ORNL-4134
UC-34 – Physics

NEUTRON PHYSICS DIVISION
ANNUAL PROGRESS REPORT
FOR PERIOD ENDING MAY 31, 1967

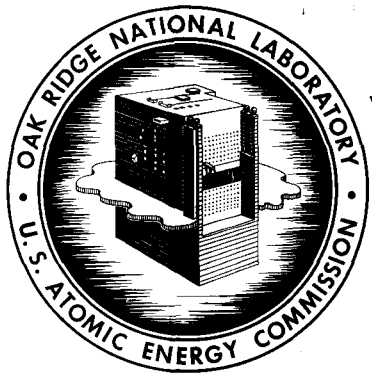

OAK RIDGE NATIONAL LABORATORY
operated by
UNION CARBIDE CORPORATION
for the
U.S. ATOMIC ENERGY COMMISSION

Printed in the United States of America. Available from Clearinghouse for Federal
Scientific and Technical Information, National Bureau of Standards,
U.S. Department of Commerce, Springfield, Virginia 22151
Price: Printed Copy $3.00; Microfiche $0.65

ORNL-4134

Contract No. W-7405-eng-26

NEUTRON PHYSICS DIVISION
ANNUAL PROGRESS REPORT
For Period Ending May 31, 1967

F. C. Maienschein, Director
A. D. Callihan, Associate Director

Group Leaders

C. E. Clifford, Reactor and Weapons Radiation Shielding
R. G. Alsmiller, Theoretical Space and High-Energy Accelerator Shielding
R. W. Peelle, Experimental Space and High-Energy Accelerator Shielding

AUGUST 1967

OAK RIDGE NATIONAL LABORATORY
Oak Ridge, Tennessee
operated by
UNION CARBIDE CORPORATION
for the
U. S. ATOMIC ENERGY COMMISSION

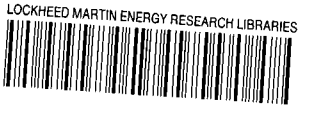

Reports previously issued in this series are as follows:

ORNL-2081	Period Ending September 10, 1956
ORNL-2389	Period Ending September 1, 1957
ORNL-2609	Period Ending September 1, 1958
ORNL-2842	Period Ending September 1, 1959
ORNL-3016	Period Ending September 1, 1960
ORNL-3193	Period Ending September 1, 1961
ORNL-3360	Period Ending September 1, 1962
ORNL-3499, Vols. I and II	Period Ending August 1, 1963
ORNL-3714, Vols. I and II	Period Ending August 1, 1964
ORNL-3858, Vols. I and II	Period Ending August 1, 1965
ORNL-3973, Vols. I and II	Period Ending May 31, 1966

Contents

1. Nuclear and Reactor Physics

1.1 RATIO OF CAPTURE TO FISSION IN ^{239}Pu AT keV NEUTRON ENERGIES[1]

A. Lottin[2] G. de Saussure
L. W. Weston J. H. Todd[3]

The neutron capture-to-fission ratio, α, was measured for ^{239}Pu for neutron incident energies from 20 to 600 keV. A pulsed beam of neutrons was collimated on a sample of plutonium placed in the center of a large hydrogenous gamma-ray scintillator poisoned with gadolinium. A capture event in the sample was characterized by a single pulse of the scintillator due to the cascade of capture gamma rays, while a fission event was characterized by a pulse due to the prompt fission gamma rays, followed a few microseconds later by additional pulses due to the gamma rays produced when the thermalized fission neutrons were captured in the gadolinium of the scintillator. Below 100 keV the neutron energies were measured by the time-of-flight technique with a resolution of 7 nsec/m. Above 100 keV approximately monoenergetic neutrons were used. Similar measurements were also performed on ^{235}U.

The ORNL 3-MV Pulsed Van de Graaff was used to accelerate protons onto a lithium target; neutrons were produced via the ^{7}Li(p,n) reaction. The proton bursts were 2 nsec wide at full width half maximum and were repeated every 32 μsec.

References

[1]Abstract of paper to be published in *Proceedings of International Conference on Fast Critical Experiments and Their Analysis, Argonne National Laboratory, October 10–13, 1966.*

[2]On assignment from CEN, Saclay, France.

[3]Instrumentation and Controls Division.

1.2 MULTILEVEL ANALYSIS OF THE ^{235}U AND ^{233}U CAPTURE AND FISSION CROSS SECTIONS IN THE ENERGY RANGE 0.4 TO 30 eV

G. de Saussure

It is now well established[1] that the neutron reaction cross sections of fissionable isotopes cannot be adequately represented by the single-level Breit-Wigner formula. Indeed there are asymmetries in the resonances caused by interference in the fission channels.

Various formulas have been developed which account for the observed asymmetries.[2,3] In particular, Adler and Adler[3] have shown that in the multilevel multichannel formalism a reaction cross section can be represented as a linear combination of single-level Breit-Wigner symmetric and asymmetric terms:

$$\sigma^{(x)}(E)\,E^{1/2} = \sum_k \frac{G_k^{(x)}\,\nu_k + H_k^{(x)}\,(\mu_k - E)}{(\mu_k - E)^2 + \nu_k^2}\,, \qquad (1)$$

where $\sigma^{(x)}(E)$ is the cross section for reaction (x) as a function of neutron energy E, and G, H, μ, and ν are resonance parameters which have only a weak energy dependence and hence are treated here as constants.

If the Doppler and instrumental resolution broadening can be approximated by Gaussian kernels,[4,5] the Doppler- and instrumental-broadened cross section corresponding to Eq. (1) is

$$\underset{\triangle}{\sigma^{(x)}}(E)\,E^{1/2} = \sum_k \frac{1}{\nu_k}\,[G_k^{(x)}\,\psi(\beta_k,x_k) + H_k^{(x)}\,\phi(\beta_k,x_k)]\,, \qquad (2)$$

where

Δ^2 = the sum of the squares of the Doppler width and of the instrumental resolution width,

$$\beta = \frac{\Delta}{\nu},$$

$$x = \frac{E - \mu}{\nu},$$

$$\psi(\beta,x) = \frac{1}{\beta\pi^{1/2}} \int \frac{e^{-(x-y)^2/\beta^2}\, dy}{1 + y^2},$$

$$\phi(\beta,x) = \frac{1}{\beta\pi^{1/2}} \int \frac{y e^{-(x-y)^2/\beta^2}\, dy}{1 + y^2}.$$

Adler and Adler[6] have developed a computer code for obtaining a least-squares fit of an experimental cross section to a trial function of the type represented in Eq. (2). However, to obtain the best possible parameters from the simultaneous measurement of the capture and fission cross sections described elsewhere,[7] it is desirable to fit *simultaneously* the two cross sections. A computer program has been written which minimizes the quantity

$$S = \sum_i \left\{ \left[(\sigma_f \sqrt{E})_e - (\sigma_f \sqrt{E})_c \right]_i^2 \omega_{fi} + \left[(\sigma_c \sqrt{E})_e - (\sigma_c \sqrt{E})_c \right]_i^2 \omega_{ci} \right\}, \quad (3)$$

where σ_f and σ_c represent the fission and capture cross sections respectively, ω_{fi} and ω_{ci} are statistical weights appropriate to the ith channel of the fission or capture measurement, and the subscripts e and c refer to the experimental data and the computed values respectively.

The trial functions for $(\sigma \sqrt{E})_c$ are of the type defined in Eq. (2). Since Eq. (2) is not linear in the parameters μ and ν, the least-squares fit is done by successive iteration by the Gauss method.[8] In its present form the least-squares program can fit up to 4000 data points with a maximum of 100 variable parameters. To fit 2000 data points with 96 variable parameters (16 levels) would take about 50 min/iteration on the CDC 1604.

Examples of least-squares fits to the cross sections of ^{233}U and ^{235}U are given in Figs. 1.2.1 and 1.2.2. The solid line in the figures is obtained by Eq. (2), using the parameters listed in Tables 1.2.1 and 1.2.2, and the dots represent the experimental data.[7]

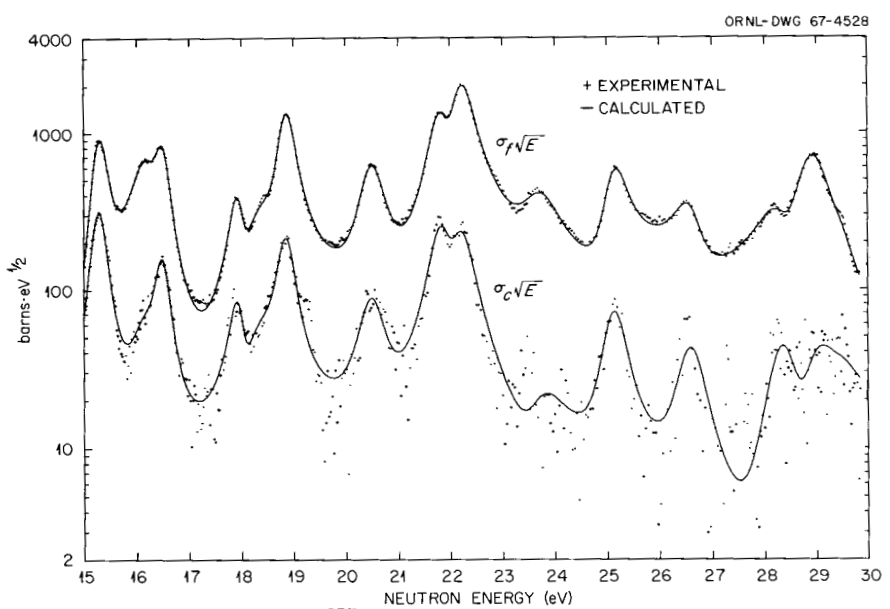

Least Squares Fit to the ^{233}U Capture and Fission Cross Sections. ORNL-RPI, 1966.

Fig. 1.2.1. Least-Squares Fit to the ^{233}U Capture and Fission Cross Sections.

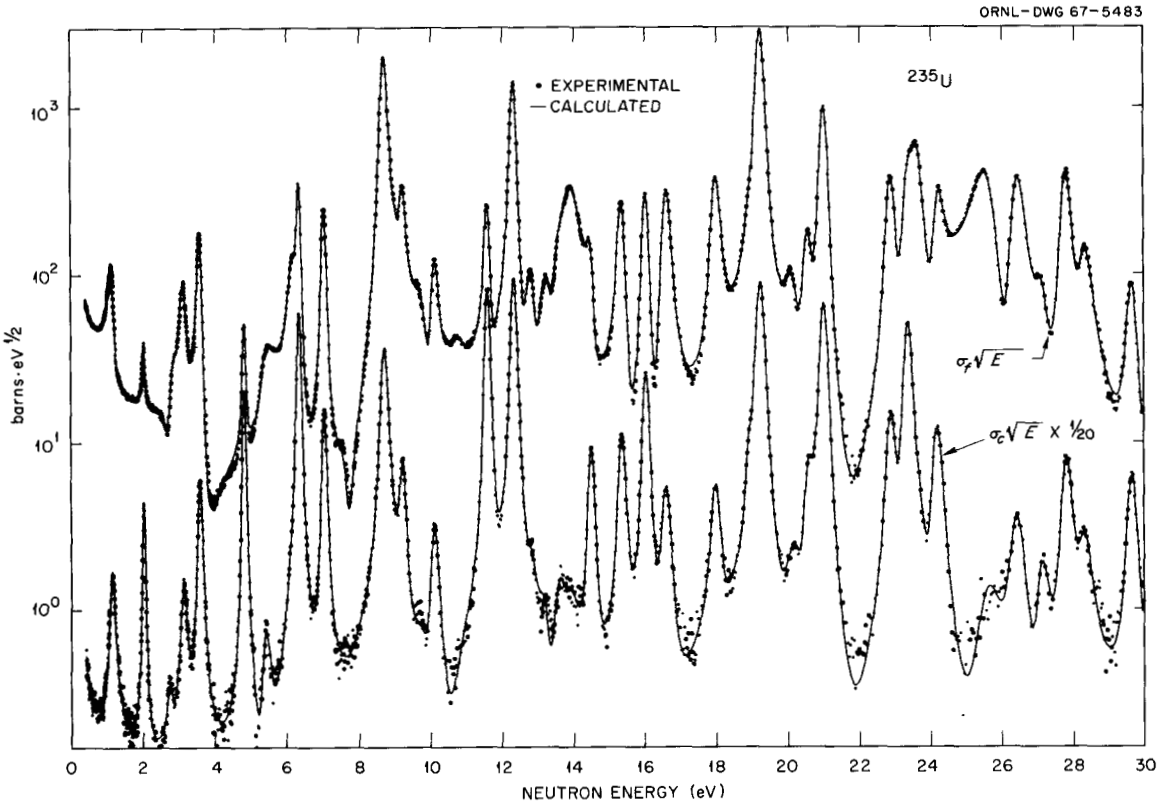

Fig. 1.2.2. Least-Squares Fit to the ^{235}U Capture and Fission Cross Sections.

References

[1]F. J. Shore and V. L. Sailor, *Phys. Rev.* **112**, 191 (1958).

[2]C. W. Reich and M. Moore, *Phys. Rev.* **111**, 929 (1958); E. Vogt, *Phys. Rev.* **112**, 203 (1958).

[3]D. B. Adler and F. T. Adler, p. 695 in *Proceedings of the Conference on Breeding, Economics and Safety in Large Fast Power Reactors, Oct. 7–10, 1963,* ANL-6792.

[4]A. W. Solbrig, Jr., *Am. J. Phys.* **29**, 257 (1961).

[5]A. Michaudon and P. Ribon, *J. Phys. Radium* **22**, 712 (1961).

[6]D. B. Adler and F. T. Adler, *Analysis of Neutron Resonances in Fissile Elements: Programs CØDILLI, CURVEPLØT, and SIGMA,* COO-1546-3 (1966), and *Multilevel Analysis of the Low Energy Level Structure of U-235, Final Report,* BNL-006977 (1966).

[7]G. de Saussure *et al.*, Paper CN-23/48 in *Conference on Nuclear Data, Microscopic Cross Sections, and Other Data Basic for Reactors, Paris, October 1966,* IAEA, Vienna (to be published).

[8]W. E. Deming, *Statistical Adjustment of Data,* Wiley, New York, 1943.

1.3 MEASUREMENT OF THE NEUTRON FISSION AND CAPTURE CROSS SECTIONS FOR ^{233}U IN THE ENERGY REGION FROM 0.4 TO 1000 eV[1]

L. W. Weston
R. Gwin
G. de Saussure
R. W. Ingle[2]
R. R. Fullwood[3]
R. W. Hockenbury[3]

The neutron capture cross section and fission cross section for ^{233}U have been measured simultaneously in the neutron energy range 0.4 to 1000 eV. The data are presented in graphical, tabular, and integral form. Comparisons with previously published data, using similar and different methods, are given.

References

[1]Abstract of ORNL-TM-1751 (May 1967).

[2]Instrumentation and Controls Division.
[3]Rensselaer Polytechnic Institute.

Table 1.2.1. Resonance Parameters Used in Computing the Cross Sections of Fig. 1.2.1.

(See Eq. 1 for definition of parameters.)

μ (eV)	ν (eV)	G_c (b·eV$^{3/2}$)	H_c (b·eV$^{3/2}$)	G_f (b·eV$^{3/2}$)	H_f (b·eV$^{3/2}$)
11.23257	.37193	2.53955	−15.72331	96.13184	−2.07796
12.76202	.17587	29.08414	2.33186	240.79899	46.94795
13.64409	.28946	13.80681	4.48138	113.72068	.89875
15.28876	.13216	46.45394	−1.41190	126.57257	−25.15996
16.18062	.29172	13.63612	−.69397	174.17748	18.00839
16.49905	.10886	16.82734	−.37380	75.00973	−3.39215
17.96900	.08320	4.87096	4.44572	21.83851	19.50060
18.29557	.53031	27.11174	−11.81989	177.75448	−76.48076
18.86678	.14045	29.22909	−.60966	179.20116	−38.20580
20.51572	.23168	17.81964	.85860	128.18506	−6.14011
21.87813	.20002	50.14075	21.92113	260.60050	166.39538
22.18681	.21254	46.93940	−25.43428	417.75994	−276.22732
23.70461	.38540	3.01877	−4.90698	91.86347	−24.40996
25.13599	.20232	14.38984	−1.91289	89.55819	−40.97917
26.60049	.25676	10.60590	−.67868	50.05842	26.50938
28.36096	.29654	15.74693	−1.05474	13.17368	70.10236
28.93349	.35504	6.62019	−14.29076	272.10981	−2.56740
29.50000	.20000	.76271	−.66177	10.25634	.61969
31.20000	.22250	9.85892	0	87.63484	0

1.4 SIMULTANEOUS MEASUREMENT OF THE NEUTRON FISSION AND CAPTURE CROSS SECTIONS FOR ^{235}U FOR NEUTRON INCIDENT ENERGIES FROM 0.4 eV TO 3 keV[1]

G. de Saussure
L. W. Weston
R. Gwin
R. W. Ingle[2]
R. W. Hockenbury[3]

The neutron fission and capture cross sections for ^{235}U have been measured simultaneously for incident neutron energies from 0.4 eV to 3 keV. In addition, the fission cross section has been measured up to a neutron energy of 20 keV. This memorandum contains a brief description of the experimental technique and a discussion of the results. A complete tabulation of the data is given in an appendix.

References

[1]Abstract of ORNL-TM-1804 (in preparation).
[2]Instrumentation and Controls Division.
[3]Rensselaer Polytechnic Institute.

1.5 MEASUREMENTS OF INELASTIC SCATTERING OF FAST NEUTRONS

F. G. Perey
W. E. Kinney
J. A. Biggerstaff[1]
J. W. McConnell[2]
J. K. Dickens
P. H. Stelson[1]

For several years we have worked on setting up a program of fast-neutron inelastic scattering making use of the three ORNL Pulsed Van de Graaff accelerators. By selecting appropriate targets we can now produce monoenergetic neutron sources suitable for inelastic-scattering measurements in the energy range 0.3 to 29 MeV. We have concentrated our efforts in developing a system which would be particularly suitable to produce data in the energy region above 4 MeV, where there are few data and where many requirements exist for the United States reactor development program.

The main purpose of these experiments is to measure $\sigma(E_n, E_{n'}, \theta)$. All our measurements to date have been in the energy region between 4 and 8 MeV, using the D(d,n) reaction to produce the primary neutrons. A deuterium gas target has been

Table 1.2.2. Resonance Parameters Used in Computing the Cross Sections of Fig. 1.2.2.

(See Eq. 1 for definition of parameters.)

μ (eV)	ν (eV)	G_c (b·eV$^{3/2}$)	H_c (b·eV$^{3/2}$)	G_f (b·eV$^{3/2}$)	H_f (b·eV$^{3/2}$)
−1.45000	.05500	770.15114	17.18756	4541.91182	36.12302
.28400	.07500	1.20231	.01072	3.32652	1.39922
1.13947	.06902	2.22347	−.19384	6.00199	2.64885
2.03120	.02439	2.90223	.06887	.82595	.05986
2.77150	.07054	.28941	.07423	−.28258	−1.02058
3.15154	.07380	2.15970	.08477	5.76045	1.72781
3.61278	.04867	6.80327	.06562	9.78259	2.93938
4.84166	.02424	17.22747	.00624	1.77571	.13642
5.40611	.10846	1.39121	−.88268	1.56906	−1.20620
5.64455	.45830	−3.90929	.00357	5.38645	−.39711
6.20306	.08812	1.43881	−.15321	9.26188	3.15553
6.38050	.02963	59.20833	1.72814	16.65094	1.17987
7.07920	.03882	17.92462	.12223	14.25560	.76116
7.67358	.46885	−1.29428	.29702	−2.32421	2.57974
8.76627	.07481	66.02073	.53074	181.25212	−15.39117
9.28574	.05825	9.92533	2.22708	18.06119	.54588
9.93854	.23616	−.89374	3.93113	−.76911	20.36651
10.14982	.09832	7.32092	−.66392	14.00283	−5.46172
10.71943	.30240	−1.39089	−.54101	7.33841	−.85938
11.65764	.03103	101.22633	1.82925	13.76491	3.38214
12.39653	.04537	138.31752	3.74425	102.90316	12.41064
12.86373	.07870	.82028	.59987	8.48599	1.39027
13.28679	.10988	.68803	1.66443	8.71831	2.28077
13.64601	.13810	3.26927	.77161	8.61804	−7.78812
14.00367	.25223	5.58913	1.06927	76.44795	3.44376
14.55257	.04683	13.55299	.29876	5.94236	4.63964
15.41923	.06222	18.09368	1.23731	23.64296	6.53652
16.09221	.04512	40.72848	1.96754	23.67437	3.20808
16.66009	.08597	11.42740	1.09002	34.98103	−4.58885
18.04589	.08719	10.90030	1.85998	40.27001	−2.49589
18.95287	.03084	4.62271	−2.17266	2.85830	.11221
19.30077	.07056	179.50668	12.01284	296.07015	14.90732
20.18719	.18930	7.70002	−.05780	13.38123	8.18879
20.60773	.06614	9.64642	−4.11001	14.21872	−.14958
21.07232	.05587	122.97042	9.01999	92.17404	5.61273
22.94443	.07080	28.62818	3.34544	38.28515	2.90291
23.42480	.05581	99.25659	10.01077	28.90408	3.74486
23.62740	.12359	13.11558	−7.21894	85.76428	−13.63375
24.22956	.08654	29.69650	−3.14958	22.01775	−18.38219
25.64412	.34972	9.76606	−2.21947	138.25995	80.49222
26.44799	.16557	13.47069	−.97383	71.74169	−29.51954
27.13103	.11845	4.47223	−2.32165	7.91285	−.04342
27.83094	.09149	19.30573	−2.02018	51.12444	−3.33743
28.32958	.15400	7.66445	−1.11256	20.68871	−7.80845
29.66914	.07216	13.95004	.56708	9.13855	.70060
30.59000	.07500	12.01990	0	12.67852	0
32.06000	.05900	103.11204	0	99.67498	0
35.21000	.08500	183.05887	0	310.90951	0

perfected for use in the high-intensity deuteron beams available which would minimize the effects of occluded deuterium. At an energy $E_n = 5$ MeV, the energy spread of the neutrons was measured to be less than 90 keV. Since this energy spread is due mostly to deuteron energy loss in the gas cell, it decreases as the neutron energy increases.

The energy $E_{n'}$ is obtained by measuring the time of arrival of scattered neutrons relative to the time of production of the primary neutrons. Scattered neutrons are detected in a liquid organic scintillator (NE-213). Gamma-ray-induced pulses are rejected by pulse-shape analysis. The pulse height and flight time for each event are recorded. The retention of pulse-height information enables correction for time slewing in the electronics as a function of pulse height. This correction used to be done off-line by recording a two-dimensional array in a multichannel analyzer but is now done on-line on an event-by-event basis using our PDP-7 computer. A block diagram of the electronics is shown in Fig. 1.5.1. The PDP-7 has now replaced the multichannel analyzers shown in the figure.

The detector is enclosed in a massive shield and is mounted on a polar coordinate system which enables positioning of the detector at distances up to 6 m from the scatterer and at angles from 0 to 140°.

Scatterers until now have been right cylinders less than one-third of a mean free path in diameter and 2 to 3 cm high. They are located at the center of rotation of the polar coordinate system at distances from 8 to 12 cm from the neutron source.

A typical time-of-flight spectrum is shown in Fig. 1.5.2. The data have been processed and corrected for time slewing and have been summed over the pulse-height distribution. Note that the flight time increases to the left so that the energy scale has the usual sense, although it is of course nonlinear. These data were taken with a 4-m flight path and with a time resolution from ~2 nsec for the first energy group, corresponding to the electronics resolution, to ~4 nsec for the lowest energy shown, corresponding to the incident neutron energy spread.

The measurements performed using a multichannel analyzer to store the data are shown in Table 1.5.1. Considerable effort was spent to reduce the spectra to cross sections using the CDC 160 computer at ORNL without succeeding in automating the data reduction.

In October 1966 a PDP-7 computer system was installed and adapted to do the "walk correction" on-line (see Sect. 6.9). Inelastic-scattering data, using the computer on-line, were obtained in November 1966. The measurements were performed at $E_n = 7.6$ MeV on C, Mg, Al, Si, S, Fe, Co, and Y.

Computer programs were written to reduce the data using the light pen facility of the system (see Sect. 6.9). This has enabled us to reduce data at a much greater rate, approximately 10 times faster, than using the large computer. All the 7.6-MeV data and all the iron inelastic-scattering data (see Sect. 1.6) have now been converted to cross sections and corrected for multiple scattering (see Sect. 1.7). Final results of the 7.6-MeV elastic-scattering data are shown on Fig. 1.5.3. Final results for some of the inelastic cross sections are shown on Fig. 1.5.4.

All the spectra which were obtained using the multichannel analyzers have now been converted to a form in which they can be reduced to cross sections using the PDP-7 computer.

The data acquisition system is being extended to include two additional detectors so that measurements can be performed at three angles simultaneously.

References

[1]Physics Division.
[2]Instrumentation and Controls Division.

1.6 NEUTRON SCATTERING CROSS SECTIONS FOR ^{56}Fe FROM 4.5 TO 7.6 MeV

W. E. Kinney
J. A. Biggerstaff[1]
J. K. Dickens
M. V. Harlow, Jr.[2]
J. W. McConnell[3]
F. G. Perey
P. H. Stelson[1]

Neutron scattering cross sections for ^{56}Fe were measured by the time-of-flight method[4,5] at 4.5, 5.0, 5.6, 6.2, 6.6, and 7.6 MeV, yielding angular distributions for 11 groups of neutrons up to an excitation energy of 4.72 MeV.

The cylindrical scattering samples of natural iron were placed from 7 to 12 cm from the D_2 gas target where neutrons were produced by the (d,d) reaction. Most of the data were taken with a 1.58-cm-diam, 2-cm-high sample; at 5 MeV, however,

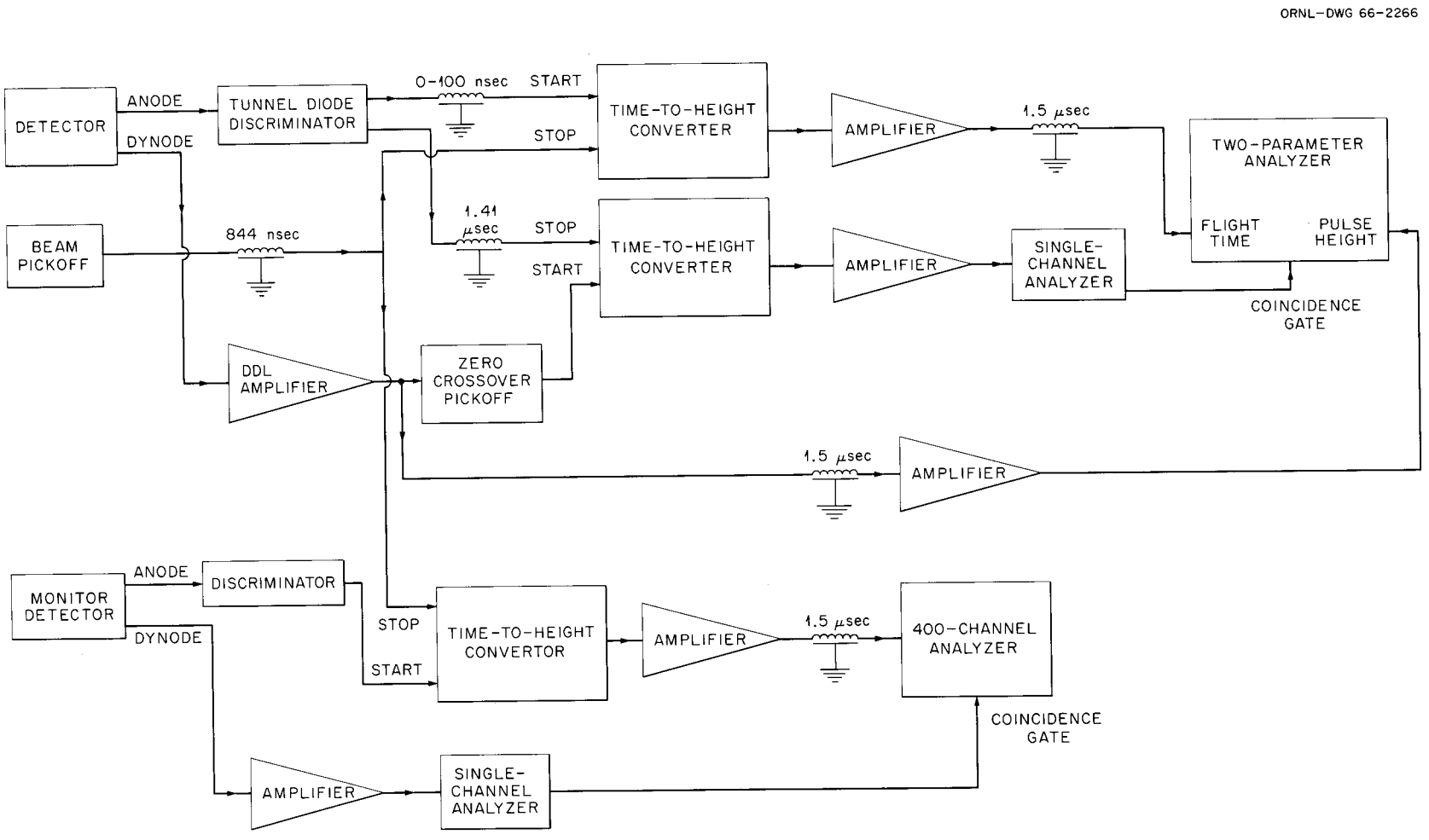

Fig. 1.5.1. Schematic Diagram of the Electronic System.

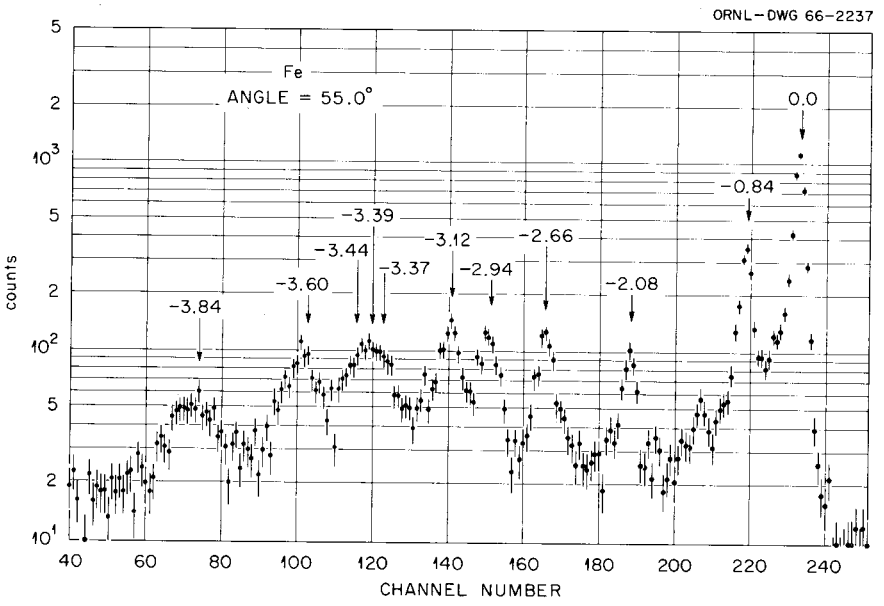

Fig. 1.5.2. Scattered Neutron Spectrum for Fe at E_n = 5.0 MeV. The flight path was 4 m. Sample-out background was not subtracted.

Table 1.5.1. (n,n') Measurements Performed to Date with Multichannel Analyzer.

Element	Incident Energy (MeV)	Number of Angles	Angular Range (deg)	Number of Neutron Groups Resolved	Maximum Excitation Energy (MeV)
			Angular Distributions		
C	4.5	9	32–135	1	~3
	5.0	9	32–135	1	~3
	5.6	8	23–128	1	~3
Na	5.0	9	43–132	7	3.7
Al	5.0	3	63–104	4	3
Si	5.0	8	21–133	2	3
	5.6	7	21–133	2	3
K	5.0	9	43–132	6	3.6
Ca	5.0	9	43–132	4	4
V	5.0	16	25–141	9	3.2
Fe	4.5	9	30–132	8	3.6
	5.0	15	30–141	8	3.6
	5.6	9	30–132	8	3.6
	6.2	12	25–114	10	4.1
	6.6	15	25–114	10	4.1
	7.6	3	25–114	10	4.1
Co	5.0	17	25–141	7	2.6
Y	5.0	9	43–132	8	3.1
			Excitation Functions		
Si	4.4–5.0	2	57 and 111	2	3
Fe	4.5–5.4	1	111	2	1

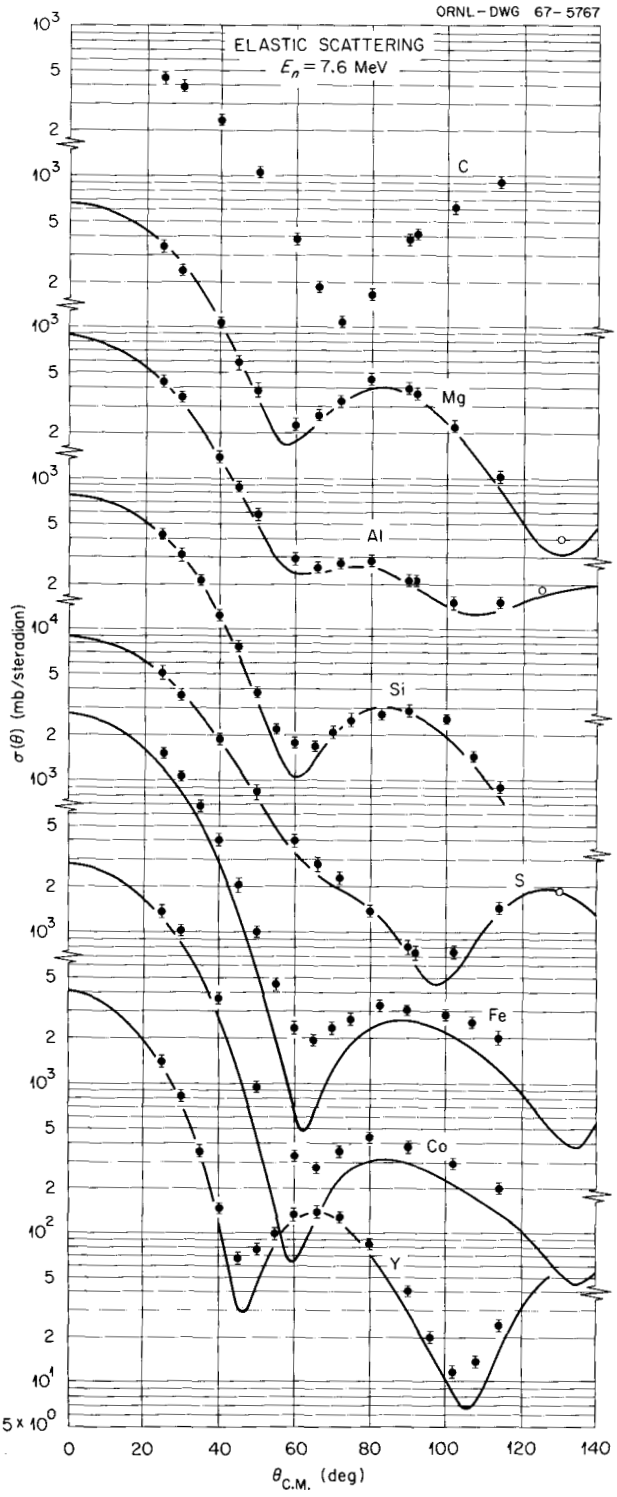

Fig. 1.5.3. Elastic Scattering of 7.6-MeV Neutrons. The dots indicate the data points and the solid line the microscopic cross section which will reproduce the data points with contributions from multiple scattering in the scatterer.

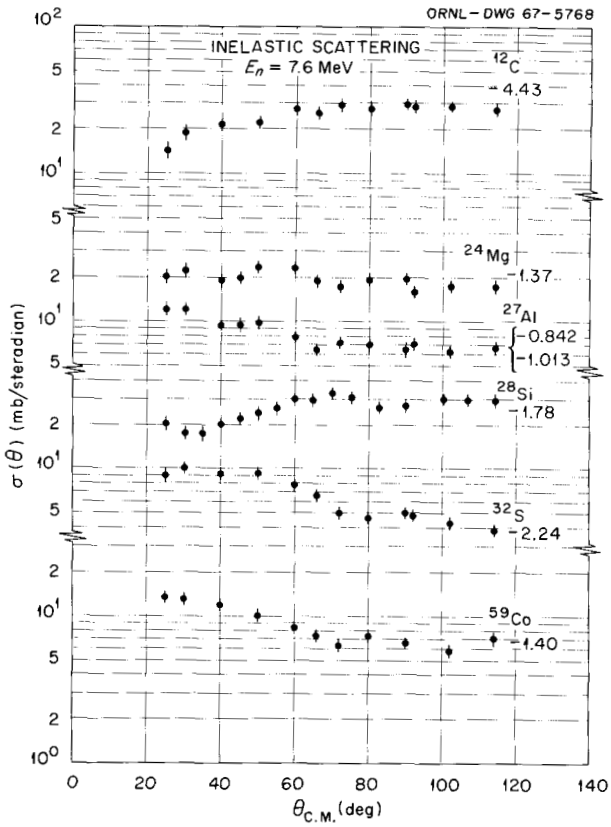

Fig. 1.5.4. Inelastic Scattering of 7.6-MeV Neutrons from Some of the Low-Lying Levels of the Studied Element.

the sample was 1 cm in diameter and 3 cm high. Flight paths ranged from 3.8 to 5.6 m.

The PDP-7 data reduction program (Sect. 6.9) was used to extract peak areas which were then converted into raw cross sections and corrected for multiple scattering and beam attenuation (Sect. 1.7) to arrive at the final results. An error analysis indicates 7% to 10% errors on the elastic cross sections and 10% to 20% on the inelastic.

In Fig. 1.6.1, a plot of the integrated cross sections as a function of energy, our results may be compared with existing data of Gilboy and Towle,[6] Hopkins and Silbert,[7] and Holmqvist and Wielding.[8] Hopkins and Silbert measured at 50° only and multiplied by 4π to arrive at an integrated cross section, a procedure which is quite satisfactory if the angular distribution is isotropic. The other investigators measured angular distribution. Our results are seen to be in agreement with those of Gilboy and Towle in all cases. They disagree with the data of Hopkins and Silbert for the 0.845-MeV level in part because of the anisotropy of the

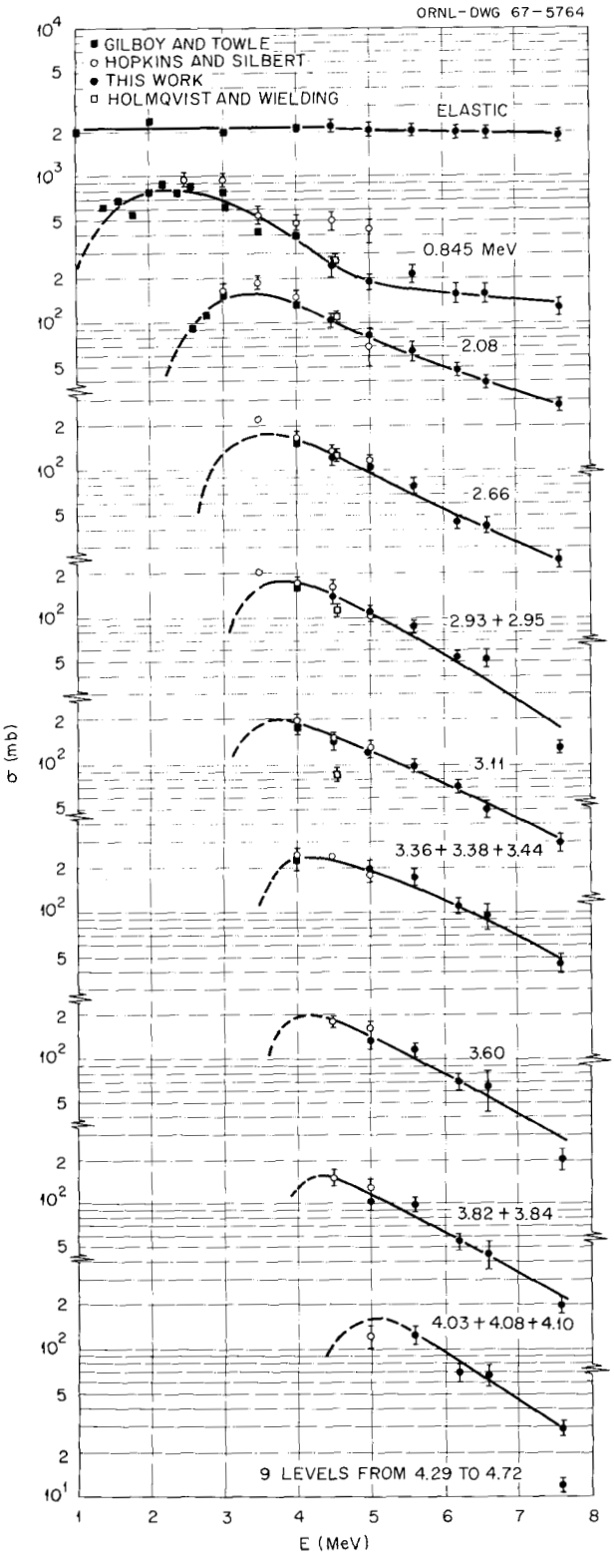

Fig. 1.6.1. Integral Cross Sections for ^{56}Fe As a Function of Energy. Numbers with each curve are -Q for the levels.

angular distribution of neutrons scattered from this level; however, from our measured angular distributions this cannot explain all of the disagreement. The distributions resulting from scattering from the higher levels are isotropic within experimental error. There appears also to be a disagreement with the data of Holmqvist and Wielding for the 3.11-MeV level. Otherwise, our data are in generally good agreement. The levels higher than the 0.845-MeV level all show about the same fall-off with increasing energy as more levels compete in the compound nucleus decay. The slower decrease of the 0.845-MeV level is an indication that direct as well as compound nucleus processes are involved in the excitation of this level.

The data for the elastic differential scattering cross section are given in Fig. 1.6.2. A comparison at 4.5 MeV may be made with the results of Gilboy and Towle at 4.0 MeV and with Holmqvist and Wielding at 4.56 MeV. Agreement is generally good with the latter data, and differences with the former are what would be expected from a 0.5-MeV difference in energy. The curves are the results of optical-model fits to the data with a standard set of parameters but with real- and imaginary-well depths varied as indicated in the figure.

Figure 1.6.3 presents the differential inelastic-scattering cross sections from the 0.845-MeV level. At 4.5 MeV the distribution is isotropic but at higher energies anisotropies appear. Distorted-wave Born approximation calculations of the direct interactions are in progress in order to fit the data with a sum of contributions from direct processes and compound nucleus mechanisms and so determine the amount of competition between these two modes of inelastic scattering. Hauser-Feshbach calculations will also be made to determine the shape of the compound nucleus angular distributions as they may very well be anisotropic. In addition, it is planned to extend measurements to larger angles at the higher energies.

References

[1]Physics Division.

[2]Present address: Los Alamos Scientific Laboratory.

[3]Instrumentation and Controls Division.

[4]J. A. Biggerstaff *et al., Neutron Phys. Div. Ann. Progr. Rept. Aug. 1, 1965,* ORNL-3858, Vol. I, p. 1.

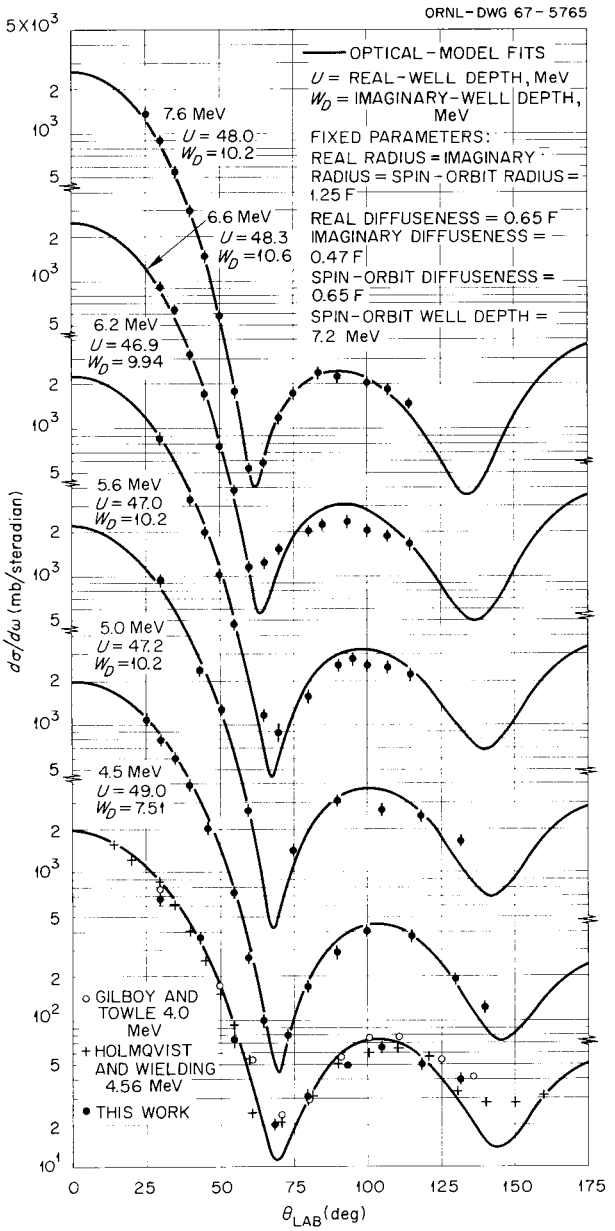

Fig. 1.6.2. Differential Elastic-Scattering Cross Sections for ^{56}Fe.

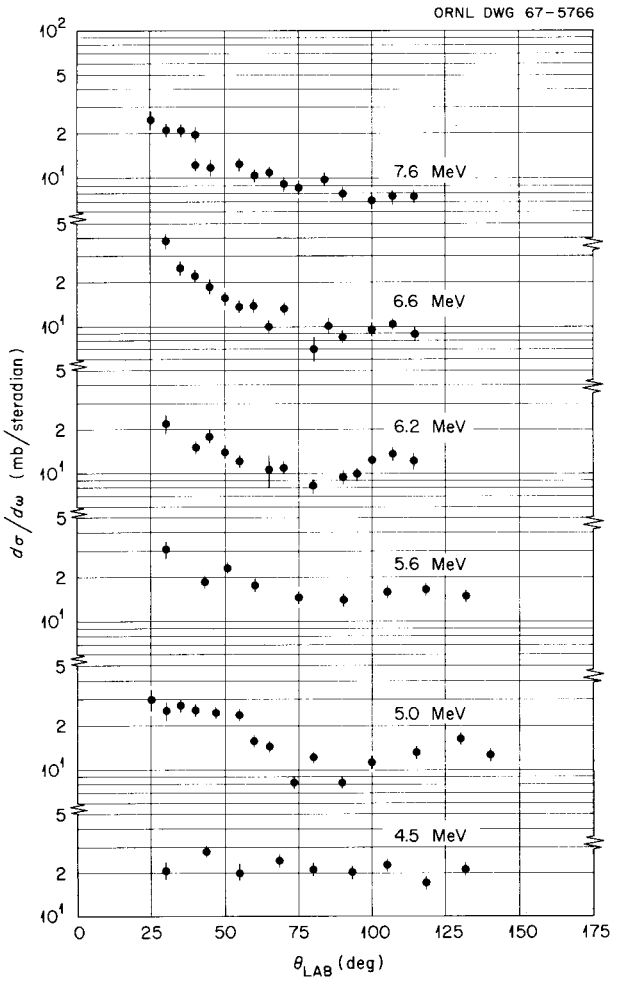

Fig. 1.6.3. Differential Inelastic-Scattering Cross Section from 0.845-MeV Level for ^{56}Fe.

1.7 MULTIPLE-SCATTERING CORRECTIONS TO NEUTRON SCATTERING DATA

W. E. Kinney F. G. Perey

Neutron scattering measurements performed at the ORNL Van de Graaff accelerator have to be corrected for the effect of the finite size of the scatterers which gives rise to incident neutron attenuation, multiple scattering, and finite angular resolution. The experimental geometry used consists of a cylindrical scatterer, usually less than 2.5 cm in diameter and 2.5 cm high, placed between 8 and 12 cm from the center of a 0.25-cm-diam, 0.5-cm-long gas cell. The detector is a proton recoil liquid scintillator about 10 cm in diameter located

[5]J. A. Biggerstaff *et al., Phys. Div. Ann. Progr. Rept. Dec. 31, 1965,* ORNL-3924, p. 54.

[6]W. B. Gilboy and J. H. Towle, *Nucl. Phys.* **64**, 130 (1965).

[7]J. C. Hopkins and M. G. Silbert, *Nucl. Sci. Eng.* **19**, 431 (1964).

[8]B. Holmqvist and T. Wielding, *Fast Neutron Scattering Cross Section Measurements on Fe and Co,* EANDC(OR) 51 "L" (1966).

from 4 to 6 m from the scatterer. An ORNL report which is in preparation describes the manner in which the time-of-flight data are reduced to cross section and the way that the "finite geometry" and multiple-scattering corrections are applied to the data with a Monte Carlo computer program. A brief résumé is given here of the fashion in which the corrections are performed.

Several simplifying assumptions have been made to perform the multiple-scattering corrections; some of them can easily be removed with slight modifications to the code. The major simplifications are as follows:

1. The neutron source is a point source.
2. The incident neutron flux is uniform over the scatterer.
3. The total cross section, for purposes of calculating attenuation in the scatterer, is constant over the energy range considered.
4. Only elastic and inelastic scattering to one level are explicitly considered; all other reactions are treated as absorption.
5. The detector is infinitely far away; i.e., we neglect the angular spread of the detector, and the detector solid angle is uniform over the scatterer.

Neutrons are required to make one collision in the sample and are assigned a statistical weight for doing so. Thereafter, analog Monte Carlo is used to transport the neutrons within the sample until they escape. At each collision, a statistical estimation is made of the contribution of that neutron to both elastic and inelastic counts at specified angles.

Any number of elastic collisions before a neutron leaves the scatterer contribute to the elastic-scattering peak. Any number of elastic scatterings and one inelastic scattering contribute to the inelastic peak.

The symbols pertaining to the geometry are defined in Fig. 1.7.1. The primary purpose of the code is to evaluate Eq. (1) for all the angles θ_D used in the experiment:

$$N(\theta_D) = \int e^{-\Sigma(\Delta r + \Delta r')}\, \sigma(\theta)\, \frac{dV}{r^2} + \int F\, dV\,, \qquad (1)$$

where Σ is the macroscopic total cross section,

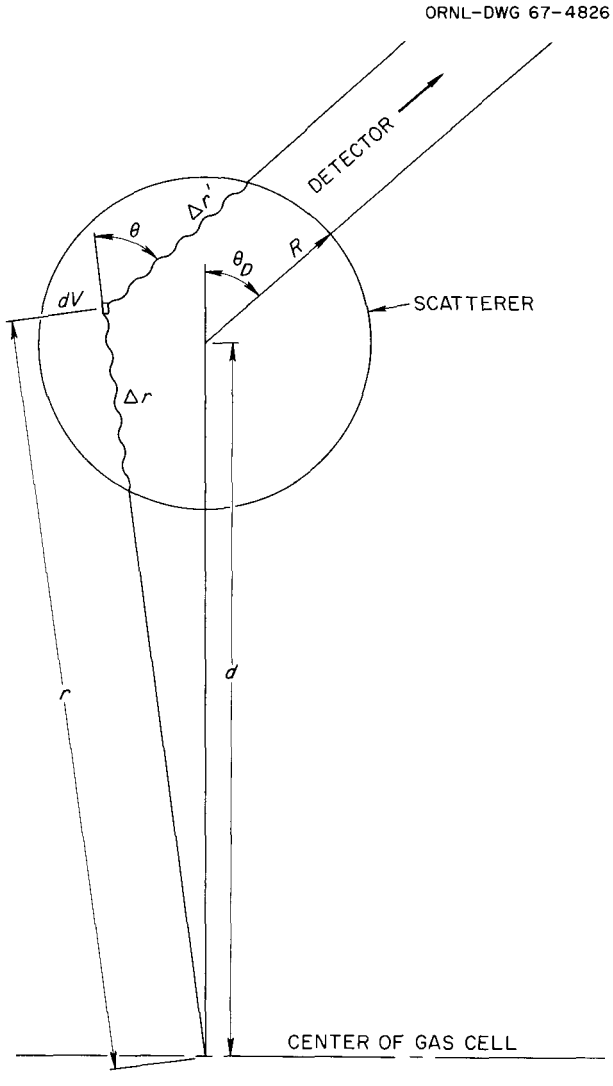

Fig. 1.7.1. Scattering Geometry.

the first term of Eq. (1) gives the contributions due to single scattering, and the second term gives the contributions due to multiple scattering.

We define the counter response $\sigma_{CR}(\theta_D)$ as

$$\sigma_{CR}(\theta_D) \equiv \frac{N(\theta_D)\, d^2}{V}\, e^{2\Sigma R}\,. \qquad (2)$$

This cross section $\sigma_{CR}(\theta_D)$ is exactly identical in form to that we obtain from our data reduction when we have applied corrections to our peak areas for efficiency of the detector, integrated neutron flux, etc.

We define the total correction factor Λ_T as

$$\sigma_{CR}(\theta_D) \equiv \Lambda_T(\theta_D)\, \sigma(\theta_D) . \qquad (3)$$

Combining Eqs. (1), (2), and (3), we have

$$\Lambda_T(\theta_D) = \frac{\int e^{-\Sigma(\Delta r + \Delta r')}\, \sigma(\theta)\, dV/r^2}{e^{-2\Sigma R}\, \sigma(\theta_D)\, V/d^2} + \frac{\int F\, dV}{e^{-2\Sigma R}\, \sigma(\theta_D)\, V/d^2} . \qquad (4)$$

The first term of Eq. (4) is called $\Lambda_S(\theta_D)$, and the second $\Lambda_M(\theta_D)$. The ratio of single-to-total scattering at any angle is given by Λ_S/Λ_T. In addition to calculating the quantities of primary interest, the Λ's, the code also keeps track, at all measured angles, of the average scattering angle and its variance and of the average outgoing neutron energy and its variance. A neutron time-of-flight spectrum can also be generated at all angles; once the system time resolution has been folded-in with the incident neutron energy spread, we can obtain a direct comparison with the measured time-of-flight spectra.

Several iteration schemes have been tried, all with about equal success, and in general three or four iterations are required so that a calculated counter response agrees with the measured one. As a practical matter, the code first fits the measured counter response by a Legendre polynomial expansion, and it is the fitted experimental counter response that the code attempts to reproduce by suitable readjustment of a guessed microscopic cross section. The lack of agreement between the individually measured points and the fitted curve is then reflected in the departure of the corrected microscopic points from the smoothed assumed microscopic cross section. First, the observed counter response is corrected for the calculated contribution due to the multiple scattering and then the correction for finite geometry is made. Figure 1.7.2 gives an example of calculated and measured counter response, together with the fit to the measured counter response for our measurement on Y at 7.6 MeV.

The computer code was checked against a complete analog Monte Carlo code written for a different computer, and very good agreement, within statistics, was obtained between the two codes.

1.8 DISTORTED-WAVE ANALYSIS OF INELASTIC SCATTERING OF 61.7-MeV PROTONS FROM ^{60}Ni[1]

F. E. Bertrand[2] J. K. Dickens
T. A. Love

Differential cross sections for the scattering of 61.7-MeV protons from the first excited level (E_x = 1.33 MeV) of ^{60}Ni have been measured between 15 and 40° with an experimental resolution of 0.3%. The data are reproduced well by a distorted-wave calculation using the vibrational model with β = 0.20.

References

[1]Abstract of paper to be published in *Physics Letters*; work partially funded by National Aeronautics and Space Administration under NASA Order R-104(1).

[2]Oak Ridge Graduate Fellow from Louisiana State University under appointment from the Oak Ridge Associated Universities, Inc.

1.9 DISTORTED-WAVE BORN ANALYSIS OF 11-MeV PROTON SCATTERING

C. M. Perey[1] J. K. Dickens
F. G. Perey R. J. Silva[2]

In previous annual reports we reported on a series of measurements of 11-MeV proton scattering from 18 isotopes between ^{48}Ti and ^{76}Ge. The analysis of the elastic-scattering data on all isotopes and of the inelastic-scattering data to the collective 2^+ and 3^- levels of the even-even isotopes is now complete, and an ORNL report describing this analysis is in preparation.

The elastic-scattering data were analyzed using the optical-model potential. For this analysis, we have made use of the elastic polarization data of Rosen *et al.*[3] on the same isotopes but taken at 10.5 MeV. Starting from the parameters obtained in a previous survey of elastic scattering,[4] we have attempted to find an optical-model potential which would best describe these measurements. The results of this search for an average optical model potential are shown in Figs. 1.9.1 and 1.9.2. The geometrical parameters of the potentials are the same for all nuclei, and only the well depths for the real,

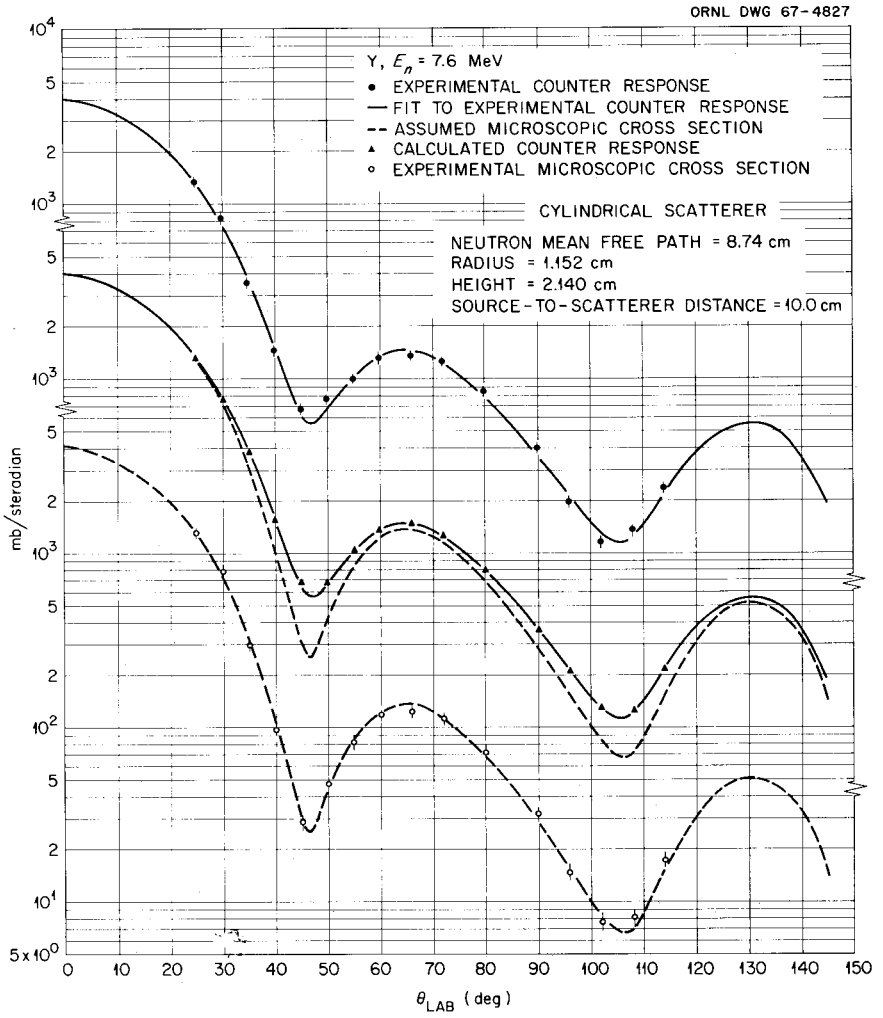

Fig. 1.7.2. Example of Multiple Scattering Correction.

imaginary, and spin-orbit potentials were adjusted to give a best fit for each nuclei. The real part of the potential is of the Wood-Saxon type with a radius parameter of 1.285 F and a diffuseness parameter of 0.65 F. The well depth slowly increases from 46.5 to 49.3 MeV as we go to heavier nuclei. The imaginary part of the potential has the shape of the derivative of a Wood-Saxon potential with a radius parameter of 1.285 F and a diffuseness parameter of 0.53 F. With the exception of the germanium isotopes, the imaginary-well depth increases slowly from 10 to 11 MeV as we go to heavier nuclei. The spin-orbit potential is of the Thomas form with a radius parameter of 1.285 F and a diffuseness parameter of 0.53 F. The well depth slowly decreases from 8 to 6 MeV as we go to heavier nuclei.

The results of the elastic-scattering analysis are very similar to those of a previous analysis,[4] except for the change in radius parameter, which was 1.25 F in the previous analysis, and imaginary diffuseness, which was 0.47 F. They are at variance with the results of analysis at higher energies,[5] where the real central potential radius parameter required is smaller and the radius parameter of the spin-orbit term is less than the one of the real part of the potential. They also differ from the analysis of the polarization data alone,[4] which gave an imaginary potential diffuseness parameter of 0.70 F.

The analysis of the inelastic-scattering data was done using the collective model calculated in the distorted-wave Born approximation. The predictions for inelastic scattering to the first 2^+ level were in

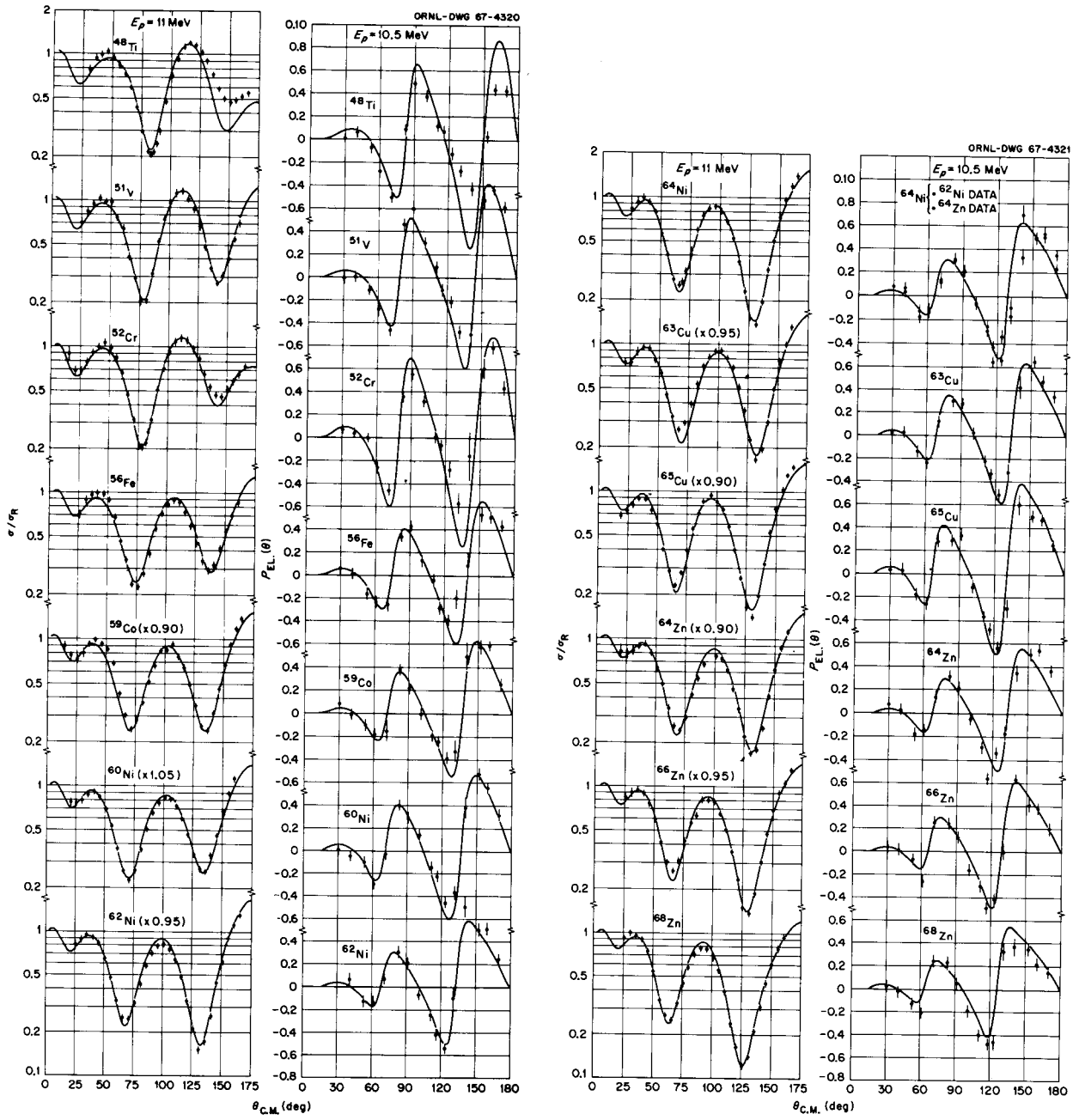

Fig. 1.9.1.*a* and *b*. Comparison of 11-MeV Proton Elastic-Scattering Data and 10.5-MeV Elastic Polarization Data with the Curves from the Average Optical-Model Potential. Only the well depths for the real, imaginary, and spin-orbit potentials were adjusted for the lowest χ^2.

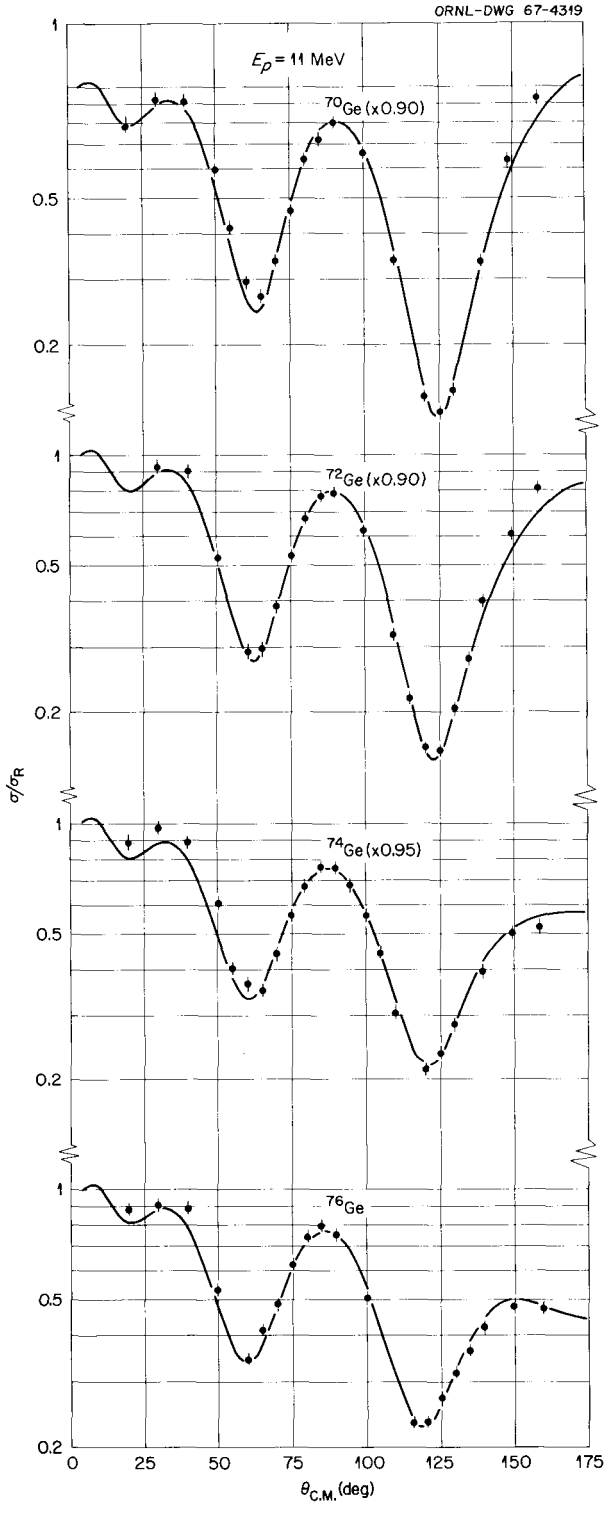

Fig. 1.9.2. Comparison of 11-MeV Proton Elastic-Scattering Data from the Ge Isotopes with the Curves from the Average Optical-Model Potential. Only the well depths for the real, imaginary, and spin-orbit potentials were adjusted for the lowest χ^2.

good agreement with the data for those nuclei which have a low Q value for the (p,n) threshold, provided that both the real part and the imaginary part of the optical-model central potential are given identical deformations. However, in several cases the agreement with the data was very significantly improved when an isotropic component was added to the cross sections predicted by the collective model. The amount of isotropic component, for a good fit, is well correlated to the Q value for (p,n) threshold, indicating that, in addition to direct reaction, we have a contribution due to compound nucleus mechanism when few channels are open to the decay of the compound system. The results of the analysis for the 2^+ levels are shown in Fig. 1.9.3, together with the value of the quadrupole deformation parameter and the fraction of the integrated cross section for each nuclei, which was added isotropically, identified as the fraction of compound nucleus contribution to the excitation of this level.

For the strongly excited low-lying 3^- collective levels the situation is similar to the case of the first 2^+ level. As was expected, the fraction of compound nucleus decay contribution is larger than that for the lower-lying 2^+ level. The major difference is that the predictions, when we assume that only the real part of the central potential undergoes octupole vibrations, are in general in better agreement with the data. The results of the analysis are shown on Fig. 1.9.4. For all cases we have shown the predictions for vibrations of the real part of the potential only and in some of the cases, where the fits were equivalent or better, the predictions when both real and imaginary parts vibrate.

The lack of a consistent picture for the interpretation of both quadrupole and octupole inelastic scattering may be due to the nonnegligible contribution of compound nucleus mechanisms at this energy or may indicate a breakdown of this simple collective model at this energy for the excitation of octupole vibrations.

References

[1]Consultant.

[2]Present address: University of California at Berkeley.

[3]L. Rosen *et al.*, *Ann. Phys.* **34**, 96 (1965).

[4]F. G. Perey, *Phys. Rev.* **131**, 745 (1963).

[5]G. R. Satchler, *Nucl. Phys.* **A92**, 273 (1967).

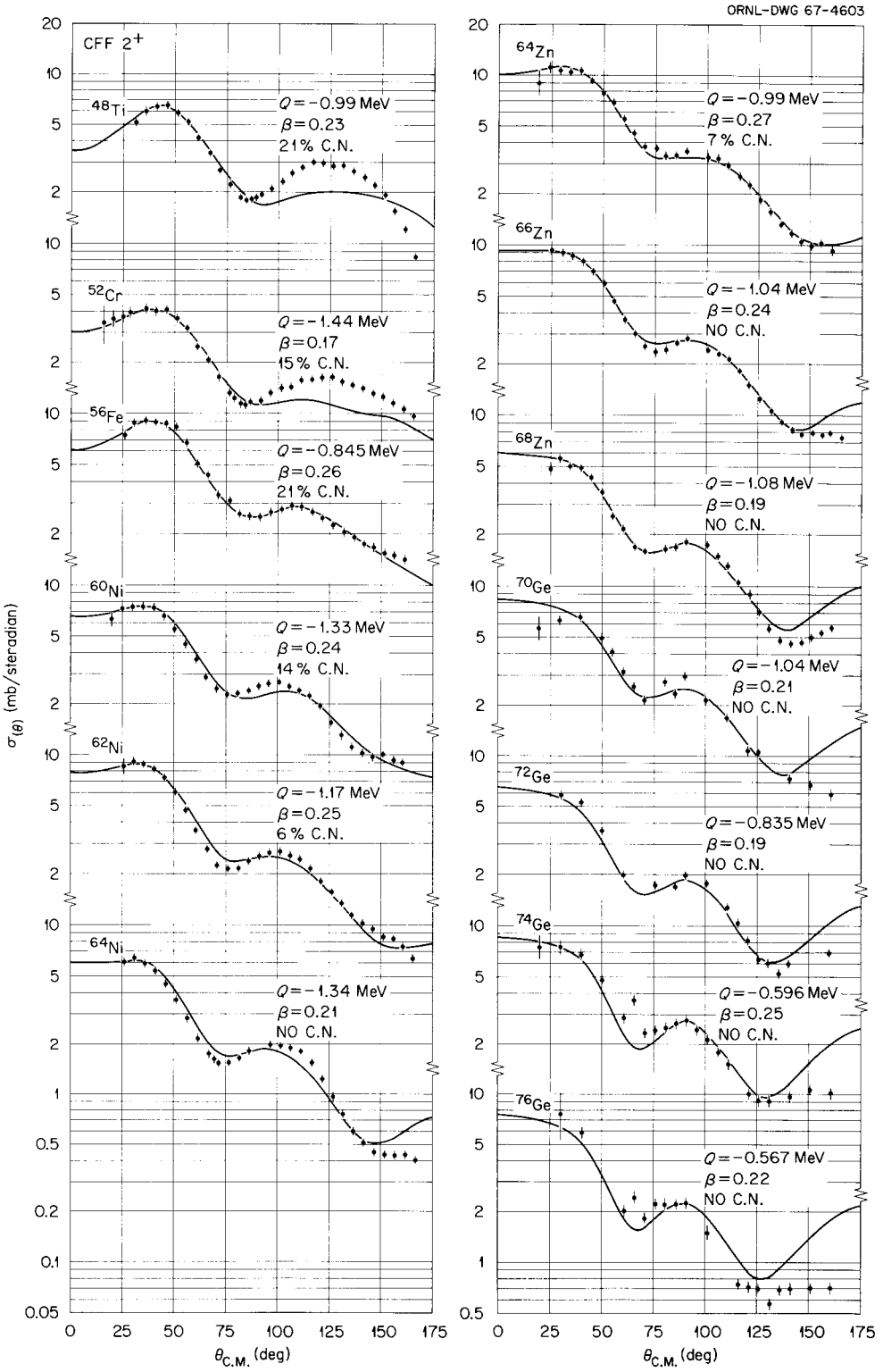

Fig. 1.9.3. Comparison of the Inelastic-Scattering Data from the First 2^+ Level of Even-Even Nuclei with Predictions from the Collective Model. Complex form factor is used with the quadrupole deformation parameters shown. To improve the fits, an isotropic component, representing compound nucleus mechanism, was added. The percentage of the total integrated cross section added as compound cross section is indicated.

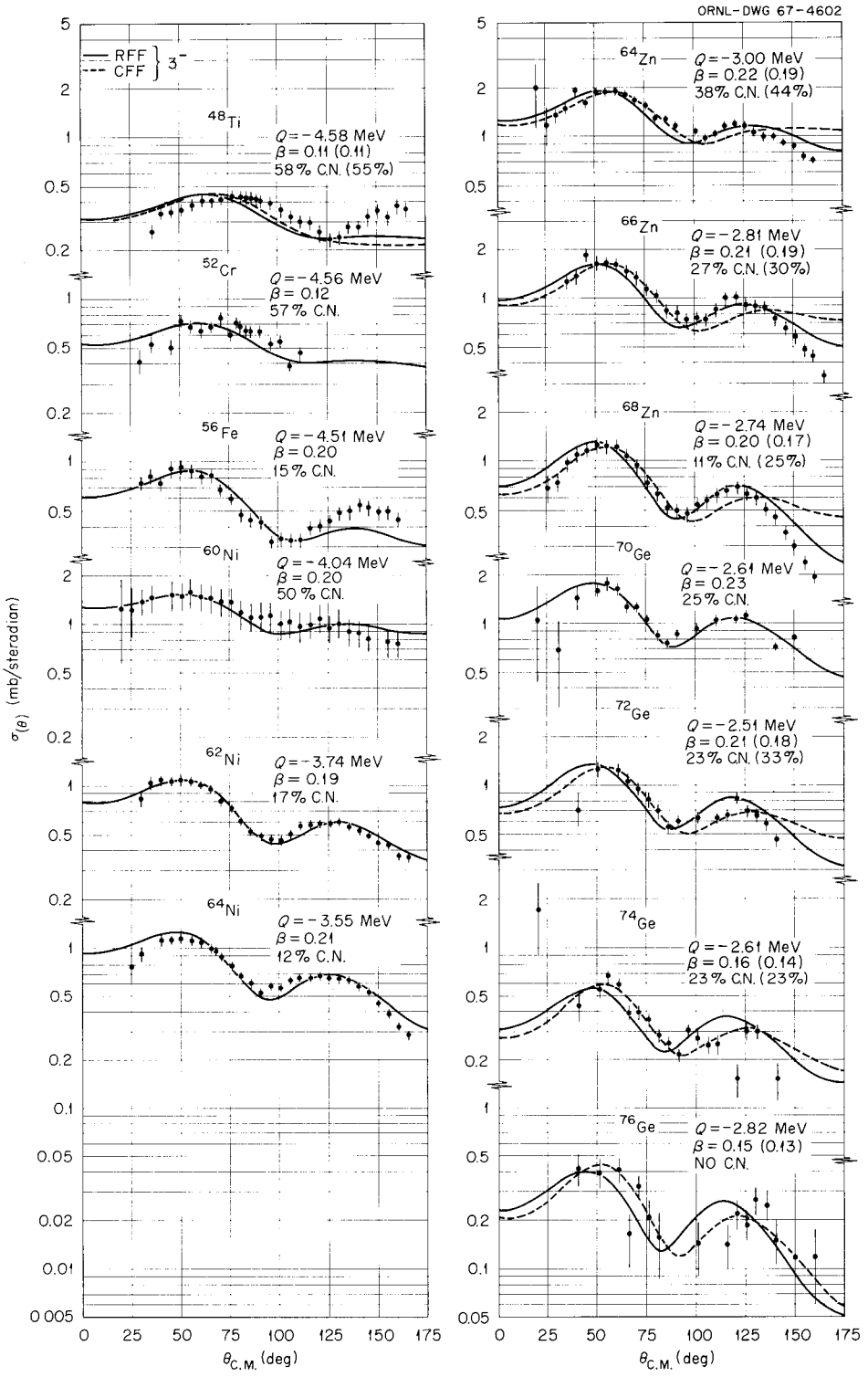

Fig. 1.9.4. Comparison of the Inelastic-Scattering Data from the First 3^- Level of Even-Even Nuclei with Predictions from the Collective Model. The full curves are calculated using the real form factor, the dashed curves using the complex form factor, with the octupole deformation parameters shown. To improve the fits, an isotropic component, representing compound nucleus mechanism, was added. The percentage of the total integrated cross section added as compound cross section is indicated.

1.10 MEASUREMENTS OF (*d*,*n*) REACTIONS

A. L. Marusak[1] J. W. McConnell[2]
J. K. Dickens F. G. Perey
W. E. Kinney P. H. Stelson[3]

A series of preliminary measurements of the reactions ^{58}Ni(*d*,*n*) ^{59}Cu and ^{60}Ni(*d*,*n*) ^{61}Cu at 5 MeV were carried out in December 1966 on the 5.5-MeV Van de Graaff using the time-of-flight technique. The purpose of these measurements was to find out what sort of problems would be involved in this type of experiment on medium-weight nuclei.

The targets used were 0.5 mg/cm^2 thick, which resulted in an energy spread of 35 keV for 5-MeV deuterons. With a 13-m flight path the resolution for lower neutron energies (2 MeV), corresponding to the excitation of higher excited states of the residual nuclei, was equal to the beam energy spread due to target thickness. It was found that with the beam intensity used, 4.5 μamp, at a repetition rate of 1 Mc/sec counting rates were such that good statistics were obtained at 13 m in about 2 hr.

A flight-path length up to 13.5 m is available, with the scattering chamber located close to the 90° analyzing magnet. The analyzing magnet is rotated on its gun mount to change the scattering angle, and the detector is only slightly moved to view the target through a hole in the shielding wall of the magnet room.

Because of the lack of a suitable scattering chamber we used a converted 4-in. beam viewer. Due to the shape of the viewer, attenuation varied from angle to angle, being higher at smaller angles. The small size of the viewer, which resulted in mass being near the target, added to the background. These problems made accurate determination of differential cross sections difficult. This series of measurements enabled us to design a new scattering chamber, which is now being fabricated. The new chamber is cylindrical in shape, is 12 in. in diameter and 12 in. in height, and has walls of 0.019-in. stainless steel.

From the ^{58}Ni data, about 25 energy levels were accurately extracted. These, along with some possible "impurity" levels, are shown in Fig. 1.10.1 for $\theta = 75°$ for the ^{58}Ni(*d*,*n*) ^{59}Cu reaction.

We extracted differential cross sections for the most prominent peaks and in particular for the ground state and the first excited state of the ^{58}Ni(*d*,*n*) ^{59}Cu reaction. Most of these showed marked angular variation. Fair agreement with the angular distributions calculated using DWBA with the Julie computer code for a stripping reaction were obtained for the $^3/_2^-$ and $^1/_2^-$ states of ^{59}Cu, the ground state, and the 0.492-MeV first excited state.

These measurements are being continued in order to gain an understanding of the deuteron interaction with nuclei at low energies. We will also use these data to determine proton single particle strength in medium-weight nuclei.

References

[1]Oak Ridge Graduate Fellow from University of Tennessee under appointment from the Oak Ridge Associated Universities, Inc.

[2]Instrumentation and Controls Division.

[3]Physics Division.

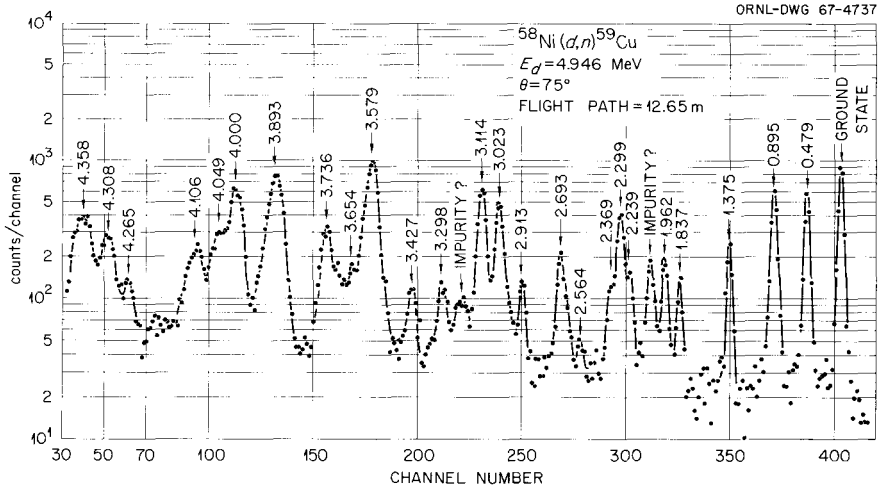

Fig. 1.10.1. Neutron Time-of-Flight Spectrum. The energies of the excited states in ^{59}Cu are indicated.

1.11 STUDIES OF (*p,n*) REACTIONS USING TIME OF FLIGHT

J. K. Dickens
W. E. Kinney
A. L. Marusak[1]
J. W. McConnell[2]
F. G. Perey
P. H. Stelson[3]

We are extending the use of the neutron detection system using time of flight for neutron energy determination (as discussed in Sect. 1.5) to study (*p,n*) reactions. To date we have investigated the reaction $^{51}V(p,n)^{51}Cr$, $^{53}Cr(p,n)^{53}Mn$, $^{55}Mn(p,n)^{55}Fe$, $^{58}Fe(p,n)^{58}Co$, $^{59}Co(p,n)^{59}Ni$, $^{65}Cu(p,n)^{65}Zn$, and $^{96}Mo(p,n)^{96}Tc$.

For all of these measurements we used the pulsed-proton beam extracted from the 5.5-MeV Van de Graaff in the High Voltage Laboratory. The targets ranged in thickness between 5 and 20 keV for the proton energy used. Flight paths up to 13 m were used, and the electronic analyzing system was capable of ~1 nsec time resolution. The energy resolution for high-energy neutrons ($E_n \gtrsim 2$ MeV) was limited by the electronic timing resolution, and that for low-energy neutrons ($E_n \lesssim 750$ keV) was limited by the target thickness. We took advantage of this experimental condition to study some of these reactions at several bombarding energies. Most (*p,n*) reactions are endoergic by several million electron volts. Thus, even with proton bombarding energies sufficient to penetrate the Coulomb barrier, the emitted neutrons were of sufficiently low energy so that the neutron energy resolution was not severely limited by the electronic timing resolution.

The spectra obtained are being studied to determine energies of excited states in the residual nucleus and the strengths of their excitations via this reaction. Preliminary results from the $^{59}Co(p,n)^{59}Ni$ and $^{65}Cu(p,n)^{65}Zn$ reactions have been reported.[4]

Two examples of our spectra are shown in Figs. 1.11.1 and 1.11.2. The first figure presents data for the $^{59}Co(p,n)^{59}Ni$ reaction for which the ^{59}Co target was ~6 keV thick to the bombarding protons. The peak numbered 0 corresponds to the ground state $^{59}Co(p,n)^{59}Ni$ transition. The first four

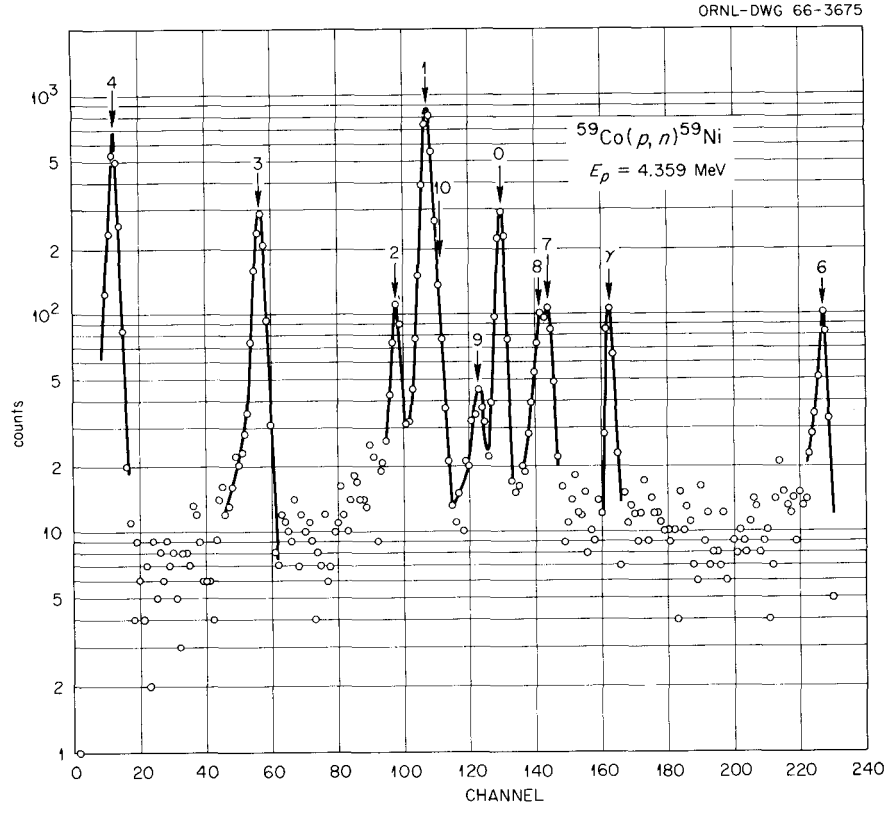

Fig. 1.11.1. Time-of-Flight Spectrum of Neutrons from the Reaction $^{59}Co(p,n)^{59}Ni$ for E_p = 4.359 MeV. The numbers above the peaks correspond to excited states in ^{59}Ni.

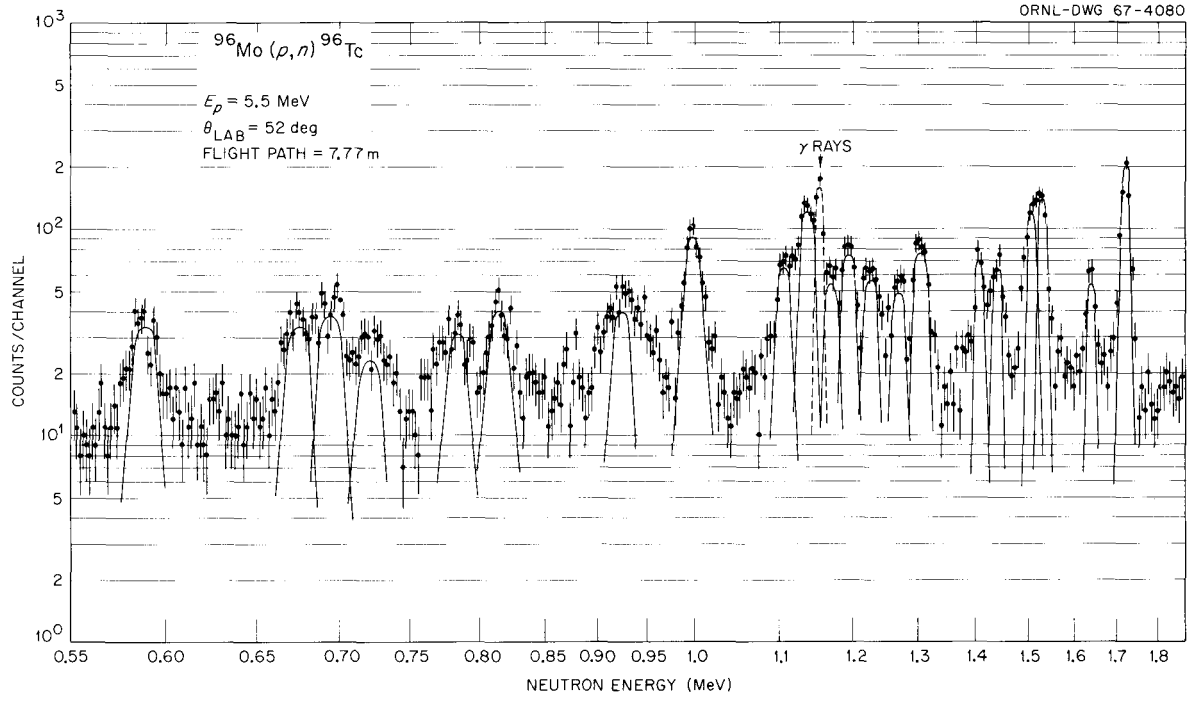

Fig. 1.11.2. Time-of-Flight Spectrum of Neutrons from the Reaction ^{96}Mo(p,n)^{96}Tc for E_p = 5.5 MeV.

excited states in ^{59}Ni correspond to groups numbered 1 to 4; neutrons with energy less than those leaving ^{59}Ni in its fourth excited state are "wrapped around" and neutron peaks reappear at the high-energy end of the spectrum. The resolving power of the system is indicated by analysis of peaks numbered 7 and 8. These peaks represent two neutron groups with an energy difference of ~8 keV.

Figure 1.11.2 indicates results for the ^{96}Mo(p,n) ^{96}Tc reaction for which the ^{96}Mo target was ~20 keV thick to the bombarding protons. The broadening in the lower energy neutron groups is due to the target thickness. Analysis to obtain the level structure of ^{96}Tc is complicated by the fact that the beta decay[5] of ^{96}Tc suggests that the ground state of this nucleus has $J^{\pi} = 7^+$. A (p,n) reaction populating a state with a spin this large will have a very small cross section at our bombarding energy, and it is very doubtful that the large peak seen at $E_n \sim 17.2$ MeV corresponds to the ^{96}Mo(p,n) ^{96}Tc ground-state transition. More likely this peak corresponds to excitation of an isomeric state in ^{96}Tc with a much lower spin. The other states in ^{96}Tc strongly excited by the (p,n) reaction should decay by prompt gamma emission to this isomeric state. Good agreement is obtained for gamma-ray energies from the ^{96}Mo(p,nγ) study reported in Sect. 1.14 and the neutron-energy differences determined from analysis of the data shown in Fig. 1.11.2. There are several neutron groups shown in this figure whose widths are greater than our energy resolution, for example, the group seen at 0.92 MeV. Careful study of our gamma-ray results may indicate the details of the level structure of ^{96}Tc in this region of excitation. The neutron spectrum and the gamma-ray spectra definitely complement each other in the study of this nucleus.

References

[1]Oak Ridge Graduate Fellow from University of Tennessee under appointment from the Oak Ridge Associated Universities, Inc.

[2]Instrumentation and Controls Division.

[3]Physics Division.

[4]P. H. Stelson *et al.*, *Bull. Am. Phys. Soc.*, Ser. II, **2**, 365 (1966).

[5]S. Monaro, G. B. Vingianai, and R. Van Lieshout, *Physica* **28**, 52 (1962); R. Cesareo, H. Langhoff, and A. Flammersfeld, *Z. Physik* **197**, 426 (1966).

1.12 THE $^{91}Zr(d,p)^{92}Zr$ REACTION AT $E_d = 6.25$ MeV[1]

J. K. Dickens E. Eichler[2]

The reaction $^{91}Zr(d,p)^{92}Zr$ has been studied at $E_d = 6.25$ MeV. Energies for 31 levels in ^{92}Zr were determined, and angular momentum transfer values were obtained for 15 of these levels. The differential cross-section data were compared with distorted-wave calculations, some of which used nonlocal potentials.

References

[1]Abstract of paper to be published in *Nuclear Physics*.

[2]Chemistry Division.

1.13 THE $^{59}Co(p,n\gamma)^{59}Ni$ REACTION FOR $4.3 \leq E_p \leq 6$ MeV

J. K. Dickens E. Eichler[1]
P. H. Stelson[2]

Using the experimental method outlined in Sect. 1.14, we have obtained spectra of gamma rays following proton bombardment of ^{59}Co. Proton bombarding energies were 4.3, 5.0, 5.3, and 6.0 MeV. A spectrum obtained at $E_p = 4.3$ MeV is shown in Fig. 1.13.1. Gamma-ray energies and relative yields have been extracted from the data. We are attempting to relate these data with the ^{59}Ni level structure deduced from the $^{59}Co(p,n)^{59}Ni$ results of Sect. 1.11 and high-precision $^{58}Ni(d,p)^{59}Ni$ data.[3] Gamma rays with energies of 339.5, 465.3, 878.1, 1188.8, 1338.7, 1680.2, 1735.0, 1745.7, 1777.9, 1948.3, 2629, 2682, and 2698 keV are apparently associated with excited-to-ground-state transitions in ^{59}Ni. Remaining gamma-ray assignments are very tentative.

References

[1]Chemistry Division.

[2]Physics Division.

[3]E. R. Cosman *et al.*, *Phys. Rev.* **142**, 673 (1966).

1.14 STUDY OF GAMMA RADIATION IN THE $^{92,94,96}Mo(p,n\gamma)^{92,94,96}Tc$ REACTIONS

J. K. Dickens I. R. Williams[1]
E. Eichler[1] R. Kuebbing[2]

We have started a program to measure gamma-ray energies and yields following (p,n) reactions. The gamma-ray detectors are lithium-drifted germanium counters, capable of 2- to 3-keV energy resolution.

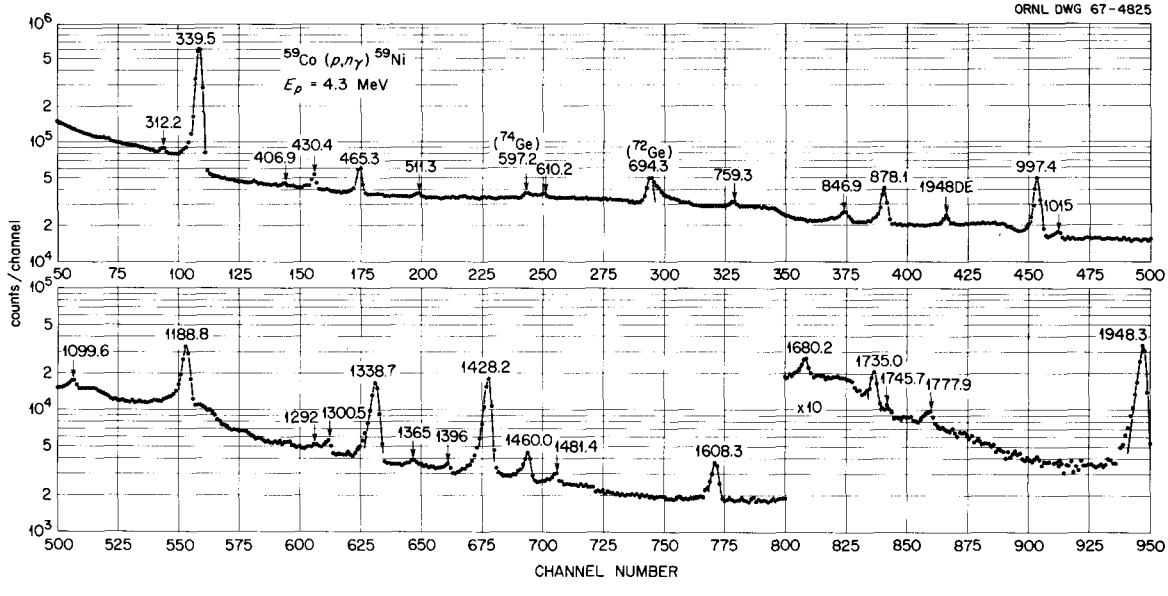

Fig. 1.13.1. Gamma-Ray Spectrum from $^{59}Co(p,n\gamma)^{59}Ni$ Reaction at $E_p = 4.3$ MeV. Gamma-ray energies shown above peaks are in keV.

To ensure that the gamma rays are associated with the (p,n) reactions, a time coincidence with the outgoing neutron is required. The neutron detector is the same one used in the (n,n'), (p,n), and (d,n) experiments discussed in Sects. 1.5, 1.11, and 1.10.

The physical quantities for each gamma transition of interest include the energy threshold for the transition, the gamma-ray energy, and the excitation function of the transition (i.e., gamma-ray yield as a function of bombarding energy). From the first two quantities one can obtain the level structure of the residual nucleus and from the third quantity, information as to the spin and parity of the levels.

Most of the data are accumulated without the neutron-coincidence requirement so that a spectrum may be obtained in a reasonable period of time and so that known sources may be used for energy calibration of the pulse-height analyzer and amplifier system. The neutron-gamma coincidence spectra "certify" the (p,n) gamma rays. In this case both the gamma-ray detector and the neutron detector are as close to the target as the mechanical system of beam tubing and target chamber will allow.

A block diagram for the electronic circuitry for the coincidence mode is shown in Fig. 1.14.1. Both neutrons and gamma rays are detected by the neutron detector. Pulses from this detector corresponding to neutrons are discriminated from those due to gamma rays in the γ-n discrimination circuitry, and a single-channel analyzer is set to gate on the pulses corresponding to neutrons. Tunnel-diode fast pickoff signals are obtained from both detectors. These provide start and stop pulses in a time–to–pulse-height converter, and another single-channel analyzer is set to gate on the "prompt" peak corresponding to a pulse in the gamma detector in time coincidence with a pulse from the neutron detector. Coincidence between this prompt peak pulse and the neutron pulse from the γ-n discriminator enables the gate, permitting a gamma-ray pulse to be registered in the pulse-height analyzer.

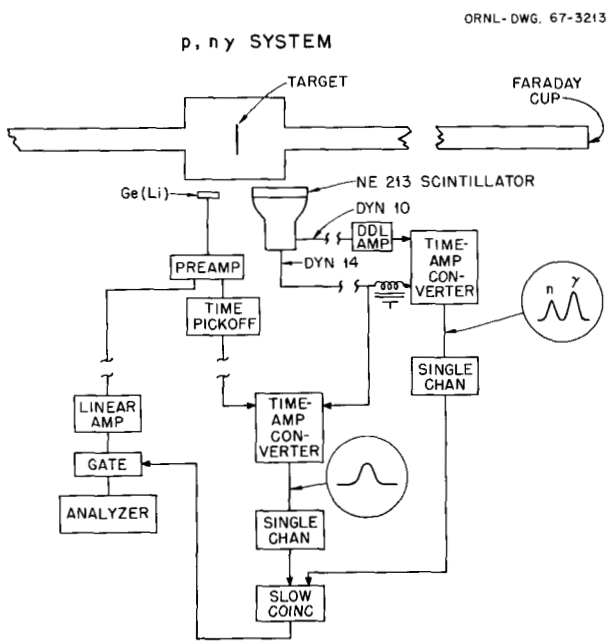

Fig. 1.14.1. Electronics Block Diagram for $(p,n\gamma)$ Experiment.

A comparison of spectra obtained with and without coincidence requirement is shown in Fig. 1.14.2 for protons on ^{94}Mo. As was expected, the counting rate in the coincidence mode is severely reduced over that obtained in the noncoincidence mode. The coincidence spectrum required 20 hr compared with 1 hr for the singles spectrum. However, the background from the (p,p') gamma radiation has been reduced by coincidence by a factor of $\sim$6. In this case the coincidence spectrum not only indicated which gamma rays seen in the singles spectrum were associated with the (p,n) reaction but also reduced the background so that a gamma ray of 520 keV became evident.

Our first experiments with this system have been the study of ^{92}Mo$(p,n\gamma)^{92}$Tc, ^{94}Mo$(p,n\gamma)^{94}$Tc, and ^{96}Mo$(p,n\gamma)^{96}$Tc. For the ^{92}Tc experiment two prominent gamma rays are seen, with energies of 209 and 259 keV. Their thresholds suggest that they are due to prompt decay of excited states in ^{92}Tc with excitation energies of 209 and 468 keV.

From the ^{94}Mo$(p,n\gamma)^{94}$Tc reaction we observed gamma rays with energies (thresholds) of 142 (5600), 145 (5270), 234 (5530), 237 (5360), 367 (5480), 379 (5520), 520 (undetermined), 728 (5860), and 750 (5860) keV. Errors of 1 and 25 keV were assigned to the gamma-ray energies and the center-of-mass thresholds respectively. In addition, the threshold for producing the 52-*min* isomer in ^{94}Tc is 5130 $\pm$ 25 keV. Assuming 107-keV excitation energy for this isomer[3] we propose a tentative level structure for ^{94}Tc including levels with excitation energies (relative to the 5-hr ground state) of 107, 252, 344, 474, 486, 619, (627), 835, 857, and 998 keV.

From the ^{96}Mo$(p,n\gamma)^{96}$Tc reaction we observed gamma rays with energies of 84, 102, (193), 204, 225, 232, 265, 285, (293), 345, (383), (393), 410, 423, 257, (480), 495 (doublet?), 523, 588, and (610) keV, with the small and uncertain assignments in

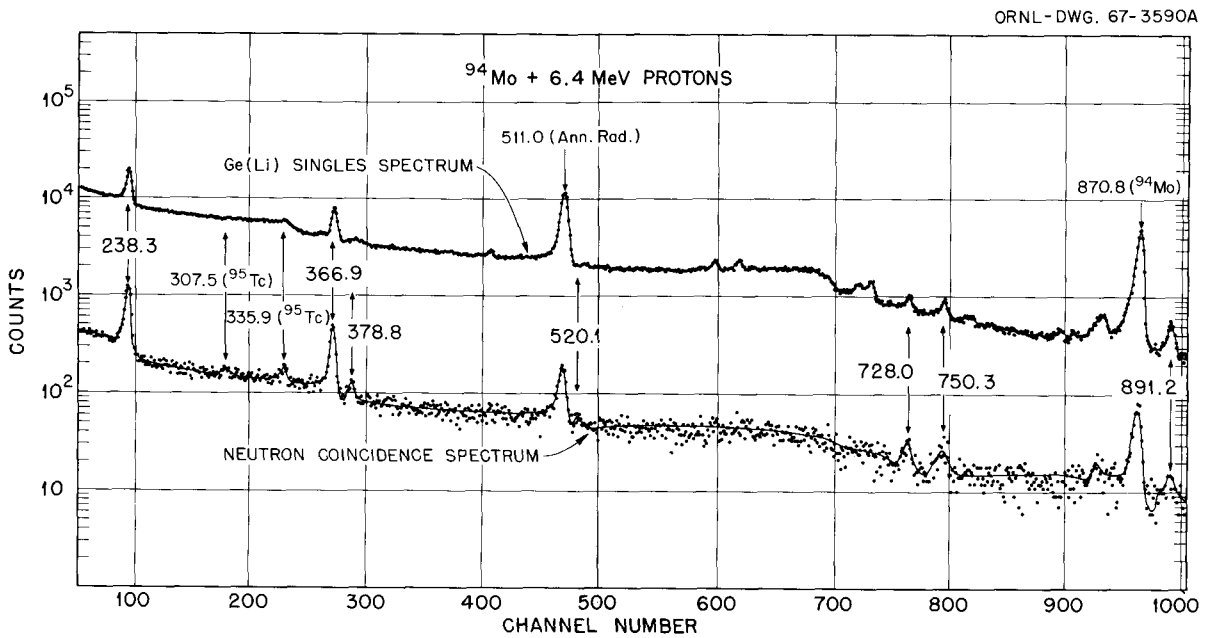

Fig. 1.14.2. Gamma-Ray Spectrum from 6.4-MeV Protons on ^{94}Mo.

parentheses. Several of these gamma rays have energies in very good agreement with neutron-energy differences reported in Sect. 1.11. These are (gamma-ray energy, neutron-energy difference) the pairs (84, 86), (232, 231), (285, 284), (423, 420), and (588, 588). We have not yet obtained energies for gamma transitions >610 keV, but intend to do so.

References

[1]Chemistry Division.
[2]Graduate Student, Physics Department, Western Reserve University.
[3]J. H. Hamilton *et al.*, *Physica* **30**, 1802 (1964).

1.15 THE OPTICAL-MODEL POTENTIAL FOR DEUTERONS[1]

F. G. Perey G. R. Satchler[2]

The elastic scattering of deuterons from nuclei is compared with the predictions of an optical-model potential whose real part is obtained by averaging a neutron and proton optical potential over the internal motion of the deuteron. Good agreement is obtained if the depth of the potential is changed by 10 to 20%. The optimum imaginary potentials extend to much larger radii than are predicted by this model. The significance of the results is discussed in some detail.

References

[1]Abstract of paper submitted to *Nuclear Physics* (in press).
[2]Physics Division.

1.16 ANOMALOUS ISOTOPE SHIFT OF THE NUCLEAR CHARGE RADIUS[1]

F. G. Perey J. P. Schiffer[2]

It is shown that the isospin dependence of the shell-model potential gives rise to the experimentally observed anomalous isotopic shift of nuclear charge radii. The charge radii calculated from a Wood-Saxon potential are in qualitative agreement with experimental determinations from electron scattering and from muonic x rays.

References

[1]Abstract of *Phys. Rev. Letters* **17**(6), 324 (1966).
[2]Argonne National Laboratory.

1.17 NEUTRON ANGULAR DISTRIBUTIONS FOR ^{9}Be(α,n) REACTIONS FOR BOMBARDING ENERGIES OF 6 TO 10 MeV[1]

V. V. Verbinski, W. E. Kinney, F. G. Perey, J. K. Dickens

Neutron cross sections were measured as a function of neutron energy and angle at several values of E_α. The n_0, n_1, and n_2 neutron groups from the ^{9}Be(α,n)^{12}C reaction were well resolved. Angular distributions of these groups varied appreciably for E_α = 6-10 MeV, but in the 8- to 10-MeV region they appeared to be much the same as those measured elsewhere at 10 to 14 MeV. This slow energy variation signifies the dominance of direct reactions at 8 to 14 MeV, with probable interference from compound nucleus effects below this. A strong low-energy component of neutrons that is present at forward angles can most easily be accounted for by lower Q-value, three- or four-body breakup reactions such as ^{9}Be(α,^{8}Be)^{5}He $\rightarrow$ ^{4}He + n ($t \cong 10^{-21}$ sec), ^{9}Be(α,α')^{9}Be* $\rightarrow$ ^{8}Be + n, or ^{9}Be(α,n)3α.

Reference

[1]Work partially funded by the National Aeronautics and Space Administration under NASA order R-104(1).

1.18 EVALUATION OF NEUTRON CROSS SECTIONS FOR ^{10}B[1]

D. C. Irving

The neutron cross sections for ^{10}B have been evaluated from 0.0253 eV to 15 MeV. The existing experimental data are reviewed, and theoretical calculations and other reasoning are used to fill in the gaps. A complete and consistent set of cross sections is presented and an explanation is given for the choices made in developing this cross-section set.

Reference

[1]Abstract of ORNL-TM-1872 (in preparation).

1.19 MEASUREMENTS OF THE NEUTRON SPECTRA OF Po-Be, Pu-Be, AND Am-Be NEUTRON SOURCES WITH AN NE-213 SCINTILLATOR[1,2]

R. M. Freestone, Jr., F. J. Muckenthaler, E. A. Straker, K. M. Henry

A close examination of previously published measurements of the neutron spectrum of (α,n) sources shows large disagreements between individual investigators, even when apparently similar techniques and methods were used. For instance, the Po-Be spectrum reported by Whitmore and Baker,[3] a nuclear emulsion measurement which was perhaps the first of the more precise determinations, differs significantly from the later nuclear emulsion data of Notarrigo *et al.*[4]

The work reported here is essentially a spinoff from the measurements of neutron spectra recently reported by Clifford *et al.*[5] Data for the cited work were obtained using a large organic scintillator (NE-213), pulse-shape discrimination to distinguish between neutron and gamma events, and analysis of the observed pulse-height distributions by the matrix inversion techniques of the FERDoR code of Burrus.[6] In order to maintain a relatively constant check upon the consistency and "good behavior" of all components, careful measurements of the spectra of Po-Be, Pu-Be, and Am-Be sources were made regularly. The results for all three sources are shown in Fig. 1.19.1, each curve normalized to unit area. The curve for a particular source is the mean of all of the runs for that source which displayed good statistics in the raw counts. (In the final report on this work we plan to compare our data with previously published observations and with calculations.)

It is clear from Fig. 1.19.1 that the spectra from the three sources are not significantly different in shape. This is as it should be, since the energies of the three alpha emitters (Po: 5.3 MeV; Pu: 5.15 MeV; Am: 5.48 MeV) are very nearly the same. Somewhat sharper peak resolution appears evident for the Pu-Be source, but this effect may be due to a difference in its construction. Differences of this nature have not yet been investigated.

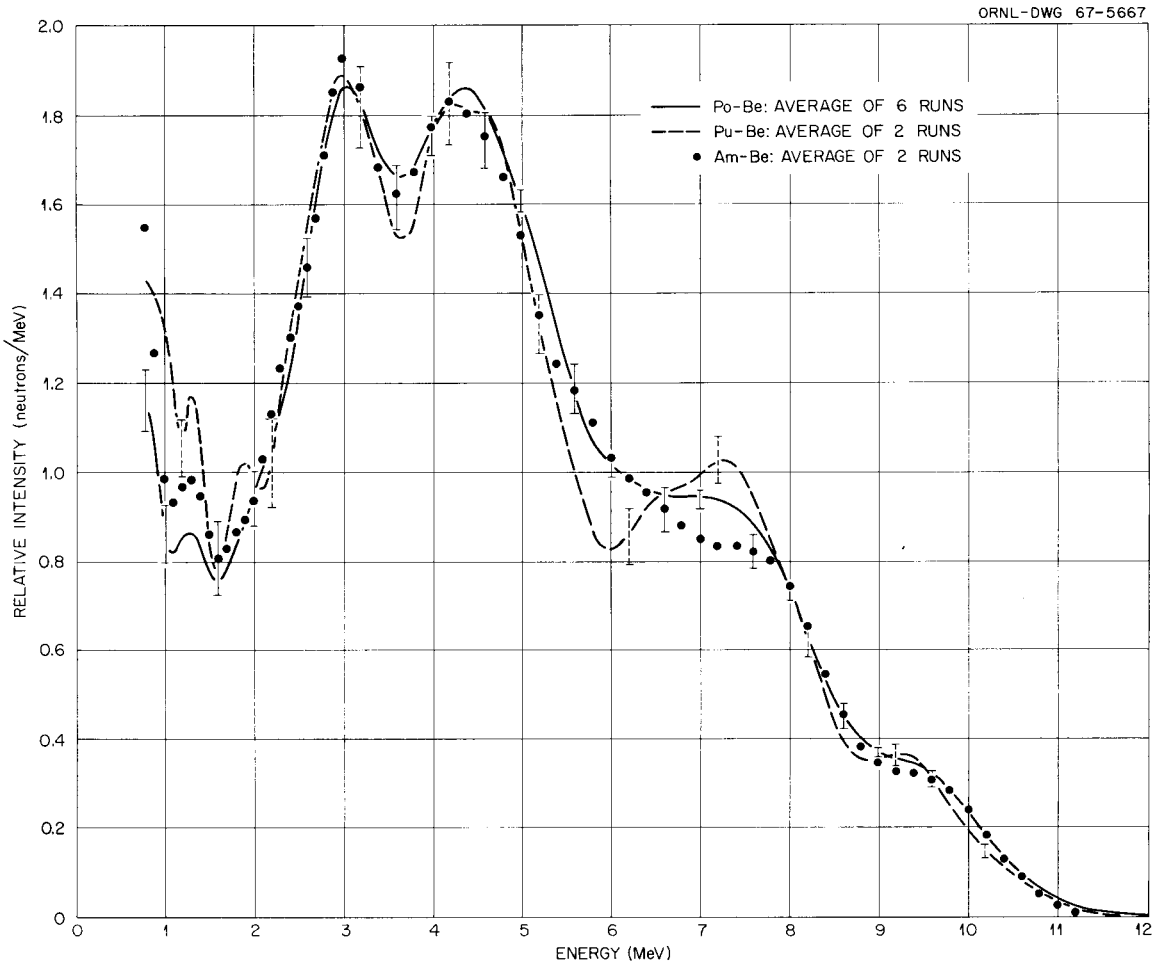

Fig. 1.19.1. Neutron Spectra from Po-Be, Pu-Be, and Am-Be Sources.

The spectra we observed are in essentially general agreement with the older (1950) Po-Be spectrum of Whitmore and Baker. In particular, we see the strong double peaking at 3 and 4.5 MeV, a feature which is notably absent in some of the later work.

An interesting and possibly debatable feature of the curves shown is the apparent tendency of all three curves to go toward a peak somewhere between 0 and 1 MeV. At the present time we are not sufficiently confident of the accuracy of our response matrix in the region below 1.5 MeV to unequivocally defend this portion of the curves, particularly when the data contain large contributions from high-energy neutrons. (The matrix responses are currently being remeasured.[7]) However, a similar shape was observed by Anderson and Bond[8] with a Pu-Be source and emulsion techniques, which they ascribe to secondary reactions (e.g., $n,2n$) occurring within the source.

As we noted earlier, surprising disagreement can be found between various measurements of the spectra of common α,n sources. Our confidence in the validity of the present work is substantially reinforced by the success achieved by the methods and equipment in the spectral measurements previously referred to,[5] in which the results were amenable to checks by analytic calculations.

References

[1]Work partially funded by Defense Atomic Support Agency under DASA orders EO-802-65 and EO-800-64.

[2]The authors wish to acknowledge the assistance of V. V. Verbinski who was principally responsible for the development of the spectrometer and its associated electronics.

[3]B. G. Whitmore and W. B. Baker, *Phys. Rev.* **78**, 799 (1950).

[4]S. Notarrigo *et al.*, *Nucl. Phys.* **29**, 507 (1962).

[5]C. E. Clifford *et al.*, *Nucl. Sci. Eng.* **27**, 299 (1967).

[6]W. R. Burrus *et al.*, "Fast-Neutron Spectroscopy with Thick Organic Scintillators, Part I"; V. V. Verbinski *et al.*, "Neutron Response of the NE-213 Scintillator from 0.2 to 22 MeV, Part II," to be submitted for journal publication.

[7]V. V. Verbinski, private communication.

[8]M. E. Anderson and W. H. Bond, Jr., *Nucl. Phys.* **43**, 330 (1963).

1.20 OAK RIDGE ELECTRON LINEAR ACCELERATOR (ORELA)

F. C. Maienschein

During the past year, Varian Associates, Palo Alto, California, has proceeded with the manufacture of the electron linear accelerator to be used at ORNL as a source of short intense pulses of neutrons. The overall design and fabrication of the accelerator was 52% complete as of May 26, 1967. In December 1966, Blount Brothers Corporation, Montgomery, Alabama, started construction of the building to house the accelerator. As of May 26, 1967, the building construction was 25% complete. The progress achieved in the construction of both the accelerator and the building is consistent with the previously established schedule which calls for delivery of accelerator parts to the site starting in October 1967, and completion of the building and initial operation of the accelerator by March 1968. Completion of acceptance tests and full use of the facility for research are planned for September 1968.

The pulsed-neutron source provided by ORELA will be used primarily for making neutron cross-section measurements by the time-of-flight technique. Particular emphasis in these measurements will be placed upon those energy regions and materials of most interest for the United States breeder reactor programs. A five-year plan outlining the experiments to be performed was transmitted to the Division of Reactor Development and Technology, U.S. Atomic Energy Commission.

The intensity of the neutron source available at ORELA will permit the acquisition of data at a very rapid rate; however, in the performance of multiparameter experiments the demands placed upon the data-acquisition system exceed the capabilities of standard systems. Therefore, a study was made of a computer-based data-handling system for ORELA. This system is divided into two phases, the first primarily concerned with data acquisition and the second with the prompt analysis of the results of the experiments. In the planned data-storage devices, up to 4×10^5 channels can be addressed at data rates up to 4×10^3 events/sec. Experience at other facilities has indicated the futility of obtaining masses of experimental data which cannot be analyzed without unreasonable delays. The ORELA system is designed to provide direct access to time-shared computing facilities from remote consoles with display and light-pen capabilities located at the experiments. For calculations requiring maximum computing capacity, block transfer of data by wire to the ORNL central processor will be provided ultimately. Bids have been received and equipment ordered for Phase I of the system.

On March 7, 1967, safety aspects of ORELA were reviewed by the AEC Advisory Panel on Accelerator Safety. Members of this panel are: Dr. Fred Cowan, Brookhaven National Laboratory; Dr. Roger Wallace, LRL-Berkeley; Mr. Keran O'Brien, HASL (NY); Dr. Miguel Awschalom, Princeton-Penn Accelerator; and Mr. Robert Wheeler, Argonne National Laboratory.

ORELA will be operated jointly by the Neutron Physics and Physics Divisions. ORNL participants in the design of ORELA include W. R. Burrus, G. de Saussure, R. Gwin, F. C. Maienschein,[1] E. G. Silver, V. V. Verbinski, and L. W. Weston from the Neutron Physics Division; E. C. Campbell, J. W. T. Dabbs, J. A. Harvey,[1] R. L. Macklin, and G. G. Slaughter from the Physics Division; A. L. Boch[2] from the Director's Division; J. A. Murray from the General Engineering and Construction Division; R. King, T. A. Lewis, J. R. Reynolds, and H. A. Todd from the Instrumentation and Controls Division; and N. A. Betz from the Mathematics Division.

References

[1]Program Codirector.

[2]Construction Project Director.

2. Critical Experiments

2.1 HOMOGENEOUS CRITICAL ASSEMBLIES OF LOW-ENRICHMENT UF_4 IN PARAFFIN

S. J. Raffety

The program of critical experiments with homogeneous hydrogen-moderated assemblies of low-enrichment UF_4 in paraffin reported previously[1-3] has been extended to include a mixture of 2% ^{235}U-enriched UF_4 and paraffin with a H:^{235}U atomic ratio of 614 and a mixture of 3% ^{235}U-enriched UF_4 and paraffin with a H:^{235}U atomic ratio of 277. The U(2) material with H:^{235}U = 614 contained 78.8 wt % UF_4 and had a density of 2.88 g/cm^3. The U(3) material with H:^{235}U = 277 contained 84.6 wt % UF_4 and had a density of 3.44 g/cm^3. However, it was found that due to the 1-mil aluminum foil used to cover the blocks and to small irregularities in the blocks the average density of the UF_4-paraffin mixture in the assemblies constructed was 98% of the values above.

Several critical parallelepipeds have been constructed from each of these materials, and the extrapolation distance for each material was determined from flux measurements through the center of the critical assemblies. The values of the extrapolation distances for the U(2) and U(3) materials are respectively 2.21 ± 0.11 and 2.32 ± 0.06 cm. From these extrapolation distances and the dimensions of the critical assemblies (corrected for reflection from support structure), the material bucklings were found to be (6.207 ± 0.037) × 10^{-3} cm^{-2} for the U(2) material and (10.204 ± 0.054) × 10^{-3} cm^{-2} for the U(3) material. The minimum critical volumes and masses for unreflected parallelepipeds, cylinders, and spheres were determined from these data and are shown in Figs. 2.1.1 and 2.1.2, along with the results of previous experiments.[1,2] The reflector savings for assemblies completely reflected by an effectively infinite thickness of polyethylene on the sides and top and of methacrylate plastic on the bottom were found to be 3.81 ± 0.06 and 4.44 ± 0.08 cm for the

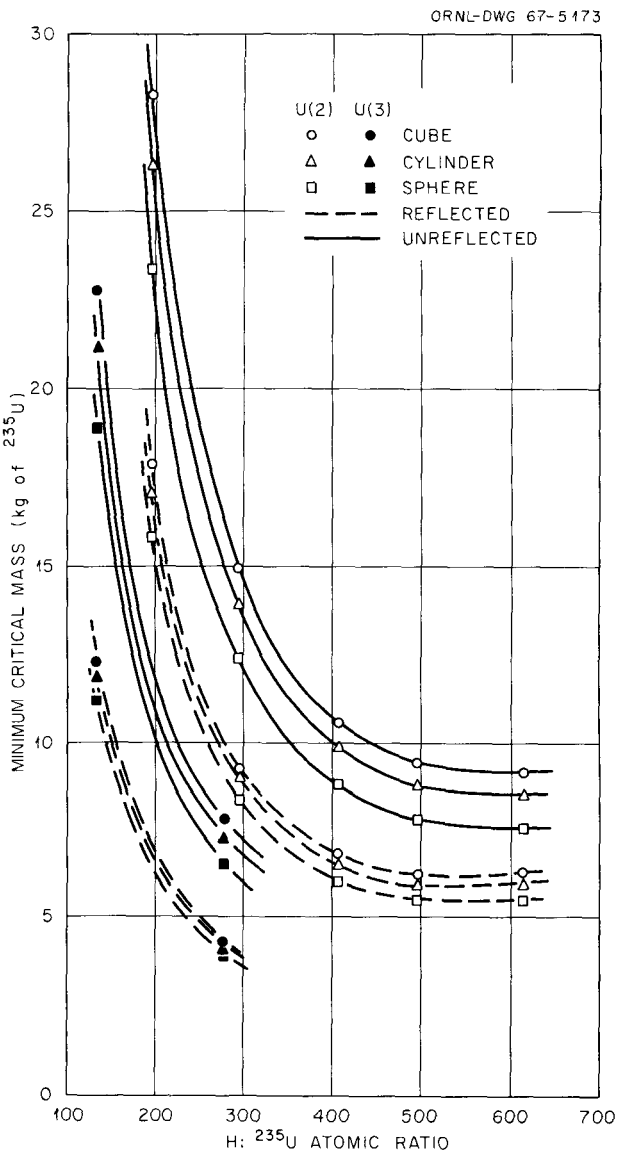

Fig. 2.1.1. Critical Mass of 2% and 3% ^{235}U-Enriched UF_4 and Paraffin Mixtures as a Function of the H:^{235}U Atomic Ratio. The values were derived from experimental data by buckling conversions.

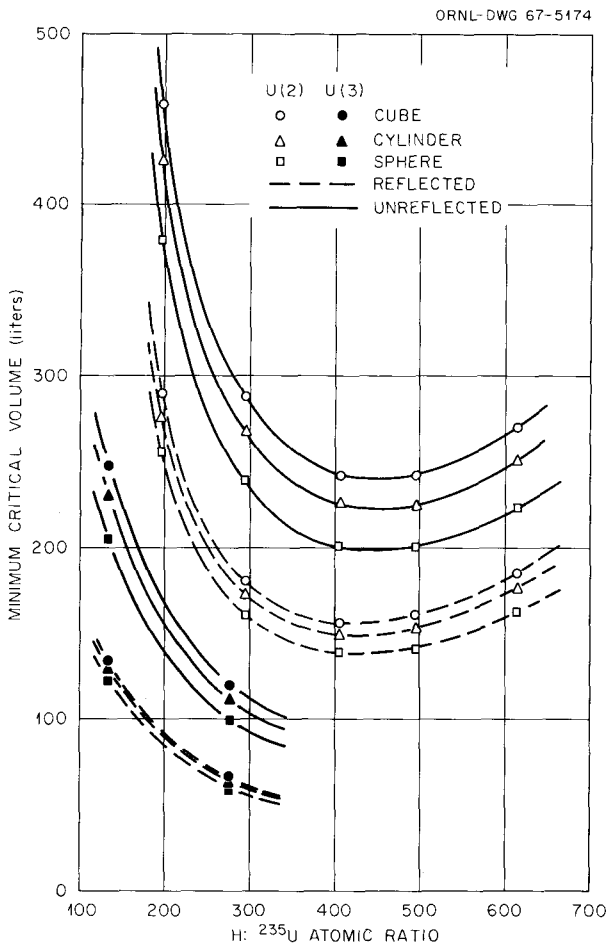

Fig. 2.1.2. Critical Volume of 2 and 3% ^{235}U-Enriched UF_4 and Paraffin Mixtures as a Function of the H:^{235}U Atomic Ratio. The values were derived from experimental data by buckling conversions.

U(2) and U(3) materials respectively. Minimum critical volumes and masses for reflected geometries are also shown in Figs. 2.1.1 and 2.1.2.

The prompt-neutron decay constants, α, in unreflected and reflected delayed-critical parallelepipeds of these two materials were determined by the pulsed-neutron technique. In the unreflected assemblies α was 139 $\pm$ 2 sec^{-1} and 242 $\pm$ 2 sec^{-1} for the U(2) and the U(3) mixtures respectively, and in the reflected assemblies α was 137 $\pm$ 2 sec^{-1} and 208 $\pm$ 2 sec^{-1} respectively.

References

[1]J. T. Mihalczo and J. J. Lynn, *Neutron Phys. Div. Ann. Progr. Rept. Sept. 1, 1960,* ORNL-3016, p. 71.

[2]J. T. Mihalczo and J. J. Lynn, *Neutron Phys. Div. Ann. Progr. Rept. Sept. 1, 1961,* ORNL-3193, p. 131.

[3]J. T. Mihalczo, *Neutron Physics Div. Ann. Progr. Rept. Sept. 1, 1962,* ORNL-3360, p. 37.

2.2 O5R MONTE CARLO CRITICALITY CALCULATIONS FOR A THERMAL REACTOR WITH 2% ENRICHED URANIUM

J. Wallace Webster

Probably the most important activity in the field of reactor computations today is the attempt to determine point-set representations of cross sections, for those nuclides commonly used in reactors, which give agreement with experiment. The most direct way to check these cross-section sets in an integral manner is to use them in Monte Carlo calculations of clean critical experiments. Once satisfactory point-set representations have been established, it will be easy to compute accurate group cross sections for use in multigroup transport and diffusion theory codes for practical reactor computations in which the machine computing times must be kept reasonable.

The critical experiment chosen for the present study was a U(2%)F_4-paraffin ($C_{25}H_{52}$) system[1-3] with abundant ^{238}U capture, which was simple in geometry – an unreflected parallelepiped, essentially homogeneous – for which both critical and k_∞ measurements had been made, the latter at the Hanford PCTR facility, as well as various foil measurements of spectral indices. Also, measurements[4] had been made, at General Atomic, of the energy spectrum of the thermal neutrons which permitted an accurate, yet simple, one-group treatment[5] of the thermal neutrons.

The O5R Monte Carlo code[6] was chosen for the analysis because, of all the Monte Carlo codes in existence, it seems to provide the greatest opportunity to represent with the greatest rigor the physical processes incurred by neutrons. O5R is well documented, is composed of a set of subroutines which can be modified at the will of the user, and produces as its output a series of collision history tapes for which the user can write analysis routines to examine any particular aspect of neutron behavior in which he is interested.

Many preliminary computations were made and analysis routines written and employed to ensure that the code was working properly and being used properly,

this being the first application of O5R to critical assemblies of this type. It was found, for example, that in the input to O5R the quantities WTLOW ("neutrons having weights below this value will be subjected to Russian roulette") and WTAVE ("if a neutron is not killed by Russian roulette it will be assigned a new weight equal to WTAVE") must be given quite small values. The first trial values – WTLOW = 0.2 and WTAVE = 0.4 – gave errors in k_{eff} of up to 3% even for 6000 neutron histories. These were then decreased to WTLOW = 0.02 and WTAVE = 0.04, and this error became negligible.

Other tests and numerical studies performed by analyzing the collision history tapes were concerned with (1) the spatial and energy distribution of fission neutrons to see whether subroutine SOURCE[7] was working properly, (2) the average cosine of the scattering angle for each nuclide in the various energy ranges of the Hansen-Roach scheme to see whether subroutine SCATR[6] and the Coveyou technique[6] for selecting neutron scattering angles from anistropic and isotropic distributions were giving reasonable results, (3) the average energy loss for collisions of neutrons with each type of nuclide, and (4) the neutron "balance" to ensure that neutrons absorbed plus neutrons leaked equaled neutrons originating from fission (except for a small difference due to the statistical nature of the game of Russian roulette).

Concerning the systems data tape which puts data on nonabsorption probabilities, fission probabilities, etc., into O5R and is prepared in advance, experiments were conducted to ensure that the number of subgroups per supergroup was adequate. It was found that no significant change in k_{eff} resulted in increasing this from 256 to 512, so the discretization error here was eliminated. Also, a printout of the information on the systems data tape was obtained and the values for a few subgroups were checked by hand computations.

With respect to the microscopic cross-section data the major effort was concentrated on ^{238}U and fluorine. For ^{238}U, point-set representations (over 900 points for each cross-section type) were obtained[8] for Doppler-broadened cross sections corresponding to 300°K and for no Doppler broadening (0°K). The 0°K case gave a k_{eff} about 5% higher than the 300°K case. In addition to the fundamental value of knowing how large the Doppler coefficient is for systems of this type, the cross-section data at 0°K, which are easy to calculate, provide a check on the data at 300°K, which are relatively difficult to calculate in that the resonance integrals over lethargy are temperature independent.

Forming the point-set representations of the fluorine cross sections required some effort because they were not previously in the O5R library. It developed that considerable care must be exercised in representing the resonances of fluorine, even though they are mostly scattering resonances. O5R determines absorption (weight loss) from the quantity Σ_s/Σ_t (the nonabsorption probability), where Σ_s and Σ_t are the macroscopic cross sections for the mixture. The logarithms of the total and scattering cross sections for fluorine were taken to vary linearly with the logarithm of energy between points. With this interpolation scheme the difference, $\sigma_a = \sigma_t - \sigma_s$, can be nonmonotonic and suprisingly large between two points even though it is small at both points. This condition occurs if the changes in σ_t and σ_s are large in going from one point to the other, as in a resonance.

Also, with respect to fluorine, Morrison's subroutine INELAS was modified to add its substantial inelastic scattering[9] to that of the uranium isotopes. However, the effect on k_{eff} was negligible.

For ^{235}U cross sections the British compilation of Freemantle[10] was used at first and then later the data of de Saussure[11] were substituted. The latter data increased k_{eff} by about 2%.

The possible effect of heterogeneity of the UF_4 particles, which were about 150 μ in diameter, on the average, in the experiment, was estimated using the method of Bartels[12] to be less than 0.5% in k_{eff}. An even smaller effect is estimated from the results of a substitution experiment.

The final computed value of k_{eff} was 0.98 ± 0.01 for 6000 neutron histories. Starting with a different initial random number (RANDM) did not affect this result appreciably. This somewhat low computed value of k_{eff} for this assembly is in qualitative agreement with the conclusions of Stratton[13] concerning the comparison of theory with experiment for low-enriched uranium systems in general. He attributes the discrepancy to errors in the cross sections of ^{238}U. They could be due to (1) inaccuracies in the measurements of the resolved resonance parameters, (2) lack of good knowledge of the cross section in the higher energy statistical region, or (3) the model[14] used to determine the Doppler broadening of the resonances.

The computed value of k_∞ was 1.15 as compared with about 1.20 as measured[2] in the Hanford PCTR, or about 4% discrepancy.

The calculated ratio of fission neutrons produced by ^{235}U plus ^{238}U to neutrons produced by ^{235}U alone is 1.068, in good agreement with 1.066 from the foil measurements.

In general, however, one must conclude that there is growing evidence that the basic microscopic cross-section data do not lead to satisfactory agreement with integral experiments for thermal systems of low enrichment.

References

[1]J. T. Mihalczo *et al.*, *Preliminary Report on 2% ^{235}U Enriched UF_4-$C_{25}H_{52}$ Critical Assemblies*, ORNL CF-59-4-120 (1959).

[2]J. T. Mihalczo *et al.*, *Nucl. Sci. Eng.* **13**, 6 (1962); see also J. T. Mihalczo *et al.*, *Comparison of k_∞ Measurements in a Critical Assembly with k_∞ Measurements in the Physical Constants Testing Reactor*, ORNL CF-60-4-24 (1960).

[3]J. T. Mihalczo and C. B. Mills, *Nucl. Sci. Eng.* **11**, 95 (1961).

[4]J. R. Beyster *et al.*, "Integral Neutron Thermalization," *Quarterly Progress Report for Period Ending December 31, 1963*, GA-4881 (1964).

[5]J. Wallace Webster, *Neutron Phys. Div. Ann. Progr. Rept. May 31, 1966*, p. 16, ORNL-3973, Vol I.

[6]D. C. Irving *et al.*, *O5R, A General Purpose Monte Carlo Neutron Transport Code*, ORNL-3622 (1965).

[7]J. T. Mihalczo, G. W. Morrison, and D. C. Irving, *SOURCE, A Neutron Distribution Routine for the O5R Monte Carlo Code*, ORNL-TM-1192 (1965).

[8]J. Wallace Webster, *Point-Set Representation of ^{238}U Cross Sections; Values and a FORTRAN Program for Computation*, ORNL-TM-1448 (1966).

[9]J. Wallace Webster, "Neutron Cross Sections for Fluorine," letter to D. C. Irving and C. W. Cravens, Jr., dated July 7, 1966.

[10]R. G. Freemantle, *The Reactions of Neutrons with ^{235}U – An Interim Revision of the File in the UK Nuclear Data Library*, AEEW-M502 (1965).

[11]G. de Saussure, personal communication (1967).

[12]W. J. C. Bartels, *Self Absorption of Monoenergetic Neutrons*, KAPL-336 (1950).

[13]William R. Stratton, p. 91 in *Proceedings of Nuclear Criticality Safety, December 13–15, 1966*, SC-DC-67-1305 (1967).

[14]L. Dresner, *Resonance Absorption in Nuclear Reactors*, Pergamon Press, New York, 1960.

2.3 CRITICAL LATTICES OF U(4.89) METAL RODS IN WATER[1,2]

E. B. Johnson

The critical dimensions of lattices of U(4.89) metal rods are reported. All the available rods are 30 cm long and have diameters of 1.31, 2.07, and 2.49 cm. Lattices of 30- and 60-cm height have been assembled in both square and triangular patterns.

The optimum lattice spacing for each rod diameter has been established by varying the separation and determining the number of rods required for criticality at each of several spacings. Figure 2.3.1 shows the data for critical lattices of rods of each diameter; critical mass is plotted as a function of the average ^{235}U density in the lattice.

Clark[3] has calculated masses of critical spherical water lattices of U(5.00) metal rods for a variety of diameters and uranium concentrations (or lattice spacings). The results for 1.52- and 1.02-cm-diam rods were interpolated to allow the comparison with the measurements with 1.31-cm rods, shown by curves A and B of Fig. 2.3.2. Curves B, C, and D were obtained from the data of Fig. 2.3.1 by equating bucklings using an extrapolation distance of 6.0 cm. No calculations of the larger diameter rods are available for comparison with curves C and D.

It has been reported[4] that a difference of as much as a factor of 2 was found between the critical masses of lattices of large cylindrical annuli of U(1.95) metal (18.3 cm OD and 6.6 cm ID) when

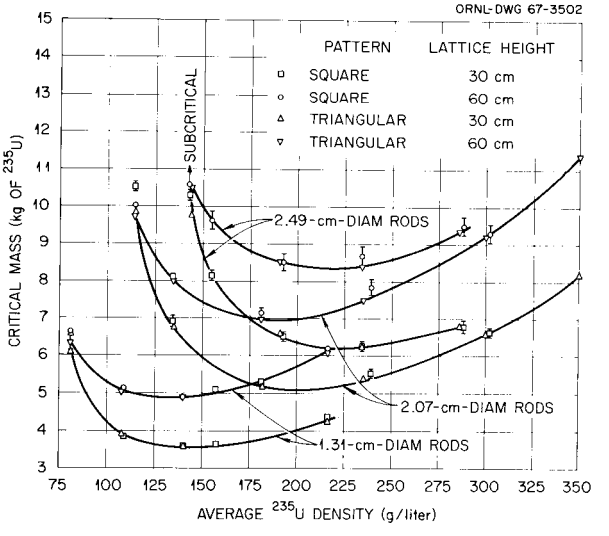

Fig. 2.3.1. Critical Mass of Lattices of U(4.89) Metal Rods in Water.

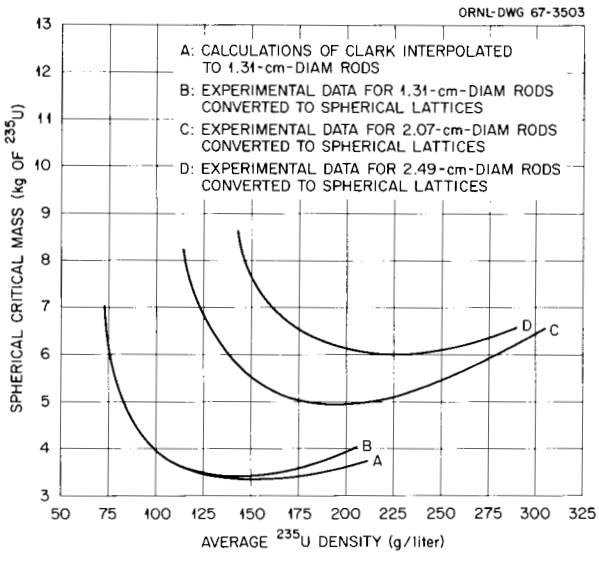

Fig. 2.3.2. Comparison of Calculated and Experimental Critical Spherical Lattices of Uranium Metal Rods in Water.

arranged in water in square and triangular patterns at the same average ^{235}U density, the triangular pattern having the lower mass. In the case of the U(4.89) rods no consistent difference was observed between lattices of the rods arranged in the two patterns.

References

[1]Summary of paper to be presented at Thirteenth Annual Meeting of the American Nuclear Society, San Diego, Calif., June 11–15, 1967; to be published in *Trans. Am. Nucl. Soc.*, vol. 10 (1967).

[2]U(4.89) represents uranium enriched to 4.89 wt % in the ^{235}U isotope.

[3]H. K. Clark, *Critical and Safe Masses and Dimensions of Lattices of U and UO_2 Rods in Water,* DP-1014 (February 1966).

[4]E. B. Johnson, *Trans. Am. Nucl. Soc.* 9, 185 (1966).

2.4 CRITICALITY OF AQUEOUS SOLUTIONS OF 5%-ENRICHED URANIUM[1]

J. Wallace Webster E. B. Johnson

As part of the continuing criticality-safety program at the Critical Experiments Facility, a comparison has been made of the analytical and experimental results describing the criticality of an aqueous U(4.98) O_2F_2 solution (H:^{235}U = 496). A single sphere, a single cylinder, and arrays of cylinders were studied; structural materials were minimized. Two analytical methods were used for the single units: (1) the Carlson S_n method using the DTF code with $n = 4$ and the Hansen-Roach 16-group cross sections, and (2) the Monte Carlo method using the O5R code with point-set representations of the cross sections. The arrays were calculated by only the O5R code.

The times required for the Monte Carlo calculations on the CDC 1604-A computer ranged between 125 and 204 min for 6000 neutron batches. This number of neutron histories resulted in an accuracy of about 1% in k_{eff}. The variance reduction techniques used consisted in (1) reducing the weight of neutrons according to the absorption probability for each collision rather than allowing their absorption, and (2) playing Russian roulette with neutrons whose weight became less than 20% of their weight at birth.

The description of the experiments and the results of the Monte Carlo calculations are presented in Table 2.4.1.

Values of k_{eff} of the two single units, i.e., the first and second entries in the table, obtained by S_4 transport calculations were 1.002 and 0.993 respectively. The analysis gave the spectrum of neutrons causing fission shown in Fig. 2.4.1. About 85% of the fissions were caused by thermal neutrons.

Reference

[1]Summary of paper presented at the 1966 Winter Meeting of the American Nuclear Society, Pittsburgh, Oct. 30–Nov. 3, 1966; published in *Trans. Am. Nucl. Soc.* 9, 514 (1966).

2.5 ENRICHED URANIUM METAL AND POLYETHYLENE CRITICAL EXPERIMENTS FOR H:^{235}U RATIOS FROM 0 TO 5

D. W. Magnuson

In a continuing program for providing critical parameters for nuclear criticality safety, critical experiments in rectangular geometry have been performed for H:^{235}U atomic ratios ranging from 0 to 5 using layers of enriched uranium metal (93.15

Table 2.4.1. Comparison of Critical Experiments with Monte Carlo Calculations

Description of Critical System					Computed k_{eff}	CDC 1604-A Running Time (6000 Neutrons) (min)
Containers			Center Separation (in.)	Solution* Height (in.)		
Geometry	Material	Inside Diameter (in.)				
Unreflected cylinder	0.031-in.-thick stainless steel	15.5		39.49	1.00 ± 0.010	147
Unreflected sphere	0.020-in.-thick stainless steel	19.99			0.99 ± 0.012	125
7 unreflected cylinders in triangular pattern	0.126-in.-thick aluminum lateral walls, 0.252-in.-thick bottom	9.49	10.48	24.02	1.00 ± 0.009	199
7 unreflected cylinders in triangular pattern			11.75	55.98	0.99 ± 0.009	204
9 unreflected cylinders in square pattern			10.26	24.02	0.98 ± 0.013	147
9 unreflected cylinders in square pattern			11.95	55.98	0.99 ± 0.010	158

*Aqueous $U(4.98)O_2F_2$ solution, H: ^{235}U atomic ratio = 496, density = 2.020 g/cm^3, concentration = 901.4 g of uranium per liter. For the sphere the density was 2.03 g/cm^3 and the uranium concentration was 910 g/liter at 18°C.

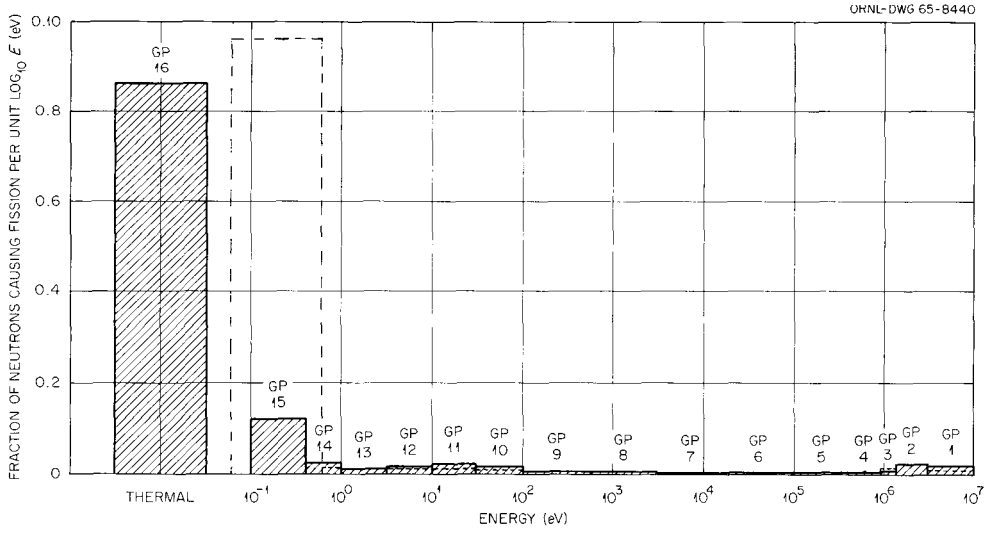

Fig. 2.4.1. Spectrum of Neutrons Causing Fission. Total number of neutrons causing fission = 1.00.

wt % ^{235}U) and polyethylene. Base dimensions of 10 × 10 in. (18 experiments) and 5 × 10 in. (8 experiments) were used because the enriched uranium metal was available in 5- × 5-in. and 5- × 10-in. slabs of varying thicknesses. The critical assemblies were constructed on the split table apparatus,[1] each half supported on a $\frac{1}{16}$- × 4- × $10\frac{3}{4}$- or $\frac{1}{16}$- × 4- × $5\frac{3}{4}$-in. aluminum plate. Each of the latter was supported, by four $\frac{3}{16}$-in.-diam stainless steel rods, approximately $27\frac{3}{4}$ in. above a 2- × 6-ft aluminum plate $\frac{1}{4}$ in. thick.

Metal assemblies were made critical by adding more metal; the moderated assemblies were made critical by adding moderator to a preselected layer arrangement of uranium metal. Using a constant extrapolation distance of 2.1 cm for all geometries, the experimental near-critical assemblies were converted to spherical geometry. The observed reactivities were corrected for the effects of the aluminum support plates. Corrections to the spherical critical masses were made for the reactivity differences from delayed critical and for the density variations of the assemblies to a standard density based on densities of 18.70 g/cm^3 for uranium metal and 0.92 g/cm^3 for polyethylene. Heterogeneity effects were found to be small from experiments having different layer thicknesses. These data are shown in Fig. 2.5.1 as a plot of spherical critical ^{235}U mass vs H:^{235}U atomic ratio. In the range of H:^{235}U from 0 to 0.6, the mass is approximately constant before the onset of a decrease with further increased moderation with polyethylene. The curves reported[2] for uranium-water mixtures show an increase in critical mass of approximately 10 to 15% before the onset of the decrease with increased moderation at H:$^{235}U \cong 1.5$. The unmoderated critical masses are approximately 1.5 kg higher than the value reported for Godiva,[3] and this may be due to differences in density or ^{235}U enrichment or to the buckling conversion.

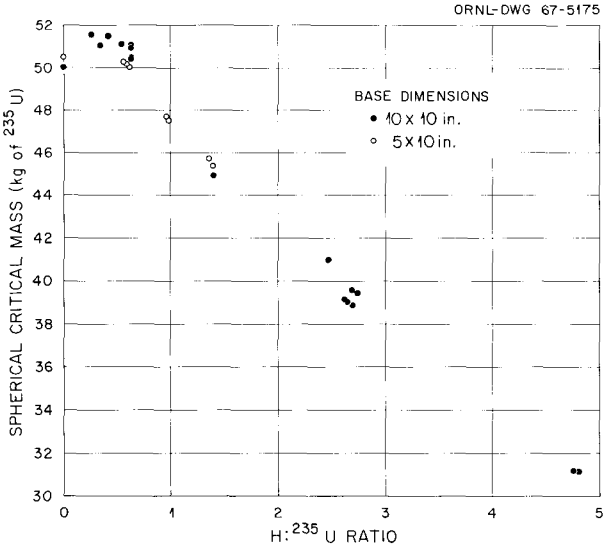

Fig. 2.5.1. Spherical Critical Mass vs H:^{235}U Ratio.

References

[1] *A Safety Analysis of the Oak Ridge Critical Experiments Facility*, ORNL-TM-349 Rev. 1 (1967).

[2] H. C. Paxton *et al.*, *Critical Dimensions of Systems Containing U^{235}, Pu^{239}, and U^{233}*, TID-7028, Fig. 8, p. 14 and Fig. 53, p. 66 (June 1964).

[3] H. C. Paxton, *Los Alamos Critical-Mass Data*, LAMS-3067 (May 1964).

2.6 CRITICALITY OF LARGE SYSTEMS OF SUBCRITICAL U(93) COMPONENTS[1]

J. T. Thomas

Methods for estimating the number of components required for criticality of unreflected and paraffin-reflected arrays of subcritical units are described. A neutron nonleakage fraction parameter is defined and leads to a correlation confirmed to within 5% of the number of units by comparison with experimental data for three-dimensional cuboidal arrays. A density analogue representation of the arrays is readily derivable and is shown to approximate the results from the above method, but is less precise. Factors by which the number of units in an unreflected critical array is reduced by adding a paraffin reflector are found to range from about 6 to greater than 30, depending on the material and on the average uranium density considered. The methods are supported by Monte Carlo calculations demonstrated to be reliable by comparison with the results of critical experiments.

Reference

[1] Abstract of ORNL-CDC-1 (in press).

2.7 CRITICALITY OF ARRAYS OF UNITS OF BASIC GEOMETRIES[1]

J. T. Thomas

Assuming the ability to compute critical arrays of cylindrical units of fissile material by the method

described in Section 2.6, it is of interest to establish the dimensions of other units of simple geometry which, when assembled in the same number and at the same average density, will also constitute a critical array.

The ratio of the surface area to the volume of cubes, spheres, and cylinders of equal height and diameter is

$$\frac{S}{V} = \frac{6}{d}, \qquad (1)$$

where d is the length of the edge of the cube and the diameter of the sphere and cylinder. The k_{eff} of individual units of these simple shapes as a function of d was computed by the KENO Monte Carlo code[2] utilizing the Hansen-Roach 16-group cross section set.[3] The results for the three shapes correlate by the empirical equation

$$k_{eff} = \left(\frac{1}{C}\frac{S}{V}\right)^{-0.924}, \qquad (2)$$

where C is 0.386, 0.345, or 0.406 cm^{-1} for cylinders, spheres, or cubes respectively. Equation 2 gives values of k_{eff} to within 1.5% of those from the KENO code over the range 0.37 $cm^{-1} < S/V < 1.00$ cm^{-1}.

Criticality of an array of identical units, each with a given k_{eff} and fraction of neutrons leaking from the unit, $f(\alpha)$, is controlled by adjusting the average uranium density (by spacing) and hence the fraction of neutrons leaking from the array. Since the value of $f(\alpha)$ of a unit having a given k_{eff} is independent of the unit shape, the size of units of other shapes necessary to maintain criticality in an array of the same number of units and the same array density can be determined. As an example, an array of 216 U(93) metal cylinders,[4] each having a mass of 20.9 kg, a diameter of 11.484 cm, a height-to-diameter ratio of 0.94, and a computed k_{eff} of 0.759, was chosen as a reference. Equation 2 then provided the size of each of the three other shapes having the same k_{eff} and $f(\alpha)$ as the array unit. The spacing in arrays of each of these three unit shapes was determined from the average uranium density in the 216-unit reference array (ρ = 1.18 g/cm^3). The k_{eff} of these three arrays from Monte Carlo calculations are compared in Table 2.7.1 with that of the reference array. The procedure was repeated for two other arrays of metal cylinders of different height-to-diameter ratios and the results are also presented in Table 2.7.1.

Except for the arrays of cubes the agreement is good. Cubes effect a better utilization of neutrons leaking from the units; hence their arrays have a greater k_{eff}.

Table 2.7.1. Computed k_{eff} of Arrays of Uranium Metal Units Having Simple Geometry

	Height / Diameter	Unit Dimension d (cm)	Unit Mass (kg)	k_{eff} of Unit	k_{eff} of Array
		Reference Array: 216 Units, Density = 1.180 g/cm^3			
Cylinder, reference array	0.94	11.484	20.9	0.759	0.994
Cylinder	1.00	11.528	22.6	0.759	1.006
Sphere		12.891	21.3	0.759	1.006
Cube		10.967	24.7	0.759	1.031
		Reference Array: 64 Units, Density = 1.778 g/cm^3			
Cylinder, reference array	1.17	11.486	26.1	0.800	1.002
Cylinder	1.00	12.203	26.8	0.800	1.008
Sphere		13.646	25.0	0.800	0.996
Cube		11.609	29.4	0.800	1.017
		Reference Array: 1000 Units, Density = 1.112 g/cm^3			
Cylinder, reference array	0.47	11.509	10.5	0.566	0.992
Cylinder	1.00	8.389	8.7	0.566	0.976
Sphere		9.380	8.1	0.566	0.975
Cube		7.980	9.5	0.566	0.993

References

[1]Summary of ORNL-CDC-4 (to be published).
[2]G. E. Whitesides, G. W. Morrison, and E. C. Crume, *Trans. Am. Nucl. Soc.* **9**, 133 (1966).
[3]G. E. Hansen and W. H. Roach, *Six and Sixteen-Group Cross Sections for Fast and Intermediate Critical Assemblies*, LAMS-2543 (1961).
[4]J. T. Thomas, p. 189 in *Proceedings of Nuclear Criticality Safety, December 13–15, 1966*, SC-DC-67-1305 (1967).

2.8 MINIMUM THICKNESS OF A WATER-REFLECTED INFINITE SLAB OF AN AQUEOUS SOLUTION OF $^{235}UO_2F_2$ AT OPTIMUM CONCENTRATION[1]

J. Wallace Webster

For the purpose of defining safety standards for the storage, processing, and transport of solutions of fissile material, it is important to establish certain limiting sizes under the assumption of optimum uranium concentration. This summary concerns a study that was made to determine the minimum critical thickness of an infinite slab of uranium-bearing solution.

Fox *et al.*[2] reported a series of critical experiments with thin slabs of an aqueous solution of UO_2F_2 with a methacrylate plastic container and a water reflector. The uranium concentration was near that which results in minimum thickness. From these experiments they arrived at an estimate of 1.76 in. as the critical thickness of the solution if the transverse dimensions were infinite and the reflector was all water, i.e., no plastic included.

New methods of reactor analysis developed since those experiments were conducted (1958) – in particular the S_n method with Hansen-Roach 16-group cross sections – make possible a different interpretation of the experiments, yielding an estimate of 2.03 in. for the minimum critical thickness instead of 1.76 in. Part of the reason for the difference apparently rests with the linear extrapolation that was made in ref. 2 to estimate the effect of extending the height of the solution to infinity.

A critical thickness of 2.03 in., if correct, would make possible a 15% increase in the safe limits designated in safety standards for the thickness of slab-shaped storage, processing, and shipment containers.

References

[1]Summary of paper submitted to *Nuclear Science and Engineering*.
[2]J. K. Fox *et al.*, *Nucl. Sci. Eng.* **3**, 694 (1958).

2.9 CALCULATED NEUTRON MULTIPLICATION FACTORS OF UNIFORM AQUEOUS SOLUTIONS OF ^{233}U AND ^{235}U[1]

J. Wallace Webster

Computations of the effective neutron multiplication factors of single units of aqueous solutions of $^{233}UO_2F_2$ and $^{235}UO_2F_2$ have been made for guidance in the specification of limits applicable to processes, such as storage and transport, for these fissile isotopes. The calculations were performed with transport theory (DTF) codes in the S_n approximation and used Hansen-Roach cross sections. In all cases an infinite water reflector was assumed, and the results are presented as plots of k_{eff} as a function of mass of the fissile material, chemical concentration, dimensions of spheres and infinitely long cylinders, and thickness and areal density of infinite slabs. The computed values agree with relevant experiments to within 0.01 k_{eff}. Limits corresponding to a computed k_{eff} of 0.97 for ^{235}U and ^{233}U systems respectively are: mass, 710 and 510 g; volume, 5.4 and 3.3 liters; uranium concentration, 11.1 and 10.6 g/liter; diameter of infinite cylinder, 13.6 and 11.3 cm; thickness of infinite slab, 4.4 and 2.8 cm; and density of uranium per unit area for infinite slab, 0.39 and 0.34 g/cm^2. Limits corresponding to any other value of k_{eff} deemed more appropriate for particular conditions may be easily read from the graphs.

Reference

[1]Abstract of ORNL-CDC-2 (in press).

2.10 EXPERIMENTS WITH THE ABERDEEN PULSE REACTOR

J. T. Mihalczo
J. J. Lynn
J. R. Taylor
E. R. Rohrer
J. F. Ellis
W. C. Tunnell
James Watson[1]
R. W. Dickinson[1]
J. Reuscher[2]
Kenneth Haynes[3,4]
Jerry Richter[3]

A series of critical experiments were performed with the Aberdeen Pulse Reactor (APR) both at low power and under superprompt critical conditions. The APR is basically an unreflected and unmoderated right cylinder of 90 wt % U–10 wt % Mo, with the uranium enriched to 93.2 wt % in ^{235}U. The APR is similar in design and purpose to the Oak Ridge Health Physics Research Reactor (HPRR).

The core of the APR consists of a 22.6-cm-OD, 10.1-cm-ID, 20.2-cm-high outer annular cylinder made up of U-Mo plates of several thicknesses held together by nine 2.0-cm-diam U-Mo bolts. A movable inner annulus of U-Mo (16.7 kg of U-Mo), the safety block, is attached to a steel member which is coupled magnetically to a drive. The APR contains three movable fuel rods having diameters of 1.6, 2.0, and 2.5 cm which are used to adjust the reactivity to delayed critical and to provide excess reactivity for pulse generation.

In the low power experiments, fission rate distributions were measured, reactivity calibration of the movable parts was made, and the reactivity effects of the presence of various stainless steel parts of the reactor were determined. The prompt neutron decay constant was measured by the Rossi-α technique.

The time-dependent behavior of the neutron population in the assembly following the rapid establishment of a superprompt critical condition was investigated in order to provide data to establish the maximum size pulse that could be produced without damage to the core. In these tests the pulse size was increased until the reactor core parts were damaged. The stress in various stainless steel members supporting the reactor and the mechanical vibrations of the various core parts produced by the pulses were measured in a cooperative program with the Sandia Corporation and White Sands Missile Range.

A series of pulses produced by the rapid introduction of reactivities to ~14 cents above prompt critical resulted, finally, in a pulse of 3.7×10^{17} fissions with a reactor period of 12.5 μsec and temperature increase of 900°C. The characteristics of this pulse are given in Fig. 2.10.1.

As in the HPRR, pressure waves generated in the safety block by pulses yielding more than about 6×10^{16} fissions caused it to disengage from the magnet ~170 μsec after the peak of the pulse. Removal of the safety block by this pressure wave terminated

ORNL PHOTO – 87638

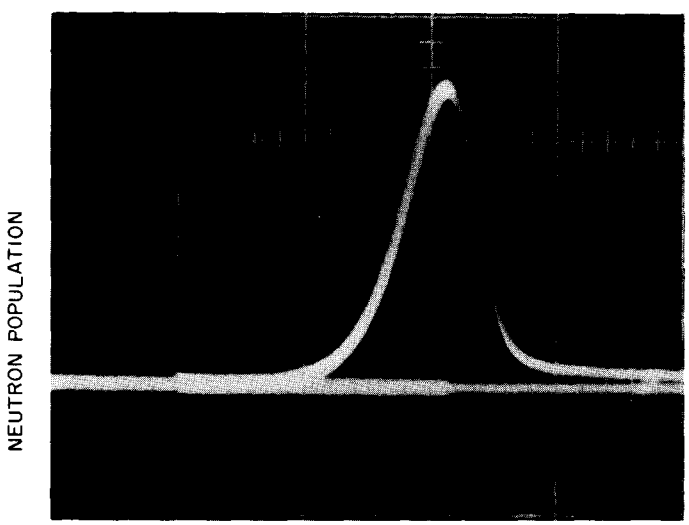

Fig. 2.10.1. Photograph of Oscillograph Trace of a 3.7×10^{17} Fission Pulse.

the low amplitude tail sustained by delayed neutrons and resulted in a large percentage of the fissions occurring in the peak of the pulse. This phenomenon enhances the safety of the operation of the system in the pulse mode. No distortion of the fuel components occurred in pulses of less than 2.1×10^{17} fissions (570°C peak temperature change). There was some distortion, principally bolt elongation, at pulses of 2.3×10^{17} fissions (610°C peak temperature change). This series of pulses, terminating in one of 3.7×10^{17} fissions, produced the following changes in the core: blistering, flaking, and rippling of all the nickel plating on U-Mo parts (aluminum plating on other parts did not fail); permanent elongation of the bolts amounting to 0.059 to 0.090 in.; three vertical (longitudinal) cracks in the central fuel plate of the outer annulus originating on the inside surface at the radial holes, provided for thermocouple insertion, and extending outward a distance not yet determined; bending of the mass adjustment and pulse rods; shearing of the stainless steel support for mass adjustment rod; and buckling of the top fuel plate sufficient to reduce the reactivity of the core 9 cents. There was no evidence that the alloy melted.

References

[1]On assignment from the Ballistics Research Laboratory, Aberdeen Proving Grounds, U. S. Army.

[2]Sandia Corporation.

[3]White Sands Missile Range.

[4]Deceased.

2.11 PROMPT-NEUTRON DECAY IN COUPLED URANIUM METAL CORES

J. T. Mihalczo

Identical cylinders of unmoderated and unreflected uranium metal, 27.94 cm in diameter, have been assembled coaxially in pairs at a separation of 36.94 cm between flat surfaces. The cylinders were of three heights: 6.042, 6.676, and 7.314 cm. The uranium metal was enriched to 93.15 wt % in the ^{235}U isotope and had a density, when assembled, greater than 18.64 g/cm^3. The prompt-neutron time behavior in these three subcritical assemblies was measured by the Rossi-α technique and, in one assembly, by the pulsed neutron method with the detectors in a variety of locations. The asymptotic decay constants compared very well with those predicted by calculations in which a pair of equations represented the kinetics of a coupled-core assembly. The equations neglected delayed neutrons and assumed space-independent kinetics for each cylinder, with a time lag representing the flight time of neutrons from one cylinder to the other. The coupling coefficients and the flight time were calculated by a Monte Carlo method. For one assembly the reactivity determined from the asymptotic prompt-neutron decay constants was compared with that measured by an analog computer whose input was the response of an ionization chamber to power changes when the separation of the components was decreased from delayed criticality to one of the above subcritical configurations.[1]

Pairs of these cylinders have also been assembled in a like manner to delayed criticality. Prompt-neutron decay constants of the assemblies were measured by the Rossi-α technique, and the results agreed with those predicted by the model described above. Neutron multiplication factors calculated for the assemblies using S_8 transport theory agreed with the experimental values.[2]

Delayed-critical systems of three identical coaxial 38.09-cm-diam cylinders have been assembled, with equal spaces between the flat faces, by adjusting the thickness of the cylinders and the spacing between them. The prompt-neutron decay constant of these assemblies, also measured by the Rossi-α technique, was observed to be independent of the detector locations and is plotted as a function of cylinder thickness in Fig. 2.11.1.

The kinetic equation used to describe the prompt-neutron time behavior in core i is[3]

$$\frac{dN_i(t)}{dt} = \alpha_i N_i(t) + \sum_{\substack{i=1,2,3 \\ j \neq i}} \gamma_{ji} N_j(t - \tau_{ji}) + S_i \delta(t) \quad ,$$

where

$N_i(t)$ = prompt-neutron population in core i at a time t,

α_i = prompt-neutron decay constant in core i when isolated from the others,

$\gamma_{ji} = \epsilon_{ji}/(l_i/\beta)$,

ϵ_{ji} = reactivity contribution of core j to core i,

l_i = prompt-neutron lifetime in the isolated core i,

β = effective delayed-neutron fraction,

τ_{ji} = flight time of neutrons traveling from core j to core i,

S_i = fraction of neutrons born in core i.

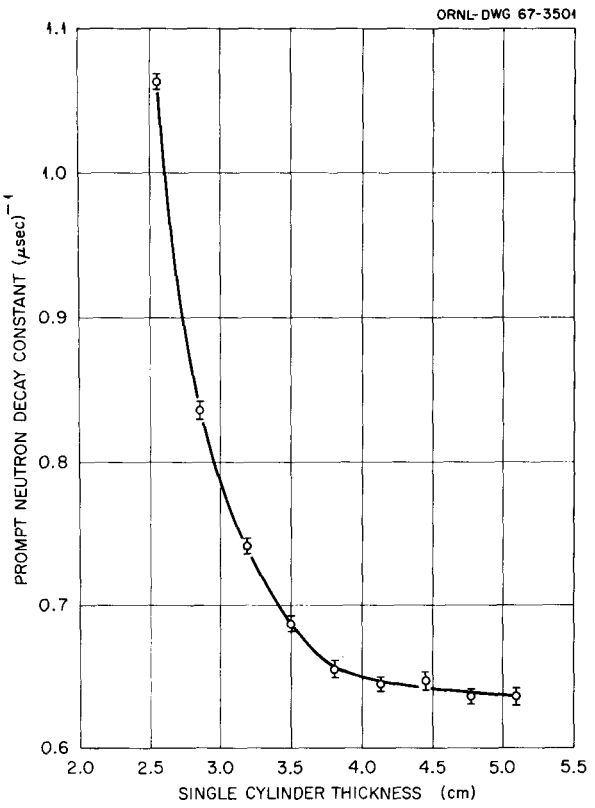

Fig. 2.11.1. Prompt-Neutron Decay Constant in Unreflected Critical Assemblies Consisting of Three Identical, Coaxial, Equally Spaced Cylinders of Enriched Uranium Metal 38.09 cm in Diameter.

The solutions of a set of three of these equations were used to compute the asymptotic prompt-neutron decay constant for the critical system with three 5.094-cm-thick cylinders. The prompt-neutron decay constant, α_i, of isolated cylinders of this thickness has been measured previously by the Rossi-α technique.[4] The prompt-neutron lifetime in a single subcritical cylinder, l_i, was obtained from the lifetime determined from the prompt-neutron decay constant measured in isolated cylinders at delayed criticality and the change in the lifetime as the cylinder was made subcritical. The values of ϵ_{ji}, τ_{ji}, and S_i used in the calculation were determined with the O5R Monte Carlo neutron transport code.[5] The calculated and measured prompt-neutron decay constants differed by less than 5%.

References

[1]This paragraph is an abstract of a paper presented at the American Nuclear Society Topical Meeting, *Coupled Reactor Kinetics*, in January 1967 (proceedings in press).

[2]This paragraph is an abstract of a paper presented at the *International Conference on Fast Critical Experiments and Their Analysis* in October 1966 [proceedings (ANL-7320) in press].

[3]R. Avery, *Proc. U. N. Intern. Conf. Peaceful Uses At. Energy, 2nd, Geneva, 1958* **12**, 182 (1958).

[4]J. T. Mihalczo, *Prompt Neutron Decay in Subcritical Uranium-Metal Cylinders by the Rossi-α Technique*, ORNL-TM-1736 (in press).

[5]D. C. Irving *et al.*, *O5R, A General-Purpose Monte Carlo Neutron Transport Code*, ORNL-3622 (February 1965).

2.12 INTERACT: A FORTRAN PROGRAM FOR CALCULATING NEUTRON PRODUCTION RATES

G. W. Morrison[1] D. C. Irving
J. T. Mihalczo

A FORTRAN program, INTERACT, has been developed for analyzing the history tapes produced by the O5R Monte Carlo neutron transport code[2] to obtain the neutron production rate in a given region due to neutrons that were born in another region. The production rate $P_{ijk\ldots m}$ is the fission weight produced in region m from neutrons starting in region i and passing through regions $j,k,\ldots$, etc., before entering region m and producing fissions. The regionwise k_{eff} is then calculated from the regionwise production rates P_{ii}. Only those neutrons which start in a given region and stay in that region are scored for the production rate P_{ii}.

An experimental critical assembly of three separate units (or regions) was calculated with INTERACT. The results are in good agreement with the experimental values as well as with calculations performed with S_n calculations. The coupling coefficients[3] have been used in the interpretation of prompt-neutron time decay measurements in coupled systems.

References

[1]Computing Technology Center, Union Carbide Corporation, Oak Ridge.

[2]D. C. Irving *et al., O5R, A General Purpose Monte Carlo Neutron Transport Code,* ORNL-3622 (1965).
[3]R. Avery, *Proc. U. N. Intern. Conf. Peaceful Uses At. Energy, 2nd, Geneva, 1958* **12**, 182 (1958).

2.13 CODES FOR SOLUTION OF COUPLED NEUTRON KINETIC EQUATIONS

J. T. Mihalczo P. Stewart[1]
G. Westley[1]

Codes have been developed to predict the prompt-neutron time behavior in a pair of coupled critical and subcritical assemblies. The equations[2] which are solved are

$$\frac{dN_1(t)}{dt} = \alpha_1 N_1(t) + \gamma_{21} \int_0^t P(T)\, N_2(t-T)\, dT + A_1 S(t) ,$$

$$\frac{dN_2(t)}{dt} = \alpha_2 N_2(t) + \gamma_{12} \int_0^t P(T)\, N_1(t-T)\, dT + A_2 S(t) ,$$

where

$N_{1,2}(t)$ = neutron population in core 1 or 2,
$\alpha_{1,2}$ = prompt-neutron decay constant in isolated core 1 or 2,
$\gamma_{21}(\gamma_{12})$ = coefficient coupling core 2 to core 1 (core 1 to core 2),
$P(T)$ = distribution of neutron transit time between cores,
$S(t)$ = neutron source distribution normalized to unity,
$A_{1,2}$ = fraction of source neutrons in core 1 or 2.

The codes determine $N_{1,2}(t)$ for a specified time interval when the other quantities are specified as input. The Rossi-α correlation probabilities can be computed for all possible locations of two detectors in a two-core assembly. The distribution of transit time can be a delta function in time corresponding to a specified transit time, an exponential function $(1/\tau)e^{-T/\tau}$ which corresponds to considering the interacting neutrons as a delayed-neutron group with an average flight time τ, or a completely arbitrary and specified numerical input. The source $S(t)$ can be a delta function or can be specified in numeric form as input. The output lists and/or plots the neutron populations and the Rossi-α two-detector correlation probabilities as a function of time.

References

[1]Computing Technology Center, Union Carbide Corporation, Oak Ridge.
[2]C. G. Chezem and H. H. Helnick, *Pulsed Neutron Analysis in the Los Alamos Reactor Experiment,* LA-3263 (1965).

2.14 PROMPT-NEUTRON DECAY CONSTANTS CALCULATED FOR HIGHLY ENRICHED URANIUM METAL ASSEMBLIES[1]

G. W. Morrison[2] D. C. Irving
J. R. Knight[2]

The discrepancy between the multigroup-calculated and the measured prompt-neutron lifetimes in unreflected highly enriched uranium metal assemblies motivated a study of the group-averaged cross sections used in S_n multigroup lifetime and neutron decay constant calculations.[3] It has been shown that prompt-neutron life time and other spectral-dependent quantities in metal assemblies can be successfully calculated by the Monte Carlo method if detailed point cross-section data are used; however, using detailed cross sections has the disadvantages of requiring a great deal of data handling and, in general, consuming excessive amounts of computing time.

A new set of multigroup cross sections with the energy structure of Hansen and Roach[4] was obtained for these assemblies by averaging the detailed point cross-section data. This averaging was carried out by using the fluxes generated in a Monte Carlo calculation of the Godiva I assembly. This new set of multigroup cross sections was used in S_n transport calculations to obtain the prompt-neutron decay constants for several systems. A comparison of the new cross-section set with the Hansen-Roach cross sections is shown in Table 2.14.1.

The general-purpose Monte Carlo neutron transport code used for the calculations allowed detailed

Table 2.14.1. Six-Group Macroscopic Cross Sections for Unreflected Highly Enriched Uranium (93.2% ^{235}U) Metal Assemblies

	Cross Section (cm^{-1})					
	Group 1	Group 2	Group 3	Group 4	Group 5	Group 6
Averaged by Monte Carlo						
Σ^A	0.0581	0.0626	0.0604	0.0582	0.0723	0.1116
$\nu\Sigma^f$	0.1731	0.1587	0.1409	0.1277	0.1463	0.2032
Σ^{TR}	0.2026	0.2313	0.2350	0.2625	0.4036	0.5522
$\Sigma_{g\to g}$	0.0423	0.0760	0.1017	0.1670	0.3212	0.4407
$\Sigma_{g-1\to g}$	0	0.0139	0.0148	0.0279	0.0297	0.0102
$\Sigma_{g-2\to g}$	0	0	0.0207	0.0396	0.0385	0.0077
$\Sigma_{g-3\to g}$	0	0	0	0.0392	0.0340	0.0061
$\Sigma_{g-4\to g}$	0	0	0	0	0.0256	0.0043
$\Sigma_{g-5\to g}$	0	0	0	0	0	0.0028
V (cm/sec) $\times 10^{-8}$	28.47	19.51	14.58	10.70	6.46	3.16
Hansen-Roach Set						
Σ^A	0.0585	0.0602	0.0604	0.0613	0.0753	0.1337
$\nu\Sigma^f$	0.1654	0.1476	0.1395	0.1347	0.1586	0.2574
Σ^{TR}	0.2034	0.2158	0.2229	0.2499	0.3803	0.5757
$\Sigma_{g\to g}$	0.0578	0.0852	0.1122	0.1675	0.3011	0.4419
$\Sigma_{g-1\to g}$	0	0.0131	0.0118	0.0271	0.0172	0.0038
$\Sigma_{g-2\to g}$	0	0	0.0180	0.0330	0.0197	0.0038
$\Sigma_{g-3\to g}$	0	0	0	0.0316	0.0222	0.0034
$\Sigma_{g-4\to g}$	0	0	0	0	0.0214	0.0034
$\Sigma_{g-5\to g}$	0	0	0	0	0	0.0029
V (cm/sec) $\times 10^{-8}$	28.5	19.9	14.7	11.0	6.7	2.7

representation of the cross-section data.[5] The energy range from 10 eV to 15 MeV was divided into 21 groups, and each group was further divided into 256 subgroups with the cross sections represented by an average value for each subgroup. An 11th order Legendre expansion was used to represent the differential cross sections. The inelastic scattering was treated by sampling from a combination of an evaporation model and a level excitation model.

In addition to the spherical Godiva I assembly, several solid uranium metal cylinders enriched to 93.15 wt % in ^{235}U and ranging in diameter from 7 to 15 in. were used in the S_n calculations.[6,7] Table 2.14.2 shows the measured and calculated values of the prompt-neutron decay constants for these assemblies. The results indicate that the multigroup cross sections generated from Monte Carlo calculations with detailed cross-section data are quite successful in predicting prompt-neutron decay constants.

References

[1]Summary of paper to be presented at Thirteenth Annual Meeting of American Nuclear Society, San Diego, Calif., June 11–15, 1967; to be published in *Trans. Am. Nucl. Soc.*, Vol. 10 (1967).

Table 2.14.2. Prompt-Neutron Decay Constant in Uranium Metal Assemblies

System Description	Ref.[a]	Prompt-Neutron Decay Constant, α (10^6 sec^{-1})	
		Measured	Calculated
Godiva I: unreflected 8.718-cm-radius metal sphere	3	1.10	1.12
Solid Cylinders:	8		
17.77-cm-diam × 12.63 cm		1.082	1.075
22.85-cm-diam × 9.75 cm		1.088	1.093
27.93-cm-diam × 8.64 cm		1.076	1.062
33.01-cm-diam × 8.08 cm		1.071	1.073
38.09-cm-diam × 7.71 cm		1.063	1.064

[a]See list of references at end of paper.

[2]Computing Technology Center, Union Carbide Corporation, Oak Ridge.

[3]G. E. Hansen, p. 453 in *Proceedings of a Seminar on Physics of Fast and Intermediate Reactors*, vol. 1, IAEA, Austria, 1962.

[4]G. E. Hansen and W. H. Roach, *Six and Sixteen Group Cross Sections for Fast and Intermediate Critical Assemblies*, LAMS-2543 (1961).

[5]D. C. Irving *et al.*, *O5R, A General Purpose Monte Carlo Neutron Transport Code*, ORNL-3622 (1965).

[6]W. W. Engle, *A User's Manual for ANISN, A One-Dimensional Discrete Ordinates Transport Code with Anisotropic Scattering*, K-1693 (Mar. 30, 1967).

[7]F. R. Mynatt, *A User's Manual for DOT, A Two-Dimensional Discrete Ordinates Transport Code with Anisotropic Scattering*, K-1694 (to be published).

[8]J. T. Mihalczo, *Nucl. Sci. Eng.* **20**, 60–65 (1964).

2.15 ADJOINT MONTE CARLO CALCULATIONS FOR ENRICHED URANIUM METAL ASSEMBLIES[1]

G. W. Morrison[2] G. W. Whitesides[2]
D. C. Irving

Solutions to the adjoint transport equation in complicated geometries of multiplying media are of great importance to those involved in core physics analysis. Perturbation and neutron lifetime calculations usually require such solutions. However, the adjoint solutions that may be obtained from transport and diffusion theory codes are limited to one or two dimensions.[3,4] These limitations do not apply in general to the Monte Carlo method. It was shown in a recent paper[5] that a generalized Monte Carlo code using few-group cross sections could calculate multiplication constants for complicated geometries with a statistical accuracy of a few percent. In this work we were able to demonstrate the feasibility of obtaining multigroup adjoint Monte Carlo predictions of the multiplication constants for complicated geometries.

The Monte Carlo program used to perform the adjoint calculations is similar to the program used in ref 3 for solutions of the forward transport equation. A set of 16-group cross sections was input for each element in a medium. This set contained the transport, scattering, and fission cross sections, as well as the fission spectrum χ_g. The scattering of the adjoint particles is treated by sampling from the transposed transfer matrix for a given element. All scattering is assumed to be isotropic in the laboratory system. At each collision the statistical weight of the "adjuncton"[6] is multiplied by the factor

$$P_g = \frac{\sum_{i=1}^{g} \sigma_i^{S \rightarrow g}}{\sigma_g^S}$$

to conserve balance in group g. This factor is necessary to account for the outscattering to higher energy groups.

As in the conventional Monte Carlo, the "adjuncton" histories are started in batches of 400 with a given spatial distribution. Source biasing was used to start the particles in the various energy groups. The source routine sampled from a

forward power distribution rather than from a normalized distribution of $\nu\Sigma^f$. The multiplication constant for a batch is taken to be the ratio of the adjoint production weight and the adjoint source weight.

The results of the calculations are given in Table 2.15.1. The multiplication constants reported are averages of all the batches for a system, with the exception of the first few, which are still affected by the initial source distribution. It can be seen in

Table 2.15.1. Monte Carlo Calculated Multiplication Constants (k_{eff}) for Experimentally Critical Systems[a]

System Description	Ref.[b]	k_{eff}	
		Adjoint	Forward
Godiva I: 8.718-cm-radius U(93.8) metal sphere, unreflected	7	0.992 ± 0.012	1.005 ± 0.011
Unreflected annular cylinder of U(93.2)-Mo alloy, 5.08 cm ID, 10.16 cm OD, 19.74 cm high	8	1.001 ± 0.009	1.003 ± 0.009
Unmoderated, unreflected 8-unit cubic array of 15.7-kg U(93.2) metal cylinders; each unit a 9.12-cm-diam × 4.32-cm-high cylinder between two 11.49-cm-diam × 2.69-cm-high cylinders; surface separation of units = 0.229 cm	12	0.983 ± 0.009	0.998 ± 0.007
Unmoderated, unreflected cylindrical annulus with parallelepiped inside; U(93.2); parallelepiped and annulus each 12.93 cm high; annulus 38.10 cm OD, 27.94 cm ID	11	1.001 ± 0.011	0.990 ± 0.009
Eight-unit ring of various metal U(93.2) pieces, consisting of cylinders, parallelepipeds, and a hemisphere; unreflected	10	1.002 ± 0.011	1.013 ± 0.008
Unreflected 8-unit cubic array of 20.9-kg U(93.2) metal cylinders, each 11.506 cm diam × 10.765 cm high and enclosed in iron cylinders 14.1 cm diam × 13.2 cm high; iron wall thickness = 0.66 cm; surface separation of units = 3.239 cm	10	0.989 ± 0.010	0.997 ± 0.007
Carbon-reflected cylindrical U(93.2) metal annulus, 15 cm OD, 11 cm ID, 4.332 cm high; reflector thickness 3 in. with void in center of core	9	1.002 ± 0.013	0.982 ± 0.011

[a] 10,000 neutron histories were run for each system.

[b] See list of references at end of paper.

Table 2.15.1 that the calculated adjoint multiplication constants are in agreement with the experiments and with the forward calculations within an accuracy of 1 or 2%. Furthermore, the running time per particle history and the number of histories required for a given statistical accuracy are comparable to those observed in forward calculations.

References

[1]Paper presented at Winter Meeting of American Nuclear Society, Oct. 31–Nov. 3, 1966, Pittsburgh; *Trans. Am. Nucl. Soc.* **9**, 440 (1966).

[2]Computing Technology Center, Union Carbide Corporation, Oak Ridge.

[3]B. Carlson, C. E. Lee, and J. W. Warlton, *The DSN and DC Neutron Transport Codes,* LAMS-2346 (1960).

[4]W. J. Fader, *TDP – A Two Dimensional Perturbation Calculation Code Based on TDC, for IBM-7090,* PWAC-446 (1964).

[5]G. E. Whitesides, G. W. Morrison, and E. C. Crume, *Trans. Am. Nucl. Soc.* **9**, 133 (1966).

[6]R. R. Coveyou in a private communication has suggested the use of the term "adjuncton" to describe the particles whose transport is described by the adjoint Boltzmann equation.

[7]G. E. Hansen, *Proc. U. N. Intern. Conf. Peaceful Uses At. Energy, 2nd, Geneva, 1958* **12**, 84 (1958).

[8]J. T. Mihalczo and W. E. Kinney, *Trans. Am. Nucl. Soc.* **4**, 302 (1961).

[9]J. T. Mihalczo, *Trans. Am. Nucl. Soc.* **8**, 442 (1965).

[10]D. C. Irving and J. T. Mihalczo, *Trans. Am. Nucl. Soc.* **7**, 287 (1964).

[11]J. T. Mihalczo, *Nucl. Sci. Eng.* **27**, 557 (1967).

[12]J. T. Thomas, *Critical Three-Dimensional Arrays of Neutron-Interacting Units, Part II – U(93.2) Metal,* ORNL-TM-868 (1964).

2.16 INVESTIGATION OF FACTORS AFFECTING THE BURST WAIT TIME OF THE HPRR

L. B. Holland L. W. Gilley
J. W. Poston[1]

In pulse reactors the neutron population in the core just prior to a pulse is reduced to nearly the natural background that would be associated with the subcritical assembly of the fissionable material in the core in order to keep the number of preinitiated pulses to a minimum. (A preinitiated pulse is a pulse which starts before all the excess reactivity has been added to the assembly, with the result that the total number of fissions in the pulse is less than the desired number.) In the Health Physics Research Reactor (HPRR) it has been the practice to reduce the neutron population by withdrawing the neutron source, which has a strength of 1.76×10^6 neutrons/sec, into its shield and removing the safety block from the core. The resulting shutdown reactivity is approximately 20 dollars (that is, the total worth of the safety block). A burst is initiated by reinserting the safety block, which brings the reactor back to the delayed-critical condition, and then adding excess reactivity by inserting a burst rod into the core with momentary delays associated with sequential operation. The number of preinitiated bursts associated with this procedure has been too high, however, which has prompted an investigation to determine the effect of the amount of shutdown reactivity used and the strength of the neutron source on the wait time between the addition of the excess reactivity and the initiation of the burst.

First, a series of eight experiments were performed by the standard procedure. Five of the eight bursts were preinitiated, and the average wait time of the remaining three bursts was only 17 msec. Next, a series of 14 experiments were performed in which the safety block was only partially withdrawn, giving a shutdown reactivity of 2 dollars; a smaller neutron source was used (source strength = 0.38×10^6 neutrons/sec) and the burst rod was always fired with no delay the moment the safety block was fully inserted. Of the 14 bursts, only 1 was preinitiated and the average wait time of the 13 remaining bursts was increased to 778 msec.

In the second group of experiments limited data were also obtained on the average wait time associated with the reactivity of the burst rod. For reactivities of 101, 104, and 108.5 cents, the average wait time was 1135, 857, and 778 msec respectively.

Since the lower value of shutdown reactivity appears to be satisfactory, a control rod much smaller in diameter than the safety block can be used which minimizes errors due to repositioning fuel and thereby tends to increase the accuracy of achieving the target yield. Accordingly, design studies will be made to modify the HPRR to use a shutdown rod worth 2 dollars rather than the safety block for reducing the neutron population. Also, to make the wait time longer the smaller source will be used, a more ef-

fective source shield will be designed, and the procedure to immediately fire the burst rod as soon as the safety block is completely inserted in the core will be continued. After the possibility of using small values of shutdown reactivity was demonstrated at the HPRR, the critical experiments with the Aberdeen Pulse Reactor (see Sect. 2.10) were successfully conducted using the lower value of shutdown reactivity and the procedure of inserting the burst rod the moment the shutdown rod was fully reinserted in the core.

Reference

[1]Health Physics Division.

2.17 TSR-II HEAT TRANSFER[1]

J. Lewin L. B. Holland

The temperature distribution in the fuel elements of the TSR-II has been calculated for a measured power distribution for the nominal operating conditions of a power level of 2 MW and a total cooling-water flow rate of 800 gpm. The distribution was also obtained for operation at a 3-MW power level and a total flow rate of 400 gpm. Under the latter conditions the maximum fuel plate temperature was 258°F, well below the saturation temperature of the water in the core, which is 283°F at the minimum core pressure of 36.5 psig.

Reference

[1]Abstract of ORNL-TM-1779 (in press).

2.18 CALCULATIONS OF THE POWER DISTRIBUTION IN THE TSR-II[1]

J. H. Wilson[2] L. B. Holland

The power distribution and heat flux of the TSR-II fuel plates have been calculated for the final core configuration, which includes the fuel-bearing cover shell on the control mechanism housing. Calculations for the clean-cold condition of the reactor were based on gold-foil activation measurements of the thermal-neutron density distribution in the core, and those for high-power operation were based on GNU-II[3] code calculations for the thermal-neutron density distribution. The data are presented for operation of the reactor at 1 MW.

References

[1]Abstract of ORNL-TM-1821 (in press).

[2]On loan from Lockheed. Present address: Dept. 7369, Lockheed Ga. Co., Marietta.

[3]C. L. Davis, J. N. Bookston, and B. E. Smith, *GNU-II, A Multigroup One-Dimension-Diffusion Program,* GMR-101 (1957).

3. Reactor and Weapons Shielding

3.1 MEASUREMENT OF THE ANGLE-DEPENDENT NEUTRON ENERGY SPECTRA EMERGENT FROM LARGE LEAD AND POLYETHYLENE SLAB SHIELDS[1]

F. J. Muckenthaler K. M. Henry
J. J. Manning J. L. Hull
R. M. Freestone, Jr.

An experiment was performed at the Tower Shielding Facility to obtain results for comparison with neutron transport calculations (see Sect. 3.2) of the energy distribution of neutrons emerging at discrete angles with respect to the normal from a 6-in.-thick polyethylene slab and an 11-in.-thick lead slab. Spectral measurements were made using an NE-213 organic scintillator for neutron energies above about 0.8 MeV and the $1/E$ detector developed by T. V. Blosser for the energy range from thermal to about 10 keV. Fast-neutron dose-rate measurements were obtained with a Hurst-type dosimeter (FND) at each of the spectral measurement locations.

The geometry for this experiment is shown in Fig. 3.1.1. The TSR-II was placed inside the spherical lead-water beam shield to provide a convenient means of collimating the neutron beam and at the same time reducing the background. The collimator consisted of a cylindrical section, $4\frac{1}{4}$ in. in inside diameter and 40 in. long, and also of conical sections, $19\frac{1}{2}$ and 22 in. long, which were added at the reactor end and detector end of the collimator, respectively, to reduce the neutron scattering in the collimator. Six inches of lead was inserted in the collimator adjacent to the reactor vessel to reduce the gamma-ray intensity at the detector.

A 36- by 30-in. lead collar, 8 in. thick and containing a 15-in.-diam hole, was placed around the end of the collimator to simplify the geometry for the measurements with lead slabs in the beam where reflected neutrons were found, through calculations, to be important. The lead collar extended $5\frac{3}{16}$ in. beyond the outermost edge of the collimator. The lead and polyethylene shielding slabs were placed against the surface of the lead collar. Lithiated paraffin blocks were arranged around the lead collar and at one end of the lead slabs to minimize neutron streaming into the detector collimator when it was rotated to large angles.

A photograph of the configuration is shown in Fig. 3.1.2. The lead sample consisted of 5- by 5-ft slabs that were 1 and $1\frac{1}{2}$ in. thick. Measurements were made at an angle of 70° to the beam center line to show that the 5-ft width was sufficient to mock up an infinite slab. Results indicated that practically all the neutrons penetrating a lead thickness of 11 in. and reaching the detector with an energy above 0.8 MeV came from a circle about 3 ft in diameter with the beam axis as its center. For polyethylene the source area was even smaller.

Fast-neutron spectra and dose-rate measurements were made with the detector located in a lead and water shield placed on a carriage that rotated in a horizontal plane about a point where the reactor beam center line intersected the back surface of the 11-in.-thick lead slab (Fig. 3.1.1). The neutrons impinged on the detector through a collimator which allowed the detector to view the full width of the slabs when the detector was placed 27.4 ft from the surface of the lead slab from which the neutrons emerged. The low-energy neutron spectra measurements were made at a point 18 ft 10 in. from the same reference point.

The neutron intensity incident on the shield sample was mapped using a Hornyak button and an FND at the surface of the lead collar. Traverses were made both in the horizontal and vertical planes at $1\frac{3}{4}$ in., 4 ft, and 30 ft from the lead collar. A traverse along the beam center line was made for a distance of 15 to 27 ft from the point about which the detector shield rotated. Slow- and fast-neutron spectral and dose-rate measurements of the bare beam were made for angles of 0, 4.16, and 8.6° with respect to the beam center line.

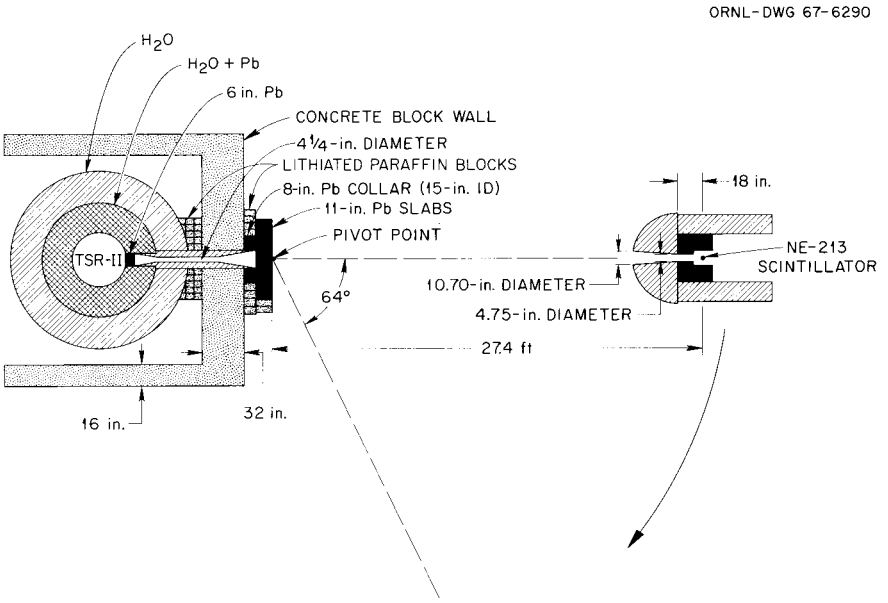

Fig. 3.1.1. Schematic Diagram of Experimental Arrangement.

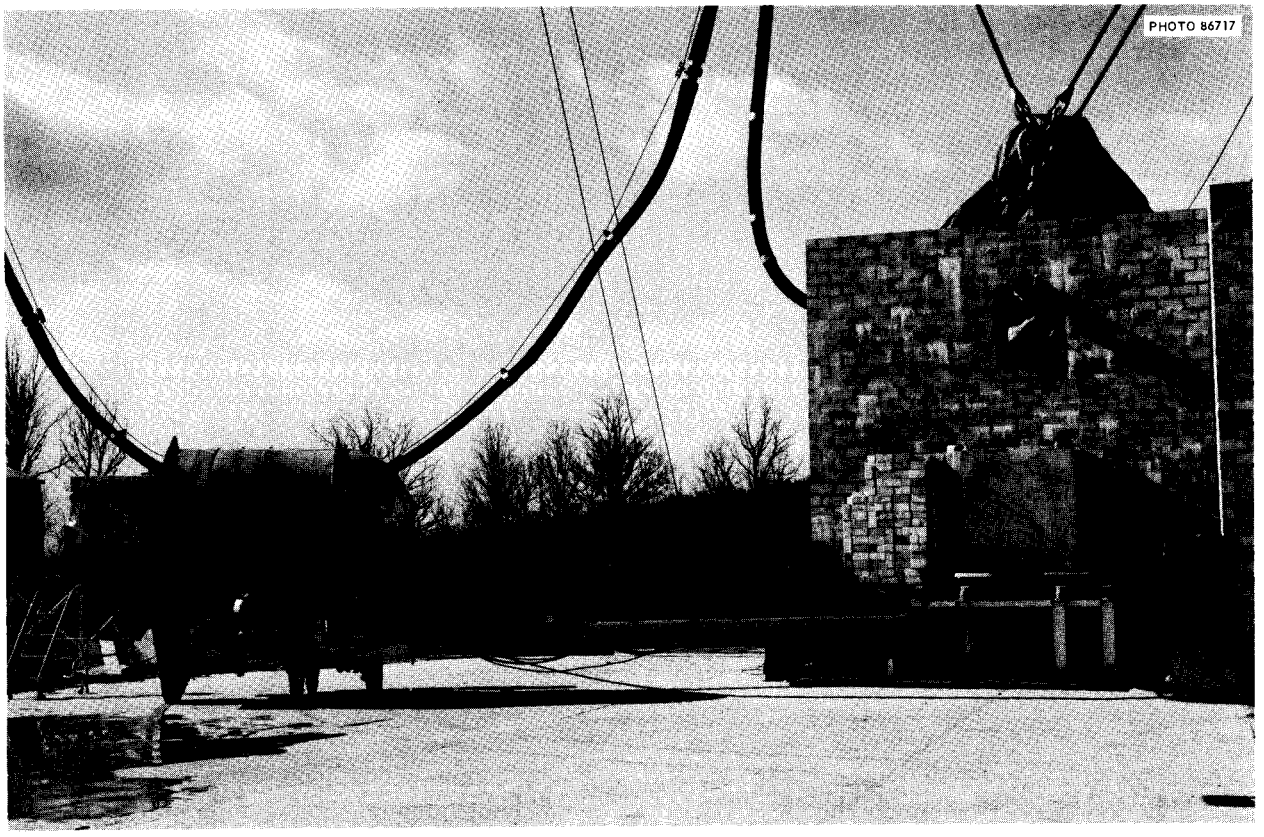

Fig. 3.1.2. Photograph of Experimental Arrangement.

Foreground and background measurements, for both fast-neutron spectra and dose rate, were made with the detectors rotated to angles of 0, 13, 30, 47, and 64° when 11 in. of lead was placed in the beam. Background measurements were obtained with a 12-in. thickness of lithiated paraffin bricks placed midway between the lead slabs and the detector. This thickness was determined through a series of experiments to minimize the reduction in gamma rays reaching the detector while providing sufficient neutron attenuation. Low-energy neutron spectra were obtained at only 0 and 30°.

High- and low-energy neutron spectra and fast-neutron dose were measured for the polyethylene slabs at angles of 0 and 30°.

Reference

[1]Work funded by Defense Atomic Support Agency under DASA Task Number A2-11.037.

3.2 PRELIMINARY TWO-DIMENSIONAL DISCRETE ORDINATES CALCULATIONS OF ANGLE-DEPENDENT NEUTRON SPECTRA EMERGENT FROM LARGE LEAD AND POLYETHYLENE SLAB SHIELDS AND COMPARISONS WITH EXPERIMENT[1]

F. R. Mynatt[2] F. J. Muckenthaler
R. M. Freestone, Jr.

As part of a study of fundamental characteristics of neutron shields and the verification of calculational techniques, a shielding experiment and calculational comparison program is being pursued. The purpose of the experiment is to provide comprehensive data for comparison with two-dimensional transport calculations rather than to simulate any practical shielding application. The fundamental element or result of a two-dimensional transport calculation is the flux $\phi(r_i, z_j, E_g, \mu_d, \eta_d)$, a function of two space dimensions, energy, and two angles. The ideal experiment would produce a direct comparison with this five-dimensional flux. This, however, is currently impossible and comparisons must be made with measurements of integral quantities. A two-dimensional dose comparison reported in Sect. 3.4 demonstrates the r and z variation. For many shielding problems the angular flux as a function of energy, space, and angle on the exit face of the shield is the quantity of most interest. The most meaningful and practical physical quantity for comparison is the energy-dependent flux or scalar spectrum at some point in the space exposed to the exit face of the shield. The location of the point emphasizes certain angles and surface areas.

In order to preclude any geometric transformations, the experiment was constructed so that it might be represented exactly in cylindrical r-z geometry. The only noncylindrical components are the square slab shields. It was thus desirable that the slabs appear infinitely large for neutrons in the energy range of most interest (0.9 to 15.0 MeV). Collimated source neutrons enter the slab over a small area and spread symmetrically over a larger area at the exit face. The widest distribution is for neutrons of the lowest energy range of interest which have the largest angle with respect to the normal. From an S_8P_3 calculation using a fission source distribution, for the energy range between 0.74 and 0.82 MeV, and for an angle at 79°25′ with respect to normal and in the plane containing the normal, it was determined that for R = 25 in. the integral

$$\frac{\int_0^R \phi(E_g,\Omega)\, dA}{\int_0^\infty \phi(E_g,\Omega)\, dA} = 0.99 . \qquad (1)$$

Thus for this extreme case 99% of the neutrons in this energy range and angle are from a circle with a radius of 25 in., and the slab is effectively infinite.

Since the comparisons of the emergent flux data and calculations are to be made on an absolute basis, the neutron source at the shield entrance face must be well-defined with respect to intensity, angular, and spatial distributions. The radial distribution is determined from a Hornyak button traverse at 1.75 in. from the collimator, and the angle and energy distribution is determined from NE-213 measurements in a 27.4-ft arc centered about the source exit. The NE-213 data showed that it is reasonably correct to assume that the total source distribution is a product of the radial, space, and angle distributions. The intensity of the source is given by scaling the NE-213 data at 0°, 27.4 ft to the slab entrance face, using the ratio of fast-neutron dose at the two points as a scale factor. The source spectrum below the NE-213 range is to be determined by combining results inferred from variable boron filter spectrom-

eter data and a discrete ordinates calculation of the TSR-II reactor and collimator assembly. The energy range below the NE-213 data is of interest only for dose and capture gamma-ray data comparisons.

The two-dimensional discrete ordinates (DOT)[3] calculations performed to date were performed as a check on the experimental data rather than for final comparison. The source for most of these calculations used the measured energy distribution but was assumed to be monodirectional and was distributed evenly over a 4.25-in.-diam circle with the normalization defined by the total integral intensity. Some later calculations used the radial source distribution, and the answers agreed with those for the evenly distributed source. The geometry used is a right circular cylinder slab using 675 mesh points to describe the 11-in.-thick by 67.75-in.-diam lead or the 6-in.-thick by 67.75-in.-diam polyethylene. Vacuum boundary conditions were applied to exterior surfaces except for the entrance face for which a flux boundary condition was used to describe the source. Two angular quadratures were used, an S10 (70 angles) half-symmetric set based on Gaussian zeros and an S10 completely symmetric set having directions within an angle of 0° 3.5′ with respect to normal, which should improve the treatment of the source and uncollided flux. Thirty-group GAM II[4] cross sections were used for the energy range of 0.74 to 14.9 MeV. The flux at points on the 27.4-ft arc about the exit face is calculated by the ray tracing code SPACETRAN described in Sect. 3.3. This routine calculates the ray connecting an arbitrary point in space to each element of area on the surface grid, uses the calculated angular flux to find the equivalent point source for the particular angle and grid element, and sums the contribution to the point in space.

Pulse-height distributions were measured by the NE-213 proton recoil scintillator on a 27.4-ft-radius arc at angles of 0, 13, 30, 47, and 64° for the lead slabs and 0 and 30° for the polyethylene. The pulse-height distributions were unfolded by R. M. Freestone using the FERD[5,6] code system, which gives a probability distribution for the neutron spectrum indicating as a function of energy the mean value and one standard deviation error limits for the spectral curve. The errors represent both the errors in the response functions and the statistical uncertainties in the experimental data. Figure 3.2.1 shows the unfolded NE-213 data and the DOT-SPACETRAN calculation for lead for a detector angle of 47°. The overall agreement in intensity and shape is good. Figure 3.2.2 shows a similar comparison for polyethylene at 30°.

Future work will include measurements and calculations for laminated lead and polyethylene slabs. A study of the effect of variation in cal-

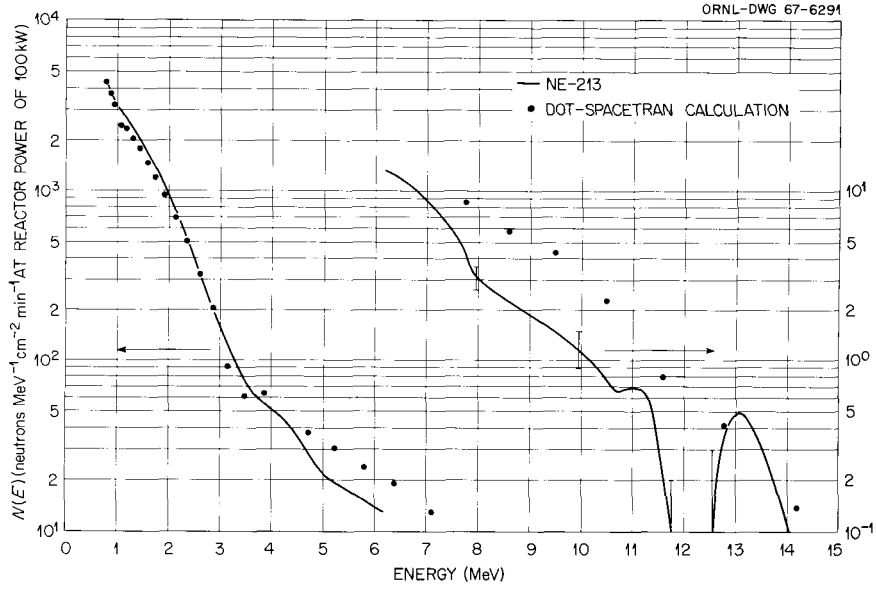

Fig. 3.2.1. Comparison of Calculated and Measured Neutron Spectra at 47° from Normal on a 27.4-ft-radius Arc from an 11-in.-thick Lead Shield.

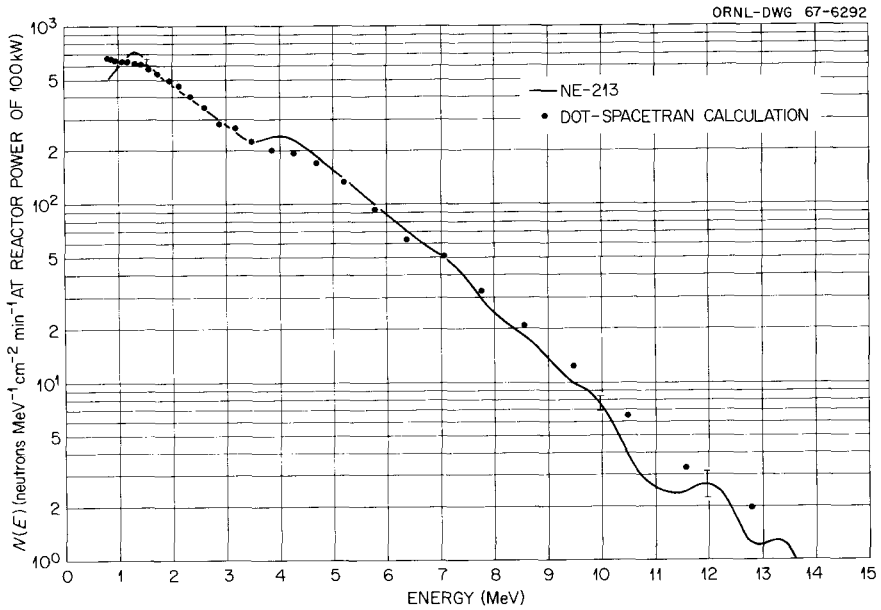

Fig. 3.2.2. Comparison of Calculated and Measured Neutron Spectra at 30° from Normal on a 27.4-ft-radius Arc from a 6-in.-thick Polyethylene Shield.

culational parameters will be made, a version of SPACETRAN using volume rather than surface integration is planned, and extensive effort will be applied toward making the calculational method rapid as well as accurate.

References

[1]Work partially funded by Defense Atomic Support Agency under DASA Task Number A2-11.037.

[2]Computing Technology Center, Union Carbide Corporation, Oak Ridge.

[3]F. R. Mynatt, *A User's Manual for DOT – A Two-Dimensional Discrete Ordinates Transport Code with Anisotropic Scattering*, K-1694 (to be published).

[4]G. D. Joanou and J. S. Dudek, *GAM-II, A B_3 Code for the Calculation of Fast-Neutron Spectra and Associated Multigroup Constants*, GA-4265 (1963).

[5]W. R. Burrus and V. V. Verbinski, p. 148 in *Proc. Special Session Fast Neutron Spectroscopy, 1964 Winter Meeting of the American Nuclear Society, San Francisco, Calif.*, ANS-SD-2 (1965).

[6]W. R. Burrus, *Utilization of a Priori Information by Means of Mathematical Programming in the Statistical Interpretation of Measured Distributions*, ORNL-3743 (1964).

3.3 THE DISCRETE ORDINATES METHOD – PROGRAM DEVELOPMENT

F. R. Mynatt[1] N. Cramer[2]
R. J. Rodgers[1] J. R. Knight[1]

During the past year the increased use of the discrete ordinates codes ANISN[3] and DOT[4] for neutron and gamma shielding calculations has encouraged the development of convenience options and peripheral programs. Many of these programs, although designed for a particular problem, may be useful for other purposes. The code modifications are discussed first, followed by the peripheral programs.

Further Development of DOT

With the advent of the IBM 360/75 computer with bulk storage at ORNL, it became possible to perform very large DOT problems (those requiring greater than 80-K but less than 325-K storage locations) and to maintain more data in computer memory. Thus, rather than storing particular data on tapes as has been required, DOT has been modified to attempt initially to maintain all data in core except cross sections, boundary fluxes, and sources. If DOT is unsuccessful in this

attempt, automatic procedures are effected wherein a second attempt to store data is made. Under these conditions, the tape storing and maneuvering of data (in particular, the flux and flux moments) is as formerly in DOT. The desired effect of this innovation should be a decrease in the computation time for some problems. This advantage should be realized to a greater extent as more energy groups are used and as the number of outer iterations for convergence is increased.

The versatility of DOT has also been enhanced with the inclusion of an albedo boundary condition at the top, bottom, and right boundaries of a given configuration. This option allows a space- and energy-dependent albedo to be specified at the boundaries mentioned above. Based on the most recent outwardly directed angular fluxes, inwardly directed (with reference to the configuration) angular fluxes are returned isotropically, proportioned by the particular albedo. Because of the nature of the DOT flux solution sequence, the returning isotropic angular fluxes at the top and right boundaries are calculated from fluxes of the previous iteration of that energy group. Hence judicious care must be taken when using this option to be assured that the albedo condition is sufficiently satisfied, as the problem gives evidence of being converged.

SPACETRAN

A program has been written to calculate the neutron or gamma flux at arbitrary points in space exterior to a two-dimensional right circular cylindrical system which has been calculated by the discrete ordinates code DOT. The output scalar flux tape from DOT contains for each group the scalar flux, the Legendre moments of the angular flux, and the emergent angular fluxes at the exterior surfaces. SPACETRAN reads the latter data, a group at a time, and performs the following calculations for each detector point which is uniquely defined by a radial and axial position:

1. The exterior surface is divided into a mesh using the DOT *r-z* mesh and an azimuthal angle mesh as shown in Fig. 3.3.1.
2. The code determines whether the detector is exposed to the top, bottom, side, or combination of side and end. A mesh sweep is then initiated over the end surface exposed, sweeping over 180° azimuthal angle and from center to outer radius. If the side is exposed, a similar mesh sweep is performed sweeping from bottom to top for only the azimuthal angle intervals that are exposed.
3. For each surface area interval in the sweep the vector **r** is calculated, along with its direction cosines μ and η relative to the two-dimensional calculation plane which is rotating with the azimuthal sweep.
4. Having the direction cosines of the vector connecting the area element and the detector, the code searches through the discrete ordinates direction set for the direction having the minimum dot product with the vector **r**. Using the calculated angular flux for the selected direction, an equivalent point source for the area element ΔA is calculated by

$$q(\Omega) = \phi(\Omega)\ |\eta|\Delta A$$

for the ends and

$$q(\Omega) = \phi(\Omega)\ |\mu|\ \Delta A$$

for the curved side. Thus the contribution of the area element ΔA to the flux at the detector is given by

$$\phi_{det} = \frac{q(\Omega)}{|\mathbf{r}|^2}\ .$$

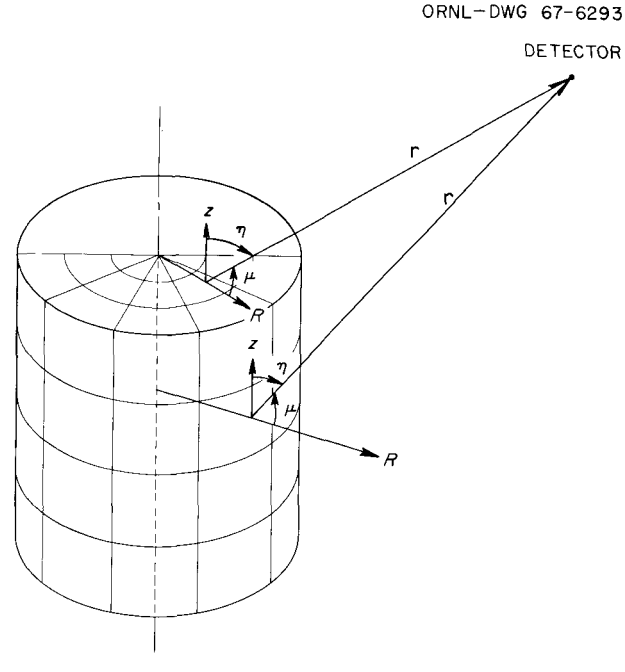

Fig. 3.3.1. A Representation of the Surface Mesh and Geometry for SPACETRAN.

In the manner described above, the contribution for each area element and energy group is calculated for each detector. For the most part the code has performed well; however, two difficulties have been observed: If the flux is essentially monodirectional over an area element (plane wave), the equivalent point source assumption is poor, and for detectors near the curved surface the size of the azimuthal intervals is very sensitive. The latter problem may be solved by using a variable mesh.

Neutron-Gamma Coupling Code

The use of discrete ordinates transport codes for the calculation of secondary gamma sources and the subsequent gamma-ray transport problem has become increasingly popular. The usual method of calculating the gamma sources involves the inclusion of activity cross sections, with each activity type corresponding to the yield for a particular gamma group. For one-dimensional problems these activities by interval and gamma group are punched on cards which are later read by a gamma problem as an isotropic fixed source. For two-dimensional calculations the tremendous volume of data requires that the gamma source be stored on tape by an activity routine. The subsequent gamma calculation reads the source tape and transfers the source information to the cross-section tape in the usual manner for a fixed-source problem. This source tape transfer method has been added to the production version of DOT and is being used for several problems.

Two new problems, the weight optimization of shields and the calculation of doubly differential neutron and gamma-ray albedos, made it very attractive, if not necessary, to run the neutron and secondary gamma problem in one calculation. The technique used for this purpose makes use of the idea that the differential transfer kernel $\Sigma(E' \rightarrow E, \Omega' \cdot \Omega)$ may represent not only the transfer of a particle from one energy-angle differential to another but also the transformation of a particle at E',Ω' to another particle at E,Ω. In particular, the treatment of secondary gammas usually assumes that the gammas are emitted isotropically in the laboratory system such that for neutron-gamma transfers the P_0 transfer coefficient is given by

$$\Sigma_0(E' \rightarrow E) = \Sigma_c(E')\, Y(E:E') ,$$

where $\Sigma_c(E')$ is the neutron reaction cross section at energy E' and $Y(E:E')$ is the gamma yield at gamma energy E per neutron reaction at E'.

A code named NγγN or NGGN has been written to assemble previously prepared neutron multigroup cross sections, gamma multigroup cross sections, neutron reaction cross sections, and gamma yield data into a single multigroup cross-section set of which the first groups are for neutrons and the following groups are for gammas.

MUG – A Multigroup Gamma Cross-Section Code

A FORTRAN IV program, MUG, has been written for the calculation of multigroup photon cross sections. The code resulted from extensive revisions of PROGRAM GAMMA[5] and is operational on IBM 7090, 360-50, and 360-75 computers. The output is in the form of a printed list and punched cards suitable for direct use in the discrete ordinates transport programs ANISN and DOT. The cross sections consist of multigroup, multitable Legendre transfer coefficients of the Compton scattering, pair-production transfer cross sections, and photoelectric-effect absorption cross sections.

The Klein-Nishina equation for the doubly differential scattering cross section is approximated by a Legendre polynomial series and is then integrated over the multigroup structure by double numerical integration using Simpson's rule, with the number of intervals in each integration used as input at execution time. The number of energy groups and the order of Legendre expansion are arbitrary (limited by program dimensions), and an arbitrary scalar weighting function may be used. The group-averaged photoelectric and pair-production cross sections are obtained by numerical integration of point values obtained from logarithmic interpolation of OGRE[6] data. Photons lost by pair production are re-emitted isotropically at the point of interaction as two new photons in the group containing 0.511 MeV (annihilation gammas).

The code will at user's option compute either energy flux or number flux cross sections. An energy absorption cross section is supplied with the number flux option. This includes energy deposited by photoelectric absorption, pair production, and Compton scattering. An additional option will generate cross sections for Compton scattering only for use with externally available absorption data.

References

[1]Computing Technology Center, Union Carbide Corporation, Oak Ridge.

[2]Consultant to ORNL.

[3]W. W. Engle, Jr., *A User's Manual for ANISN – A One-Dimensional Discrete Ordinates Code with Anisotropic Scattering*, K-1693 (1967).

[4]F. R. Mynatt, *A User's Manual for DOT – A Two-Dimensional Discrete Ordinates Code with Anisotropic Scattering*, K-1694 (in preparation).

[5]M. J. Stanley, *Klein-Nishina Photon Cross Sections (PROGRAM GAMMA)*, APEX-487 (May 1959).

[6]S. K. Penny, D. K. Trubey, and M. B. Emmett, *OGRE, A Monte Carlo System for Gamma-Ray Transport Studies*, ORNL-3805 (April 1966).

3.4 THE DISCRETE ORDINATES METHOD – SHIELDING APPLICATIONS

F. R. Mynatt[1] H. C. Claiborne
L. R. Williams[1] W. E. Ford, III[1]
M. Solomito

Calculation of the Off-Center-Line Fast-Neutron Dose in the Lid Tank Shielding Facility

With the completion of the first version of DOT,[2] a two-dimensional discrete ordinates transport code with anisotropic scattering, it was decided that the first comparison calculation should be a continuation of the extensive one-dimensional study of fast-neutron penetration in water.[3,4] A two-dimensional calculation was thus performed for the LTSF fission source plate (SP-2[5]) adjacent to one end of a large (160-cm-diam by 150-cm-length) right circular cylinder of water. The calculation contained 2660 space points, 27 energy groups, and used S10 (70 angles) quadrature and a P_2 expansion of the differential-scattering cross sections. The two-dimensional results are shown in Fig. 3.4.1 compared with a kernel integration which calculates the dose at a point (R,Z) by the equation

$$D(R,Z) = S \int_0^{2\pi} \int_0^{R_0} G(\rho)\, r\, dr\, d\alpha\ , \qquad (1)$$

where $G(\rho)$ is the point kernel for the fast-neutron dose at a distance ρ from a point fission source, R_0 is the radius of the source plate, and S is the source strength in neutrons cm^{-2} sec^{-1}. The point kernel $G(\rho)$ is taken from a one-dimensional ANISN S_{16}-P_3 calculation.[3,4] Since the same cross sections are used in the one- and two-dimensional calculations, the comparison reflects only the ability of the two-dimensional transport approximation compared with the kernel integration. The two-dimensional transport approximation, thus verified, may be used for problems in which kernel integration is inapplicable.

Calculations of the Reactivity Effect of Possible Shields on the TSF-SNAP Reactor

Since the TSF-SNAP reactor[6] is a high-leakage reactor, it was speculated that a wraparound shield might have a significant influence on the reactivity. A series of DOT[2] calculations were thus performed for the bare reactor with drums in (the only reasonable configuration for cylindrical r-z geometry) and for the same assembly with a "bucket" shield as shown in Fig. 3.4.2. The calculations contained 2365 space points for the reactor-shield assembly, 21 energy groups, S6 (30 angles) quadrature, a P_2 expansion of the scattering cross section, and solved, by source iteration, for the static multiplication factor k_0. Since the shield has a low-order effect on the fission distribution, a stringent point-wise convergence criterion was used on the inner iterations.

Three modifications of the bucket shield were calculated, the first having an inner radius of 30.21 cm, the second having an inner radius of 37.83 cm, and the third having an inner radius of 30.21 cm but with the tungsten (shown in Fig. 3.4.2) replaced by additional lithium hydride. Table 3.4.1 shows the results of these three calculations. The results indicate that a shield of this type does have a significant effect on reactivity and that the effect is sensitive to the radius and the type of material for the inner lining of the shield and can thus be easily controlled. The reactivity effect is decreased when the inner shield radius is increased, because more neutrons are allowed to escape through the open top. A larger reactivity decrease is noted when tungsten, a heavy scatterer which returns neutrons with slight energy degradation, is replaced with lithium hydride, which is characterized by forward scattering and large energy degradations.

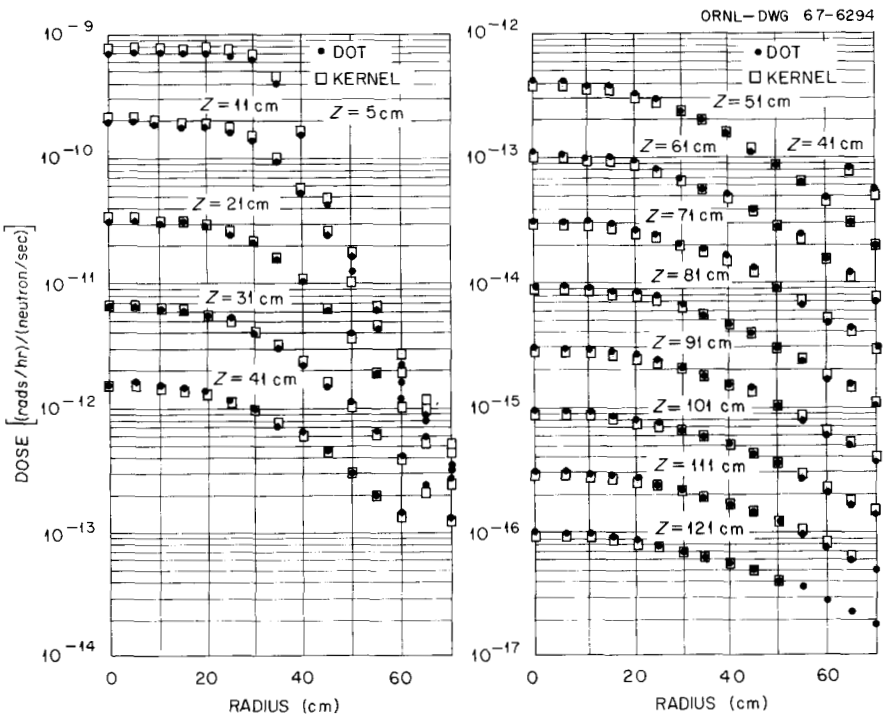

Fig. 3.4.1. Comparison of Fast-Neutron Dose Rates in Lid Tank Calculated with DOT Code and by Kernel Integration.

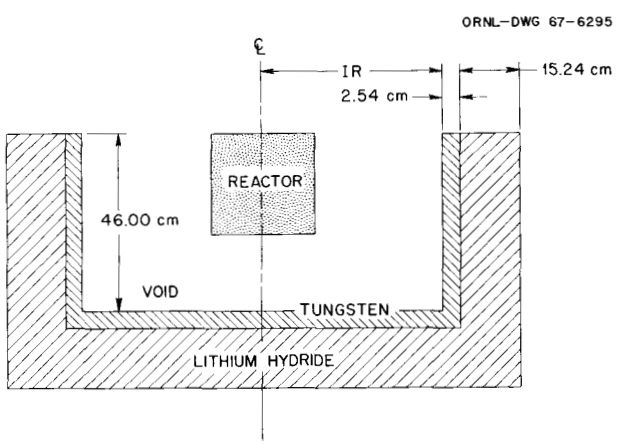

Fig. 3.4.2. Schematic Representation of the TSF-SNAP Reactor and a Cylindrical Bucket Shield.

Parametric Study of Asymmetric SNAP Shields

The completion of DOT, along with the development of convenient techniques for secondary gamma calculations, has made possible a study of several practical reactor-shield configurations. The basic purpose of the study is to provide data to indicate the feasibility of empirical design formulas and to serve as a basis for simplified transport calculations. A secondary purpose is the design of a high-efficiency shield by trial and error. The parametric study consists of the following:

1. three SNAP reactor types representing current design ideas;
2. four core sizes for each reactor type (right circular cylinders with varying weight and diameter);
3. several shields for each type and size; although all types and sizes are not calculated with all shields, an overlap is maintained so that cross comparisons may be made;
4. for each shield, reactor type, and size the neutron and secondary gamma dose is calculated by SPACETRAN (Sect. 3.3) for detector positions along the axis at distances of 50, 100, 150, and 200 ft from the reactor center and along the radius from reactor midplane for the same distance.

Table 3.4.1. Reactivity Effect of Three Shield Configurations on the TSF-SNAP Reactor

Shield	k_0	Percent change in k_0	$\Delta\rho$ ($\beta = 0.0065$)
None	1.022		
30.21-cm IR; W + LiH	1.041	1.84	\$2.72
37.83-cm IR; W + LiH	1.037	1.42	\$2.11
30.21-IR; LiH only	1.033	1.11	\$1.65

As an example of the data obtained from the study, the doses calculated for core type 1, which is a zirconium-hydride-moderated SNAP reactor, core size 1, and a type-3 asymmetric shield (see Fig. 3.4.3) are shown in Table 3.4.2.

Although the study is not yet complete, information from the first calculations is influencing plans for future shielding studies. Three of the most important shield charateristics thus disclosed are the following:

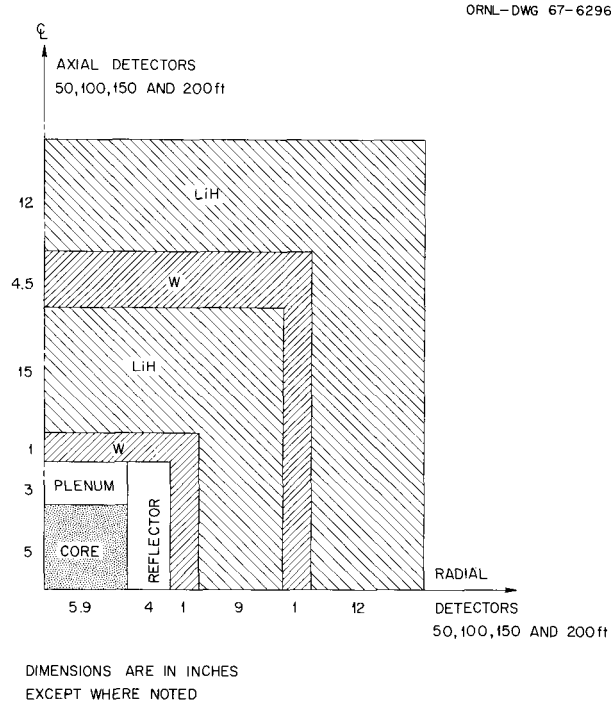

Fig. 3.4.3. Configuration of SNAP Reactor Type 1, Size 1, with Type-3 Asymmetric Shield.

Table 3.4.2. Calculated Neutron and Gamma-Ray Doses for SNAP Reactor Type 1, Size 1, with Shield 3

Detector Location (ft)	Neutron Dose (mrem hr^{-1} MW^{-1})	Gamma-Ray Dose (mrem hr^{-1} MW^{-1})
Radial Detectors		
50	385.9	11,761.0
100	92.65	2,803.7
150	40.63	1,226.8
200	22.71	684.76
Axial Detectors		
50	10.07	329.83
100	2.346	76.97
150	1.019	33.44
200	0.5667	18.60

1. As expected, secondary gamma dose is of greatest importance and the transport calculations must provide rigorous neutron transport, determination of secondary gamma sources, and gamma transport.

2. For this type of system the major part of the gamma dose (80-90%) is from gammas originating in resonance (nonthermal) capture in tungsten. For this reason much future work will be devoted to the resonance self-shielding effect and to the determination of gamma yield spectra as a function of neutron capture energy.

3. The design of asymmetric shields (e.g., axial-to-radial dose ratios of 10^{-2} or less) must be primarily based on two-dimensional calculations since radiation scattered from the radial shield toward the axial detectors (1 to 2%) may be greater than the dose transmitted through the axial shield.

Weight Optimization of Shields

Current methods used for weight optimization of shields use simplified functions to represent the radiation transport[7] and complex mathematical techniques for optimization.[8] However, the complexity of the transport problem for a high-efficiency shield suggests that a rigorous method should be used for the transport problem even if the numerical techniques preclude the attractive optimization techniques. A shield optimization program using discrete ordinates transport theory and an

automatic rule of thumb selection technique is thus under development. The method proceeds as follows:

1. A two-dimensional calculation (2D base case) is performed for a system having a reasonable shield configuration.
2. A one-dimensional base case is performed for the same system, and the results are normalized to the 2D base case. The 1D case is quite rapid and calculates both neutrons and gammas in one pass.
3. For each boundary of interest a one-dimensional calculation is performed with the boundary slightly displaced. The change of weight and dose for each boundary movement is thus determined, and a two-point approximation for dD/dW is obtained for each boundary.
4. A specified percentage, x, of weight is moved from the zone having the boundary with smallest dD/dW to the zone having the boundary with largest dD/dW. The amount of weight added to the zone with large dD/dW is less than the weight removed by the ratio (dD/dW small: dD/dW large). Thus there is a net weight loss and the total dose remains the same.
5. Steps 3 and 4 are repeated until all boundaries have essentially the same dD/dW and the shield has a minimum weight.
6. The optimized shield is calculated in two dimensions to see whether the initial normalization is still valid.

The sequence of steps 2-3-4 will be automated to be performed at one execution. Current work is proceeding toward an optimum shield based on the shield-3 calculation in the previous section using the sequence of steps listed above in a nonautomated procedure. Development is proceeding on the automated code.

References

[1]Computing Technology Center, Union Carbide Corporation, Oak Ridge.

[2]F. R. Mynatt, *A User's Manual for DOT – A Two-Dimensional Discrete Ordinates Transport Code with Anisotropic Scattering*, K-1694 (in preparation).

[3]F. R. Mynatt, W. W. Engle, Jr., and N. M. Greene, *Neutron Phys. Div. Ann. Progr. Rept. May 31, 1966*, ORNL-3973, Vol. I, pp. 43-44.

[4]F. R. Mynatt, N. M. Greene, and W. W. Engle, Jr., *Trans. Am. Nucl. Soc.* **9**, 366 (1966).

[5]D. R. Otis and J. R. Smolen, ORNL-CF-57-2-8 (classified); also D. R. Otis, *Appl. Nucl. Phys. Div. Ann. Report Sept. 10, 1956*, ORNL-2081, p. 163.

[6]J. Lewin, *TSF-SNAP Reactor Safety Analysis Report*, ORNL-4058 (in press).

[7]L. O. Ricks and R. K. Disney, *Trans. Am. Nucl. Soc.* **9**, 365–366 (1966).

[8]F. B. K. Kam and F. H. S. Clark, *Numerical Solution of the Lagrange Multiplier Problem with Several Constraints*, ORNL-3846 (1965).

3.5 MEASUREMENTS OF THE SPECTRA OF UNCOLLIDED FISSION NEUTRONS TRANSMITTED THROUGH THICK SAMPLES OF NITROGEN, OXYGEN, CARBON, AND LEAD: INVESTIGATION OF THE MINIMA IN TOTAL CROSS SECTIONS[1]

C. E. Clifford
F. J. Muckenthaler
R. M. Freestone, Jr.
E. A. Straker
V. V. Verbinski
K. M. Henry
W. R. Burrus

Minima in the total cross sections of nitrogen and oxygen have been investigated by measuring the spectra of uncollided fission neutrons transmitted through thick samples of the elements and by comparing the results with calculated spectra based on total cross sections only. Good agreement between the measurements and calculations was obtained for oxygen when the cross sections evaluated by Slaggie and Reynolds were used and for nitrogen when the cross sections measured by Foster and Glasgow were used. Calculations with other evaluated cross sections for these elements resulted in significant differences and indicate a lack of detailed knowledge of the valleys in the cross-section data. Measurements made for carbon and lead were in good agreement with calculations, as was expected since the cross sections for these elements are well known. The technique used for the spectral measurements employed an NE-213 proton-recoil spectrometer of high sensitivity.

Reference

[1]Abstract of *Nucl. Sci. Eng.* **27**, 299–307 (1967); work funded by Defense Atomic Support Agency under DASA Task Number A2-11.037.

3.6 EXPERIMENTAL EVALUATION OF MINIMA IN TOTAL CROSS SECTIONS[1]

E. A. Straker F. J. Muckenthaler
J. L. Hull K. M. Henry
J. J. Manning R. M. Freestone, Jr.

The spectra of uncollided flux of neutrons transmitted through thick samples have been measured for several materials. The technique used in the measurements and the results obtained for N, O, C, and Pb are described elsewhere.[2] Because the samples were quite thick the spectra are sensitive to the minima in the total cross sections and because of good geometry the measured spectra depend only on the source spectrum and the total cross section of the sample. The energy range covered extends from 0.8 to 11 MeV. Thus a comparison of the measured spectra with calculations of the uncollided flux using a previously evaluated cross-section set is termed an experimental evaluation. Good agreement between the measured and calculated cross sections means that the valleys are adequately represented in the cross-section set. If there is disagreement, detailed information about the specific region of disagreement is not possible unless the minima are well separated. This is due to the relatively poor energy resolution of the spectral measurements. For nonisolated minima, only the general energy range in which the disagreement exists can be noted. (This limitation prevents the interpretation of these measurements as "cross-section measurements.")

Table 3.6.1 summarizes the comparison on an absolute basis of measurements and calculations. The material and thicknesses for which data were obtained are listed in columns 1 and 2. The remainder of the table lists the source of the total cross sections which were used to calculate the uncollided spectra and comments on the comparison. The limitations of the evaluation as discussed above should serve as a basis for interpreting and understanding the comments in the last column.

For notation purposes "slight or small disagreements" between the calculated and measured spectra is used to denote differences between the measured and calculated spectra of less than 20% (generally less than 5% effect in the total cross section). This notation is used only if there is a disagreement in one energy range but agreement for higher and lower energies.

Where possible, comparisons have been made with ENDF/B cross sections (only tape 102 was available at this writing). Comparisons with ENDF/B cross sections for the other materials will be made when additional tapes are provided; however, cross sections for Ca, Si, K, and Pb will not be provided in the ENDF/B file in the near future.[3]

In general there is good agreement between the measurement and the calculations. For every material except calcium (see remarks in Table 3.6.1) there is a sizable energy range over which there is good agreement. In general the region of disagreement is below 3 MeV, where there is considerable structure in the cross sections. The calculated spectra are low for every case in which there is disagreement (calcium excluded); this indicates that minima in the cross section are not adequately represented in the cross-section set, due to either lack of energy detail or lack of resolution of the valleys.

This technique of evaluating minima in total cross sections has been very useful in deciding which evaluated set of total cross sections is adequate for shielding calculations and thereby permitting an efficient updating of cross-section libraries by updating only those cross sections that are not adequate. It also provides information about the energy regions in which new cross-section measurements should be made.

References

[1]Work funded by Defense Atomic Support Agency under DASA Task Number A2-11.037.

[2]C. E. Clifford *et al.*, *Nucl. Sci. Eng.* **27**, 299–307 (1967).

[3]Cross Section Evaluation Working Group, Brookhaven National Laboratory, Newsletter 8 (April 1967) (unpublished).

3.7 SENSITIVITY OF CALCULATIONS OF NEUTRON TRANSPORT IN OXYGEN TO VARIOUS CROSS-SECTION SETS[1]

E. A. Straker M. B. Emmett[2]

A study of the sensitivity of a neutron transport calculation to the input cross-section set has been made for a point isotropic fission source

Table 3.6.1. Comparison of Calculated and Measured Spectra – Evaluation of Total Cross Sections

Sample	Thickness (cm)	Total Cross Sections Used in Calculations	Best Cross Section	Comments on Comparison of Spectra (Calculation Based on Best Cross Section)
Be	27.28	05R,[a] BNL,[b] ENDF/B[c]		Good agreement with all three cross sections; although there are some small differences, no one cross section is best
H_2O	20.32, 30.48	H: 05R; O: UNC,[d] 05R, KAPL[e]	O: KAPL	Good agreement for all energies; primarily another test of the oxygen cross sections (see oxygen sample)
LiH	10.16, 20.32, 15.24, 25.4	H: 05R; Li: 05R, ENDF/B		Good agreement for all energies; the Li cross sections in both 05R and ENDF/B are from the same source
Al	30.48	05R, ENDF/B	ENDF/B	Slight disagreement for energies between 1.6 and 3 MeV; cross section appears to be too high
Fe	20.32	05R, KFK[f] and BNL,[g] ENDF/B	KFK and BNL	Good agreement above 2.0 MeV but all cross sections are too high for lower energies
Ni	15.24	05R, BNL[g] and BNL,[h] FZK[i]	BNL[g] and BNL[h]	Good agreement above 2.5 MeV but cross section is too high for lower energies
Na	60.96	05R, ENDF/B, BNL[b]	ENDF/B	Slight disagreement in peaks at 1.7, 3.0, and 4.5 MeV
Ca	55.56 (chips)	05R, BNL[b] and ORNL[j]	BNL and ORNL	Sample was not "thick" because of voids; therefore the comparison is not very sensitive to cross section; approximately 20% disagreement in magnitude for all energies
K	76.2	05R, BNL[b]	BNL	Good agreement except for slight differences between 1 and 2 MeV
Mg	60.96	05R, BNL,[b] ENDF/B	BNL, ENDF/B	Good agreement for energies greater than 4 MeV; for lower energies the cross sections are too high
Zr	19.526, 39.0	05R, BNL[g]		Good agreement with both cross sections
Concrete	15.24, 30.48	O: KAPL; Others: 05R	Only set tried	Good agreement except for slight difference near 2.4 MeV, the valley regions of oxygen and carbon; requires further study
W	10.63	BNL[h]	Only one available	Good agreement except for energies less than 2.0 MeV
Sand (SiO_2)	55.56	Si: 05R; O: KAPL	Only set tried	Slight disagreement for energies around 2.4 MeV, the valley region of oxygen; requires further study
U^{238}	8.69	05R, ENDF/B		Very good agreement for both cross sections for all energies

Table 3.6.1. Continued

Sample	Thickness (cm)	Total Cross Sections Used in Calculations	Best Cross Section	Comments on Comparison of Spectra (Calculation Based on Best Cross Section)
Lead	2.45, 5.08, 7.62, 10.16, 20.32, 30.48	BNL,[h] BNL[h] and ORNL[k]	BNL and ORNL	Very good agreement at all energies when Pb^{208} cross sections[k] are used for energies less than 4.3 MeV; disagreement (see ref. 1 in text) for energies less than 2.0 MeV was eliminated
C	10.64, 20.32, 30.48	05R, ENDF/B	ENDF/B	Good agreement for both cross sections, with ENDF/B slightly better around 8 MeV (see ref. 1 in text)
N	60.96, 91.44	05R, UNC, ORNL[l]	ORNL	See ref. 1 in text
O	60.96, 91.44, 152.4, 182.88	05R, UNC, KAPL	KAPL	See ref. 1 in text; good agreement even for 5- and 6-ft samples
$Ni + H_2O$	Ni: 10.16; H_2O: 15.24	Ni: 05R, BNL[g] and BNL;[h] H: 05R; O: KAPL	Ni: BNL[g] and BNL;[h] O: KAPL	Primarily another test of nickel cross section; disagreement for energies less than 2.5 MeV

[a]D. C. Irving, *05R Cross Section Library, Memo 2*, Code Package CCC-17, Radiation Shielding Information Center, ORNL (1965).

[b]J. R. Stehn *et al.*, *Neutron Cross Sections*, Vol. I, 2d ed., Suppl. 2, BNL-325 (1964).

[c]ENDF/B Tape 102, Cross Section Library, Brookhaven National Laboratory.

[d]J. H. Ray, G. Grochowski, and E. S. Troubetzkoy, *Neutron Cross Sections of Nitrogen, Oxygen, Aluminum, Silicon, Iron, Deuterium, and Beryllium*, UNC-5139 (1965).

[e]E. L. Slaggie and J. T. Reynolds, *0-16 Fast Neutron Cross Sections and Legendre Moments*, KAPL-M-6452 (1965).

[f]S. Cierjacks *et al.*, *A Novel Method for Very High Resolution Cross Section Measurements*, KFK-453, Institut fur Angewandte Kernphysik, Karlsruhe (1966).

[g]M. D. Goldberg *et al.*, *Neutron Cross Sections, Vol. IIA*, BNL-325, 2d ed. (1966).

[h]D. J. Hughes and R. B. Schwartz, *Neutron Cross Sections*, BNL-325, 2d ed. (1958).

[i]J. J. Schmitt, *Neutron Cross Sections for Fast Reactor Materials*, KFK-120, Vol. I, Institute fur Neutronenphysik und Reaktortechnik (1966).

[j]P. H. Stelson, *Some Recent Nuclear Cross Section Measurements at ORNL Oct. 1, 1966 – Mar. 31, 1967*, ORNL TM-1801 (1967).

[k]J. L. Fowler, E. G. Corman, and E. C. Campbell, p. 474 in *Proceedings of the International Conference on Nuclear Structure, Kingston, 1960*, University of Toronto Press, Canada.

[l]J. W. Craven, private communication concerning evaluated cross sections submitted to ENDF/B library.

in liquid oxygen. The importance of adequately representing the energy structure and of updating cross sections in transport codes is demonstrated by comparing dose and spectra calculated with four different sets of oxygen cross sections.

The 05R Monte Carlo code[3] was used in the investigation because of the ease of inputting cross sections and because of the detail in which cross-section data can be utilized. The complete detail available in the cross-section sets was used in the calculations; a set includes both the total and all the partial cross sections in a given evaluation. In addition, a comparison was made of the Monte Carlo calculations with the results of an $S_{16}P_3$ discrete ordinate calculation[4] which used fine-group GAM[5] cross sections that were updated[6] in the 5- to 7-MeV energy range.

Figure 3.7.1 illustrates the wide variation in the results of the calculation of the dose versus depth obtained with flux-to-dose conversion factors from

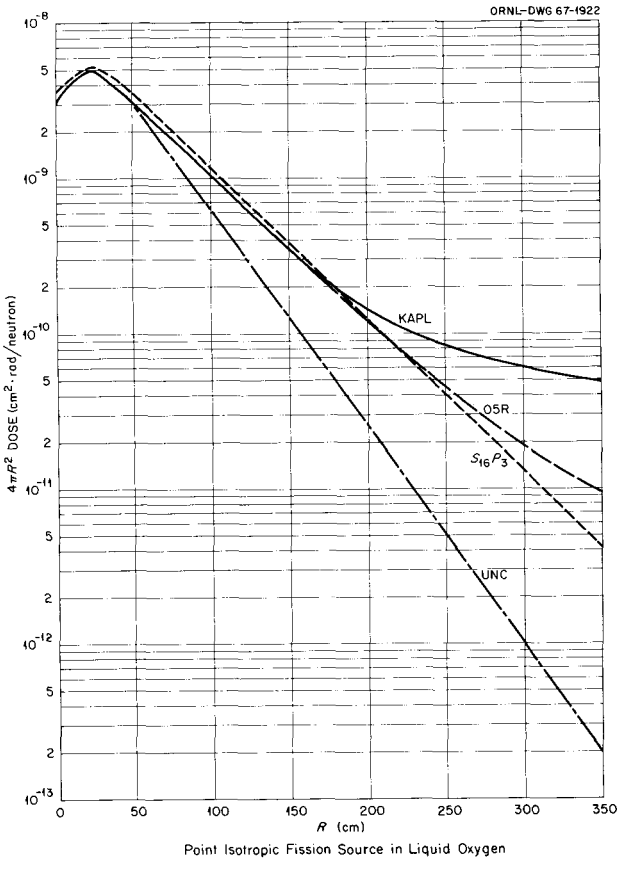

Fig. 3.7.1. Neutron Dose versus Depth in Liquid Oxygen Calculated with Various Cross-Section Sets for a Point Isotropic Fission Source.

ref. 7. At deep penetrations (greater than R = 200 cm) the divergence between the calculations using KAPL[8] and 05R[9] cross sections is primarily due to differences in the slope of the uncollided doses; this results from the fact that the neutrons which penetrate this far have energies around 2.37 MeV, the energy of the deep valley in the total cross section. At small distances the differences in the two cross-section sets have little effect on the dose.

The UNC cross sections[10] yielded results which are in considerable disagreement even relatively close to the source and are considered to reflect the lack of detail in representing the cross-section structure; this results in high values for the cross sections in the region of deep, narrow minima. The results of the $S_{16}P_3$ calculations agree with the results obtained with the 05R cross sections for attenuation factors up to ~100 but have a steeper slope for larger attenuations.

A comparison of the energy spectra at 200 cm illustrates differences which are correlated to the differences in the total cross section; that is, the peak in the spectra at 2.37 MeV is highest for the KAPL cross sections and lowest for the UNC cross sections. Similarly, the spectrum in the energy range from 5 to 7 MeV is highest for the KAPL cross sections and lowest for the 05R cross sections. The relative variations in the total cross sections alone would account for these general differences.

The above comparisons indicate the importance of representing the minima in the cross section with adequate detail. Because of the lack of experimental data on neutron transport in liquid oxygen, there is no basis for determining which cross-section set yields the best results; however, the KAPL total cross sections have been shown to give good agreement with measured uncollided spectra.[11] Even though neutrons with energies around 2.37 MeV dominate the transport at deep penetrations, the magnitude of the dose is also influenced by the partial cross sections.

References

[1]Summary of paper to be presented at Thirteenth Annual Meeting of the American Nuclear Society, San Diego, Calif., June 11–15, 1967; to be published in *Trans. Am. Nucl. Soc.*, Vol. 10 (1967); funded by the Defense Atomic Support Agency under DASA Task Number A2-11.037.

[2]Mathematics Division.

[3]D. C. Irving *et al., 05R, A General-Purpose Monte Carlo Neutron Transport Code,* ORNL-3622 (1965).

[4]F. R. Mynatt, private communication.

[5]G. D. Joanou and J. S. Dudek, *GAM-II, A B_3 Code for the Calculation of Fast Neutron Spectra and Associated Multigroup Constants,* GA-4265 (1963).

[6]G. E. Whitesides, private communication.

[7]B. J. Henderson, *Conversion of Neutron or Gamma-Ray Flux Absorbed Dose Rate,* XDC 59-8-179 (1959).

[8]E. L. Slaggie and J. T. Reynolds, *O-16 Fast Neutron Cross Sections and Legendre Moments,* KAPL-M-6452 (1965).

[9]D. C. Irving, *05R Cross-Section Library Memo 2, Radiation Shielding Information Center,* Oak Ridge National Laboratory, Code Package CCC-17 (1965).

[10]J. H. Ray, G. Grochowski, and E. S. Troubetzkoy, *Neutron Cross Sections of Nitrogen, Oxygen, Aluminum, Silicon, Iron, Deuterium, and Beryllium,* UNC-5139 (1965).

[11]C. E. Clifford *et al.*, *Nucl. Sci. Eng.* **28**, 299 (1967).

3.8 CALCULATIONS OF THE EFFECT OF THE AIR-GROUND INTERFACE ON THE TRANSPORT OF FISSION NEUTRONS THROUGH THE ATMOSPHERE[1]

E. A. Straker F. R. Mynatt[2]

Two-dimensional discrete ordinates calculations have been performed for neutron transport in an air-over-ground geometry for water, dry sand, and wet sand. Results for a fission neutron source at 92 m above the ground interface are compared with infinite-air results. The calculated values of single-collision dose and thermal-neutron flux are compared with results from Operation BREN. Although the ground interface has a significant effect on the transport, the hydrogen content of the ground has an equally large effect. Agreement between calculations and the BREN results is quite good.

References

[1]Abstract of ORNL TM-1819 (in preparation); work funded by Defense Atomic Support Agency under DASA Task Number A2-11.037.

[2]Computing Technology Center, Union Carbide Corporation, Oak Ridge.

3.9 CALCULATIONS, USING THE ALBEDO CONCEPT, OF THERMAL-NEUTRON FLUXES, EPICADMIUM NEUTRON FLUXES, AND FAST-NEUTRON DOSE RATES ALONG THE CENTER LINES OF ONE-, TWO-, AND THREE-LEGGED SQUARE CONCRETE OPEN DUCTS; COMPARISON WITH EXPERIMENT[1,2]

R. E. Maerker F. J. Muckenthaler

Monte Carlo calculations, using previously determined differential albedo data for concrete,[3–5] in conjunction with the AMC duct code,[6] were made of the fast-neutron single-collision dose rates, epicadmium-neutron fluxes, thermal-neutron fluxes, and secondary gamma-ray wall-capture dose rates along the center lines of one-, two-, and three-legged rectangular ducts. The results are compared with those from a series of parallel experiments conducted at the Tower Shielding Facility, in which measurements were made with a Hurst dosimeter, cadmium-covered and bare BF_3 detectors, a boron filter spectrometer,[7] and a multicollision dosimeter.[8] For the particularly demanding source geometry and spectrum employed in these comparisons, agreement within about 25% over five decades of attenuation was attained for each neutron component.

References

[1]Abstract of ORNL-4147 (in preparation), which represents an amalgamation of *Nucl. Sci. Eng.* **27**, 423 (1967), "Neutron Fluxes in Concrete Ducts Arising from Incident Thermal Neutrons," *Nucl. Sci. Eng.* (to be published), "Neutron Fluxes in Concrete Ducts Arising from Incident Epicadmium Neutrons: Calculations and Experiment," *Nucl. Sci. Eng.* (to be published).

[2]Work funded by Defense Atomic Support Agency under DASA Task Number A2-11.037.

[3]R. E. Maerker and F. J. Muckenthaler, *Nucl. Sci. Eng.* **22**, 455 (1965).

[4]R. E. Maerker and F. J. Muckenthaler, *Nucl. Sci. Eng.* **26**, 339 (1966).

[5]W. A. Coleman *et al.*, *Nucl. Sci. Eng.* **27**, 411 (1967).

[6]R. E. Maerker and V. R. Cain, *AMC: A Monte Carlo Code Utilizing the Albedo Approach for Calculating Neutron and Capture Gamma-Ray Distributions in Rectangular Concrete Ducts,* ORNL-3964 (1967).

[7]T. V. Blosser and R. M. Freestone, Jr., *Neutron Phys. Div. Ann. Progr. Rept. Aug. 1, 1965,* ORNL-3858, Vol. I, p. 59.

[8]T. V. Blosser, *Neutron Phys. Div. Ann. Progr. Rept. May 31, 1966,* ORNL-3973, Vol. I, p. 60.

3.10 DIFFERENTIAL NEUTRON CURRENT ALBEDOS FOR CONCRETE IN THE INCIDENT ENERGY RANGE 0.5 eV TO 200 keV. I. DESCRIPTIONS OF MONTE CARLO CALCULATION AND TSF EXPERIMENT AND COMPARISON OF CALCULATED AND EXPERIMENTAL RESULTS[1]

W. A. Coleman R. E. Maerker
F. J. Muckenthaler

Extensive Monte Carlo calculations were performed to determine the distribution in energy and angle of neutrons reflected from steel-reinforced concrete for five incident directions and ten incident energy groups extending from 0.5 eV to 200 keV. The reflected distributions were determined in terms of a doubly differential albedo for each of 54 emergent directions for each energy group lying between and including the incident group and the tenth group (0.5 to 1.8 eV). The standard deviation of the doubly differential albedo averaged around 10%. The angular slowing-down density of the incident epicadmium neutrons within the slab was computed at 0.5 eV and used as the source distribution for a Monte Carlo single-velocity diffusion calculation using 0.025-eV cross sections. From the diffusion calculation the differential angular albedos of the reflected subcadmium neutrons and the depth distributions of captures occurring at subcadmium energies were obtained. Measurements of the differential angular albedo of emergent subcadmium neutrons due to a measured spectrum of incident monodirectional beams of epicadmium neutrons were performed at the Tower Shielding Facility in an experiment geometrically identical to that previously reported for incident subcadmium beams. Of the 35 common points of calculation and measurement, the two largest discrepancies were 23 and 36%; the remaining 33 comparisons produced a root mean square deviation of 4.5%.

Reference

[1]Abstract of ORNL-3967, Vol. I (1967); work funded by the Defense Atomic Support Agency under DASA Task Number A2-11.037.

3.11 DIFFERENTIAL NEUTRON CURRENT ALBEDOS FOR CONCRETE IN THE INCIDENT ENERGY RANGE 0.5 eV TO 200 keV – VOLS. II–VI[1]

W. A. Coleman R. E. Maerker

These reports present the machine output in detail of Monte Carlo calculations of the doubly differential current albedos (i.e., differential in reflected energy and direction). Each volume gives the results for a different angle of incidence as follows: Vol. II, 0°; Vol. III, 45°; Vol. IV, 60°; Vol. V, 75°; and Vol. VI, 85°. The results in each case are for ten incident energy bands; the reflected energy structure is identical to the incident grouping, with the addition of a subcadmium group (reflected energies below 0.5 eV). The bulk of the calculations (reflected energies above 0.5 eV) were performed using the 05R computer code, while the diffusion at subcadmium energies was performed using a simple one-velocity model.

Reference

[1]Abstract of ORNL-3967, Vols. II-VI (1966); work funded by Defense Atomic Support Agency under DASA Task Number A2-11.037.

3.12 AMC: A MONTE CARLO CODE UTILIZING THE ALBEDO APPROACH FOR CALCULATING NEUTRON AND CAPTURE GAMMA-RAY DISTRIBUTIONS IN RECTANGULAR CONCRETE DUCTS[1]

R. E. Maerker V. R. Cain

This report describes the AMC code and is intended to serve as a reference manual to be used with the code. This code can be used to calculate the fluxes and dose rates inside large rectangular ducts constructed of concrete walls that arise from neutrons of all energies incident upon the duct mouth. An option in the code allows a simultaneous calculation of the secondary gamma-ray dose rates arising from wall capture as well. The code treats duct transmission by employing the albedo concept in conjunction with a Monte Carlo

treatment of history generation. The present description is limited to six distinct types of rectangular duct geometries, but includes ducts having up to three legs with two right-angled bends.

Reference

[1]Abstract of ORNL-3964 (in press); work funded by Defense Atomic Support Agency under DASA Task Number A2-11.037.

3.13 NEUTRON SPECTRA, AFTER VARIOUS ORDERS OF REFLECTION, FROM MONOENERGETIC SOURCE NEUTRONS REFLECTED BETWEEN TWO INFINITE PARALLEL CONCRETE SLABS[1]

R. E. Maerker

The calculations described in this summary were requested by L. V. Spencer.[2] The results are general enough, however, that they should provide considerable insight into the slowing-down properties of concrete ducts and entryways.

The problem is essentially to calculate the relative spectra of neutrons inside a cavity between two infinite parallel concrete slabs for various orders of reflection. The source is assumed to have a cosine angular distribution of incident neutron current with respect to a slab normal and to lie uniformly over both slab surfaces. The neutron spectral fluxes under these idealized conditions are independent of spatial position within the cavity, so that spatial coordinates are not necessary to determine the relative spectra.

The doubly differential albedos for concrete used in the AMC computer code[3] for incident energies from thermal to 10 MeV were incorporated into a Monte Carlo random-walk procedure similar to that used in AMC, except that the infinite slab geometry required that the incident polar angle for a particular reflection be the supplement of the reflected polar angle of the preceeding reflection. Incident and reflected energies were banded into the groups shown in Table 3.13.1.

At each reflection the statistical weight of a neutron was multiplied by the total current albedo for the particular incident energy group and incident polar angle. Statistical estimates were made to all possible reflected energy groups of the probability of reflection into each of these groups.

Table 3.13.1. Energy Group Structure

J	ΔE^J(MeV)	J	ΔE^J(keV)	J	ΔE^J(eV)
1	3–10	5	15–55	9	87–320
2	0.75–3	6	4.2–15	10	24–87
3	0.2–0.75	7	1.2–4.2	11	6.6–24
4	0.055–0.2	8	0.32–1.2	12	1.8–6.6
				13	0.5–1.8
				14	< 0.5

The reflected polar and azimuthal angles and reflected energy groups were sampled from appropriate distribution functions, and the random-walk procedure was continued until a source neutron had undergone 35 reflections. Fourteen problems were run, one for each source energy group J_0.

Typical spectral results are shown in Table 3.13.2 and Fig. 3.13.1, where the spectra after various orders of reflection are presented for the case $J_0 = 4$.

It can be seen from Fig. 3.13.1 that, even for source energies lying between 55 and 200 keV, approximately one third of the neutrons remaining after three reflections have already been thermalized, and only 4% still remain in the source energy group.

Figure 3.13.2 illustrates the rate of thermalization of various source energy groups with order of reflection. It is to be observed that roughly 90% of the reflected neutrons have been thermalized after two reflections for $J_0 = 13$ ($\Delta E_0 = 0.5$ to 1.8 eV) and after ten reflections for $J_0 = 1$ ($\Delta E_0 = 3$ to 10 MeV). Figure 3.13.3 shows, however, that the number of neutrons lying in the thermal group is about 40% of the source strength of neutrons lying in the $J_0 = 13$ group and is 4% of the source strength of neutrons lying in the $J_0 = 1$ group after the above orders of reflection. This results from the albedos being only of the order of 0.7 for all source energies (including thermal energy) since capture of thermalized neutrons occurs in the concrete with appreciable probability for neutrons of all incident energies undergoing a single wall reflection.

Since the albedos are relatively independent of incident energy, once thermalization occurs, the number of thermal neutrons existing in the cavity is sensibly independent of the original source energy for a given order of reflection. This surprising conclusion is verified by Fig. 3.13.3,

Table 3.13.2. Spectra as a Function of Order of Reflection for $J_0 = 4$ (25,000 Histories)

J	Reflected Neutrons Lying in ΔE^J Per Source Neutron for						
	1 Reflection	2 Reflections	3 Reflections	4 Reflections	5 Reflections	6 Reflections	8 Reflections
4	2.49×10^{-1}	6.47×10^{-2}	1.67×10^{-2}	4.24×10^{-3}	1.15×10^{-3}	2.90×10^{-4}	1.61×10^{-5}
5	1.63×10^{-1}	7.89×10^{-2}	2.90×10^{-2}	9.40×10^{-3}	2.85×10^{-3}	8.43×10^{-4}	6.07×10^{-5}
6	8.04×10^{-2}	6.43×10^{-2}	3.28×10^{-2}	1.35×10^{-2}	4.96×10^{-3}	1.66×10^{-3}	1.66×10^{-4}
7	5.82×10^{-2}	5.35×10^{-2}	3.29×10^{-2}	1.60×10^{-2}	6.79×10^{-3}	2.56×10^{-3}	3.47×10^{-4}
8	4.20×10^{-2}	4.68×10^{-2}	3.27×10^{-2}	1.83×10^{-2}	8.72×10^{-3}	3.76×10^{-3}	5.61×10^{-4}
9	3.21×10^{-2}	3.98×10^{-2}	3.13×10^{-2}	1.97×10^{-2}	1.03×10^{-2}	4.88×10^{-3}	8.57×10^{-4}
10	2.46×10^{-2}	3.34×10^{-2}	2.93×10^{-2}	1.99×10^{-2}	1.14×10^{-2}	5.82×10^{-3}	1.20×10^{-3}
11	1.90×10^{-2}	2.78×10^{-2}	2.63×10^{-2}	1.92×10^{-2}	1.19×10^{-2}	6.54×10^{-3}	1.53×10^{-3}
12	1.60×10^{-2}	2.47×10^{-2}	2.42×10^{-2}	1.86×10^{-2}	1.25×10^{-2}	7.28×10^{-3}	1.91×10^{-3}
13	1.17×10^{-2}	2.02×10^{-2}	2.11×10^{-2}	1.75×10^{-2}	1.24×10^{-2}	7.67×10^{-3}	2.21×10^{-3}
14	5.27×10^{-2}	9.81×10^{-2}	1.25×10^{-1}	1.32×10^{-1}	1.24×10^{-1}	1.08×10^{-1}	6.91×10^{-2}
Sum	7.48×10^{-1}	5.52×10^{-1}	4.01×10^{-1}	2.89×10^{-1}	2.07×10^{-1}	1.49×10^{-1}	7.79×10^{-2}
Albedo	7.48×10^{-1}	7.38×10^{-1}	7.27×10^{-1}	7.20×10^{-1}	7.17×10^{-1}	7.19×10^{-1}	7.25×10^{-1}

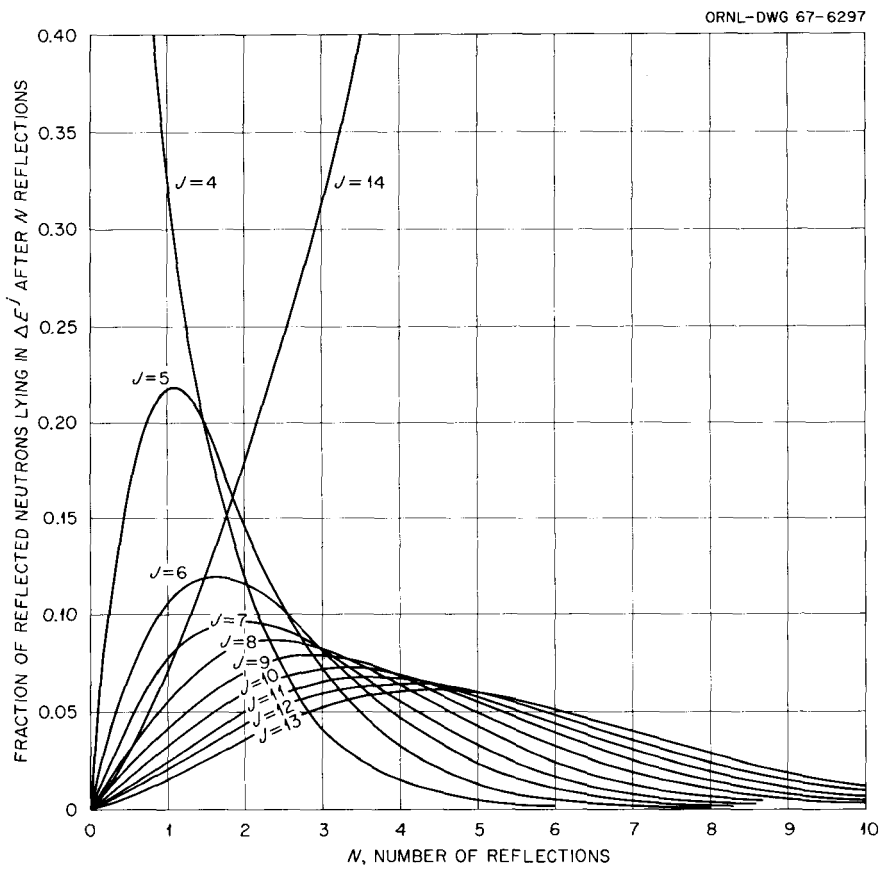

Fig. 3.13.1. Fraction of Reflected Neutrons Lying in the ΔE^J as a Function of Order of Reflection N for the Case $J_0 = 4$.

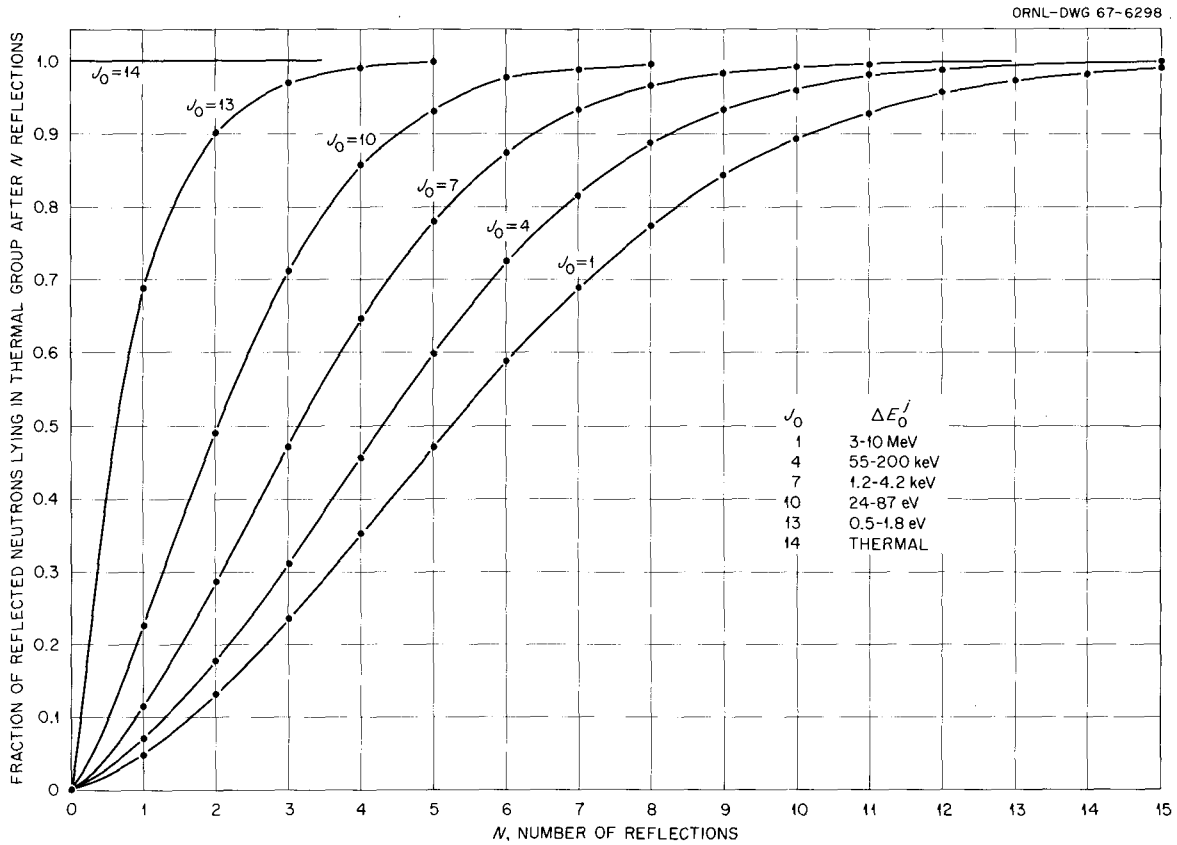

Fig. 3.13.2. Fraction of Reflected Neutrons Lying in Thermal Group After N Reflections for Various Source Energy Groups J_0.

where after about ten reflections the curves for all $J_0 \neq 14$ are seen to merge. The number of thermal neutrons remaining from a purely thermal source always remains slightly higher than that from a nonthermal source for a given order of reflection, but this difference is small.

A noteworthy conclusion to be drawn from this study is that, providing the differential angular albedos for nonthermal neutrons are not significantly different from those of thermal neutrons and hence that spatial considerations are not important, the thermal-neutron flux and associated secondary gamma rays arising from wall capture constitute the only important sources of dose deep inside a multilegged concrete duct, and these doses are essentially independent of the source spectrum at the mouth.

References

[1]Work funded by Defense Atomic Support Agency under DASA Task Number A2-11.037.

[2]L. V. Spencer, Ottawa University, Ottawa, Kansas, private communication.

[3]R. E. Maerker and V. R. Cain, *AMC: A Monte Carlo Code Utilizing the Albedo Approach for Calculating Neutron Capture Gamma-Ray Distributions in Rectangular Concrete Ducts*, ORNL-3964 (1967).

3.14 MEASUREMENTS AND SINGLE-VELOCITY CALCULATIONS OF DIFFERENTIAL ANGULAR THERMAL-NEUTRON ALBEDOS FOR CONCRETE[1]

R. E. Maerker F. J. Muckenthaler

Measurements and single-velocity Monte Carlo calculations have been performed to determine the differential angular thermal-neutron albedos for a reinforced concrete from monodirectional beams of incident thermal neutrons. Preliminary calculations using a statistical estimation technique indicate that up to 50 scatterings should be fol-

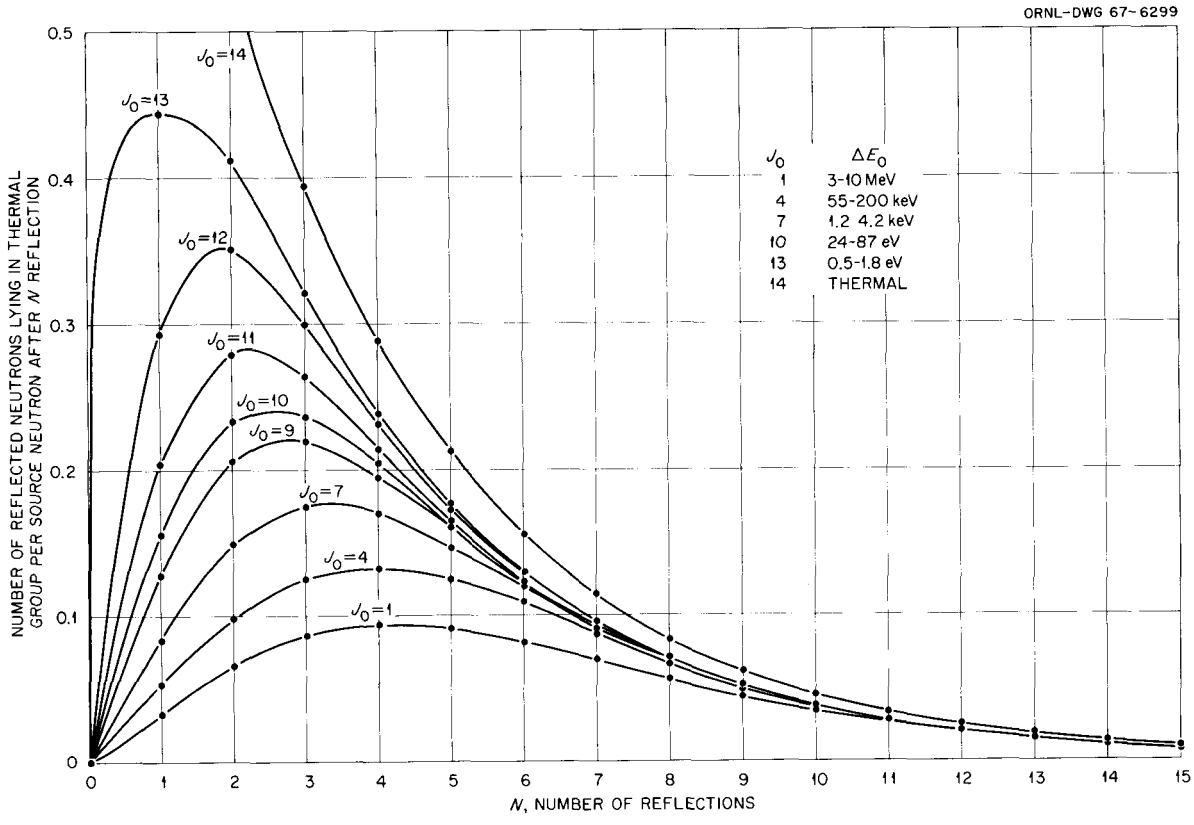

Fig. 3.13.3. Number of Reflected Neutrons Lying in Thermal Group After N Reflections Per Source Neutron Lying in Energy Group J_0.

lowed for each neutron in order to produce good estimates of the capture-gamma-ray differential dose albedos. Deviation between experiment and calculation can be reduced to an average of 4.1% for 72 points of comparison if an anisotropic-scattering law for water deduced from earlier Argonne National Laboratory measurements is assumed.

Reference

[1]Abstract of ORNL-4090 (in press); work funded by Defense Atomic Support Agency under DASA Task Number A2-11.037.

3.15 PRELIMINARY MEASUREMENTS OF THERMAL-NEUTRON CAPTURE GAMMA-RAY SPECTRAL INTENSITIES FROM SEVERAL SHIELDING MATERIALS[1]

F. J. Muckenthaler
J. J. Manning
J. L. Hull
K. M. Henry

As the initial part of a study on secondary gamma-ray production in shields, an attempt was made to measure the gamma-ray spectra resulting from thermal-neutron capture for a number of different shielding materials placed in a beam of neutrons from the TSR-II. Where possible, materials were chosen (1) to provide a single-energy gamma ray (due to

thermal-neutron capture) so that these results could be used to accumulate a series of response functions for a 3-in. NaI detector, (2) to have a known cross section for the interaction, (3) to have a known number of gamma rays emitted per thermal-neutron capture, and (4) to provide a range of gamma-ray energies sufficient to provide extrapolated response functions needed. Other materials were then chosen to test the response functions and verify their validity. The materials used are listed in Table 3.15.1.

Table 3.15.1. List of Shielding Samples

Sample	Thickness (in.)
Cement	1
Polyethylene	$\frac{1}{32}$, $\frac{1}{16}$, 2, 4
Fe	$\frac{1}{16}$, $\frac{1}{2}$, 1, $1\frac{1}{2}$
Al	$\frac{1}{4}$, $1\frac{1}{4}$, $2\frac{1}{2}$
Pb	$\frac{1}{4}$
Concrete	6, 9, 12, 18
Soil (TSF)	1
Sand	1
H_2O	1
Graphite	$\frac{3}{4}$
^{16}N (in circulating reactor water)	

A highly collimated beam of neutrons was obtained by placing a thick water shield adjacent to the 15-in.-diam beam port of the TSR-II beam shield as shown in Fig. 3.15.1. This additional shielding contained a stepped collimator with the neutron beam emerging through a duct $2\frac{3}{4}$ in. in diameter and 30 in. long. The thin-slab sample of material was placed in the beam at an angle of 45° to the beam center line in the horizontal plane.

The detector, a 3-in.-diam by 3-in.-long NaI crystal, was located inside a lead-water shield placed at an angle of 90° to the beam center line (45° with respect to the slab normal) so that the detector looked at the beam-emergent side of the slab. This geometry was chosen to minimize incidence of reactor capture and fission gamma rays on the crystal and to reduce to 0.5 MeV or less the energy of those gamma rays scattered by the sample to the crystal. The stepped collimator in the detector shield permitted the gamma rays to reach the crystal with minimum interference. A concrete block wall between the irradiated sample and the detector shield, containing another collimator, served to minimize the background reaching the crystal. Both collimator openings were sufficient to allow the crystal to view the full width of the slab sample. The neutron intensity incident on the crystal was reduced sufficiently by placing 2 in. of borated polyethylene in front of the detector shield collimator.

The profile of the thermal-neutron flux incident on the slab sample was mapped using bare and Cd-

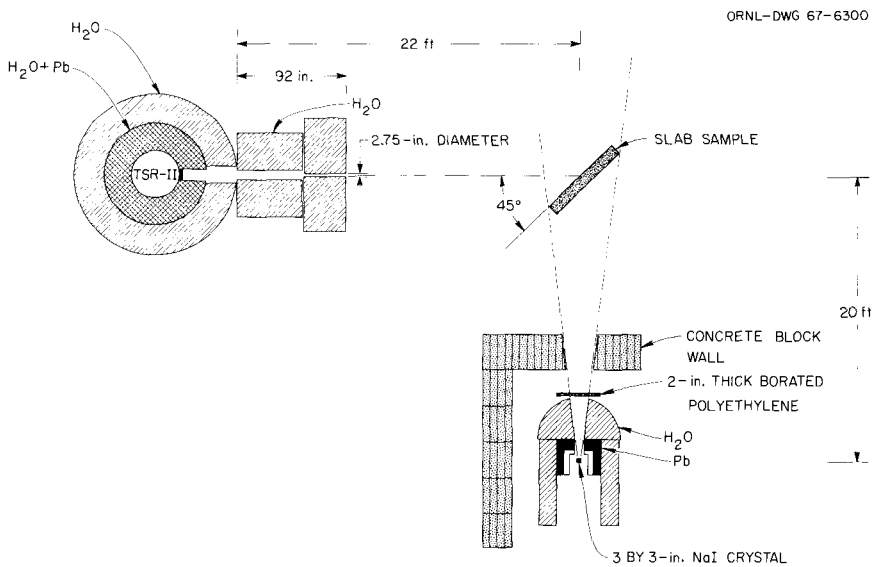

Fig. 3.15.1. Schematic Diagram of Geometry for Thermal-Neutron Capture Gamma-Ray Experiment.

covered spherical BF_3 counters. Traverses were made perpendicularly to the beam at the sample location, 14 ft 4 in. from the end of the $2\frac{3}{4}$-in.-diam collimator, in both the vertical and horizontal direction through the beam center line, and the intensity (bare – Cd readings) under this profile was determined through integration. The width of the beam was such that the width of the slab at 45° always exceeded it.

The relative response functions for the crystal obtained through the use of radioactive gamma-ray sources ^{137}Cs (0.661 MeV), ^{65}Zn (1.12 MeV), ^{60}Co (1.33 MeV), ^{24}Na (2.76 MeV), and the gamma ray from the decay of ^{16}N in the reactor water. The energy scale of the pulse-height spectra was checked several times daily through the use of the ^{60}Co gamma rays. The absolute response functions were determined using ^{65}Zn and thermal-neutron capture gamma rays from hydrogen (2.23 MeV), Pb (7.38 MeV), and Fe (9.29 MeV).

Spectral measurements were obtained for the samples shown in Table 3.15.1. The thicker samples were used either to increase the intensity of the source or to provide data for comparison with calculated results using the discrete ordinates and Monte Carlo methods. To determine the pulse-height spectra due to thermal-neutron capture only, data were obtained with and without cadmium over the reactor collimator, when the samples were in and out of the beam. A proper sequence of subtractions provided spectra of the gamma rays due to thermal-neutron capture.

A typical pulse-height spectrum obtained from thermal-neutron capture in a 9-in.-thick concrete sample placed in the beam is shown in Fig. 3.15.2.

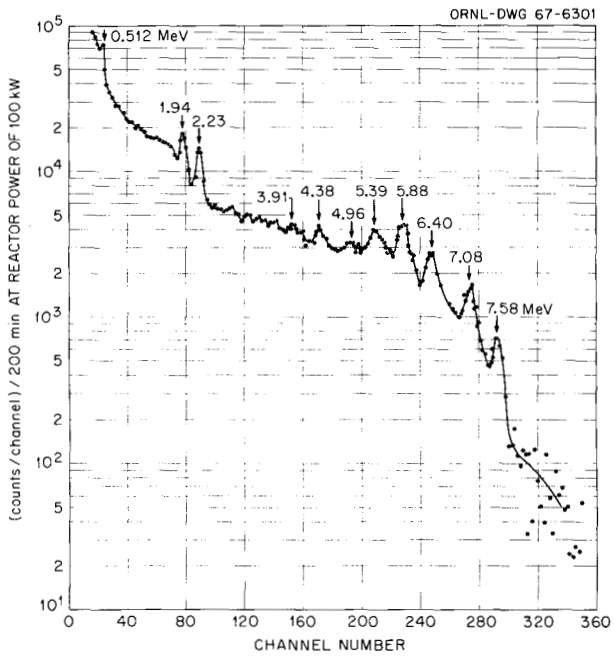

Fig. 3.15.2. Thermal-Neutron Capture Gamma-Ray Pulse-Height Spectrum for 9-in.-thick Concrete Slab Containing Iron Rod Reinforcements.

Reference

[1]Work funded by Defense Atomic Support Agency under DASA Task Number A2-11.037.

3.16 PRELIMINARY ANALYSIS OF THERMAL-NEUTRON CAPTURE GAMMA-RAY SPECTRAL INTENSITIES FROM SHIELDING MATERIALS[1]

R. E. Maerker

A preliminary analysis has been made of the experiments discussed in Sect. 3.15, which were performed at the TSF to determine the spectral intensities of gamma rays emitted following capture of thermal neutrons in various materials. It was hoped that the calculations would help to determine the accuracy of some existing tabulations of gamma-ray spectral intensities following thermal-neutron capture, of some existing tabulations of thermal-neutron capture cross sections, and of a single-velocity treatment of thermal-neutron diffusion through thick slabs in predicting secondary gamma-ray source intensities. It is further hoped that similar questions can be answered regarding secondary gamma-ray spectral intensities and neutron capture cross sections in the epi-cadmium energy range.

Details of the experiment are given in Sect. 3.15. The absolute response of the NaI crystal spectrometer was first determined for each of four monoenergetic gamma rays: the 1.12-MeV gamma ray following activation of ^{65}Zn, the 2.23-MeV gamma ray following thermal-neutron capture in hydrogen, the 7.38-MeV gamma ray following thermal-neutron capture in lead, and the 9.29-MeV gamma ray following thermal-neutron capture in iron. The number of photons incident upon the crystal for each of these sources was obtained in the latter three cases from a knowledge of the capture cross section and, in the case of iron, from recent spectral intensity measurements due to Bostrom.[2]

The slabs of polyethylene, lead, and iron were sufficiently thin that the incident thermal neutrons suffered few scattering collisions in the slab and the resulting capture gamma rays essentially none. Thus the calibrated responses do not depend on the use of a single velocity diffusion approximation to describe the transport of the thermal neutrons or on knowledge of the gamma-ray buildup within the slab. The absolute intensity of the total absorption peak was found to be a slowly varying function of source energy. Additional relative responses (i.e., shapes of the response functions only) were measured for four other source energies and were converted to absolute responses by interpolation along the total absorption peak curve. The absolute responses thus obtained are shown in Fig. 3.16.1.

A method of interpolation to any source energy in the range 1–10 MeV was devised using the curves of Fig. 3.16.1. It is based on the fact that the shape of the response is a more slowly varying function of the source energy than the absolute response itself. Thus linear interpolation of values a fixed number of channels from the total absorption peak is performed rather than interpolation of values at a fixed channel.

The accuracy of the response functions shown in Fig. 3.16.1, together with the interpolation scheme discussed above, was tested with two additional measurements. In the first experiment a $\frac{1}{16}$-in.-thick slab of iron was placed in the TSF collimated beam and the response of the spectrometer measured. Calculations were made of the expected response using the spectral intensities of Bostrom. The results are compared in Fig. 3.16.2. It is to be noticed that, except in the vicinity of the 9.29-MeV calibration line, where the two obviously must agree, the predicted response is consistently about 15% low but that the two shapes agree remarkably well. Since the spectral intensities used account for only 82% of the binding energy in iron, the calculated results could be brought into almost perfect agreement with the measured values by increasing the spectral in-

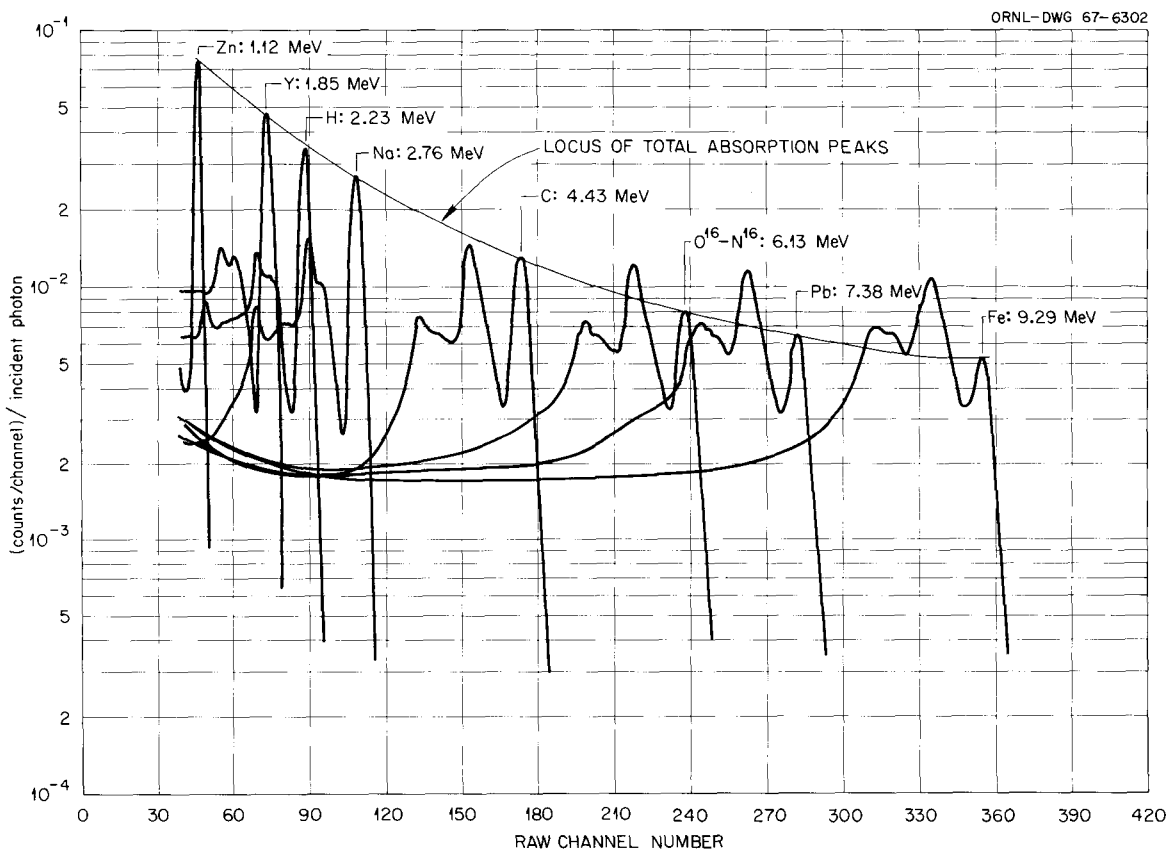

Fig. 3.16.1. Measured Responses of NaI Crystal to Gamma Rays in the Energy Range 1 to 10 MeV.

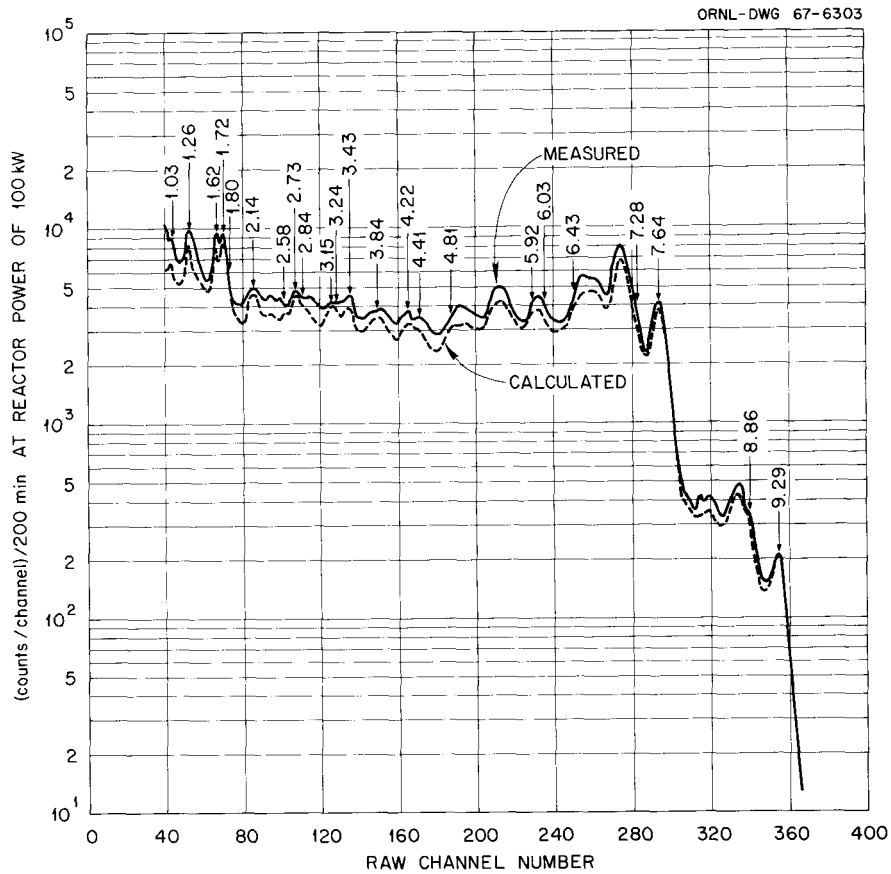

Fig. 3.16.2. Comparison of Measured and Calculated Spectrometer Response to Gamma Rays Arising from Thermal-Neutron Capture in Iron (Thickness of Iron Slab = $\frac{1}{16}$ in.).

tensities of Bostrom by 18% except for the 9.29-MeV transition. In all, some 23 transitions are involved in the region above 1 MeV, and the corresponding energies are depicted in Fig. 3.16.2.

In the second experiment, a $\frac{1}{4}$-in.-thick slab of aluminum was placed in the collimated beam and the response measured. Calculations were made of the response using spectral intensities previously reported by Groshev *et al.*,[3] and by Bartholomew and Higgs[4] and amended where applicable to include the later work of Draper and Bostrom.[5] The results are compared in Fig. 3.16.3. In all, some 35 transitions were included, the more important of which are labeled in the figure. Again, agreement is good, with the calculations consistently being about 10 to 15% low. The sum of all spectral intensities used accounts for 89% of the binding energy in aluminum. Comparison of the regions 4.2 to 6.2 MeV seems to indicate that the source intensities were somewhat underestimated in this range, but the overall agreement is very satisfying.

The tentative conclusion reached from the analysis of the iron and aluminum measurements is that the response functions and interpolation scheme are sufficiently accurate for analyzing complex spectra and that spectral intensities reported in the *Reactor Handbook*[6] can be in error by as much as 35% for the highest energy transitions.

Further measurements on gamma-ray responses following incident thermal-neutron capture have been made for several concretes and soils, in addition to thicker slabs of iron, aluminum, lead, and polyethylene. The analysis of these data has not yet been started.

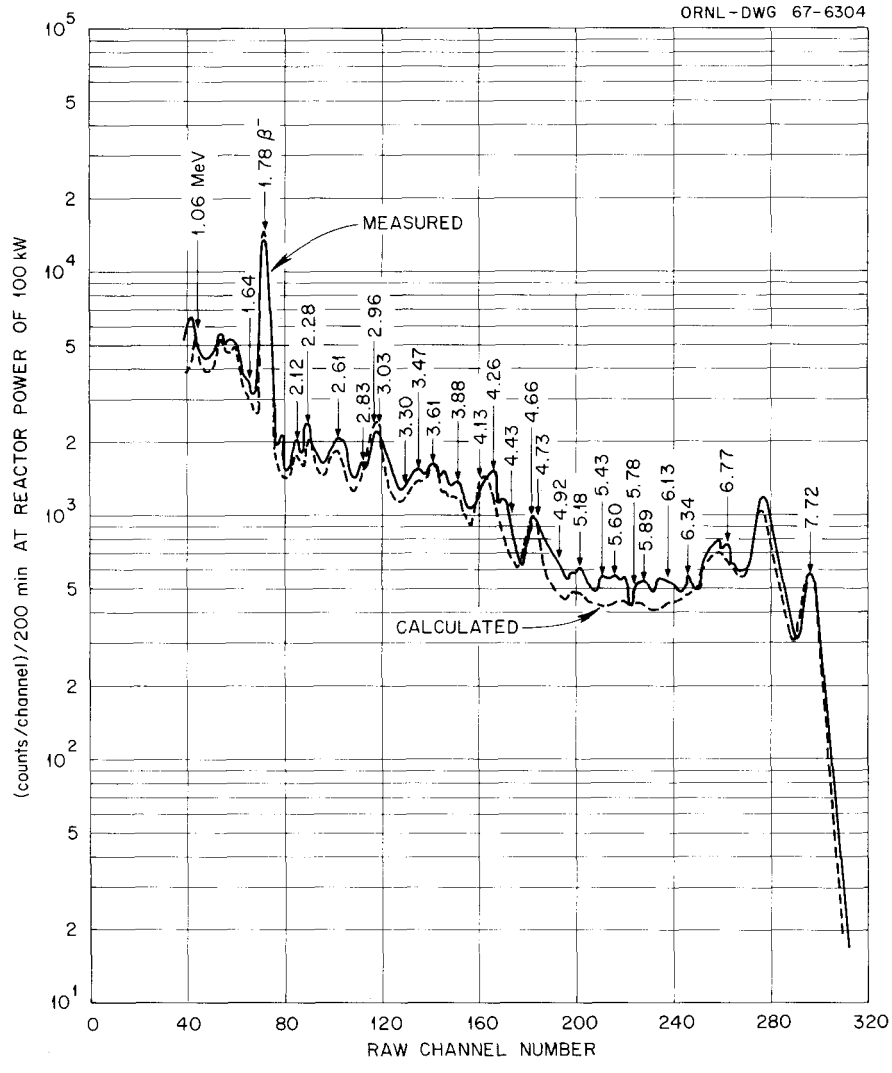

Fig. 3.16.3. Comparison of Measured and Calculated Spectrometer Response to Gamma Rays Arising from Thermal-Neutron Capture in Aluminum (Thickness of Aluminum Slab = $\frac{1}{4}$ in.).

References

[1]Work funded by Defense Atomic Support Agency under DASA Task Number A2-11.037.

[2]C. O. Bostrom, Ph. D. thesis, Yale University (1962).

[3]L. V. Groshev, B. P. Adyasevich, and A. M. Demidov, *At. Energ. (USSR)* **3**, 187 (1957).

[4]G. A. Bartholomew and L. A. Higgs, *Compilation of Thermal Neutron Capture Gamma Rays*, CRGP-784 (AECL-669) (1958).

[5]J. E. Draper and C. O. Bostrom, *Nucl. Phys.* **47**, 108 (1963).

[6]H. Goldstein, pp. 44–62 in *Reactor Handbook*, 2d ed., Vol. III, Part B, "Shielding," edited by E. P. Blizard and L. S. Abbott, Interscience, New York, 1962.

3.17 MULTIGROUP ^{6}Li AND ^{7}Li CROSS SECTIONS

N. M. Greene[1]

Recent successes[2] in predicting the fast-neutron dose through water suggest the use of the S_n method

for deep penetration problems. With the availability of large high-speed computers, such calculations can be very detailed and are comparatively fast. To check the feasibility of using the S_n codes for penetration problems involving lithium hydride, the one-dimensional S_n code ANISN[3] was used to calculate the dose from a point fission source in a large lithium hydride medium. An S_8 calculation with a P_3 expansion on all cross sections, as they are given in the GAM-II[4] library, was run.

A very precise Monte Carlo calculation for the same problem was performed by Kam and Clark[5] using the general-purpose Monte Carlo code 05R.[6] The calculation gave the fast-neutron dose rates out to 90 cm within an accuracy of ±10%. The most up-to-date cross-section data for lithium were used, and all important nuclear processes were treated in great detail. The ability of these cross sections to reproduce experimental results for shielding calculations was checked in a separate study.[7] The agreement between the S_8P_3 calculation noted above and these Monte Carlo calculations was very poor, the fast-neutron dose being underestimated by a factor of nearly 3 at 90 cm. Most of the disagreement can be traced to differences in the lithium cross sections used in the two calculations.

It was felt that the best way to compare an S_n calculation with the 05R calculation would be to take the raw 05R data and put them in the 100-group energy structure for the lithium cross-section sets which is identical with the 99-group GAM-II structure with one thermal group added. To accomplish this, the following major nuclear processes experienced by a neutron in lithium were used to produce group-averaged transfer matrices: elastic scattering, inelastic scattering $(n,n'\gamma)$, n-$n'\alpha$, n-$2n'\alpha$, and n-$2n'\gamma$ (for ^{7}Li only) reactions, and absorption ($n\gamma$, $n\alpha$, np, or nd as required).

Experience has shown that a P_3 expansion on cross sections used in the S_n codes is sufficient for calculating deep neutron penetration in water. The P_3 elastic-scattering matrices in a 100-group energy structure were produced by the cross-section averaging code TRANSFER,[8] using the f_8 center-of-mass expansion coefficients of the 05R data. These data were taken from BNL-400.[9]

The level-model data from 05R are used in the group-averaging code TACS[10] to obtain the inelastic-scattering transfer matrix. This process is assumed to be isotropic in both the center-of-mass and the laboratory system.

The $(n,n'\alpha)$ transfer matrix was obtained from the smoothed secondary neutron distribution curves of Rosen and Stewart as given in reports[11,12] on ^{6}Li and ^{7}Li respectively. A special routine was written to perform the required calculations.

Another special routine was written to get the $(n,2n)$ matrices, again using the recommended data of refs 11 and 12.

The cross sections for the absorption processes were obtained by averaging 05R data with the TACS code.

All the cross sections except those for elastic scattering were averaged over a fission spectrum from 15 MeV to 20 keV; a $1/E$ spectrum was used from 20 keV to thermal. TRANSFER allowed only $1/E$ weighting in calculating the elastic-scattering transfer matrices. In any event, the type of weighting will not be too important as most of the cross sections are fairly constant within a group.

The final cross sections were obtained by combining the elastic, inelastic, $(n,n'\alpha)$, and $(n,2n)$ matrices.

The results of an $S_{16}P_3$ calculation using these cross sections for the point source in a lithium hydride problem are given in Fig. 3.17.1. The flux to fast neutron dose conversion factors used in this calculation were obtained by averaging the Hurst dose factors[13] over a fission spectrum with the TACS code. As is shown, the agreement with 05R results leaves little to be desired. The relative ease of problem preparation and speed of the S_n codes should make these cross sections very useful in doing lithium hydride shield design studies involving fast-dose calculations.

References

[1]Computing Technology Center, Union Carbide Corporation, Oak Ridge.

[2]F. R. Mynatt, N. M. Greene, and W. W. Engle, Jr., *Trans. Am. Nucl. Soc.* **9**, 366 (1966).

[3]W. W. Engle, Jr., *A User's Manual for ANISN, A One-Dimensional Discrete Ordinates Transport Code with Anisotropic Scattering*, K-1693 (1967).

[4]G. D. Joanou and J. S. Dudek, *GAM-II: A B_3 Code for the Calculation of Fast-Neutron Spectra and Associated Multigroup Constants*, GA-4265 (1963).

[5]F. B. K. Kam and F. H. S. Clark, "Fission Spectrum Neutron Dose Rate Attenuation and Gamma-Ray Exposure Dose Buildup Factors," to

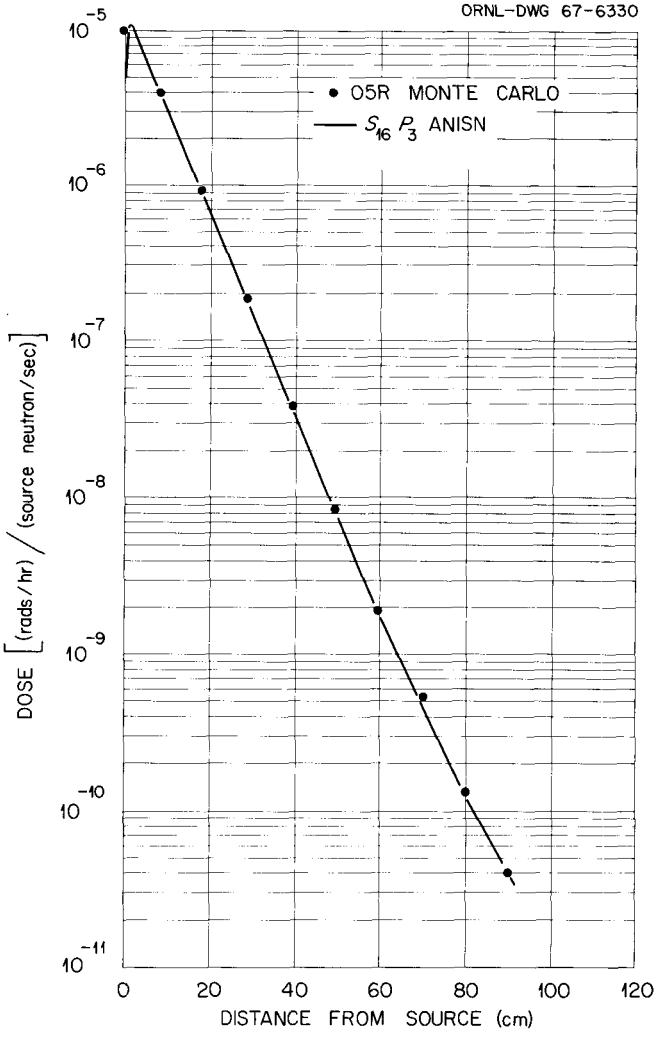

Fig. 3.17.1. Fast-Neutron Dose from a Point Isotropic Fission Source in Lithium Hydride (ρ = 0.75 g/cm^3).

be published in July 1967 issue of *Nuclear Applications.*

[6]D. C. Irving *et al., 05R, A General-Purpose Monte Carlo Neutron Transport Code,* ORNL-3622 (1965).

[7]F. H. Clark and F. B. K. Kam, *Neutron Phys. Div. Ann. Progr. Rept. Aug. 1, 1964,* ORNL-3714, Vol. I, p. 62.

[8]C. W. Craven, Jr., *TRANSFER: A Program to Calculate P_n Multigroup Scattering Matrices,* ORNL TM-1537 (1966).

[9]M. D. Goldberg *et al., Angular Distributions in Neutron-Induced Reactions, Volume I, Z = 1 to 22,* BNL-400 (1962).

[10]O. L. Smith, *TACS – A Code to Calculate Fast Reactor Group Cross Sections from Point Data for Primary Use in S_n Transport Codes,* ORNL TM-1610 (1966).

[11]E. D. Pendlebury, *Neutron Cross Sections of Li-6 in the Energy Range 0.001 eV – 15 MeV,* AWRE 0-60/64 (1964).

[12]E. D. Pendlebury, *Neutron Cross Sections of Li-7 in the Energy Range 0.001 eV – 15 MeV,* AWRE 0-61/64 (1964).

[13]H. Goldstein, *Fundamental Aspects of Reactor Shielding,* p. 18, Addison-Wesley, Reading, Mass., 1959.

3.18 SHIPPING CASK SHIELDING REQUIREMENTS

M. Solomito H. C. Claiborne

Present ICC regulations for shipping radioactive materials require that the gamma-ray dose rate not exceed 200 mr/hr or equivalent at any point on the surface of the shipping cask and 10 mr/hr at a distance of 3 ft from the surface. Various methods to determine the wall thickness required to attenuate the radiation to these acceptable levels are currently being compared since considerable interest has developed in shipping cask design. The lead thickness required to give a dose rate of 100 mrad/hr at the surface of a lead shipping cask was determined for various reactor operating times and fuel cooling times using the point kernel code QAD.[1] These results were compared with similar calculations made using the SDC code[2] and with values obtained from a nomogram by Zahn *et al.,*[3] which is based on a point kernel method but with an infinite slab geometry which has been proposed for use in preliminary design and evaluation as a reasonably good approximation.

It was found that the Zahn nomogram gave values of lead thicknesses which were either greater than or less than the QAD results, depending upon the reactor operating and cooling times. Generally, agreement in thickness was within 5%, with the extremes being −7.6% and +5.3%. In all cases the SDC code gave a lead thickness which was less than that calculated with QAD, the average being about 5% less and the maximum 7.6%. Some initial Monte Carlo and S_n calculations have been made in order to have a check on the point kernel method (Table 3.18.1). Additional work is in progress in order to complete the evaluation of the point kernel method for this application.

Table 3.18.1. Shipping Cask Radial Dose

Distance from Surface Source (ft)	Calculated Dose (mrad/hr)	
	QAD	S_n
0.0	103	116
0.1	94	88
0.4	75	75
0.8	59	57
1.0	53	51
1.5	42	41
3.0	27	24

References

[1]R. E. Malenfant, *QAD: A Series of Point-Kernel General-Purpose Shielding Programs*, LA-3573 (1967).

[2]E. D. Arnold and B. F. Maskewitz, *ADC, A Shielding-Design Calculation Code for Fuel Handling Facilities*, ORNL-3041 (1966).

[3]L. L. Zahn, C. L. Brown, and J. W. Langhaar, *Transportation of Radioactive Materials*, TID-8541 (1966).

3.19 NEUTRON FLUX-TO-DOSE CONVERSION FACTORS FOR TISSUE

J. J. Ritts[1] P. N. Stevens[2]
M. Solomito

Multicollision flux-to-dose conversion factors used to obtain the dose in tissue exposed to a neutron flux are being calculated. These factors, which are based on the energy deposited per unit mass in tissue, have previously been calculated by Snyder and Neufeld[3] by Monte Carlo techniques. The new calculations are being performed by the S_n technique, which solves the Boltzmann transport equation numerically. The S_n calculations yield the neutron and secondary gamma-ray flux distributions in various phantoms, and these fluxes are multiplied by single-collision flux-to-dose conversion factors to obtain the energy deposition (and consequently dose). These results, when properly normalized, are equivalent to multicollision conversion factors.

Some preliminary calculations have been made using the single-collision flux-to-dose conversion factors previously calculated by Henderson.[4] Calculations of new single-collision conversion factors for tissue are presently being made in order to improve upon existing calculations and to obtain these factors for various tissue compositions. Cross sections have been obtained for a tissue model which includes 12 elements. The code to compute the single-collision conversion factor based on the cross sections is presently being completed.

References

[1]University of Tennessee, Department of Nuclear Engineering.

[2]Consultant from University of Tennessee.

[3]W. S. Snyder and J. Neufeld, *Calculated Depth Dose Curves in Tissue for Broad Beams of Fast Neutrons*, ORNL-1872 (1955).

[4]B. J. Henderson, *Conversion of Neutron vs. Gamma Ray Flux-to-Absorbed Dose*, XDC 59-8-179 (1959).

3.20 A METHODOLOGY FOR CALCULATING NEUTRON CAPTURE GAMMA-RAY SPECTRA

K. J. Yost

A program has been initiated for the development of techniques for calculating neutron capture gamma-ray spectra. In particular, existing nuclear theories are being combined in such a way that collectively they will permit a systematic, albeit essentially phenomenological, approach to gamma spectrum calculations. The gamma cascade models under development at present include the following:

1. A continuum treatment which allows for both dipole and quadrupole transitions. Level densities for the continuum are calculated using either a "temperature" formula or Newton's formula which incorporates shell model parameters.
2. A continuum treatment which accounts for the experimentally observed enhancement of the high-energy portion of capture gamma-ray spectra as a function of proximity to the magic numbers. In this treatment cascade transition probabilities are related to the electric dipole giant resonance and associated strength function by way of the theorem of detailed balance.

The photonuclear cross section is extrapolated to energies of interest by either the Lorentzian or the "Lane and Lynn" line shapes. In order to generate transition probabilities for all possible combinations of nuclear excitation and gamma-ray energies, it is assumed that the photonuclear cross section is independent of target nucleus excitation. This appears to be a reasonable assumption from the nuclear theorists' standpoint.

3. A treatment which takes into explicit account the spin and parity of the compound nucleus energy states. Here, of course, it is assumed that capture is effected into discrete states whose spin and parity define, through the nuclear selection rules, allowed transitions to lower lying states. Electric and magnetic dipole and quadrupole transitions are allowed. At each stage of the cascade, a discrete energy level spectrum is constructed from a Porter-Thomas or chi-square distribution. The level spacing is a function of transition number and posttransition spin and parity probabilities.

3.21 *WEAPONS RADIATION SHIELDING HANDBOOK:* STATUS REPORT[1]

L. S. Abbott H. C. Claiborne
C. E. Clifford, Editors

At the request of the Defense Atomic Support Agency, the Neutron Physics Division, with the assistance of Radiation Research Associates, Inc., is preparing a handbook to aid engineers charged with the responsibility of designing shields to protect military equipment. The *Weapons Radiation Shielding Handbook* (to be identified as DASA-1892) will consist of two volumes, one presenting basic data and the other giving engineering methods.

The individual chapters are being issued as separate documents as they are completed. Chapter 5, "Methods for Calculating Effects of Ducts, Access Ways, and Holes in Shields," by Wade E. Selph and H. C. Claiborne, was issued in December 1966, and Chapter 4, "Neutrons and Gamma-Ray Albedos," by Wade E. Selph, was published in May. These two chapters, together with an introductory first chapter, will be combined with a chapter defining the radiation sources and environment at a shelter (Chapter 2) and a chapter outlining methods for calculating the attenuation of radiation through shield materials (Chapter 3) to form Volume I of the Handbook. Volume II will consist of two additional chapters (6 and 7) presenting engineering design methods that are based on the more sophisticated techniques described in Volume I. The intent is that the shield designer will use Volume I as a textbook and ready reference and Volume II as a guide for handling most of the problems with which he will be confronted.

Drafts of Chapters 2 and 3 have been prepared and are being revised. Chapter 6, "Shelter Design Against Fallout Radiation," and Chapter 7, "Shelter Design Against Initial Radiation," are partially complete; completed first drafts should be available by July 1.

Reference

[1]Work Funded by the Defense Atomic Support Agency under DASA Task Number A2-11.033.

3.22 PREANALYSIS OF TSF-SNAP EXPERIMENTS

V. R. Cain K. D. Franz[1]

As part of the preanalysis necessary for the SNAP experimental work to be started at the Tower Shielding Facility (TSF) in FY-1968, Hubner (see Sect. 3.23) made the necessary modifications to the O5R[2] and ACTIFK[3] Monte Carlo system. The calculations he performed to test the code modifications included several undesirable simplifications, such as a homogenized fuel region and a core geometry which assumed that the reactor control drums were completely inserted. Therefore the calculations have been repeated, removing all restrictions that seemed feasible. The new calculations include the power distribution in a reactor model with control drums out 30° and with a central beryllium rod, the leakage spectra at the reactor surface, the angular flux spectra to be measured by a collimated spectrometer viewing a small portion of the bottom face of the reactor, and the neutron dose penetration through a SNAP-2 shield. These data are expected to be put in published form before the experiment begins.

References

[1]Computing Technology Center, Union Carbide Corporation, Oak Ridge.

[2]D. C. Irving *et al., O5R, A General-Purpose Monte Carlo Neutron Transport Code,* ORNL-3622 (February 1965).

[3]F. B. Kam and K. D. Franz, *ACTIF, A General-Purpose Code to Analyze O5R Collision Tapes,* ORNL-3856 (September 1966).

3.23 CALCULATIONAL METHODS AND PRELIMINARY RESULTS FOR FAST-NEUTRON LEAKAGE FROM THE TSF-SNAP REACTOR[1]

R. S. Hubner[2]

The O5R Monte Carlo code and associated analysis codes were modified for use in the analyses of the ORNL TSF-SNAP experiments on the leakage of fast neutrons from a SNAP reactor. The reactor geometry is given in great detail. Anisotropic elastic scattering, beryllium $(n,2n)$ reactions, and inelastic scattering are thoroughly treated. Importance information obtained from adjoint S_n calculations was used to construct biased distributions in O5R for the selection of source neutron parameters and of neutron track lengths between reactions. Input instructions and listings for programs and subroutines that were developed are given in the appendices; flow diagrams for certain routines are also given. Power distributions, angular leakage flux, and fluxes viewed by collimated detectors were calculated for some preliminary analyses; O5R source neutron tapes for subsequent O5R calculations on the penetration of neutrons through a SNAP-2 shield were prepared. Requirements for the final analyses are given.

References

[1]Abstract of ORNL TM-1666 (in press).
[2]Atomics International.

3.24 DETERMINATION OF RESPONSE FUNCTIONS FOR THE SNAP COLLIMATOR

E. A. Straker M. B. Emmett[1]

The SNAP core-mapping collimator[2] is to be used in conjunction with the NE-213 proton recoil scintillator to determine the energy and angular distributions of neutrons leaking from the reactor. The collimator was designed[3] so that less than 5% of the flux at the detector is due to neutrons that have been scattered by or transmitted through the collimator itself. Nevertheless, it is still desirable to include the effect of the collimator in the predictions (Sects. 3.22 and 3.23) of neutron leakage from the core. Thus response functions which give the average flux over the surface of the detector as a function of the position of the neutron's last scattering event in the core have been calculated by Monte Carlo. The calculational model consisted of an isotropic ring source with a fission source energy distribution at various source distances Z from the collimator entrance. The direct, transmitted, and scattered components of the flux at the detector were determined for neutrons starting from a plane perpendicular to the collimator axis and within a ring centered about the collimator axis. These calculations determine the effective solid angle of the collimator system for any point in the reactor if interpolation of the response function is made for sources lying between the three planes for which calculations were made.

The Monte Carlo results were then reduced to a response relative to the geometrical response for an unshielded, uncollimated detector, but as a function of sin α, where α is the angle between the collimator axis and the ray between a point detector and the neutron collision point. These response functions are shown in Fig. 3.24.1. For source planes at 15.25 and 30.5 cm from the collimator entrance the relative response for a source on the collimator axis is greater than 1 because of scattering in the collimator. There is no contribution from transmitted flux for sources on the collimator axis since the whole detector surface is "visible." The general shape of the curve for sin $\alpha < 0.05$ is determined primarily by the variation of the direct flux alone due to a decrease in the fractional area of the detector which is "visible." For sin $\alpha > 0.05$ the response is due primarily to transmitted and scattered flux.

The response function for a neutron source on the axis a distance of 61 cm from the collimator entrance is less than 1.0 because the minimum opening in the collimator is smaller than the NE-213 detector. The response functions are slowly varying as a function of the source-collimator distance, and linear interpolation is assumed for distances other than those for which calculations were performed.

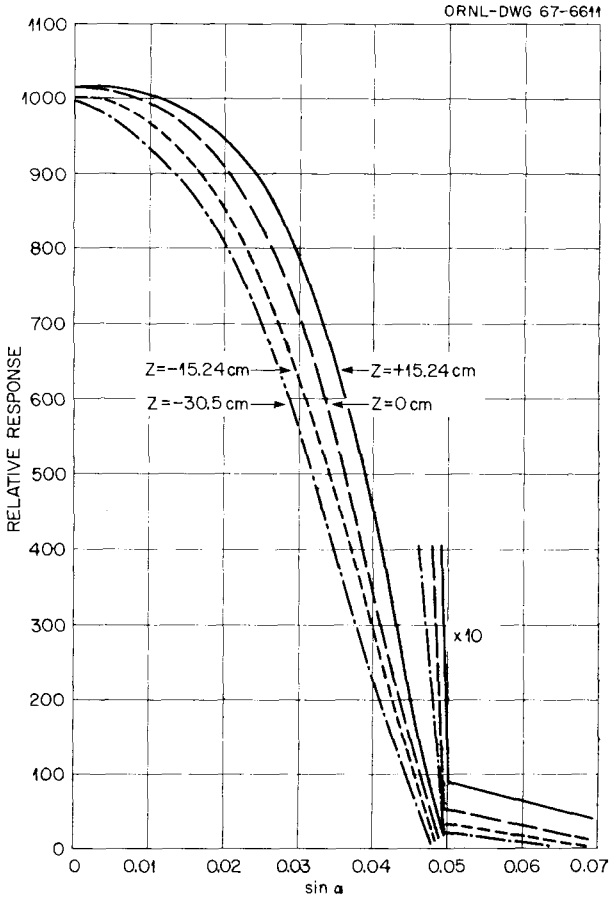

Fig. 3.24.1. Response Functions for SNAP Core-Mapping Collimator.

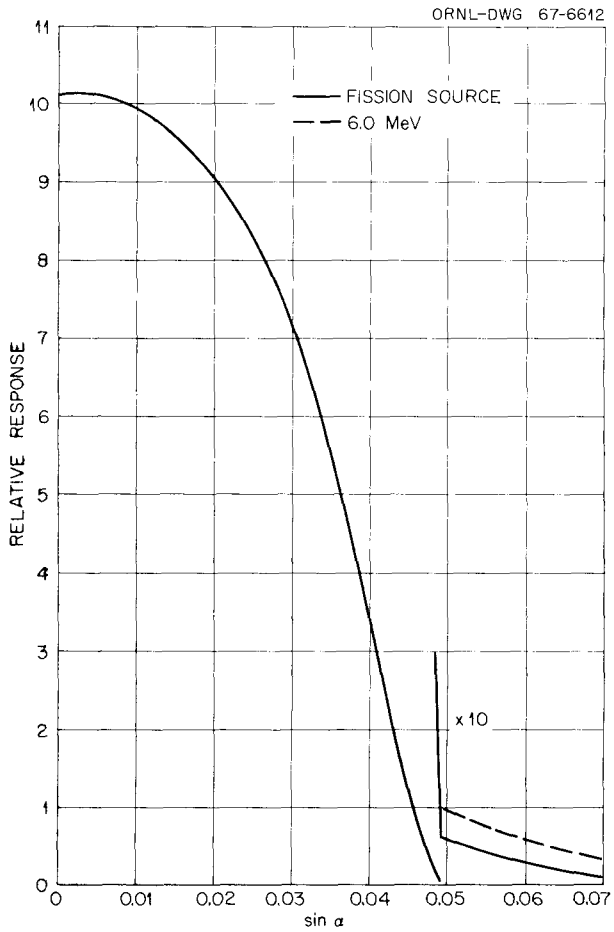

Fig. 3.24.2. Response Function for Fission and 6-MeV Source for $Z = 30.5$ cm.

To determine whether these response functions vary significantly with energy of the source neutrons, calculations were also made for one source plane location for a 6-MeV source. Figure 3.24.2 compares the response function obtained for a fission source and the 6-MeV source. It is noted that the major difference is for sin $\alpha > 0.05$; that is, the transmitted and scattered flux is higher and so the total unwanted flux is approximately 6% rather than 3%.

References

[1]Mathematics Division.

[2]E. A. Straker and M. B. Emmett, *Neutron Phys. Div. Ann. Progr. Rept. May 31, 1966,* ORNL-3973, Vol. I, p. 40.

[3]E. A. Straker and M. B. Emmett, *Trans. Am. Nucl. Soc.* **9**, 355 (1966).

3.25 INSTALLATION OF TSF-SNAP REACTOR

L. B. Holland J. Lewin
D. R. Ward

The TSF-SNAP reactor went critical on April 7, 1967. Experiments have been conducted to establish the reactivity worths of various materials both in and out of the core and to calibrate the effectiveness of the control drums. A core configuration has been established that includes a loading of 36 SNAPTRAN V fuel elements and one stainless steel rod with a small quantity of boron carbide in the center position.

The power distribution in the core has been mapped by scanning of gamma activity distribution in the fuel rods, by foil measurements, and by traversing with a small-diameter fission chamber.

Absolute power was calculated from measurements made with the small-diameter fission chamber and with fission foils, both of which were calibrated in a known thermal flux.

All control components of the reactor have been tested, and preparations are complete for welding of the NaK-containing envelope and charging the system with this coolant.

3.26 TIME-DEPENDENT NEUTRON TRANSPORT IN INFINITE AIR[1]

E. A. Straker M. B. Emmett[2]

Monte Carlo calculations of neutron transport in infinite air are being performed to determine the time dependence of both the spectral flux and dose for ranges up to 1500 m. Updated cross sections[3,4] are being used in O5R[5] and ACTIFK[6] for calculations of the transport of neutrons from both fission and 14-MeV sources.

Figure 3.26.1 illustrates the time dependence of the dose rate due to a 14-MeV point source for several ranges (air density of 1.22 mg/cm^3). The change in the shape of the dose rate curve with range indicates that the maximum dose rate shifts from the time of arrival of the 14-MeV neutrons at short ranges to a later time for the larger ranges. This is due to the change in the spectra that occurs with increasing range.

These time-dependent calculations are being extended to an air-over-ground geometry, and will also include the production and transport of neutron-induced gammas.

References

[1]Work funded by Defense Atomic Support Agency under DASA Task Number A2-11.037.

[2]Mathematics Division.

[3]E. T. Slaggie and J. T. Reynolds, *O-16 Fast Neutron Cross Sections and Legendre Moments*, KAPL-M-6452 (1965).

[4]C. W. Craven, private communication of nitrogen cross sections evaluated for ENDF/B library (1967).

[5]D. C. Irving *et al.*, *O5R, A General-Purpose Monte Carlo Neutron Transport Code*, ORNL-3622 (1965).

[6]F. B. K. Kam and K. D. Franz, *ACTIFK, A General Analysis Code for O5R*, ORNL-3856 (1966).

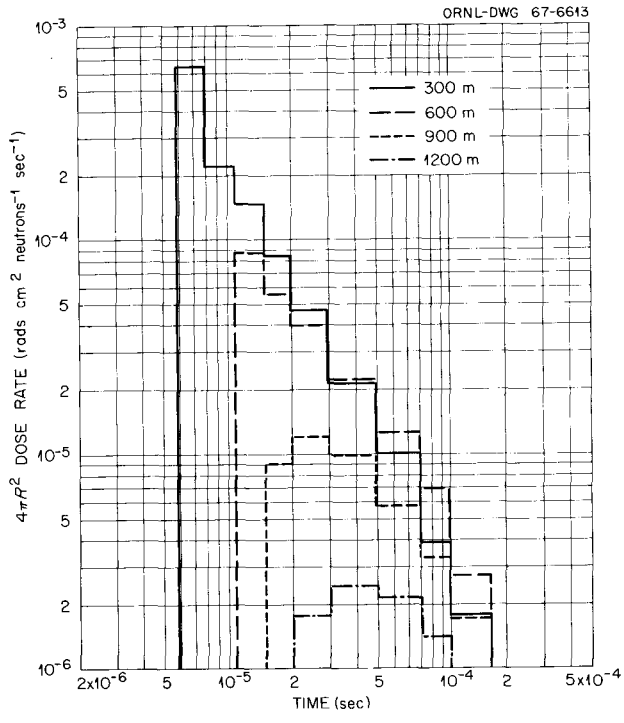

Fig. 3.26.1. Dose Rate vs Time for 14-MeV Source in Infinite Air.

3.27 GROUP AVERAGING OF CROSS SECTIONS FOR MULTIGROUP ADJOINT DISCRETE ORDINATES CALCULATIONS

F. R. Mynatt[1] W. W. Engle, Jr.[1]

The general energy-dependent reciprocity theorem is stated by the equation

$$\phi(r_1,E_1,\Omega_1;\, r_0,E_0,\Omega_0) = \phi^+(r_0,E_0,\Omega_0;\, r_1,E_1,\Omega_1)\,, \qquad (1)$$

where the term on the left is the flux at r_1,E_1,Ω_1 due to a unit source at r_0,E_0,Ω_0, and the term on the right is the adjoint flux at r_0,E_0,Ω_0 due to a unit source at r_1,E_1,Ω_1. The adjoint flux as defined above is in fact the Green's function for the flux at r_1,E_1,Ω_1. In the above notation the dose at a point r_d due to an isotropic source at r_s is given by

$$D(r_d) = \int_0^{4\pi}\int_0^{\infty}\int_0^{4\pi}\int_0^{\infty} DF(E) \times \phi(r_d,E,\Omega;\, r_s,E',\Omega')\, S(E')\, dE'\, d\Omega'\, dE\, d\Omega\,. \qquad (2)$$

Inserting Eq. (1) into Eq. (2) shows that the dose at r_d may also be given by

$$D(r_d) = \int_0^{4\pi}\int_0^{\infty}\int_0^{4\pi}\int_0^{\infty} S(E') \times \phi^+(r_s,E',\Omega';\, r_d,E,\Omega)\, DF(E)\, dE\, d\Omega\, dE'\, d\Omega' . \quad (3)$$

The quantity $D(r_d)$ may therefore be calculated by integrating either the dose factor $DF(E)$ with the flux from a forward calculation with a source, $S(E')$, or the source $S(E')$ with the Green's function from an adjoint calculation with a "source," $DF(E)$. The same relationship should hold true for forward and adjoint multigroup discrete ordinates calculations inasmuch as they are good approximations of the forward and adjoint Boltzmann equations. However, in the use of adjoint discrete ordinates calculations to determine the Green's function for the dose at deep penetrations in water, it was found that the dose determined by the two different methods differed by as much as a factor of 2.

After some investigation this discrepancy was attributed to the weighting of the multigroup cross sections. Most multigroup codes have as option an adjoint calculation, and all of these codes, when the option is used, merely transpose the scattering matrix. However, the adjoint of a matrix operator is the transpose only if the elements are self-adjoint. Unweighted multigroup transfer cross sections are self-adjoint, but weighted cross sections are not. Beginning with the adjoint Boltzmann equation and proceeding in the same manner as for deriving the forward multigroup equations, the following equation was obtained for weighting of the transfer cross section:

$$\Sigma_{G\to G'} = \frac{\dfrac{1}{\Delta u_G}\displaystyle\sum_{g\in G}\sum_{g'\in G'}\Sigma_{g\to g'}\,\phi^+_{g'}\,\Delta u_g}{\dfrac{1}{\Delta u_{G'}}\displaystyle\sum_{g'\in G'}\phi^+_{g'}\,\Delta u_{g'}}, \quad (4)$$

where the fine-group adjoint flux $\phi^+_{g'}$ is calculated using unweighted transfer cross sections $\Sigma_{g'\to g}$. Note that the transfer cross section is weighted over the sink group instead of the source group as for forward cross sections. It is for this reason that the transfer matrix elements are not self-adjoint.

In order to test the weighting method and the reciprocity theorem, four one-dimensional ANISN calculations were performed, a 99-group forward problem using unweighted cross sections, a 99-group adjoint problem using unweighted cross sections, a 27-group forward problem using cross sections weighted by the first problem, and a 27-group adjoint problem using cross sections weighted by the second problem. In the forward problems the source was an isotropic plane fission source at the left boundary of a water slab, and the dose 120 cm from the source was calculated using a single-collision dose factor. In the adjoint problems the "source" was the fast-neutron dose response at a plane 120 cm from the origin, and the dose was calculated by integrating the adjoint flux at the origin plane with the fission source. The results shown in Table 3.27.1 verify the use of the reciprocity theorem and the adjoint cross section weighting.

The spread in dose for the various calculations ($\sim$4%) when compared with the attenuation involved ($\sim 10^{-6}$–10^{-7}) is such that the answers may be considered to be identical. Besides the adjoint weighting of the transfer-cross-section matrix and the total cross section, it was found that the fission source which was integrated with the adjoint flux [similar to Eq. (3)] had to be weighted by the fine-group adjoint fluxes before use with the 27-group fluxes. This is merely the converse of the usual forward case in which the 27-group dose factors are weighted with the fine-group forward fluxes.

Table 3.27.1. Fast-Neutron Dose 120 cm from an Isotropic Plane Fission Source Calculated by Various Methods

Calculation Type	Dose Rate [rads hr^{-1} (source neutron)$^{-1}$ sec^{-1}]
Forward 99-group	1.23×10^{-12}
Forward 27-group	1.21×10^{-12}
Adjoint 99-group	1.26×10^{-12}
Adjoint 27-group	1.23×10^{-12}

The reciprocal calculations presented here are merely indicative of the large class of problems which may be solved by the adjoint method which gives a Green's function for a particular answer (i.e., the particular answer may be determined for any source configuration by merely integrating the source with the Green's function). However, adjoint problems are usually difficult to visualize, and adjoint weighting of cross sections may be necessary.

Reference

[1]Computing Technology Center, Union Carbide Corporation, Oak Ridge.

3.28 A USER'S MANUAL FOR ANISN, A ONE-DIMENSIONAL DISCRETE ORDINATES TRANSPORT CODE WITH ANISOTROPIC SCATTERING[1]

Ward W. Engle, Jr.[2]

ANISN is a FORTRAN IV, version 13, program which solves the one-dimensional Boltzmann transport equation for slab, cylindrical, or spherical geometry. As a secondary calculation the detailed flux generated as the solution to the Boltzmann equation may be used to perform a group reduction of the cross sections.

The user's manual describes in detail the format of the input data required to execute the many options available in the ANISN program. As an aid to understanding the data, the input and output of a sample problem are presented with comments.

References

[1]Abstract of K-1693 (Mar. 30, 1967).

[2]Computing Technology Center, Union Carbide Corporation, Oak Ridge.

3.29 MODIFICATION OF THE QAD-P5A CODE

M. Solomito J. R. Stockton[1]

The point kernel code QAD-P5A[2] has been converted for use on the IBM 360/75 computer. The code has also been modified to use the generalized geometry subroutines of the O5R code.[3] With the increased speed of the IBM 360 computer and the ability of the generalized geometry to describe arbitrary shapes, the overall versatility of the code is increased. Specialized O5R geometry routines such as the cylindrical and the spherical geometry have also been adapted for use with the QAD-P5A code in order to reduce the required running time when dealing with these particular geometries.

A lithium hydride kernel has been added to the QAD code for use in the neutron calculation. With this new kernel, the spectral changes associated with neutron penetration are based on lithium hydride transport data calculated by the moments-method code RENUPAK.[4]

References

[1]Mathematics Division.

[2]R. E. Malenfant, *QAD: A Series of Point-Kernel General-Purpose Shielding Programs*, LA-3573 (1967).

[3]D. C. Irving *et al.*, *O5R, A General-Purpose Monte Carlo Neutron Transport Code*, ORNL-3622 (1965).

[4]J. Certaine *et al.*, *RENUPAK, An IBM-704 Program for Neutron Moment Calculations*, NDA 2120-3 (December 1959).

3.30 ADJOINT AND IMPORTANCE IN MONTE CARLO APPLICATION[1]

R. R. Coveyou V. R. Cain
K. J. Yost

The use of the Monte Carlo method for the study of deep penetration of radiation into and through shields entails the use of sophisticated methods of variance reduction to make such calculations economical or even feasible. This paper presents an exposition of the most useful methods of variance reduction. The exposition is unified by consistent exploitation of adjoint formulations to estimate expected values, as in previous work, and further to evaluate the variance of the resulting estimates.

The connection between adjoint formulations and the choice of biasing schemes is also investigated. In particular, it is shown that the value function (the solution of the integral equation of the adjoint formulation) is always a good choice for importance function biasing; a sharp upper bound, independent

of the particular problem, is found for the resulting variance. Predicted (analytic) and experimental (Monte Carlo) results are also given for a simple one-dimensional problem.

Reference

[1]Abstract of ORNL-4093 (April 1967); also *Nucl. Sci. Eng.* **27**, 219–234 (1967).

3.31 APPLICATION OF S_n ADJOINT FLUX CALCULATIONS TO MONTE CARLO BIASING[1]

V. R. Cain

As part of the SNAP shielding program at ORNL, biasing techniques are being developed to routinely perform deep-penetration Monte Carlo calculations. Although many worthwhile biasing techniques are in use, the determination of useful (or even better, optimum) parameters for these techniques continues to be a problem. It has been known for some time that it is possible to calculate functions which would lead to good biasing procedures.[2,3] The technique uses a calculation of the solution to the inhomogeneous adjoint equation. This solution, called the "value function," represents the importance of a collision in the random walk to the desired answer, and can be used to obtain parameters for use in existing biasing techniques or as a guide to constructing desirable biasing techniques. This procedure has not been exploited since obtaining the complete value function is, on the average, just as difficult as obtaining the desired answer.

Recent work[4] has shown that the above procedure does not always lead to ideal biasing, but may give very good biasing. A practical approach is to calculate a value function with either a simpler physical model or a simpler geometry than that used in the transport calculation. The approach we have taken is to use a simpler geometry; the value function is obtained with a one-dimensional S_n code. The results are then used as biasing information for the three-dimensional Monte Carlo code. The value function has been used to obtain the biased source distribution in energy and to obtain parameters for an exponential transform which is dependent on energy and position.

Experimental data[5] taken at the Tower Shielding Facility were used for a test case. A 6-in.-diam neutron beam from the TSR-II was normally incident on the center line of a LiH SNAP-2 shield, which was surrounded by an iron and transformer oil collar. The SNAP-2 shield is about 63.5 cm thick and gives a dose attenuation of about 10^5. Measurements of fast-neutron dose rates were made with collimated detectors such that the dose from radiation leaving the LiH shield and that from radiation leaving the collar were obtained separately. The principal approximations in the Monte Carlo calculation were the use of a point source with an anisotropic angular distribution to mock up the actual source and the assumption of perfect collimation for the detector.

Table 3.31.1 gives results for this case. The second column gives results of a calculation (in the same units as the experimental data) which used biasing parameters determined from trial and error

Table 3.31.1. Comparison of Measured Kerma in Collar Shield Experiment to Calculated Kermas with Different Biasing Parameters (Arbitrary Units)

(Normal beam on shield center line, 10 in. Fe, 10 in. CH_2 collar)

	Measured	Monte Carlo Empirical Biasing	Monte Carlo Biasing Parameters from Value Function
Kerma leaving SNAP-2 shield	4.27	4.83 (23%)	4.42 (11%)
Kerma leaving collar shield	0.854	0.48 (36%)	0.59 (43%)
Running time (sec/history)		0.49	0.60

experience. The fractional standard deviation, in percent, is given in the parentheses. The last column gives results where the biasing parameters were obtained from the value function. Since the value function was obtained for a one-dimensional slab of LiH, the biasing may be expected to help only the calculation of radiation leaving the shield. As can be seen, the variance was reduced about a factor of 4 for this quantity but increased the variance for the radiation leaving the collar.

The theory predicts that if all the information contained in a precise value function calculation was used, the fractional standard deviation would have been less than 1%; thus there is a factor of 100 improvement in variance yet to be achieved. Future work will include splitting, Russian roulette, and angular scattering biasing to determine the practical limitation of achieving the theoretical variance.

References

[1]Summary of paper presented at Thirteenth Annual Meeting of the American Nuclear Society, San Diego, Calif., June 11–15, 1967; to be published in *Trans. Am. Nucl. Soc.*, vol. 10 (1967).

[2]H. Kahn, *Applications of Monte Carlo*, AECU-3259 (1954).

[3]G. Goertzel and M. H. Kalos, "Monte Carlo Methods in Transport Problems," *Progress in Nuclear Energy*, Series I, Volume II, *Physics and Mathematics*, Pergamon Press, New York, 1958.

[4]R. R. Coveyou, V. R. Cain, and K. J. Yost, *Nucl. Sci. Eng.* **27**, 219 (1967).

[5]F. J. Muckenthaler *et al.*, *Neutron Phys. Div. Ann. Progr. Rept. May 31, 1966*, ORNL-3973, Vol. I, p. 38.

3.32 DOUBLE-PRECISION VERSION OF O5R FOR IBM-360 SYSTEM

E. C. Long

After completing the transliteration of O5R for the IBM-360 computer in single precision, it was determined that a double-precision version would be desirable. A double-precision version of the routine was made in Fortran 360 and this was further modified to be compatible with Fortran 360-Fortran IV. The modification to the Fortran-360 version was necessary because of restrictions in the IBM Fortran-IV compiler. The Fortran 360-IV version has been turned over to RSIC for distribution. No further work is contemplated on the O5R transliteration.

3.33 CONTRIBUTIONS TO *ENGINEERING COMPENDIUM ON RADIATION SHIELDING*

Nine papers have been prepared by members of the Neutron Physics Division for inclusion in the *Engineering Compendium on Radiation Shielding*, a compilation of radiation shielding data which has been sponsored by the International Atomic Energy Agency, Vienna, and is being published by Springer-Verlag in Berlin. The editors are R. G. Jaeger, E. P. Blizard, A. B. Chilton, M. Grotenhuis, A. Honig, Th. A. Jaeger, and H. H. Eisenlohr. Contributions included from this Division are as follows:

"Ducts and Voids in Shields; Attenuation of Gamma Rays; Random Voids and Solids," W. R. Burrus

"Ducts and Voids in Shields; Attenuation of Neutrons; Random Voids and Solids," W. R. Burrus

"Neutron Streaming in Rectangular Ducts," R. E. Maerker, H. C. Claiborne, and C. E. Clifford

"Discrete Ordinates Method (S_n)," F. R. Mynatt

"Measurements in the Water Shield of the Bulk Shielding Reactor," F. C. Maienschein

"Prompt-Fission Gamma Rays," F. C. Maienschein

"Fission-Product Gamma Rays," F. C. Maienschein

"Photoneutrons," D. K. Trubey

"Combination Diffusion Methods," D. K. Trubey

4. Radiation Shielding Information Center

4.1 RECENT DEVELOPMENTS IN RSIC OPERATIONS

D. K. Trubey F. H. Clark
Betty F. Maskewitz

The Radiation Shielding Information Center continues to serve the technical community engaged in radiation shielding research and development.[1] This community represents a wide variety of interests, as indicated by the fact that RSIC is supported by three agencies: the Atomic Energy Commission, the National Aeronautics and Space Administration, and the Defense Atomic Support Agency. The people served by RSIC generally have interests in parallel with or are doing work for one of those agencies.

The international operations of the Center have continued to expand, partly as a result of a trip to Europe by two staff members to participate in a computer code seminar-workshop at the European Nuclear Energy Agency Computer Programme Library (ENEA-CPL) at Ispra, Italy. A number of shielding codes have been exchanged with European shielding groups and made generally available. Mr. Victor Bell, staff member of the ENEA-CPL, spent approximately a month with the RSIC staff acquiring experience with American-developed codes and helping to check out codes contributed from Europe. Mr. Hisao Yamakoshi, from the Ship Research Institute of Japan, has joined the RSIC staff for approximately a year to do work of mutual interest.

Other international activities of RSIC included computer searches of the literature file for foreign requesters, distribution of the monthly newsletter to about 140 foreign scientists and engineers, and receipt of several foreign reports and journal reprints.

Another phase of the Center's work which is continually growing is consultation with shield design engineers who are at the initial stage of design projects. It is here that the value of the computer code collection as an integral part of the Center's operations becomes most obvious. Generally, the Center can recommend specific codes to fill the requester's needs.

Evaluated Nuclear Data File

An important adjunct to any radiation transport computer code is the associated nuclear cross-section library. Unless continually updated and expanded, the library and hence the code which uses it tend to become obsolescent since improved cross-section data are constantly becoming available. The bewildering array of formats used in code development makes it nearly impossible to keep these libraries up to date. Therefore RSIC has been extremely interested in the efforts to produce a generally adopted computer-tape format which, in principle, could be used to make cross sections available to any laboratory (or computer code) by any group producing cross sections. The development of the Evaluated Nuclear Data File (ENDF) format by the AEC and contractors will provide a vehicle to communicate data of interest within the shielding community. To assure that the file will contain such data, a shielding subcommittee of the working group was appointed. The RSIC staff has been active on this subcommittee. Substantial progress has been achieved in adapting the file format to shielding needs, expanding the data file to give it the necessary scope for shielding, evaluating shielding data, and enlisting the cooperation of other groups with related needs.

Literature Store

The three sets of literature files, reactor-weapons, space-accelerator, and computer codes, have continued to increase. The new accessions were mainly current, although older literature is added as it comes to the staff members' attention. A new edition of the reactor-weapons bibliography[2] was published, and additional abstracts were issued to the holders of ORNL-RSIC-6.[3] The category list has been revised to include cross-section evaluations by integral experiment or transmission calculation, x-ray categories, and computer codes by name. The space-accelerator file is now about double the size it was when the first bibliography[4] was issued (November 1965); therefore the bibliography will probably be reissued sometime in 1967.

Newsletter

The newsletter, sent monthly to more than 900 persons and libraries, continues to carry the monthly accession list which alerts the community to new publications. A regular feature has been articles giving descriptions of current work and problems. This information has been solicited regularly.

Computer-Based Customer File

Person-to-person contact is an important aspect of the Center's operations. An important tool in this connection is the computer-based customer file and program for the IBM-360/50, which is capable of listing the customers with address, telephone number, and interests in any of several ways. For example, listings can be obtained by personal name, corporation name, country, zip code (in U.S.), or interests. Mailing labels are routinely printed by the computer.

An improved program for the Selective Dissemination of Information (SDI) has been put into effect, resulting in a 50% savings in machine time and other improvements. This program is used to print abstracts of literature entered into the system for direct mailing to persons whose interests correspond to the subject of the literature specimen. The SDI file has been merged with the customer file to yield one master file of persons who receive material from RSIC. The abstracts are printed on 5- by 8-in. cards with a "feedback" card attached. An analysis of the feedback cards is used to estimate the effectiveness of the SDI. The returned cards indicate that the recipients generally regard the abstracts as a valuable alerting service.

Code Section Operations

The computer codes collection[5-7] has continued to grow. As of April 30, 1967, 81 code packages have been assembled and are ready for distribution, with approximately 12 additional codes in various stages of checkout and packaging. On an average, approximately one code package is shipped from RSIC per workday. Each shipment normally represents the culmination of considerable information exchange between RSIC and the recipient. This information exchange continues so as to ensure the successful operation of the code by the recipient and to enable the RSIC staff to accumulate experience related to a particular code.

It was obvious as of last reporting that the activities of the codes collection have outgrown current record-keeping practices. New and more efficient methods have been initiated which should expedite processing of information and organization of records into automated systems.

The seminar-workshop method by which the originating installation places a computer code in the RSIC Code Collection has proved to be a practical and efficient means of communicating a great deal of information in a short time. Members of the RSIC codes section staff participated in a workshop-in-depth on a specific code in five different instances at the originating installation. Since considerable interest had been shown in the kernel integration code, QAD,[8] RSIC invited the originating group at LASL to present a seminar-workshop at ORNL in April of this year. By enlarging the scope to include discussions of applications of the code by other users and kernel integration as a method to design shields, additional information was exchanged by the 50 participants from 25 separate installations.

RSIC staff members continue to initiate and assist in the development of standards and practices (documentation and programming) that will facilitate the exchange of computer codes, as well as encouraging their adoption. A member of the staff serves on a subcommittee of the American Nuclear Society which was formed for the purpose of recommending practices in this area.

RSIC has initiated and continues to encourage periodic participation in the codes section work by interested members of the shielding community. Such members may be those who offer their services in checking out a specific computer code or those who want close coordination with RSIC staff members in learning how to use a code. Experience to date has demonstrated mutual profit from such cooperative effort.

References

[1]D. K. Trubey, *Nuclear News* **10**(1), 24 (1967).

[2]S. K. Penny, D. K. Trubey, and J. Gurney, *Bibliography, Subject Index, and Author Index of the Literature Examined by the Radiation Shielding Information Center*, ORNL-RSIC-5 (Rev. 1) (November 1966).

[3]*Abstracts of the Literature Examined by the Radiation Shielding Information Center*, ORNL-RSIC-6 (Vol. I) (Rev. 1) (September 1966).

[4]R. G. Alsmiller, Jr., F. S. Alsmiller, and J. Gurney, *Bibliography, Subject Index, and Author Index of the Literature Examined by the Radiation Shielding Information Center – Space and Accelerator Shielding*, ORNL-RSIC-11 (November 1965).

[5]D. K. Trubey, B. F. Maskewitz, and S. K. Penny, *Nucleonics* **24**(8), 112 (1966).

[6]B. J. Maskewitz, *Abstracts of Digital Computer Code Packages Assembled by the Radiation Shielding Information Center*, ORNL-RSIC-13 (January 1966).

[7]B. J. Maskewitz, B. L. McGill, and J. Gurney, *Bibliography of the Computer Codes Literature Examined by the Radiation Shielding Information Center*, ORNL-RSIC-15 (July 1966).

[8]R. E. Malenfant, *QAD: A Series of Point-Kernel General-Purpose Shielding Programs*, LA-3573 (April 1967).

4.2 REPORT OF A MEETING OF A WORKING COMMITTEE ON SHIELDING CONVENTIONS[1]

F. H. Clark

Staff members of RSIC met with various representatives of the shielding community and two members of the International Commission of Radiological Units and Measurements (ICRU) to discuss ways of standardizing the language and the quantities used in the communication of shielding information. Principal results of the meeting were as follows: A document will be written by RSIC interpreting ICRU nomenclature to the shielding community, especially as it affects buildup factors.[2] Recommendations will be made to the ICRU and to NBS concerning the gamma-ray energy deposition coefficients that are required in shielding. An attempt will be made to initiate a shield instrument standardization project. A study will be made of the importance of eipthermal neutrons in dosimetry. The need for additional neutron dose response functions will be explored.

References

[1]Abstract of ORNL-TM-1604 (Nov. 8, 1966).

[2]D. K. Trubey, *Use of ICRU-Defined Units in Shielding*, ORNL-RSIC-16 (in press).

4.3 USE OF ICRU-DEFINED UNITS IN SHIELDING[1]

D. K. Trubey

The recommendations of the International Commission on Radioiogical Units and Measurements (ICRU) promulgated in 1962 have not been generally adopted. By means of this document, RSIC is bringing these recommendations to the attention of the shielding community, and also making further recommendations regarding special concepts and nomenclature not covered by the ICRU.

Reference

[1]Abstract of ORNL-RSIC-16 (in press).

4.4 A MONTE CARLO CALCULATION OF THE COMPONENTS OF THE EXPOSURE IN A BASEMENT DUE TO FALLOUT[1]

D. K. Trubey

Since the standard technology[2] employed to estimate exposure in a fallout shelter, especially in a basement, does not treat geometry in sufficient detail to evaluate the various components, the Monte Carlo method has been employed to evaluate these components and to produce a total result

which can be compared with the results obtained with more conventional techniques. For this purpose a special version of the OGRE-G code,[3] which has a very general geometry capability, was used. The assumed geometry is shown in the inset of Fig. 4.4.1. The layer of concrete comprising the floor of the superstructure and the ceiling of the basement is 15 psf (lb/ft^2) thick. The ceiling of the superstructure is also of 15-psf-thick concrete, plus an additional layer of extremely high density concrete to remove the skyshine that penetrates the roof. The exposure at point *D* in the basement was obtained for wall thicknesses of 15, 30, and 60 psf. The source was taken to consist of 1.25-MeV isotropic sources uniformly distributed on the air-ground interface to a distance of 1000 m.

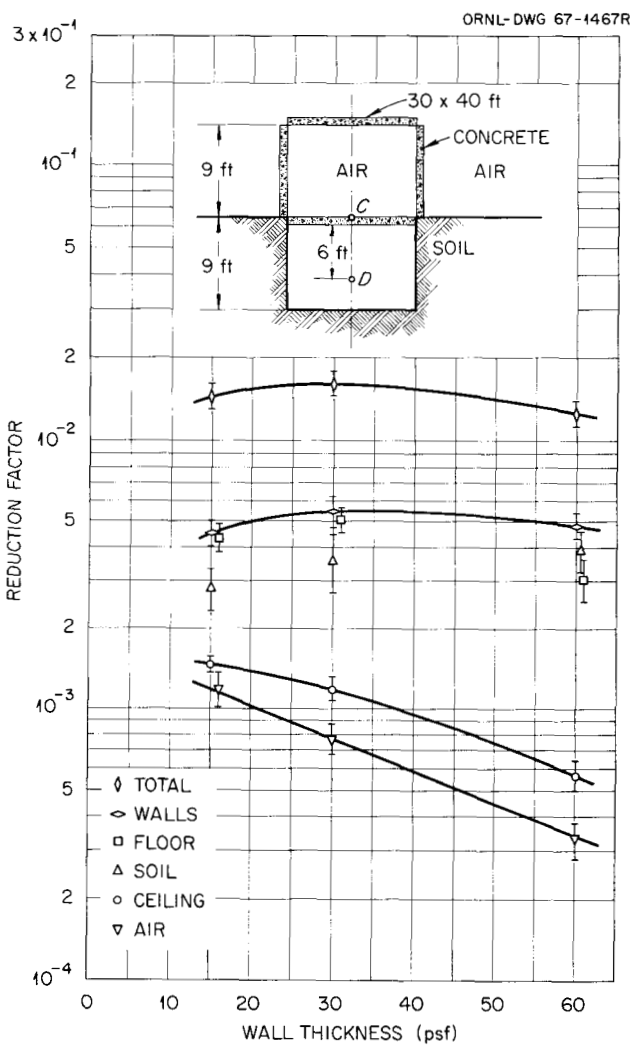

Fig. 4.4.1. Basement Reduction Factor As a Function of Wall Thickness.

Several special sampling schemes were employed. The source position was picked from a biased distribution proportional to $1/R$, where R is the distance from *C* to the source point, since the flux density near a plane source is approximately proportional to this function for sources at a distance of less than about 1 mfp. The direction of the photon was picked from a biased distribution which greatly favored a direction toward the shelter. This was done by aiming the photon at a point on a rectangle roughly coincident with the shelter walls. The point was picked from a uniform distribution over the rectangle. Approximately 80% of the photons were aimed toward the rectangle; the rest were picked isotropically.

Russian roulette was used to kill photons if the statistical weight was reduced below 10% of the starting weight or if the statistical estimation score was less than about 1% of the expected score.

The results are given in Fig. 4.4.1 as a "reduction factor," that is, the ratio of the exposure under the specified conditions to that at 3 ft in air above an infinite plane source on the ground. The reference point was calculated by a one-dimensional OGRE code. It is assumed here that exposure is equivalent to kerma, the actual quantity calculated.

The top curve shows the total exposure. The other curves show the contribution to the exposure from the walls, ceiling, floor, air, and soil as determined by the location of the collision which produced each statistically estimated score.

The reduction factor shown in Fig. 4.4.1 for 30 psf, 0.016, may be compared with a value of ~ 0.010 determined[4] by the method described in ref. 2. It can be seen that the contribution from the ceiling, air, and soil is appreciable, although the walls and floor are the major contributors.

References

[1]Summary of paper to be presented at Thirteenth Annual Meeting of the American Nuclear Society, San Diego, Calif., June 11–15, 1967; to be published in *Trans. Am. Nucl. Soc.*, Vol. 10, No. 1 (1967).

[2]C. Eisenhauer, *An Engineering Method for Calculating Protection Afforded by Structures Against Fallout Radiation*, PM-100-1 (Suppl. No. 1) (1964).

[3]D. K. Trubey and M. B. Emmett, *OGRE-G, an OGRE System Monte Carlo Code for the Calculation of Gamma-Ray Dose Rate at Arbitrary Points in an Arbitrary Geometry*, ORNL-TM-1212 (1966).

[4]A. B. Chilton, personal communication.

4.5 IMPORTANCE OF EPITHERMAL NEUTRONS RELATIVE TO THERMAL NEUTRONS IN ABSORBED DOSES[1]

F. H. Clark

There has been a growing practice, in dosimetry measurements near neutron sources, of measuring the epithermal-neutron flux density in addition to the usual fast-neutron dose rate and the thermal-neutron flux density. The importance of making these measurements was confirmed by the results of calculations using an S_n program[2] available at ORNL.

Neutron spectra were computed in simplified geometry for several interesting materials and then weighted with a dose response function. In each case the geometry is a slab of finite thickness and infinite lateral extent and the source, consisting of isotropically emitted 100-keV neutrons, is uniformly distributed over the whole volume.

The materials considered are a 30-cm slab of water, density 1 g/cm^3; a 600-m slab of air, density 1.29×10^{-3} g/cm^3, 78% nitrogen, 22% oxygen; and a 60-cm slab of concrete.

The thermal-neutron contribution in air was noted to be negligible in comparison to the epithermal-neutron contribution because of the heavy depletion of the thermal-neutron group by the nitrogen thermal-neutron-absorption cross section. For concrete shields the epithermal contributions are appreciable and ought not to be neglected. For water shields, the contribution of epithermal neutrons is perceptible but of considerably less dosimetric importance.

The data obtained strongly suggest that monitoring of epithermal flux densities should become a general practice, that more attention should be given to development of dosimetric instrumentation for the epithermal region and of standards for existing instrumentation and practice.

References

[1]Abstract of *Health Phys.* **13**, 296–297 (1967).

[2]Ward W. Engle, Jr., *A User's Manual for ANISN, A One Dimensional Discrete Ordinates Transport Code with Anisotropic Scattering*, K-1693 (March 1967).

4.6 DETERMINATION OF SHIELD REQUIREMENTS FOR NEUTRON SOURCES[1]

F. H. Clark

A number of simple computational formulas and graphs of transmission data which will assist in the rapid evaluation of common materials as neutron shields have been assembled for inclusion as a section in an NCRP handbook shortly to be issued as a replacement to NBS-63, *Protection Against Neutron Radiation Up to 30 Million Electron Volts.*

Reference

[1]Abstract of ORNL-TM-1655 (Oct. 5, 1966).

4.7 FISSION SPECTRUM NEUTRON DOSE RATE ATTENUATION AND GAMMA-RAY EXPOSURE DOSE BUILDUP FACTORS FOR LITHIUM HYDRIDE[1]

F. B. K. Kam F. H. Clark

A fission spectrum neutron dose rate attenuation curve has been computed by Monte Carlo for lithium hydride penetrations up to 67.5 g/cm^2. Gamma-ray exposure dose buildup factors have been computed for lithium hydride using moments method. Discrete gamma-ray source energies in the range 0.5 to 10 MeV were used and calculations were made out to 20 mfp (at source energy).

Reference

[1]Abstract of ORNL-TM-1774 (Jan. 13, 1967); also to be published in *Nuclear Applications.*

4.8 COMPARISONS OF RESULTS OBTAINED WITH SEVERAL PROTON PENETRATION CODES[1]

W. Wayne Scott[2] R. G. Alsmiller, Jr.

Comparisons of the results obtained on a hypothetical problem using the proton penetration codes presently included in the Radiation Shielding Information Center's code collection are presented. All the codes considered include secondary-particle production and transport in some approximation.

The hypothetical problem considered is to find the dose as a function of depth in tissue when a typical solar-flare proton spectrum is normally incident on an infinite slab shield which is followed by a slab of tissue 30 g/cm^2 thick. The solar proton spectrum considered is taken to be exponential in rigidity with a characteristic rigidity, P_0, of 100 MV and is normalized to 10^9 protons/cm^2 with energy > 30 MeV.

Graphs comparing both the total dose and the various secondary-particle contributions to the dose for aluminum and iron shields are presented. Definite inconsistencies between some of the codes are apparent.

References

[1]Abstract of RSIC-17 (in press); work funded by the National Aeronautics and Space Administration under NASA order R-104(10).

[2]Assistant Professor of Physics at Chattanooga State Technical Institute and consultant to RSIC.

4.9 ESTIMATES OF PRIMARY AND SECONDARY PARTICLE DOSES BEHIND ALUMINUM AND POLYETHYLENE SLABS DUE TO INCIDENT SOLAR FLARE AND VAN ALLEN BELT PROTONS[1]

W. Wayne Scott[2]

Primary proton and secondary particle doses (both physical and biological) have been computed behind aluminum and polyethylene slabs of varying thicknesses for normally incident solar-flare spectra of characteristic rigidities, P_0 = 50, 60, 80, 100, 120, and 195 MV, and for the Freden and White spectrum of protons in the Van Allen belt. These computations were performed with the recently developed NASA Lewis Research Center proton penetration code.

References

[1]Abstract of RSIC-18 (in press); work funded by the National Aeronautics and Space Administration under NASA order R-104(10).

[2]Assistant Professor of Physics at Chattanooga State Technical Institute and consultant to RSIC.

5. Mathematics and Computer Programs

5.1 DESCRIPTION OF THE TERP SYSTEM, A FORTRAN II/63, IV/63, 360 SYSTEM FOR EFFICIENT INTERPOLATION[1]

D. I. Putzulu[2] P. Aebersold[3]
W. R. Burrus

When repetitive calculation of complicated or nonlibrary functions is anticipated, use of an efficient numerical approximation is highly desirable. The system to be described (TERP) provides a means for obtaining such an approximation when the user can furnish routines to calculate the functions he desires. The entire system is available in FORTRAN. For increased speed, a machine-coded version of the interpolation routine is also included for IBM 7090 FORTRAN II and IV, CDC 1604 FORTRAN 63, and ORNL IBM 360 FORTRAN. Using these hand-coded routines, the time required for interpolation is 255 μsec (IBM 7090), 107 μsec (IBM 7094-II), 441 μsec (CDC 1604-A), and 45 μsec (IBM 360, MOD.-75I). The system works by table lookup and parabolic interpolation, and its accuracy depends on the functions and the number of storage locations allocated for the table. For example, the function ERF(X), 0 .LT. X .LT. 4.5, can be reproduced to 0.002% with 250 storage locations or to 0.00005% with 450 locations. The system can produce symbolic language (FAP, MAP, CODAP-2, or 360 assembly) decks for computing the functions and/or their inverses (backward interpolation). The function values may be obtained from these decks by FORTRAN statements such as Y = ERF(X) and X = ERFBAK(Y), where the names are chosen by the user.

References

[1]Abstract of ORNL-TM-1706 (December 1966); work funded by National Aeronautics and Space Administration under NASA order R-104(1).

[2]Cooperative student from Virginia Polytechnic Institute.

[3]Cooperative student from University of California at Berkeley.

5.2 STATUS OF TIME-SHARING COMPUTER SERVICES

V. R. Cain W. R. Burrus

During the last year the IBM Quiktran service[1] was discontinued, and two more-advanced services were obtained as replacements. Service with Tymshare, Inc., in Palo Alto, California (SDS 940), and with Applied Logic Corporation in Princeton, New Jersey (PDP 6), was begun in October 1966. Four 33ASR teletypes were leased for use with these services (two installed in Bldg. 4500, one in Bldg. 7702, and one in Bldg. 3010). Later, three of these teletypes were replaced by ones which were purchased. A fourth teletype was purchased for use with an acoustic coupler data set to provide a portable terminal usable with ordinary telephones. In February 1967 the Tymshare service was discontinued because of insufficient usage, and arrangements were made to obtain comparable service (also an SDS 940) from Comshare in Ann Arbor, Michigan, on a low-usage basis.

The present two services are somewhat complementary in that the Comshare system is highly developed and easy for the novice to use, does not yet have a standard FORTRAN IV compiler, and is fairly limited in executional ability, whereas the Applied Logic system is intended for the more experienced programmer, has a good FORTRAN compiler, and has significant executional capability. The software available on the SDS 940 includes CAL and BASIC, conversational languages aimed at the small numerical problems in a highly interactive environment; FORTRAN II (batch type) and FORTRAN IV (conversational but nonstandard and

incomplete as of this writing) compilers; QED, a generalized text editor; DDT, a debugging package; and a symbolic macro-assembler. The PDP-6 software, which is more powerful but not so well-defined, includes FORTRAN IV (a good standard-batch type); several editors, file manipulation systems, etc.; DDT, a debugging package; and a symbolic macro-assembler.

At the present stage of development it appears that small numerical problems are better suited to the SDS-940 system and that FORTRAN debugging and longer running problems are better suited to the PDP 6 (see Table 5.2.1 for comparison of execution times, core capacity, and file capacity). In using these systems it has been discovered that only a very small number of people in the Division have tried either system, much less made serious use of the services (seven people have tried Applied Logic, with three people accounting for 81 hr of connection time during March) and that the Division has much less demand than was thought beforehand for super desk calculator capability (quite a few people tried CAL, agreed that it would be very useful for a certain class of problems, then forgot about it). Most people seem to prefer to continue with their present techniques for most problems, until such time as they can have a console installed in their office. The level of overall usage is very close to the $1\frac{1}{2}$ hr/day/console predicted last year, even though this time is concentrated in a small number of users. It is also worth noting that the Division's experience with languages such as CAL is unique; other groups in the Laboratory are making extensive use of even simpler languages.

A summary of the approximate monthly costs with the present system is shown below, based on 100 hr/month usage of the Applied Logic system and ignoring the small Comshare usage:

Leased telephone line	$ 300
Commercial line usage	300
Data sets and one 33ASR	183
PDP-6 connection time	500
PDP-6 computation charge	750
Maintenance	40
	$2073 per month

The primary disadvantages to the present system (ignoring the lack of desirable advanced features such as CRT displays, etc.) are the inconveniences associated with insufficient numbers of teletypes, telephone lines, and input lines at the computer. We are now proposing an intermediate system with 16 teletypes and 4 frequency multiplexed channels over our present leased telephone line. The choice of this system implies that Applied Logic can handle all the Division's remote computer requirements, which should be the case in a few weeks when Applied Logic installs a language similar to CAL.

The level of usage that seems reasonable to expect with the 16-teletype system would account for about 10% of the capacity of a $1 million time-sharing computer. The same service could be provided locally (including capital depreciation) for about two-thirds the commercial rates, if there is enough local demand to justify the acquisition of such a computer. Because of this expected demand, Division personnel participated in an investigation of the possibility of acquiring a "stand-alone" time-sharing computer to service 50 consoles at the four Oak Ridge Operations plants. Serious consideration was given to the possibility of renting an SDS-940 system to provide this type of service beginning in about April 1967 for one or two years, until comparable service could be provided locally. The proposal was dropped because of uncertainties in fund availability.

Reference

[1]W. R. Burrus, *Neutron Phys. Div. Ann. Progr. Rept. May 31, 1966,* ORNL-3973, Vol. II, p. 92.

5.3 CSP: A GENERAL-PURPOSE MULTIGROUP CROSS-SECTION AVERAGING CODE

K. J. Yost N. M. Greene[1]

A code package (CSP) has been written which automates the process of obtaining group-averaged neutron cross sections for arbitrary group structures. Versions of CSP will be available which will utilize either the O5R or ENDF library tape as a source of point cross-section data. Particular emphasis has been devoted to producing cross sections in a form suitable for input to the discrete-ordinate (S_n) transport codes.

Reactions for which CSP generates group-averaged cross sections include absorption, fission, n-2n, elastic and inelastic scattering, and tabulated secondary energy reactions. Provisions are included

Table 5.2.1. Comparison of Execution Speeds, Program Sizes, and File Storage Capacities

	Arithmetic Speed (operations/sec)	Program Size (data words)	File Capacities	
			Active	Inactive
Quiktran (IBM 7040)	10	4K* (36-bit words)	60K	Cards
Comshare (SDS 940)				
BASIC, FORTRAN II	200	12K	60K	Paper tape
CAL, FORTRAN IV	40	(24-bit words)		
Applied Logic (PDP 6)				
FORTRAN IV	1000	22K (36-bit words)	50K	150K/user (10-min access)

*K = 1024.

in CSP for averaging cross sections over $1/E$, $1/v$, and arbitrary input flux spectra.

The code is programmed in FORTRAN IV. The present version for the IBM 360/75 allows for 200 energy groups and up to 2000 data points per process. The elastic-scattering routine is presently dimensioned to allow a P_{10} approximation to anisotropic elastic-scattering distributions in the laboratory system.

Reference

[1]Computing Technology Center, Union Carbide Corporation, Oak Ridge.

5.4 EFFECT OF FAULTY RANDOM NUMBER GENERATORS ON MONTE CARLO CALCULATIONS[1]

H. A. Feldman

It is possible[2] to make a priori analyses of the statistical performance of random number generators. This study reports some efforts to test the practical effect of the use of such generators, predicted to be faulty by the methods of ref. 2. Very simple problems only were treated. No clear pattern emerged, although there was a tendency for the faulty generator to produce results which were dubious or clearly wrong.

References

[1]Abstract of ORNL-TM-1625 (in press).

[2]R. R. Coveyou and R. D. MacPherson, *J. Assoc. Computing Mach.* 14(1), 100-119 (1967).

5.5 DEVELOPMENT OF ENDF/B CROSS-SECTION FORMAT PROGRAMS AND THE UTILIZATION OF ENDF/B BY THE O5R SYSTEM

D. C. Irving J. Stockton[1]
C. Whitehead[2]

In conjunction with 15 other installations receiving support from the Division of Reactor Development and Technology, AEC, a cooperative program was undertaken to develop the ENDF/B cross-section format as a useful tool in the preparation of cross-section data for neutron computer codes and to establish a complete library of cross sections in this format to serve as a calculational standard for code comparison. Our part in the establishment of the cross-section library consisted in evaluating the cross sections for ^{10}B and then distributing them to the other cooperating installations (see Sect. 1.18, "Evaluation of Neutron Cross Sections for ^{10}B").

As a part of the code development necessary for the utilization of the ENDF/B format, the following general-purpose programs have been written and are being distributed to the other installations:

EDIT – A program designed to provide readable listings of the ENDF/B data. This program also has capabilities for copying tapes, making deletions, and converting data from one mode to another. It has been completed.

MERGE – A program for the merging of two ENDF/B tapes into a single, ordered tape. It also has capabilities for copying tapes, converting, and making insertions. It has been completed.

A program for producing Calcomp plots of the ENDF/B data is partially completed but several options are still to be added.

The ENDF/B library of cross-section data has been received. In order to make use of these data, modifications have been made to the O5R cross-section handling package, XSECT, to permit the use of ENDF/B as an input format in the preparation of the macroscopic cross-section tapes actually used directly by the O5R program. As an interim measure pending full development of the ENDF/B system and its implementation in the O5R system, partial translation routines to convert data from the present O5R format to the ENDF/B format and vice versa were written.

As a part of the new O6R system, the EDIT, MERGE, and ENDF/B plotting routines will be combined with the modified macroscopic tape preparation routines to form a new XSECT package. The present simple but limited O5R format will be dropped in favor of the complex but much more comprehensive ENDF/B format as the working format for microscopic data. The adoption of ENDF/B will permit, among other things, the development of a general inelastic-scattering routine.

References

[1]Mathematics Division.

[2]Computing Technology Center, Union Carbide Corporation, Oak Ridge.

5.6 MODIFICATIONS TO THE O5R-ACTIFK MONTE CARLO SYSTEM

V. R. Cain
M. B. Emmett[1]
K. D. Franz[2]
E. A. Straker

The continuing use of the O5R[3]-ACTIFK[4] Monte Carlo system in the SNAP and DASA shielding programs has revealed many shortcomings in the system. Consequently, several modifications have recently been made, including improved bookkeeping for splitting and roulette, provision for albedo-model scattering, incorporation of time dependence, and some specific estimators and biasing techniques. In addition, a FORTRAN IV version of ACTIFK has been released to the Radiation Shielding Information Center for distribution. The modifications described here will be incorporated periodically into versions of the codes to be released.

A version of O5R containing changes in banking and splitting logic and allowing albedo collisions to occur has been written and tested on the CDC 1604 computer. Banking logic has been changed so that no neutrons having zero weight are ever stored in the neutron bank. Whenever a neutron's weight does become zero, that neutron's position in the bank is filled by the last neutron in the bank and processing is continued using the replacement neutron. This process maximizes the amount of available storage in the neutron bank during an O5R run by allowing neutrons which are generated by splitting to fill vacancies in the bank. Thus, in a problem employing splitting, more split histories can be generated during an O5R run than previously.

Splitting logic has been changed so that the parent of a neutron created by splitting is not the neutron that has just split but is the *source* neutron from which both are derived; i.e., regardless of the generation to which a neutron belongs, its parent will always be a source neutron.

In this modified version of O5R, logic allowing albedo collisions has been included. The modifications include provision for obtaining the surface normal vector at boundary crossings and for calling a user-written albedo scattering routine with this information when a scattering of this type is desired.

Time dependence has also been incorporated into O5R. The chronological age of the neutron is an added variable and is the 36th collision parameter.

An additional feature was added for a particular problem. At any specified supergroup boundary the contents of BANKR are written on a magnetic tape and the next batch is started. The magnetic tape may be used as a starting source for the continuation of the problem, and the neutrons are then followed to lower energies. This stop-start feature may be used to take full advantage of changing input cross-section detail, biasing schemes, etc.

The necessary user-written subroutines for ACTIFK have been completed for a boundary cross-

ing estimator to score a four-dimensional flux. That is, the neutrons crossing boundaries in the system may be ordered as a function of energy, angle of crossing, and time after leaving the source. Output consists of energy and angular spectra of neutrons crossing a boundary within specified time intervals. Also, the sum over angle is given for each time bin and the sum of the energy and angular flux over all time printed. Time-dependent dose and silicon damage are also outputted. All output consists of the mean and standard deviation of the results. Routines for plotting any of the outputted variables are being written.

A special nonleakage version of O5R subroutine GETETA has been written. The algorithm has been described previously.[5] This routine requires the use of subroutine EUCLID from ACTIFK to determine the number of mean free paths to the leakage boundary.

References

[1]Mathematics Division.

[2]Computing Technology Center, Union Carbide Corporation, Oak Ridge.

[3]D. C. Irving *et al., O5R, A General-Purpose Monte Carlo Neutron Transport Code,* ORNL-3622 (February 1965).

[4]F. B. Kam and K. D. Franz, *ACTIFK, a General-Purpose Code to Analyze O5R Collision Tapes,* ORNL-3856 (September 1966).

[5]F. H. Clark and N. A. Betz, *Importance Sampling Devices for Selecting Track Lengths and Directions after Scatter in O5R,* ORNL-TM-1484 (Aug. 1, 1966).

6. Radiation Detector Studies

6.1 MONTE CARLO CALCULATIONS OF THE NEUTRON FLUX WITHIN A $^{10}B_4C$ SHELL[1]

R. M. Freestone, Jr.

A Monte Carlo code, O5R, has been employed to study the transport of neutrons through a nearly spherical $^{10}B_4C$ shell. Such shells are often used to shield neutron detectors against the intense background of thermal neutrons associated with reactor or reactor-like neutron fluxes. An aluminum disk simulated a solid-state detector within the shell.

Calculations were made for isotropic monoenergetic neutrons having energies of 0.5, 1, 2, 4, 6, 8, 10, 12, and 14 MeV, for an isotropic fission spectrum source, and, for comparison purposes, for a 4-MeV normal beam source.

Results indicate that only a small distortion of the incident spectral shape is created by passage through the shell. The effect seems to be confined to incident neutron energies below 2 MeV. The degree of isotropy of the incident flux, however, importantly affects the absolute fraction of neutrons reaching the detector.

Reference

[1]Abstract of report ORNL-TM-1816 (in press).

6.2 STATUS OF ORELA SCINTILLATOR DETECTOR DESIGN STUDY

E. G. Silver

A large scintillation detector for use in time-of-flight measurements of fission and capture cross sections at the Oak Ridge Electron Linear Accelerator (ORELA) is under study. A number of codes have been written to study the effects of tank shape on the gamma leakage probability, and a preliminary decision has been made to utilize a cylindrical tank with truncated-cone end sections. The beam axis will coincide with the axis of rotation of the cylinder. An optimization code for tanks of this geometry has been written to choose the relative proportions.

It is anticipated that this detector (with a volume of between 2000 and 3500 liters) will be made of aluminum and will have a fixed drain and filling system to permit easy handling of the organic scintillator fluid.

The use of 60AVP (9-in.-diam) photomultiplier tubes is contemplated, and two such tubes have been acquired and are being tested.

The overall considerations guiding the design of this detector are flexibility in use and fast timing coupled with good energy resolution. To this end, the tank will be built so as to permit a wide range of beam-hole diameters and also lateral access for other detectors.

6.3 ESTABLISHING AN ENERGY SCALE FOR PULSE-HEIGHT DISTRIBUTIONS FROM GAMMA-RAY SPECTROMETERS BASED ON INORGANIC SCINTILLATORS[1]

R. W. Peelle T. A. Love

Devices, experimental designs, and data analysis techniques useful for the calibration of scintillation gamma-ray spectrometers are critically examined. Though the ideas have broader application, the discussion assumes the use of NaI(Tl) phosphors. The review of calibration sources includes tables of gamma-emitting radioisotopes employable for this purpose, with best energies, uncertainties, and other convenient data. The branching ratios among the naturally mixed x-ray

lines (K-L vs K-M + K-N) are tabulated for useful radioisotope x-ray sources to enable use of a simple method given for determining the appropriate "effective" energy of the mixed source. The origins of spectrometer instability and nonlinearity are reviewed, along with their relative importances, and experimental designs and data analysis techniques which will minimize these effects are discussed. For finding the central position of the peak in a pulse-height distribution from gamma rays of a single energy, all the standard numerical and graphical methods are illustrated and compared, including full and partial nonlinear least-squares analyses. Finally, interpolation methods are detailed for determining from the available calibration information an unknown gamma-ray energy and its uncertainty.

Reference

[1]Abstract of ORNL-4118 (to be published); work funded by the National Aeronautics and Space Administration under NASA order R-104(1).

6.4 SYSTEM RESPONSE FUNCTIONS FOR FLIGHT-TIME SPECTROMETRY OF SECONDARY FAST NEUTRONS[1]

R. T. Santoro

Time-channel response functions have been derived for a time-of-flight spectrometer used to measure monoenergetic secondary neutrons in the energy region from 2 to 100 MeV produced in a homogeneous slab target from the interactions of monoenergetic charged particles with the target nuclei. The effects on the flight-time distribution of the target and detector dimensions and orientation, the spatial distribution of the beam, and the pulse-height-dependent time slewing (walk) were demonstrated. Response functions were derived assuming that the neutron emission from the target is independent of the azimuthal scattering angle and the polar angle over the angular region subtended by the detector, that neutron detection may be treated in the first-collision approximation with the light being emitted uniformly from the interaction point and collected uniformly from all points in the detector volume, that the beam dimension perpendicular to the scattering plane can be ignored, and that the instrumental timing jitter can be approximated by a Gaussian distribution independent of the pulse height. The time-channel response functions were obtained from the integral over the time-analyzer response function of the convolution of the physical flight-time distribution of detected neutrons and the time-slewing response function. The maximum flight-time uncertainties, $\Delta t/t$, were derived in terms of the target and detector dimensions, assuming that all dimensions have negligible effect except the one being evaluated. Comparisons are made between the computed distributions and the distributions obtained analytically. The expected dominant effects of the detector thickness are demonstrated, along with the dependence of the target dimensions on the neutron velocity and the angular difference between the neutron scattering angle and the target rotation angle. The distributions arising from the target and detector thickness were shown to be square except for attenuation effects, while those obtained for large detector radii showed a $1/t$ dependence. The time distribution for large beam size reflects the beam spatial distribution. The numerical methods are described, and typical distributions illustrate each contribution to the overall response function. For cases in which multiple scattering does not dominate, the time integrals of the computed response functions are in good agreement with known detector efficiencies.

Reference

[1]Abstract of ORNL-4114 (in press); work funded by the National Aeronautics and Space Administration under NASA order R-104(1).

6.5 A VACUUM-HARDENED, CHARGE-SENSITIVE PREAMPLIFIER

N. W. Hill[1]

The design of a low-noise, charge-sensitive preamplifier was motivated by the need for a system which would fulfill the many experimental requirements of the charged-particle studies performed at ORIC (Oak Ridge Isochronous Cyclotron). This solid-state preamplifier was required to have good versatility without a sacrifice in other performance characteristics. The preamplifier consists only of a modified Blalock charge-sensitive loop with a charge sensitivity of from

54 mV/MeV (i.e., germanium) to as much as 2 V/MeV with from one to three field effect transistors in parallel at the input without the addition of parasitic suppressors. For 1.6-μsec RC-RC pulse shaping, this preamplifier gives a calculated noise figure at room temperature of 1.1 keV full width at half maximum (referred to germanium). This measurement is with zero detector capacity but with all other connections made, including a 1-pF test pulse capacity. Either polarity input pulse is accepted with a maximum output of either plus or minus 3.5 V into 93 ohms with better than 0.05% linearity.

The temperature stability is better than 0.05% from $-10°$ to 50°C and as measured is determined by the temperature stability of both the charge injection capacitor and the feedback capacitor. The stability of the gain of this preamplifier under prolonged vacuum operation inside a scattering chamber has been better than 0.05% for 5 hr, and under actual experimental conditions in vacuum seems to be better than 0.1% for several days. This latter figure includes the stability of the pulser, the main amplifier, and the analog-to-digital converter, and in the case of the preamplifier used with the germanium detector, it includes the differential heating caused by the germanium cryostat.

In order to increase the signal seen by the fast amplifiers used simultaneously with these slow preamplifiers and also to minimize the loop closure time, little if any bandwidth suppression is used even for the larger feedback ratios with three field effect transistors. Under similar conditions these preamplifiers have proved to be stable for input cable impedances from 50 to 125 ohms, which have continuously variable lengths of 0 to 4 ft with input capacities at the ends of these cables from zero to several hundred picofarads.

One of the design considerations was that the dc bias conditions be sufficient to ensure linear operation for the large dynamic range of energies expected. This includes energy depositions in a 500-μ diode of approximately 36 MeV with a collection time essentially faster than the response time of the charge-sensitive loop.

The design includes an internal feedback network whose adjustment permits the preamplifier to operate from 0- to 100-pF detector capacitance with less than 0.01% loss in pulse height.

Reference

[1]Instrumentation and Controls Division.

6.6 DECAY TIMES OF SCINTILLATION INDUCED BY ELECTRONS, PROTONS, AND ALPHA PARTICLES IN SOME ORGANIC SCINTILLATORS[1]

T. A. Love R. W. Peelle
N. W. Hill[2]

For several years various investigators[3–6] have used organic scintillators for the detection of neutrons and in some cases[7–9] for the spectral measurements of neutron flux. Most of these scintillators exhibit light decay of more than one period when excited by charged particles, and the intensity relation between the two or more time components at a given energy is a function of the particular incident particle. The total light production has been studied by several investigators,[10] and Voltz *et al.*[11] have described qualitatively the production of both the fast and slow components.

The data on the relationship of the total light output to the energy of the charged particle have often been fitted assuming that scintillations induced by electrons have no energy variation of their fractional slow component. Experiments which use both fast timing and total light spectra would benefit from detailed knowledge of both fast and slow components.

Spectral measurements of neutrons in general are made in environments where appreciable gamma-ray flux is present. The difference in decay characteristics has been exploited to enable the experimenters to distinguish between pulses induced by gamma rays and those induced by neutrons incident upon the detector. The method, although it has several variations, is usually called pulse-shape discrimination and was first described by Brooks.[12] NE-213 is a liquid organic scintillator which exhibits a difference in time behavior of the light produced by electrons, neutrons (proton recoil), and alphas, and is extensively used for neutron measurements.

Measurements were undertaken to establish the magnitude relationship of the two decay components. Many single oscilloscope traces, each of which represented the light from a single particle integrated over time, were photographed and later analyzed for amplitude as a function of time.

Experimental Setup

All scintillators used were coupled to 56AVP phototubes. For most of the measurements made in this experiment the detectors were two 1.5- by 1.5-in. aluminum cylinders, with a glass end, each containing NE-213 scintillator. One of the scintillators has a ^{234}U alpha-particle source evaporated on a piece of platinum glued to the top of the detector, and the other has a ^{242}Cm source in the same position. The alpha particles were of energies 4.76 and 6.10 MeV respectively. A few measurements were made on stilbene and NE-211 for comparison with NE-213.

Protons measured were the recoil protons generated by neutrons from a ^{252}Cf or a Po-Be source incident on the scintillator. Gamma rays from several sources were used to generate electrons and to allow energy calibration.

Figure 6.6.1 shows a block diagram of the electronics. Because of statistical variance, averages over a number of comparable pulses were required. This was accomplished by obtaining the oscilloscope and analyzer trigger from a circuit sensitive to a narrow band of fast-light pulse heights. A 25-nsec clipped signal from dynode 13 of the phototube defined the fast component. Whenever possible, the window bias position was adjusted using calibrated attenuators.

The anode circuit has a long time constant (RC = ~41 μsec). The anode pulse was fed into a mixer circuit (along with test pulse generator pulses) and into the cathode follower probe ordinarily used with the Tektronix model 661 sampling oscilloscopes. The output of the probe was fed into a high-quality delay line, 50-ohm attenuators (variable in 1, 2, 4, and 5 factors), and then into a Tektronix type 585 oscilloscope which is terminated in 50 ohms. Only one sensitivity setting was used on the type 82 dual trace plug-in unit. Figure 6.6.2 shows the anode circuit used, and Fig. 6.6.3 shows typical alpha, electron, and test pulses at a fast bias of 100 keV. Considerable effort was required to obtain correct pulse shapes.

Analysis

Geometric and time corrections of the oscilloscope were determined and incorporated into the analysis program, as well as corrections for the decay constants of the circuits involved. Resulting uncertainties are small compared with the statistical uncertainties introduced by the broad spreads and the small total number of pulses analyzed. Mercury pulser pulses, one per photograph, were analyzed and used to demonstrate gain and circuit time constant stability.

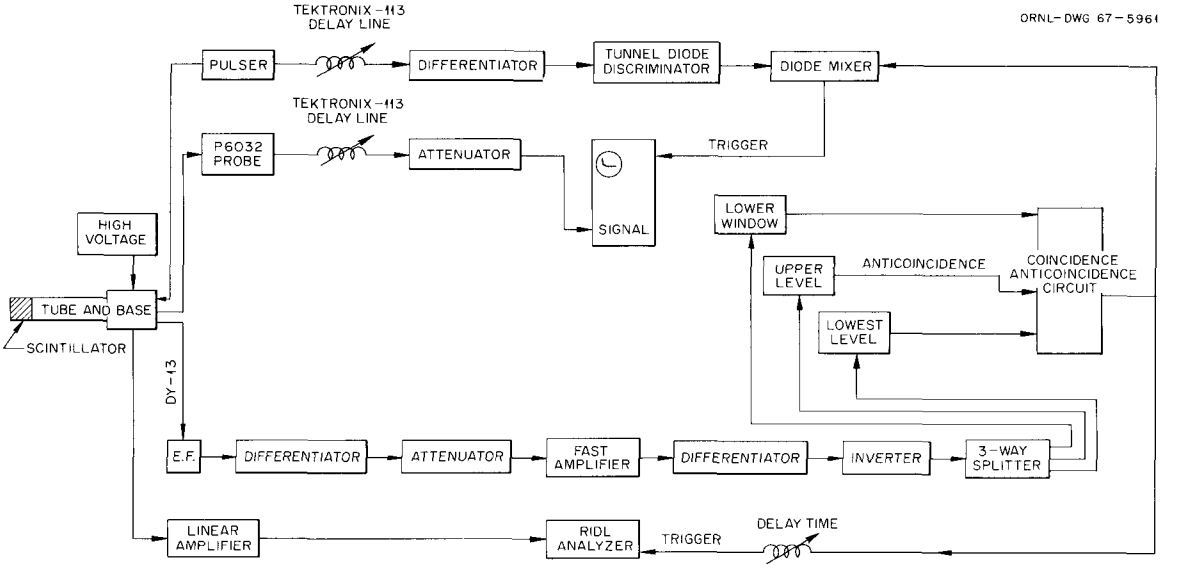

Fig. 6.6.1. Block Diagram of Electronics.

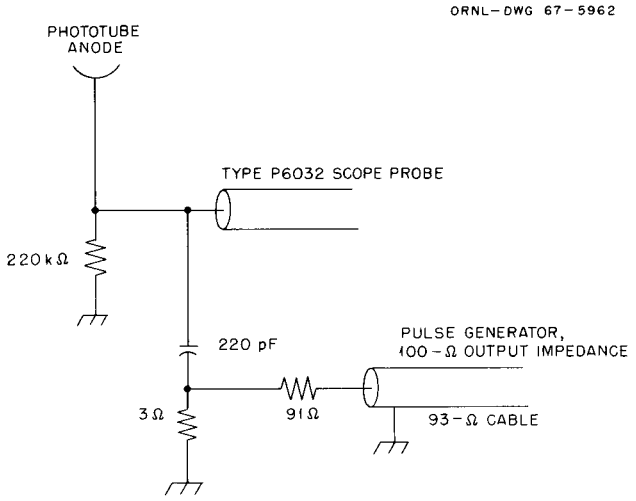

Fig. 6.6.2. Anode Circuit Used to Mix Pulser Pulses at Real Pulses.

Slow light has been arbitrarily defined as the light which appears after ~20 nsec. Table 6.6.1 gives the percent slow light, integrated to 0.91 μsec, for electrons, protons, and alpha particles in terms of total electron energies. The extreme value of 11% for the electron light from the 2- by 2-in. NE-213 is not understood, nor is the one of 17.5% at ~1.5 MeV bias from the 1.5- by 1.5-in. NE-213. Slow light from the alphas at an electron bias of 325 keV was corrected downward because the window actually corresponded to an alpha energy of 5.9 MeV rather than 6.1 MeV.

The ratio of the total light from the protons to the total light from the electrons for the 1.5-in. scintillators is in serious disagreement with that published several years ago.[13] However, for the previous data the incident particles were ~14-MeV neutrons and light below a bias of about 1 MeV (electron light) was a mixture of recoil protons and alphas from the carbon n,α and carbon $n,3\alpha$ reactions. Figure 6.6.4 shows the data from the two 1.5- by 1.5-in. NE-213 detectors.

Examination of the integral of the decay curves given by Yates and Crandall[14] shows ~6% slow light for NE-213 and NE-211, and ~12% for stilbene when excited by 1.11-MeV gamma rays. These values are in substantial agreement with those given in Table 6.6.1.

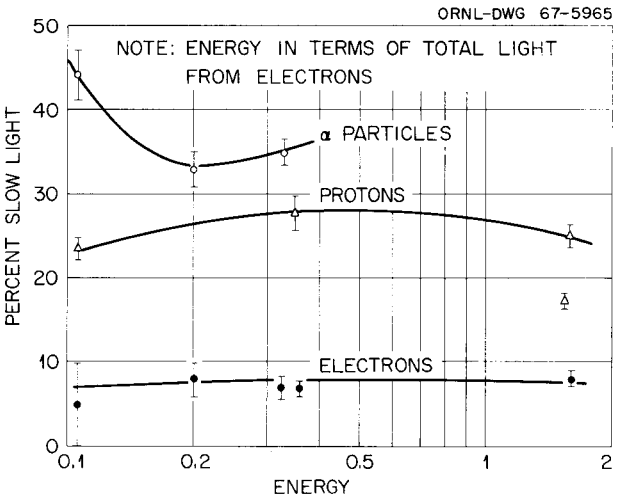

Fig. 6.6.4. Percent Slow Light in an NE-213 Scintillator for Alphas, Protons, and Electrons.

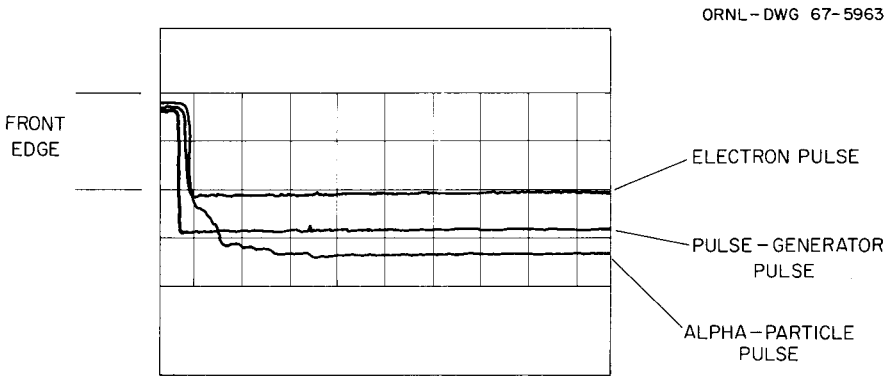

Fig. 6.6.3. Typical Oscillogram Showing an Electron, Pulser, and Pulse Generator Pulses.

Table 6.6.1. Percentage Slow Light from Organic Scintillators

Scintillator	Bias (MeV)	Electrons		Protons		Alphas		Particle Energy[a] (MeV)	
		% Slow Light	No. of Pictures	% Slow Light	No. of Pictures	% Slow Light	No. of Pictures	Alphas	Protons
NE-213;	0.105	5 ± 0.36	136	23 ± 1.0	71	44 ± 2.5	19	2.3	0.462
1.5 by 1.5 in.	0.200	8 ± 2.3	10			33 ± 1.5	43	4.8	
with	0.325	7 ± 1.1				35 ± 1.2	69	5.7	
internal	0.360	7 ± 0.5	46	28 ± 1.6	20				1.6
alpha sources	1.55			17.5 ± 0.9	18				4.5
	1.60	8 ± 0.35	55	25 ± 1.3	18				4.6
NE-213;	0.111	11 ± 1.7	12						
2 by 2 in.	0.300	8 ± 1.1	10	35 ± 2.1	7				1.5
	1.40	8 ± 0.88	8	20 ± 1.0	5				4.3
NE-211;	0.300	5 ± 0.89	17	22 ± 2.3	6				1.5
2 by 2 in.									
Stilbene,	0.289	16 ± 1.2	50	42 ± 3.2	17				1.5
1 cm high by									
5 cm diam									
Stilbene	1.40	19 ± 1.1	16	35 ± 2.3	12				4.3

[a]Energy calculated from Schuttler's (ref. 13) light curve.

References

[1]Work partially funded by the National Aeronautics and Space Administration under NASA order R-104(1).

[2]Instrumentation and Controls Division.

[3]F. G. Perey, *Inelastic Scattering of 14-Mev Neutrons in Carbon, Oxygen, and Lithium*, Ph.D. thesis, University of Montreal, June 1960.

[4]N. A. Bostrom *et al.*, *Inelastic Scattering of Fast Neutrons from Nitrogen and Oxygen*, WADC-58-88 (February 1958).

[5]R. W. Peelle *et al.*, *Space Radiation Shielding Research Ann. Progr. Rept. Aug. 1962* (unpublished report).

[6]R. Batchelor *et al.*, *Nucl. Instr. Methods* **13**, 70 (1961).

[7]J. C. Courtney, *Fast-Neutron Scattering from Small Cylinders of Steel, Aluminum, and Graphite*, ORNL-TM-1156 (1965).

[8]V. V. Verbinski, "Proton-Recoil Spectrometry with Organic Scintillators," *IAEA Symposium on Neutron Monitoring for Radiological Protection*, Vienna, 1966.

[9]V. V. Verbinski *et al.*, paper SD-2 in *Proceedings of Special Session on Fast Neutron Spectroscopy*, ANS Meeting, San Francisco, 1964.

[10]J. B. Birks, *The Theory and Practice of Scintillation Counting*, Pergamon Press, London, 1964.

[11]R. Voltz *et al.*, *Influence of the Nature of Ionizing Particles on the Specific Luminescence of Organic Scintillators*, Centre de Recherches Nucléaires, Departement de Chimie Nucléaire, Strasbourg-Cronenbourg, France (to be published).

[12]F. D. Brooks, *Progress in Nuclear Physics*, vol. 5, p. 252, Pergamon Press, London, 1956.

[13]T. A. Love and R. J. Schuttler, *Neutron Phys. Div. Ann. Progr. Rept. Aug. 1, 1964*, ORNL-3714, vol. II, pp. 136–138.

[14]E. C. Yates and D. G. Crandall, pp. 153–158 in *IEEE Transactions on Nuclear Science*, NS-13 (June 1966).

6.7 CALIBRATION OF THE PROTON-RECOIL NEUTRON SCINTILLATOR FROM 0.2 TO 22 MeV[1]

V. V. Verbinski
R. E. Textor[2]
J. Drischler
W. R. Burrus
W. Zobel
T. A. Love
N. W. Hill[3]

A 2- by 2-in.-diam NE-213 liquid organic scintillator was calibrated with monoenergetic neutrons with the use of time of flight to reduce spurious background. The pulse-height distributions were taken over a broad range of pulse heights from about 0.03 standard light unit (1 light unit corresponds to about a 1.27-MeV electron) to the maximum possible. At low neutron energies, the low cutoff was below 0.01 light unit (below 0.2 MeV recoil proton energy). Up to four different gains were necessary to cover the range with adequate detail. The data are now being corrected for accelerator beam normalization, for residual background, for a slight nonlinearity of the lower pulse-height channels, for a small zero channel offset, and for a gradual droop in the vicinity of the low pulse-height cutoff that is due to pulse-shape discriminator characteristics.

The Forté-Hill pulse-shape discriminator was used for these measurements. The loss of counts at low pulse heights was determined by measuring the count loss with and without the discriminator using the associated particle technique with the $^{2}H(d,n)^{3}He$ reaction for rejection of background counts due mostly to gammas and photomultiplier tube noise. The correction extended from about 0.08 light unit down to about 0.03 light unit, where the count loss is about 50%.

After final corrections, the data will be compared with Monte Carlo calculations of pulse height from monoenergetic neutrons. Discrepancies between the calculation and experiment are minor below 15 MeV and major above 15 MeV since the ^{12}C cross-section information for the calculation has been

empirically adjusted (without altering the total elastic and nonelastic cross sections) to agree with previous experiments below 15 MeV. These discrepancies will be resolved in a semiempirical way such that the absolute normalization of the Monte Carlo calculations will prevail.

The use of the new pulse-height distributions in the FERDoR unscrambling code should significantly improve the overall results below 1.5 MeV and above 15 MeV.

References

[1]Work partially funded by the National Aeronautics and Space Administration under NASA order R-104(1).

[2]Computing Technology Center, Union Carbide Corporation, Oak Ridge.

[3]Instrumentation and Controls Division.

6.8 BORANAL: A FOLDING PROGRAM TO SIMULATE THE RESPONSE OF A BORON FILTER NEUTRON SPECTROMETER

R. M. Freestone, Jr.

Previous reports[1,2] have described the design and current status of an epithermal neutron spectrometer based upon a series of ^{10}B filters having graduated thicknesses. The immediate product of an examination of an unknown spectrum by this spectrometer is a set of count rates, one for each filter of the series. Since each count rate represents an integration of the response of the counter with a particular filter combination over all neutron energies, the unknown spectrum is not readily deducible from the raw count rates.

When the first tests of the spectrometer were made, an effort was made to utilize the unscrambling methods contained in the FERD code of Burrus.[3] These efforts failed, principally because the combination of a $1/v$ absorber and a $1/v$ detector inherent in the device resulted in response functions having a rather steep rise at low energy, an extremely broad peak, and a slowly descending tail having appreciable values in energy regions far beyond the range for which the device was intended. The approach now being taken consists in attempting to calculate analytically a series of count rates which the spectrometer would produce upon exposure to an arbitrarily proposed "guess" spectrum. The calculated counts are compared graphically and numerically with the measured counts for the unknown spectrum, a more or less intelligent modification of the first guess is made, and the calculation is rerun. With a sufficient number of guesses, a series of counts are arrived at which are statistically in agreement with the experimental counts, and the final guess represents a possible solution to the unknown spectrum. These ideas are contained in the program called BORANAL, presently written for and running on the CDC 1604 computer.

The premise underlying BORANAL is that the counts obtained experimentally behind any ^{10}B filter can be represented by

$$\text{counts}(i) = \int_0^\infty \phi(E)\, T(E)\, \epsilon(E)\, dE\,, \qquad (1)$$

where

$\phi(E)$ = neutron flux, per unit area per unit time per unit energy interval,

$T(E)$ = filter transmission,

$\epsilon(E)$ = efficiency of the $^{10}BF_3$ counter behind the filter.

The only effect in the experimental configuration that is not accounted for by Eq. (1) is the scattering in the ^{10}B shell which surrounds the counter. The importance of such scattering has been evaluated, however, both experimentally and by (unpublished) Monte Carlo calculations to be (1) not evident, according to the experiment, and (2) less than a few percent, according to the calculations.

The term $\phi(E)$ in the integral is, of course, the arbitrary guess of the flux. The transmission T is obtained from least-squares fits to the filter transmissions measured at the ORNL Fast Chopper Facility. The counter efficiency ϵ is essentially derived during the calculation by utilizing the foil measurement of the thermal flux that is routinely made prior to each use of the instrument.

The BORANAL package consists of the main program, BORANAL, and a set of subroutines. BORANAL does little but call the subroutines at proper times. The subroutines (EGEN, MAXWELL, FLXGES, YINTEG, NORM, CORRECT, TRANS, COUNTS, and OUTPUT) compute energy meshes, Maxwellian distributions, and "guess" fluxes; do normalizations; calculate transition curves; compute counts; perform numerical integrations; and output the results.

The computed data are normalized to the experimental data in the following fashion. Three normalization parameters are input to the code: the thermal flux, as measured by an indium or gold foil; the counts due to thermal neutrons, as determined by the difference between the counts from a bare counter and those from a cadmium-covered counter; and the counting rate behind an arbitrarily chosen filter of the series. The Maxwellian distribution is first computed for an arbitrary total number of neutrons. The area under the distribution then is compared with the true value from the foil data, and the calculated values are corrected accordingly. The counts resulting from the corrected distribution are then calculated, and this value is compared with the experimental value of the same quantity to establish a value for the true counter efficiency. This efficiency is used to calculate the counts due to the guessed epithermal flux. Finally, the computed counts for some filter sufficiently thick to be completely black to thermals (presently filter 10) are made to agree with the experimental values for the same filter by adjusting the epithermal flux values.

BORANAL is, admittedly, far from an ideal solution to the problem of understanding the data obtained from the boron filter spectrometer. However, it has yielded some useful, apparently quite accurate, information and in addition has helped to clarify some of the problems that are encountered in using the spectrometer. One of these problems is created by the fact that the spectrometer attempts to look at epithermal neutrons but is strongly affected by higher energy neutrons. In looking at some data obtained with the Tower Shielding Facility reactor, for instance, it is possible to see the effect of moving the observation point from zero degrees, or directly on the reactor beam axis, to a point 8.6° off the axis, where the high-energy neutrons are not so numerous. As a result of this sensitivity to high energies, in many situations it is necessary to obtain a simultaneous measurement of the high-energy range in order to understand the epithermal data.

As the previous paragraph notes, the program thus far has been used to successfully analyze several pieces of TSR data. Making a satisfactory assumption for the trial spectrum has been somewhat tedious, but a library of typical curves is being accumulated which should facilitate future guessing. A major weakness of the method, of course, is that it does not offer any way to assign errors to the final results. The most reasonable scheme may be to compare the results of multiple runs.

The program does have the small virtue of a short running time. Four assumed spectra can be computed on the CDC 1604 in just over 1 min. The program probably should be converted for use with the remote consoles now available in the Division, so that variations in the flux assumptions could be studied without the loss of time due to computer turnaround now existing.

References

[1]T. V. Blosser, *Neutron Phys. Div. Ann. Progr. Rept. May 31, 1966,* ORNL-3973, vol. 1, p. 59.

[2]T. V. Blosser and R. M. Freestone, Jr., *Neutron Phys. Div. Ann. Progr. Rept. Aug. 1, 1965,* ORNL-3858, vol. 1, p. 59.

[3]W. R. Burrus *et al., Neutron Phys. Div. Ann. Progr. Rept. May 31, 1966,* ORNL-3973, vol. 1, p. 61.

6.9 ON-LINE DATA ACQUISITION AND DATA REDUCTION USING A PDP-7 COMPUTER

J. A. Biggerstaff[1] A. L. Marusak[2]
J. K. Dickens J. W. McConnell[3]
W. E. Kinney F. G. Perey

A PDP-7 computer was received from Digital Equipment Corporation in October 1966 for acquiring on-line neutron time-of-flight data, and was put into use in November 1966. Experiments performed using the computer include (p,n) reactions (Sect. 1.11), (d,n) reactions (Sect. 1.10), and (n,n) elastic and inelastic scattering (Sect. 1.6).

A program for data reduction was written, and has been used to process data accumulated both before and after the computer was delivered. This program has effectively reduced the time required to extract areas of peaks from the raw spectra and thereby has eliminated the bottleneck previously involved in data reduction.

A number of routines have been written which improve the software provided by the manufacturer by taking advantage of our complete computer configuration. In addition, routines have been written for cross-section determination which are used in

conjunction with large programs written for the large ORNL data processing units (IBM 360, CDC 1604). Present programming efforts include continually improving and melding these routines so that on-line decisions, based on analysis of the data, can be promptly effected.

Computer Configuration

The computer system consists of a PDP-7 central processing unit, having 8K memory and 1.75-μsec cycle time; an extended arithmetic unit with hardware integer multiplying, dividing, and long-shift operations; standard Teletype model 33 keyboard for input-output, Digitronics model 2500 fast paper tape reader, and Teletype model BRPE II fast paper tape punch; two IBM-compatible magnetic tape drive units; four TMC model 217A 4096-channel analog-to-digital converters; and a Hewlett-Packard model 141A storage oscilloscope. A light-pen facility was added in February. A patch-panel interface unit accepts the digital output from the ADC's, and forms computer-size words. These data are stored in a buffer region in the central processor on a cycle-stealing basis. The data buffer region is designated under program control, and a flag is set when the buffer is full.

Data Acquisition Program

A program has been written and used for the acquisition, processing, and display of data obtained in the neutron time-of-flight experiment. The data are stored in a basic two-dimensional array of 4096 channels consisting of 512 (or 256) channels for time of flight for each of 8 (or 16) recoil-proton energy groups. The time-of-flight axis is linear in time, but the energy axis is divided into nonlinear bins under program control. The division of the energy axis is determined by the experimentally obtained flight-time dependence on recoil-proton pulse height (i.e., the electronic "walk"). The walk-corrected, collapsed, 512-channel time-of-flight spectrum is stored. A 256-channel time-of-flight spectrum from a monitor detector is also stored. Selected spectra are displayed during data acquisition. The channel contents and running sum of any portion of any of the saved data may be typed out. All data are saved in binary form on magnetic tape, and data saved on tape may be recalled.

Data Reduction Program

A program fully utilizing the light-pen facility has been written and is being continually used to extract peak areas from the walk-corrected, collapsed spectra. Spectra from two runs may be handled simultaneously; for (n,n') data these two spectra consist of a sample-in run and its associated sample-out run. Normalization factors are obtained from the monitor spectra, and the sample-out spectrum is subtracted from the sample-in spectrum. Any further background subtraction may be drawn in, using the light pen. Areas, centroids, and second moments for peaks of interest are extracted and typed out. All commands from the user are communicated to the computer by the light pen sensing light spots on the oscilloscope face.

Other Programming Efforts

A routine to display text material on the oscilloscope, which uses the variable persistence feature of this oscilloscope, has been written and incorporated into the symbolic tape editor program (supplied by DEC). This addition has improved the efficiency of symbolic tape processing.

A "short-form" floating point package has been prepared for essential floating point operations which is much faster and requires much less memory space than the standard packages. To obtain these features, precision and range requirements were reduced. The range is from 1×10^{-8} to 8×10^{10} and the precision for most of this range is 1 part in 800. These capabilities are quite sufficient for most of our data-handling needs.

Two data read-in routines have been appended to the data-reduction program which allow reading in punched paper tapes from Nuclear Data 160 FM analyzers and data on magnetic tape in the BCD format prepared using standard programs on the High Voltage Laboratory CDC 160-A computer.

FORTRAN programming has been used to provide several useful routines, even though FORTRAN preparation is, at best, awkward for our computer. However, once a program has been successfully assembled, it may be stored on a program magnetic tape for easy recall. Routines prepared using FORTRAN include curve fitting to power series, Legendre polynomials, and Gaussian function. These routines display the data and the computed curve. A routine to perform calculations

of cross sections given the extracted peak areas, detector efficiency function, total cross sections, sample parameters, and detector geometry has been extensively used. Kinematic calculations are included in this routine.

References

[1]Physics Division.
[2]Oak Ridge Graduate Fellow from University of Tennessee under appointment from the Oak Ridge Associated Universities.
[3]Instrumentation and Controls Division.

6.10 PDP-7 SYSTEM INTERFACE

J. W. McConnell[1] J. A. Biggerstaff[2]
F. G. Perey

A Digital Equipment Corporation PDP-7 computer was installed in October. This installation consists of a standard PDP-7 computer with 8192, 18-bit words of memory, extended arithmetic for hardware multiplication, division, and long shifts, two IBM-compatible magnetic tape drives and controller, a light pen, a three-channel direct-access-to-memory interface, and four Technical Measurements Corporation, 20-MHz (megacycles/sec) analog-to-digital converters (ADC).

The ADC interface consists of three 36-bit input channels. Each channel may be independently enabled, disabled, and reset under program control. Also each channel may be independently selected for single or double word input under program control, i.e., 18- or 36-bit input. All three channels have equal priority. Thus if data are presented to channels A and B simultaneously, the computer must accept the data from both channels before a second data input request can be honored on channel A. Any combination of the four ADC's may be connected to any of the three interface channels.

An interface has been designed for reading Transistor Specialties, Incorporated, model 1535 scalers into the computer. Each dual scaler contains its own parallel to serial converters and output gating to the four output data lines. The output is 1-2-4-8 binary coded decimal. The interface provides program control for the reading and resetting of the scalers. Provision is made to allow the computer to control the counting gates of the scalers.

The computer has greatly increased the data-handling capability for the time-of-flight experiment. Use of three detectors with only minor additions to existing equipment is feasible, thereby reducing the time required to obtain a complete neutron angular distribution by a factor of 3. Figure 6.10.1 shows a system block diagram for a three-detector configuration. Each detector requires a fast-timing discriminator, a slow linear amplifier, and a zero-crossing detector. All other electronics are shared by the three detectors.

References

[1]Instrumentation and Controls Division.
[2]Physics Division.

6.11 SUPER FLICKERS – AN ON-LINE DATA ACQUISITION SYSTEM FOR THE PDP-8[1]

B. W. Rust[2] W. R. Burrus

SUPER FLICKERS is a system of PDP-8 programs for accumulating and processing four-parameter data from pulse-height and time-of-flight analyzers. It writes all incoming data on magnetic tape for later analysis by a larger computer and provides oscilloscope displays of various two-dimensional "flicker boxes" on an event-by-event basis. It also accumulates and plots certain one-dimensional combination spectra which are of interest. Program options are controlled by key switches, and plot scaling options are controlled by teletype keys.

References

[1]Abstract of ORNL-TM-1878 (in preparation); work funded by the National Aeronautics and Space Administration under NASA order R-104(1).
[2]Computing Technology Center, Union Carbide Corporation, Oak Ridge.

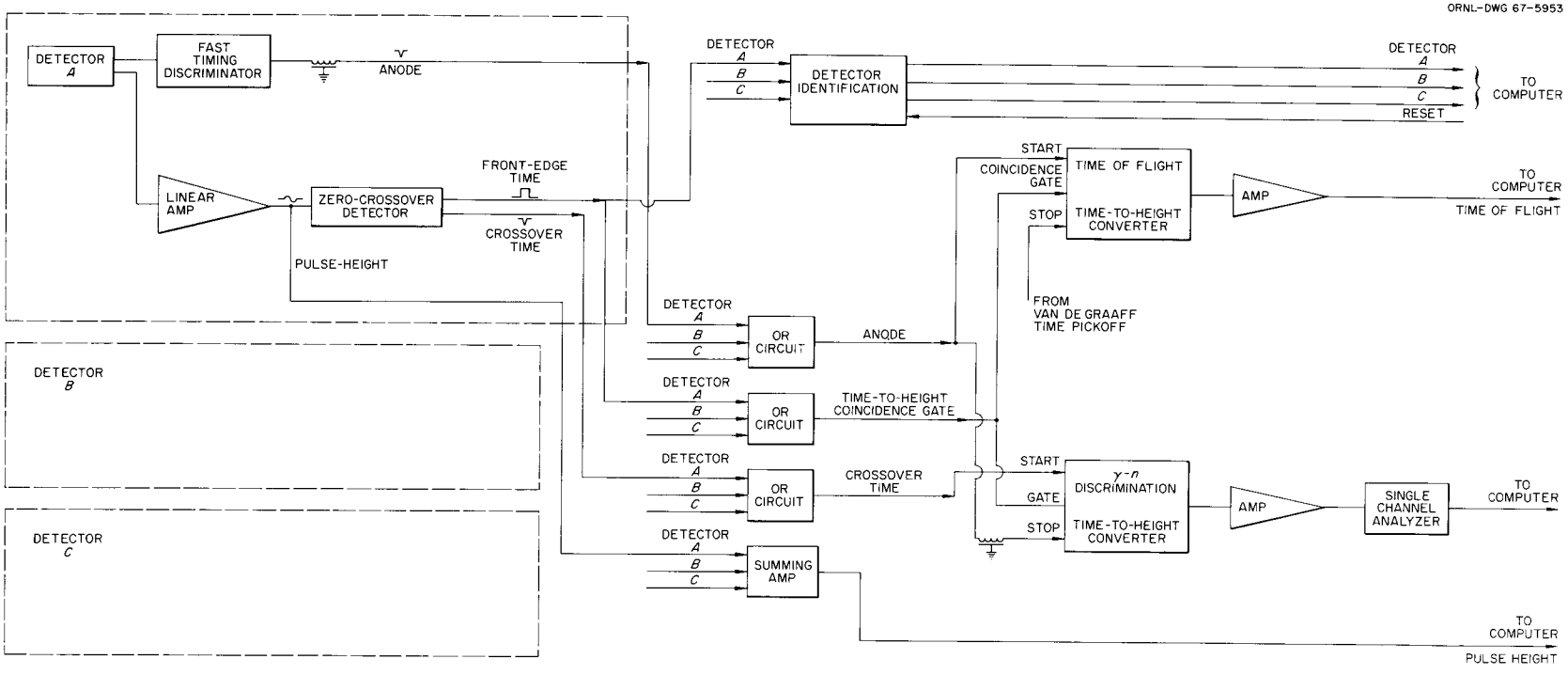

Fig. 6.10.1. Multidetector Block Diagram.

6.12 FLEXI-KLUDGE – A MULTIPARAMETER NUCLEAR SPECTRUM SUMMING SYSTEM FOR THE PDP-8[1]

B. W. Rust[2] W. R. Burrus

FLEXI-KLUDGE is a system of PDP-8 programs for the on-line accumulation and summing of multiparameter nuclear spectra. Pulse heights from four different detectors are brought into the computer, together with flags which contain coincidence, pulser, and pile-up information. Upon initialization, the operator may impose conditions for the accumulation or summing of any of the four spectra. The result is a single-dimension 2048-channel pulse-height distribution. One and one-half words (18 bits) are used for the count storage for each channel. Routines are provided for typing and integrating the spectrum between limits specified by the user and for displaying the spectrum on the oscilloscope. Routines are also provided for driving a Moseley X-Y plotter, which is connected in parallel with the scope. The full 2048 channels are plotted on two 11- by 14-in. graphs in the form of an inked histogram in less than a minute. The primary purpose of the FLEXI-KLUDGE system is to aid in the routine testing and setting up of multiparameter experiments.

References

[1]Abstract of ORNL-TM-1879 (in preparation); work funded by the National Aeronautics and Space Administration under NASA order R-104(1).

[2]Computing Technology Center, Union Carbide Corporation, Oak Ridge.

6.13 PUT-5 AND TAKE-5 – TWO MAGNETIC TAPE SYSTEM ROUTINES FOR THE PDP-8[1]

B. W. Rust[2] W. R. Burrus

Two magnetic tape system routines, PUT-5 and TAKE-5, have been written to provide fast input of programs or data to a PDP-8 computer from a DEC type 580 tape transport. PUT-5 is used to create system tapes containing the user's programs, and TAKE-5 is used to read the programs into the computer from such system tapes.

References

[1]Abstract of ORNL-TM-1805 (1967); work funded by the National Aeronautics and Space Administration under NASA order R-104(1).

[2]Computing Technology Center, Union Carbide Corporation, Oak Ridge.

6.14 BIG HOOP AND LITTLE HOOP – TWO PETER T. HOOPER ROUTINES FOR CHECKING THE DATA BREAK ON A PDP-8[1]

B. W. Rust[2] W. R. Burrus

Two routines, BIG HOOP and LITTLE HOOP, have been written to check the data break for the PDP-8. Both routines flicker for each event a dot on an oscilloscope, with the x and y coordinates equal to any two of the four signals for that event. The routines differ in that LITTLE HOOP requires the user to specify at the start of the program which two signals he wants plotted, whereas BIG HOOP contains a command program COMMND which allows the user to change the signal being plotted along each axis by typing in changes from the keyboard. COMMND also can serve as a prototype for more complex and powerful command routines which could be used to give the experimenter more flexibility in controlling what the computer does during the experiment.

References

[1]Abstract of ORNL-TM-1795 (1967); work funded by the National Aeronautics and Space Administration under NASA order R-104(1).

[2]Computing Technology Center, Union Carbide Corporation, Oak Ridge.

6.15 CALCULATION OF THE GAMMA-RAY RESPONSE OF A COMPTON DIODE DETECTOR

V. R. Cain C. Y. Fu[1]
R. Roussin[2]

The OGRE-G[3] Monte Carlo computer code has been modified to calculate the response of a Compton diode detector. Photon histories are followed as in OGRE-G and side trips are made to

estimate the electron charge transfer. Compton effect and pair production effect are treated separately by two different versions of the code.

The collector element in the Compton diode detector under consideration is a solid aluminum cylinder surrounded by Teflon insulation and enclosed in an aluminum housing. A detector may contain as many as five diodes stacked together and surrounded by a lead shield and collimator.

The response of the detector is based on the net transfer of charge to the collector element. Charge transfer is accomplished by electrons which are set in motion through interactions with photons. Some electrons are knocked from other parts of the detector and stop in the collector, whereas electrons originally in the collector are knocked into other areas. An output current is observed when the two mechanisms are unequal. For a fixed number of incident photons per unit time the response is a function of the input gamma energy.

The following assumptions are used in the calculations:

1. Monoenergetic and monodirectional gamma rays below 10 MeV are incident on the circular face of the diode.
2. An electron travels in a straight line for a distance equal to its extrapolated range.
3. Photoelectrons are unimportant.
4. The effects of the positron and the electron emerging from a pair production event cancel each other due to symmetry in their energy and angular distributions. However, the two 0.51-MeV gamma rays from annihilation of the positron are processed in the pair production version of the code.
5. Electrons are not able to cross more than one interface.

One of the important features of the code is a scheme to estimate electron transfer quantities for each leg of a photon history. The introduction of a good estimation technique is desirable because the electron crossing events which contribute to charge transfer have a small probability of occurring. A source photon or a scattered photon is assumed to continue from the source point or the collision point until it escapes from the system. A geometry routine is used to track the photon on its imaginary journey. Each time the collector-insulator interface is crossed, the crossing points and the distance to the crossing point are stored. A scattering collision is assumed to occur in a small interval about each crossing point. The direction and the extrapolated range of the Compton electron produced in such a collision are determined first. Then a triangle is formed using the direction and the extrapolated range of the electron, the original photon leg, and the collector-insulator boundary. The collision point is selected uniformly on the side of the triangle formed with the original photon leg. The electron produced in such a way is assumed to cross the interface, carrying a proper statistical weight.

The results obtained are compared in Table 6.15.1 with some experimental data.[4] The experimental data are for a three-diode detector and for ^{137}Cs (0.66-MeV), ^{60}Co (1.25-MeV), and ^{24}Na (1.37- and 2.76-MeV) sources. The calculations are for 0.66-, 1.25-, and 2.76-MeV sources. The data in the last column are a transformation to a "pure" 2.76-MeV source, based on the assumption that the sodium source consisted of a 2.76-MeV gamma and a 1.37-MeV gamma (equivalent to a Co source). The second set of numbers under the cobalt data was for a repeat run. No effort has been made to interpret the discrepancies between the computational results and the experimental data because the geometry of the detector used in the calculation is not entirely conformed to that used in the experiment (due to later changes in the detector structure). There were also experimental difficulties, primarily that approximately one-third of the dose from the sources was due to scattered gamma rays.[5]

Calculation of the pair production effect for 6-MeV photons indicates that it is a negative effect, about 4% of the Compton effect in the first diode, 7% in the second, and 9% in the third.

References

[1]Consultant, University of Tennessee.

[2]Summer student, University of Illinois.

[3]D. K. Trubey and M. B. Emmett, *OGRE-G, An OGRE System Monte Carlo Code for the Calculation of Gamma-Ray Dose Rate at Arbitrary Points in an Arbitrary Geometry,* ORNL-TM-1212 (January 1966).

[4]G. P. Lietz, Harry Diamond Laboratories, Washington, personal communication, June 14, 1966.

[5]R. C. Lamb, Harry Diamond Laboratories, Washington, personal communication, March 8, 1967.

Table 6.15.1. Calculated Response of Compton Diode Detector Compared with Experimental Results

Diode	Source			
	^{137}Cs	^{60}Co	^{24}Na	Pure 2.76 MeV[a]
		Experimental Raw Data (Coulombs/R)		
1	2.6 (−11)[b]	4.27 (−11)	3.69 (−11)	3.11 (−11)
		3.93 (−11)		
2	0.48 (−11)	2.02 (−11)	2.38 (−11)	2.74 (−11)
		1.65 (−11)		
3		0.936 (−11)	1.37 (−11)	1.804 (−11)
		0.655 (−11)		
		Experiment (transformed to net electrons per history)		
1	4.56 (−4)	1.29 (−3)		1.68 (−3)
		1.18		
2	0.841 (−4)	6.09 (−4)		1.48 (−3)
		4.97		
3		2.82 (−4)		0.974 (−4)
		1.97		
		Calculations (net electrons per history)		
1	6.51 (−4)(6%)[c]	1.256 (−3)(6%)[c]		2.49 (−3)
2	2.19 (−4)(6%)	6.733 (−4)(5%)		1.43 (−3)
3	6.58 (−5)(8%)	2.631 (−4)(7%)		0.801 (−3)
		Ratios (exp./calc.)		
1	0.70	1.027		0.674
		0.94		
2	0.38	0.904		1.034
		0.74		
3		1.071		1.22
		0.75		

[a]Obtained by multiplying the sodium-source data by 2 and then subtracting the cobalt-source data.

[b](−11) = $\times 10^{-11}$, etc.

[c]Percentages are fractional standard deviations.

6.16 FAST-NEUTRON RESPONSE FUNCTION CALCULATIONS FOR POLYETHYLENE-MODERATED FISSION CHAMBERS[1]

N. M. Greene[2] F. R. Mynatt[2]

Considerable work has been done toward predicting the count rate which a specified neutron source would produce in a special set of polyethylene–boron carbide detector systems, described in Fig. 6.16.1. A number of spectrally dependent sources striking the detectors at various positions were considered. The calculations for these cases were mockups of calibration checks for the detectors performed at the Bulk Shielding Reactor.

Initial work involved a 100-energy-group S_8P_3 transport calculation by the S_n code ANISN[3] to obtain the fast- and epithermal-neutron flux emergent from a 1-in.-diam beam tube placed in the

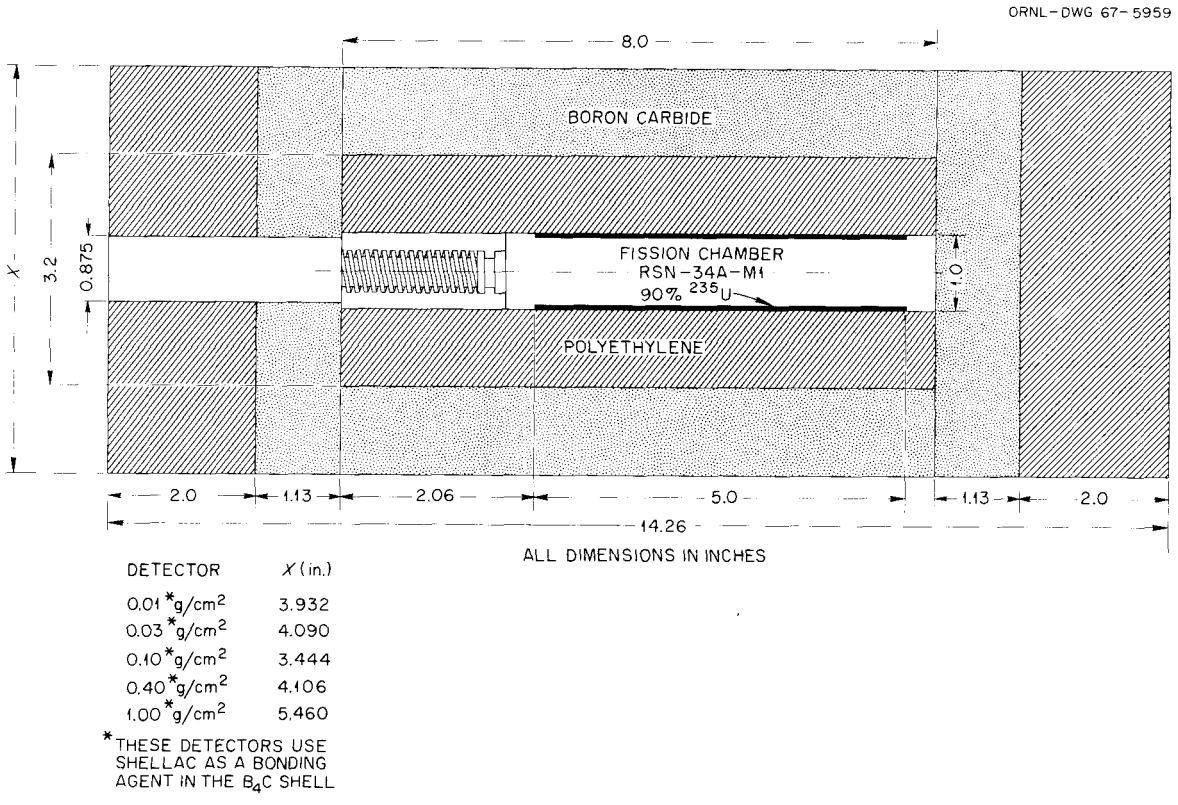

Fig. 6.16.1. Description of CH_2-B_4C Detector Systems.

BSR pool. The results of this calculation were coupled to those of Freestone[4] giving a spectral source distribution covering the energy range from thermal to 15 MeV. The variation in the source spectra was accomplished by placing ^{10}B filters of different thicknesses on top of the beam tube. The angular and spectral variation of the sources incident on the detectors was obtained in a series of S_n calculations.

A major difficulty existing prior to performing the S_n detector calculations was to obtain low-energy cross sections capable of describing the thermal transport of neutrons through polyethylene and boron carbide. The KERNEL[5] program was modified to allow up to 78 energy groups of upscatter and downscatter and to output cross sections in a format suitable for input to the S_n codes. A 78-group energy structure with a top energy limit of 3 eV was chosen.

To reduce running times, the 78-group thermal-cross-section set was reduced by a one-dimensional S_8P_3 cylinder calculation to a 13-group set in such a manner so as to make coupling with a 24-group GAM-II[6] set (fast and epithermal) possible. The coupling was accomplished by a specially written code which combined the 24 GAM-II groups with the 13 thermal groups into a single 37-group set. This set was used in any one-dimensional calculations required in the analysis, for example, the one-dimensional boron filter calculations noted above.

The 13 thermal groups of the 37-group structure contain upscatter. Because of the complexity of the upscatter problem in a two-dimensional S_n calculation – two-dimensional calculations are required for the detector system under study – it was decided to collapse the portion of the cross section containing upscatter into one group and to take the spatial spectral variation into account by using point-weighted cross sections. This resulted in 25-group cross-section sets for the two-dimensional calculations.

The detectors were mocked up as cylinders for the two-dimensional S_n code DOT.[7] S_6P_3 twenty-five energy-group calculations over a spatial mesh of 552 points (23 axial and 24 radial intervals) were performed. The scattering effects of the ^{10}B

filters were included by using the boundary source option of DOT which allows sources to be described as a function of angle, energy, and position.

Several normal (forward) calculations were run for the detector with a B_4C shell containing 0.1 g/cm^2 ^{10}B using the calculated source noted above, and the results were checked to make sure that the calibration data could be reasonably reproduced. These results were found to agree within around 10% for the cases in which the source beam struck the axial center of the detector. At this point it was decided to perform an adjoint calculation for one of the detectors. With a proper source input, one should be able to obtain numbers from which response functions for arbitrary sources can be calculated. The results of some of these calculations are given in Table 6.16.1. The response function for an isotropic flux covering the 0.1-g/cm^2 detector is shown in Fig. 6.16.2.

The advantage of the adjoint S_n method is that only one calculation is required to define the response function.

References

[1]Work supported by the Army Nuclear Defense Laboratory, Edgewood Arsenal, Maryland.

[2]Computing Technology Center, Union Carbide Corporation, Oak Ridge.

[3]W. W. Engle, Jr., *A User's Manual for ANISN, a One-Dimensional Discrete Ordinates Transport Code with Anisotropic Scattering*, K-1693 (1967).

[4]R. M. Freestone, Jr., *et al., Neutron Phys. Div. Ann. Progr. Rept. May 31, 1966*, ORNL-3973, Vol. I, p. 10.

[5]F. D. Federighi *et al., KERNEL and PAM — Programs for Use in the Calculation of the Thermal Scattering Matrix for Chemically Bound Systems*, KAPL-2225.

[6]G. D. Joanou and J. S. Dudek, *GAM-II: A B_3 Code for the Calculation of Fast-Neutron Spectra and Associated Multigroup Constants*, GA-4265 (1963).

[7]F. R. Mynatt, *A User's Manual for DOT, a Two-Dimensional Discrete Ordinates Transport Code with Anisotropic Scattering*, K-1694 (to be published).

Table 6.16.1. Comparison of Calculated Results with Calibration Data for Fission Chambers

(Beam on Axial Center of Detectors)

Cage	^{10}B Filter Thickness (g/cm^2)	^{10}B Filter Number	Measurement (counts/min)	Calculations (counts/min)	
				Forward S_n	Adjoint S_n
1[a]	0.1	0	2.991×10^4	2.99×10^4	2.99×10^4
2	0.1	1	2.700×10^4	2.77×10^4	2.73×10^4
3	0.1	10	2.009×10^4	2.02×10^4	1.94×10^4
4	0.1	15	1.444×10^4	1.51×10^4	1.36×10^4
5	0.1	20	7.371×10^3	9.63×10^4	7.58×10^3
6	0.4	0	2.068×10^4		2.07×10^4
7	0.4	10	1.596×10^4		1.62×10^4
8	0.4	15	1.236×10^4		1.22×10^4
9	0.4	20	6.766×10^3		7.22×10^3

[a]Results are normalized to this case.

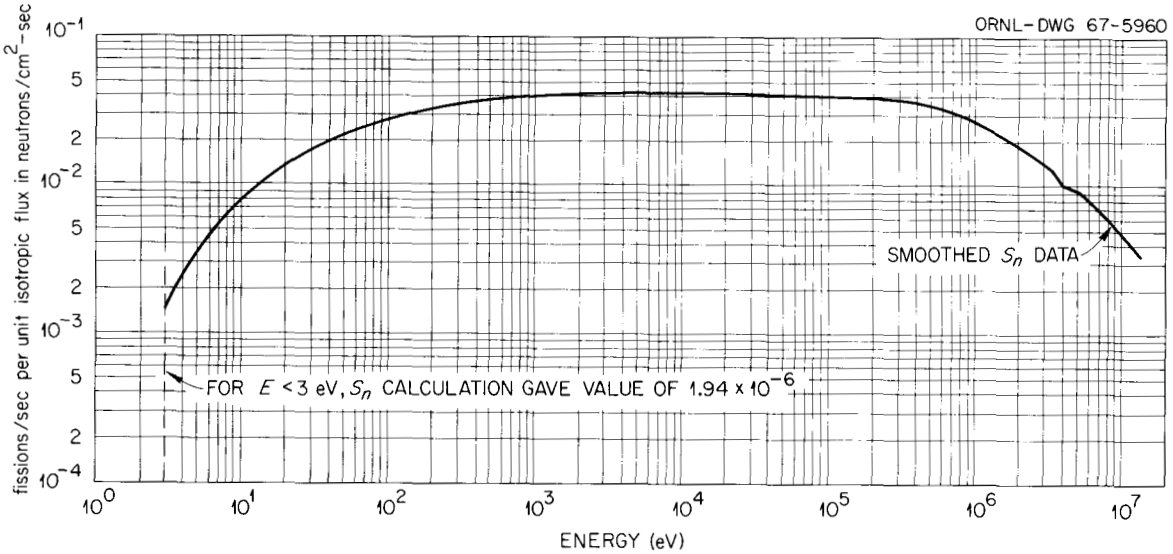

Fig. 6.16.2. Response Function for an Isotropic Flux Incident on the 0.1-g/cm^2 ^{10}B Detector.

7. Theoretical Studies for High-Energy Radiation Shielding

7.1 SOME EFFECTS OF A MODIFIED EVAPORATION PROGRAM ON CALCULATIONS OF RADIOCHEMICAL CROSS SECTIONS AND PARTICLE MULTIPLICITIES FOR PROTONS ON CARBON AND ALUMINUM TARGETS[1]

Hugo W. Bertini

Earlier calculations of radiochemical cross sections by the usual cascade-evaporation approach for 25- to 400-MeV protons incident on aluminum and carbon have been repeated to determine the effects of some of the modifications made by Peelle and Aebersold in the evaporation program originally coded by Dresner. For aluminum the effect is to improve the agreement of the calculated cross section with experiment for the two reactions calculated, but for carbon the modifications resulted in no change in one case and in a decrease in agreement in another case. The most significant change in the particle multiplicities is that the average number of neutrons evaporated in the higher energy reactions with aluminum is about 25% higher when the modified program is used.

Reference

[1]Abstract of ORNL-TM-1549 (Nov. 14, 1966); work partially funded by National Aeronautics and Space Administration under NASA order R-104(1).

7.2 SECONDARY PARTICLE SPECTRA FROM THE INTERACTION OF 30- TO 340-MeV PROTONS ON COMPLEX NUCLEI: EXPERIMENTAL DATA AND COMPARISON WITH THEORY[1]

Hugo W. Bertini

A survey was made of the measured neutron and proton spectra from the interaction of protons with nuclei in the energy region of 30 to 340 MeV, and a number of serious discrepancies or anomalies were found. One is that a pronounced quasi-elastic neutron peak appears at small forward angles as the incident proton energy is increased from 100 to 140 MeV, and there is no explanation for this energy dependence at the present time. Another is that the measured neutron spectra at small angles from 160-MeV protons have a dependence on the mass number of the target, which is inconsistent with the 140-MeV data. Also, the shapes of some of the measured secondary proton spectra are inconsistent with each other. These data have been compared with the theoretical predictions in an intranuclear-cascade calculation, but it is difficult to evaluate the predictions because of the experimental discrepancies. In order to progress in the development of the theory, additional experiments are needed to resolve some of these differences.

Reference

[1]Abstract of ORNL-TM-1652 (Feb. 27, 1967); work partially funded by National Aeronautics and Space Administration under NASA order R-104(1).

7.3 REPRESENTATIVE RESULTS IN GRAPHICAL FORM FROM COMPUTER PRODUCTION RUNS OF THE LOW-ENERGY INTRANUCLEAR-CASCADE CALCULATION[1]

Hugo W. Bertini Barbara L. Bishop
Miriam P. Guthrie

This report contains an extensive set of graphs which are meant to illustrate the mass and energy dependence of results that were selected from the output of computer production runs of a low-energy intranuclear-cascade calculation. The nuclear reactions considered are those resulting from the interaction of neutrons and protons with energies from 50 to 400 MeV and π^+ and π^- with energies from 50 to 300 MeV with nuclei ranging from carbon

to uranium. Plausibility arguments are given in an attempt to explain some of the results.

Reference

[1]Abstract of ORNL-4128 (in press); work partially funded by National Aeronautics and Space Administration under NASA order R-104(1).

7.4 COMPARISON OF EXPERIMENTAL SECONDARY PARTICLE ENERGY SPECTRA WITH RESULTS FROM INTRANUCLEAR CASCADE CALCULATION FOR PROTONS INTERACTING WITH NUCLEI AT 0.66 AND 2.9 BeV[1]

Hugo W. Bertini

The medium-energy cascade calculation described previously[2] has been debugged. The angular distribution of the isobars remains to be determined, and the latest values of the free-particle cross-section data that are required by the program must be incorporated. Work on these items is in progress.

The program is in operation, and comparisons with experiment are shown in Figs. 7.4.1–7.4.3. Figure 7.4.1 illustrates excellent agreement for the proton spectrum at 18° from 0.66-BeV protons on copper. Figure 7.4.2 contains the possibility of a large discrepancy between theory and experiment for 2.9-BeV protons on platinum. The shapes of the proton spectra at low secondary particle energies are quite different. This discrepancy will be examined in detail to determine its source. The data for emitted pions, in Fig. 7.4.3, are in reasonable agreement.

The angular distribution of the isobars that was used in making these comparisons was such that 25% of the time the isobar was emitted at zero

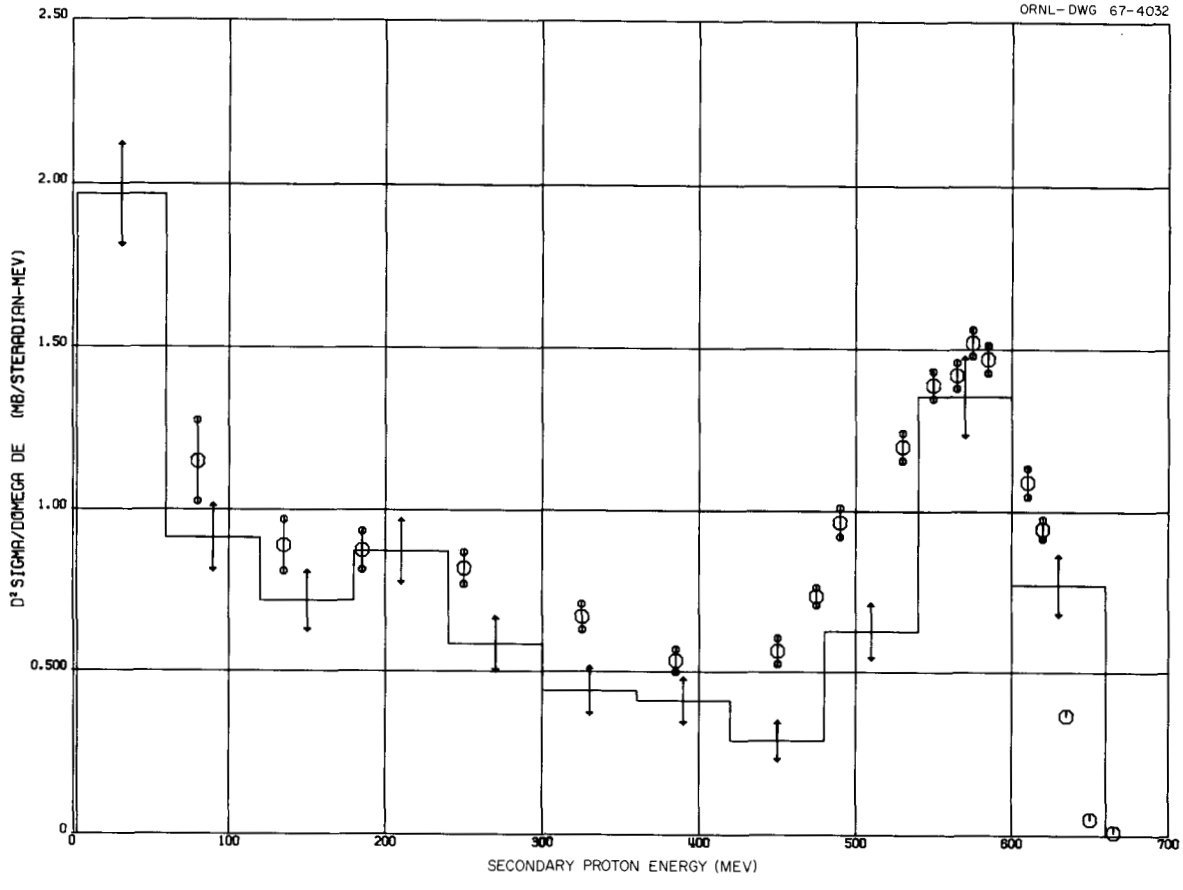

Fig. 7.4.1. Secondary Proton Spectrum at 18° from 0.66-GeV Protons on Copper. The octagonal figures represent the experimental data of L. S. Azhgirey *et al.*, *Nucl. Phys.* 13, 258 (1959). The histogram represents the calculated spectrum of protons emitted into the angular interval 13 to 23°.

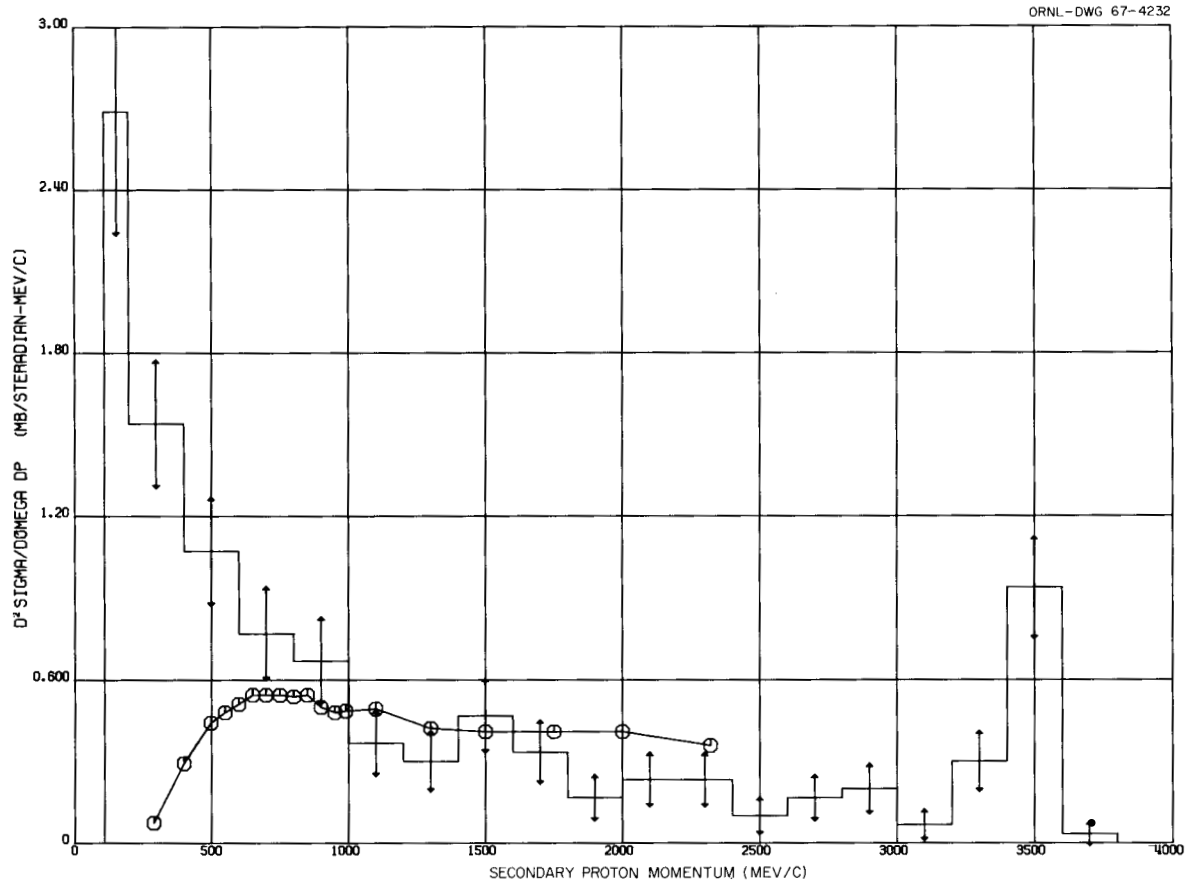

Fig. 7.4.2. Secondary Proton Spectrum at 13° from 2.9-GeV Protons on Platinum. The octagonal figures connected by straight lines represent the experimental data of P. A. Piroué and A. J. S. Smith, *Phys. Rev.* **148**, 1315 (1966). The histogram represents the calculated spectrum of protons emitted into the angular interval 10 to 15°.

degrees (in the center-of-mass system of the interacting particles), 25% of the time it was emitted at 180°, and 50% of the time it was emitted isotropically. The free-particle cross-section data that were used were published in the open literature no later than 1962.

References

[1]Work partially funded by National Aeronautics and Space Administration under NASA order R-104(1).

[2]H. W. Bertini, *Neutron Phys. Div. Ann. Progr. Rept. May 31, 1966*, ORNL-3973, Vol. II, p. 77.

7.5 EMISSION OF PROTONS AND CHARGED PIONS FROM Ag AND Br NUCLEI BOMBARDED BY 1.55-BeV NEGATIVE PIONS

D. T. King[1] Hugo W. Bertini

The differential cross sections for the emission of protons and charged pions from disintegrations produced in Ag and Br by 1.55-BeV negative pions have been measured. The results obtained from nuclear emulsions are compared with corresponding predictions of the intranuclear cascade obtained by Bertini.[2]

A stack of 3- by 4-in. Ilford K5 emulsions, each 600 μ thick, was exposed in the 1.70-BeV/c nega-

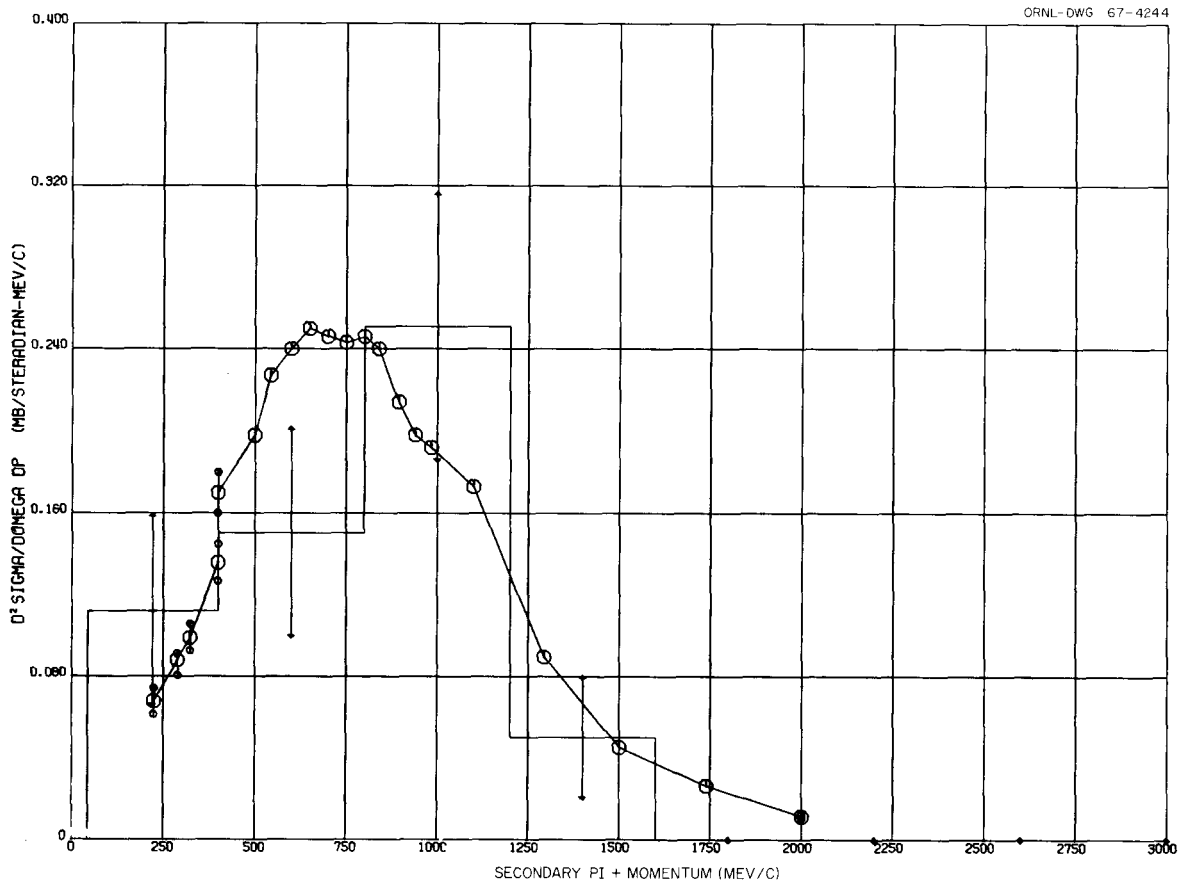

Fig. 7.4.3. Secondary π^+ Spectrum at 13° from 2.9-GeV Protons on Platinum. The octagonal figures connected by straight lines represent the experimental data of P. A. Piroué and A. J. S. Smith, *Phys. Rev.* **148**, 1315 (1966). The histogram represents the calculated spectrum of π^+ emitted into the angular interval 10 to 15°.

tive pion beam at the Lawrence Radiation Laboratory bevatron.[3] The beam intensity was 2.0×10^5 per square centimeter, and the beam direction was closely parallel to the emulsion plane. The beam momentum was checked both by kinematic analysis of elastic π^-, p collisions and by multiple Coulomb scattering of the beam tracks. From a search along the beam tracks, using oil-immersion objectives, the mean free path for inelastic nuclear collisions of beam particles was found to be 31.5 ± 1.2 cm. From the known composition of the emulsion,[4] it follows that the mean free path for nonelastic processes in Ag and Br nuclei is 45.5 ± 1.5 cm, corresponding to (70 ± 2)% of the collisions. The nonelastic cross section of 1.70 BeV/c π^- on Ag and Br is therefore found to be 1090 ± 36 mb. This result may be compared with the nonelastic cross section of 1073 ± 25 mb calculated by the Monte Carlo method for 1.55-BeV π^- on the nucleus ^{100}Ru, a weighted average of Ag and Br. Further, an inspection of the prong-number distribution for stars found by beam scan indicates that those stars with five or more heavily ionized prongs can most probably be identified as π^- collisions with the heavy nuclei of the emulsion. (This conclusion is not valid for proton-induced collisions.)

The data on emergent protons and charged pions have been gathered by a systematic examination of 3300 collisions produced by beam particles. (It is not possible here to distinguish the sign of the outgoing pions.) Stars located within 50 μ of either emulsion surface were excluded. Those outgoing tracks with ionization corresponding to singly charged particles with velocities exceeding 0.5 c and visible length exceeding 3.0 mm were recorded. If the ionization further indicated a velocity $0.5\ c < v < 0.85\ c$, an evaluation of the multiple Cou-

lomb scattering of the track was made in order to distinguish the cascade protons from emergent charged pions. (The pion beam energy was determined so that elastically recoiling protons are always distinguishable from pions; the proton energies are determined by reference to the ionization characteristic.) With small error, the outgoing tracks with velocities exceeding 0.85 c may all be attributed to pions. From 2400 stars with five or more heavily ionized prongs, we have found 175 proton tracks and 184 charged pion tracks, which satisfy our selection criteria. For each of these tracks the projected polar angle of emission, relative to the beam primary, was measured.

For 10° intervals of projected polar angle, the element of solid angle corresponding to emitted path lengths exceeding 3.0 mm in a 600-μ emulsion is readily calculated. By comparison of this element with the solid angle included within 10° intervals of polar angle, a geometric correction factor is obtained as a function of polar angle. In this way, we infer that our observations represent 1386 protons and 1530 charged pions emergent with velocities exceeding 0.5 c from 2400 π^- collisions in Ag and Br. Our measured result for the total-emission cross section (all angles) of protons with kinetic energy > 150 MeV is 630 ± 90 mb, which may be compared with the calculated value of 520 mb. Similarly, we find a total-emission cross section, 695 ± 100 mb, for charged pions (all angles) with kinetic energies exceeding 22 MeV. The calculated value is 924 mb. It may be noted that the protons are of particular interest in this experiment because they are all products of the intranuclear cascade and therefore provide a sensitive test of the Monte Carlo calculation.

Taking account of the corrected numbers of protons emitted into the indicated intervals of polar angle, we can deduce the differential cross section for proton emission at all energies > 150 MeV as a function of angle, shown in Fig. 7.5.1. The prediction of the intranuclear-cascade calculation ap-

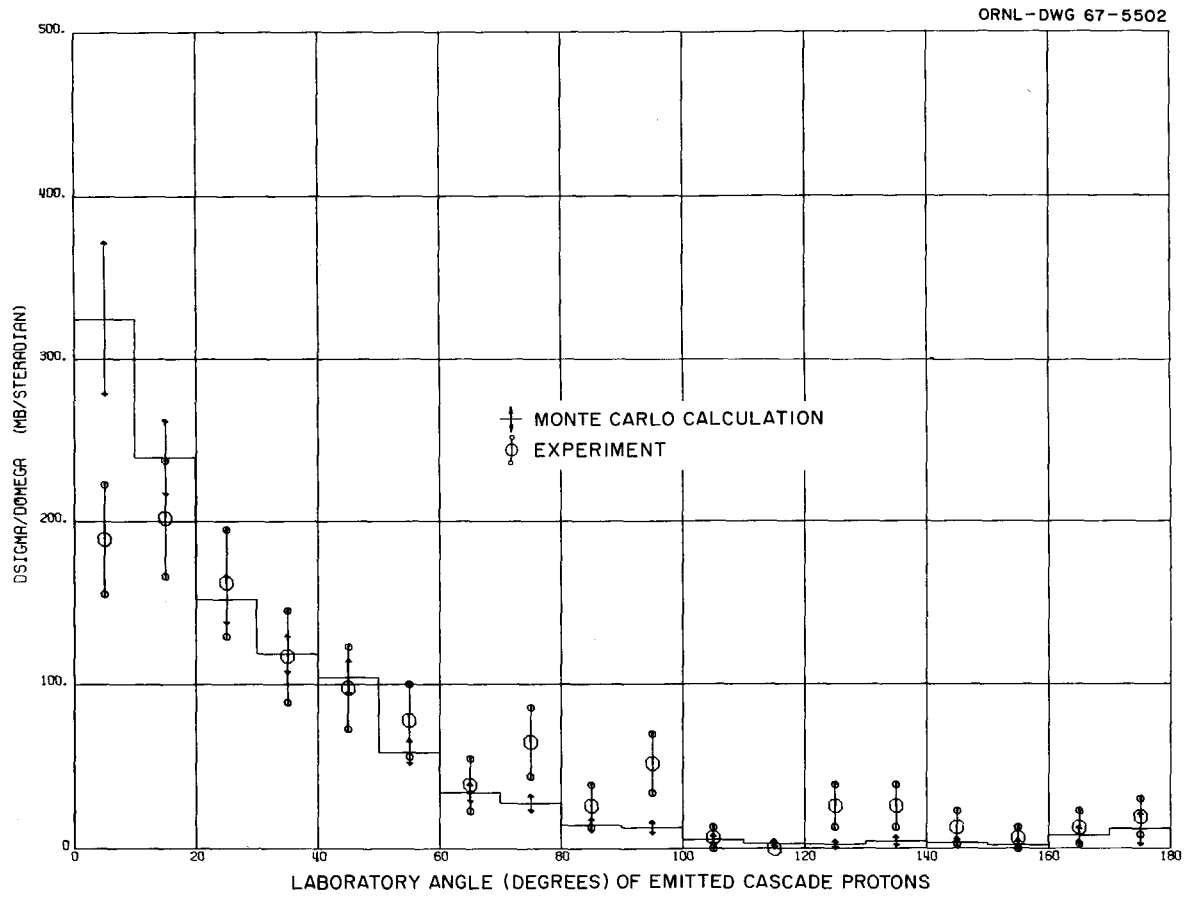

Fig. 7.5.1. Angular Distribution of Emergent Protons with Kinetic Energies > 150 keV. The experimental result is compared with the Monte Carlo prediction.

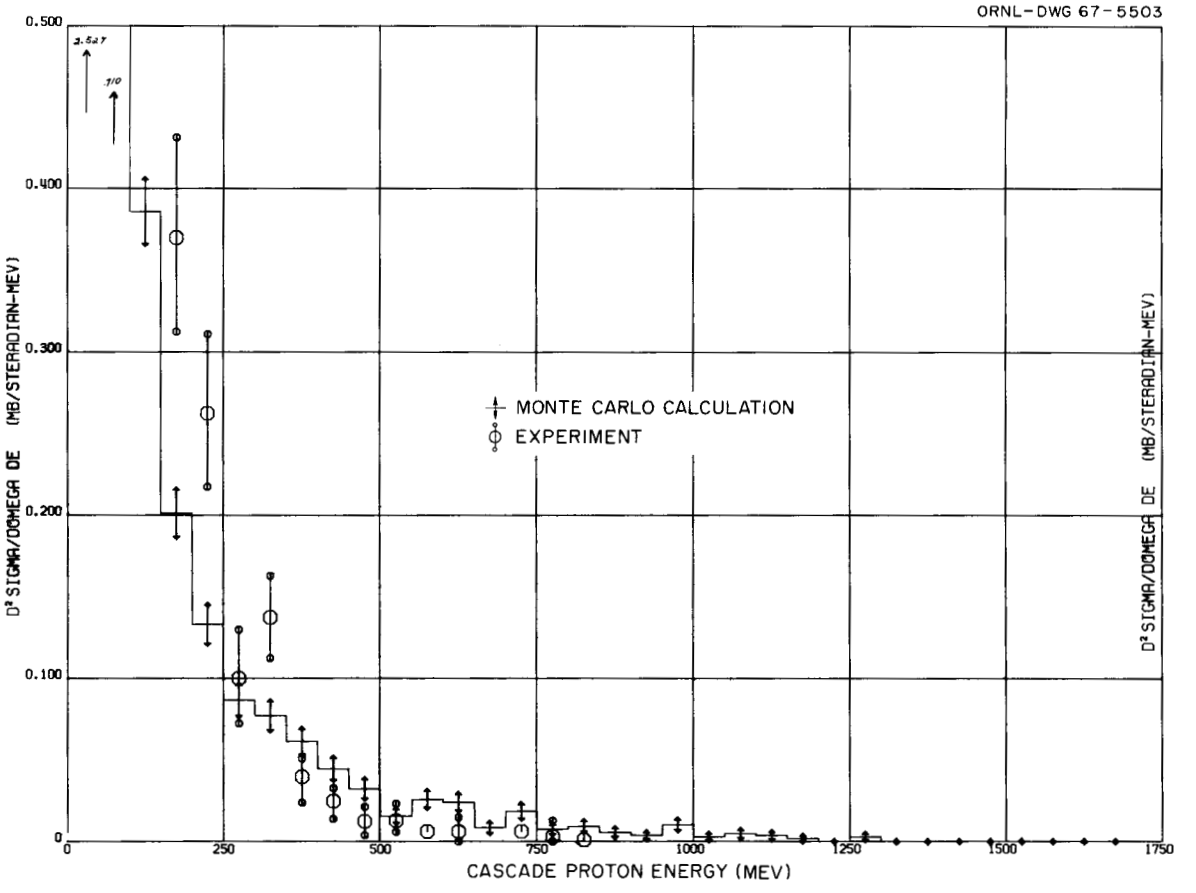

Fig. 7.5.2. Spectrum for Cascade Protons Emergent at All Angles.

pears to be in reasonable agreement with our results. In order to examine the differential cross section of the protons as a function of energy, it is necessary to tabulate the angles of emission for those protons within a given energy interval and then apply the appropriate geometric factors. The proton spectrum for all angles is compared with the prediction of the intranuclear cascade in Fig. 7.5.2, and again the two results exhibit a certain consistency. Apparently the ~20% disparity in the proton total cross sections arises chiefly from those protons with kinetic energies between 150 and 250 MeV.

For the charged pions it is possible to deduce only the differential cross section as a function of angle, as shown in Fig. 7.5.3, and here there is evidently a disagreement, with the experimental results significantly below the calculated values at the forward and backward angles. This comparison must be regarded as tentative since there is uncertainty regarding the values of the parameters in the isobar model. Observations are continuing in an effort to improve the statistical significance of the experiment.

References

[1]Consultant from the University of Tennessee.

[2]H. W. Bertini, *Neutron Phys. Div. Ann. Progr. Rept. May 31, 1966*, ORNL-3973, Vol. II, p. 78.

[3]Valuable assistance in adjusting and tuning the 1.70-BeV/c π^- beam was provided by W. Chupp and others at Lawrence Radiation Laboratory.

[4]W. H. Barkas, *Nuclear Research Emulsions*, Vol. 1, p. 74, Academic Press, New York, 1963.

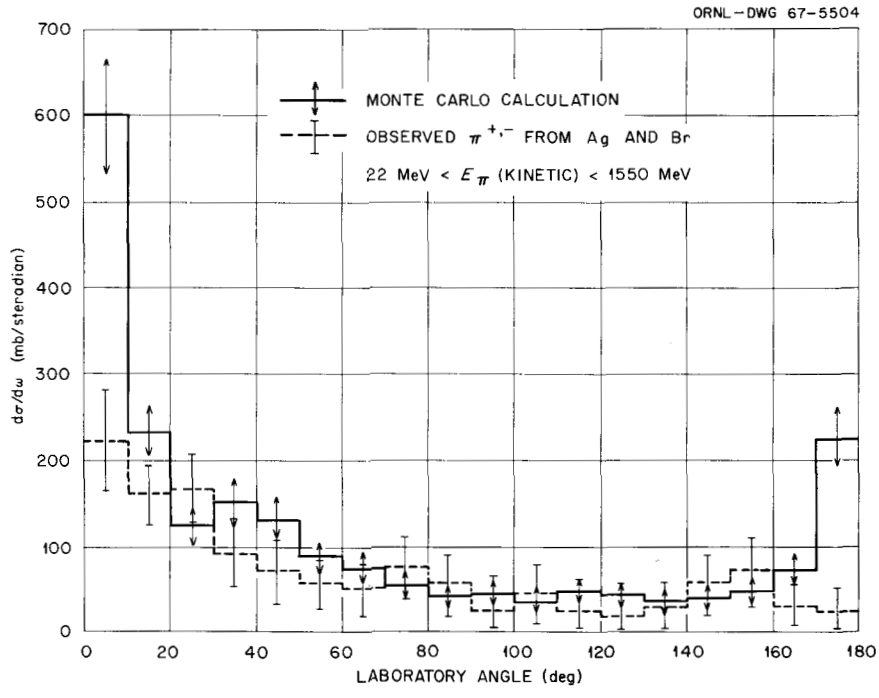

Fig. 7.5.3. Angular Distribution for Charged Pions with Emission Energies Exceeding 22 MeV.

7.6 ANALYTIC REPRESENTATION OF NONELASTIC CROSS SECTIONS AND PARTICLE-EMISSION SPECTRA FROM NUCLEON-NUCLEUS COLLISIONS IN THE ENERGY RANGE 25 TO 400 MeV[1]

R. G. Alsmiller, Jr. M. Leimdorfer
J. Barish[2]

Analytic fits, obtained by the method of linear least squares, to the intranuclear-cascade data generated by H. W. Bertini are given. For both protons and neutrons incident on the elements C, O, Al, Cr, Cu, Ru, Ce, W, Pb, and U, analytic expressions are given for the nonelastic cross section as a function of energy;[3] the cascade neutron- and proton-emission spectra in the angular intervals 0–30°, 30–60°, 60–90°, and 90–180°; the evaporation neutron- and proton-emission spectra (assumed isotropic); and the cascade neutron- and proton-emission spectra integrated over all angles.

References

[1]Abstract of ORNL-4046 (April 1967); work partially funded by National Aeronautics and Space Administration under NASA order R-104(1).

[2]Computing Technology Center, Union Carbide Corporation, Oak Ridge.

[3]Erratum to ORNL-4046: the expressions given on p. 4 for the nonelastic cross sections should read as follows:

$$\sigma(E) = \frac{1}{400} \exp\left[\sum_{j=0}^{\nu} a_j \left(\frac{E}{400}\right)^j\right], \qquad (1)$$

$$R = \sum_{E_i} \left[\log\left(400\sigma_{E_i}\right) - \sum_{j=0}^{\nu} a_j \left(\frac{E}{400}\right)^j\right]^2 ; \qquad (2)$$

that is, the coefficients *ao* printed in Table 1 are correct only if the exponential in Eq. (1) is divided by 400. When the coefficients in Table 1 are used in conjunction with Eq. (1), the cross sections are given in millibarns.

7.7 THERMAL-NEUTRON PRODUCTION FROM HIGH-ENERGY PROTONS IN THICK TARGETS AND THE EXTENSION OF THE NUCLEON TRANSPORT CODE TO 2–3 BeV[1]

W. A. Coleman[2] R. G. Alsmiller, Jr.

It is plausible that a thermal-neutron flux, comparable to those being produced in high-flux reactors, is attainable by bombarding certain target materials with a very intense beam of BeV protons. In this connection, the nucleon transport code,[3] NTC, has been used to calculate thermal-neutron flux distributions resulting from 540-MeV protons incident on cylindrical targets of lead and depleted uranium in a water moderator. The calculations were performed for the system represented schematically in Fig. 7.7.1. NTC presently incorporates a subroutine version of Bertini's low-energy intranuclear-cascade code,[4] which calculates an emitted cascade particle description at each nuclear collision. After each intranuclear cascade, an evaporation calculation is performed. Computation in this manner eliminates the need for explicit nucleon-nucleus cross-section data. In the calculations being discussed, the cascade-evaporation model was used down to 50 MeV. Neutrons below the cascade-evaporation cutoff energy are transported in NTC via the O5R neutron transport code.[5] In O5R, particle production following nonelastic collisions was treated using direct compound nucleus formation followed by evaporation.

The cross sections for the various nuclides in O5R were obtained almost exclusively from the references indicated below:

Element	Reference*
H	Irving and Gillen[6]
O	Irving and Gillen[6]
Pb	Hughes and Harvey,[7] Bertin *et al.*[8]
^{235}U	Hughes and Harvey,[7] Bertin *et al.*[8]
^{238}U	Hughes and Harvey,[7] Bertin *et al.*,[8] Webster[9]

*See list of references at end of paper.

The cross-section data in the region between 15 and 50 MeV for Pb and U are extremely sparse.

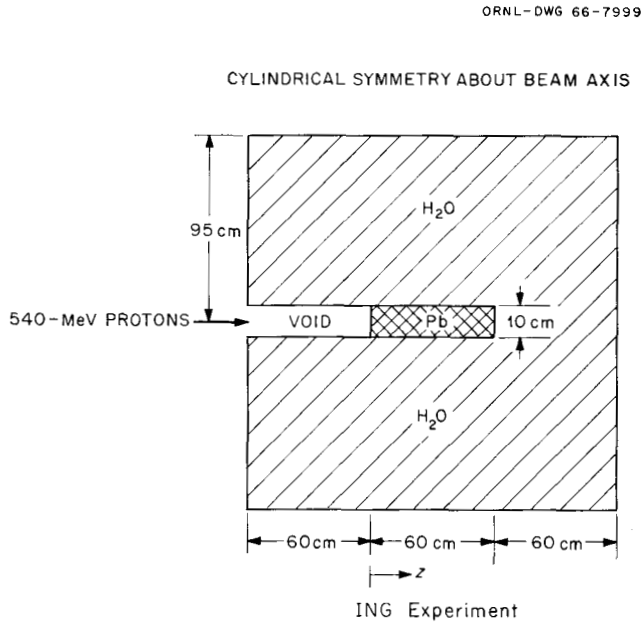

Fig. 7.7.1. Schematic Representation of a System for Thermal-Neutron Production from ~1-BeV Protons.

However, about 95% of all neutrons which enter the O5R calculation are below 15 MeV.

Neutrons slowing down past 0.5 eV were transported using the assumption of a one-speed model and isotropic scattering in the laboratory system. The thermal flux was obtained by calculating the collision density in each of 312 cylindrical annuli defined by 24 axial increments and 13 radial increments. Figures 7.7.2 and 7.7.3 illustrate radial-flux distributions for the z (axial) increments containing $z = -11.5$ and 19 cm respectively. The target-void interface defines $z = 0$, with z increasing to the right in Fig. 7.7.1. The numbers over the histograms are the calculated relative standard errors expressed in percent.

Fraser *et al.*[10] have performed a series of thermal-flux measurements at Brookhaven National Laboratory under conditions virtually identical with those of our calculations. Some of these data are presented in Figs. 7.7.2 and 7.7.3 for comparison with the Monte Carlo results.

Work is in progress to extend the valid energy range in NTC to ~2.5 BeV and include charged pion and muon transport. The revised version of NTC is being programmed for the IBM 360/2075 computer and will incorporate a subroutine version of Bertini's medium-energy cascade code (Sect.

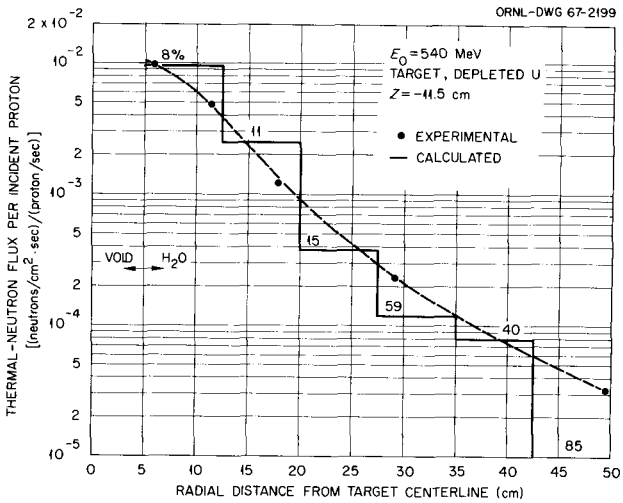

Fig. 7.7.2. Radial Distribution of Thermal-Neutron Flux at $z = -11.5$ cm Due to 540-MeV Protons Incident on a Depleted Uranium Target.

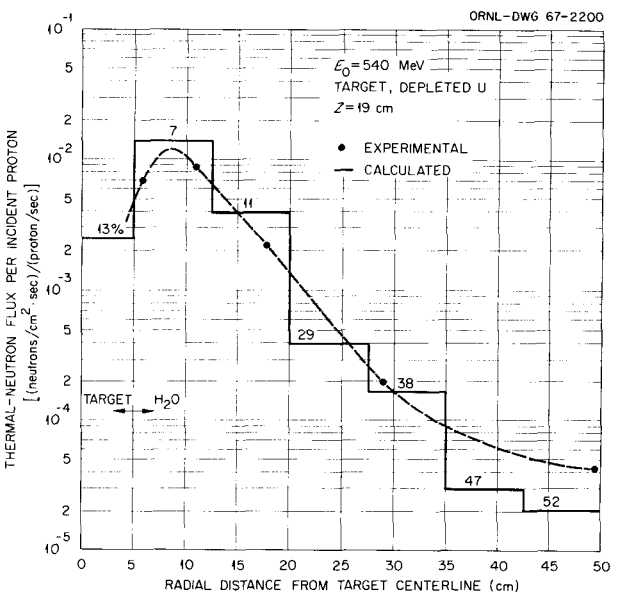

Fig. 7.7.3. Radial Distribution of Thermal-Neutron Flux at $z = 19$ cm Due to 540-MeV Protons Incident on a Depleted Uranium Target.

7.4). This is the same calculational scheme as was used in the existing version of NTC. An apparent alternative would be to use Bertini's code to generate a complete set of the cross-section and related data for each element in NTC and program these data into the code. Since this alternative is not realizable at present, the former procedure has been adopted.

References

[1]Work partially funded by National Aeronautics and Space Administration under NASA order R-104(1).

[2]University of Tennessee Graduate Fellow.

[3]W. E. Kinney, *The Nucleon Transport Code, NTC*, ORNL-3610 (1964).

[4]Hugo W. Bertini, *Phys. Rev.* **131**, 1801 (1963); and erratum *Phys. Rev.* **138**, AB2 (1965).

[5]D. C. Irving *et al.*, *O5R, A General-Purpose Monte Carlo Neutron Transport Code*, ORNL-3622 (1965).

[6]D. C. Irving and J. Gillen, *Neutron Phys. Div. Ann. Progr. Rept. May 31, 1966*, ORNL-3973, Vol. I, p. 55.

[7]D. J. Hughes and J. A. Harvey, *Neutron Cross Sections*, BNL-325 (1955).

[8]M. C. Bertin *et al.*, *Neutron Cross Sections of* U^{238}, U^{235}, U^{237}, U^{239}, U^{234}, U^{236}, Pu^{239}, Pu^{240}, *W, Pb, Ni, Cr, C,* Li^6, Li^7, *and I*, UNC-5099 (1964).

[9]J. W. Webster, *Point-Set Representation of* ^{238}U *Cross Sections; Values and a Fortran Program for Computation*, ORNL-TM-1448 (1966).

[10]J. S. Fraser *et al.*, *Phys. Can.* **21**(2), 17 (1965).

7.8 REACTION PRODUCTS RESULTING FROM THE ABSORPTION OF SLOW NEGATIVE PIONS BY THE LIGHT NUCLEI C, N, AND O[1]

B. Chern[2]

It is of interest to obtain the energy deposition in tissue by π mesons which have been essentially brought to rest. To calculate this, one needs to know the energy carried away by the reaction products resulting from the absorption of the pion by the nucleus. Evaluating the available experimental data and comparing it with the theoretical predictions, we obtain reasonable mass and energy spectra of the reaction products.

References

[1]Abstract of ORNL-4085 (to be published); work partially supported by National Aeronautics and Space Administration under NASA order R-104(1).

[2]Work performed while the author was at the Oak Ridge National Laboratory as a Summer Research Participant from the University of Florida, Gainesville.

7.9 THE VALIDITY OF THE STRAIGHTAHEAD APPROXIMATION IN SPACE VEHICLE SHIELDING STUDIES – II[1]

R. G. Alsmiller, Jr. D. C. Irving
H. S. Moran

The straightahead approximation, i.e., the approximation that the secondary particles from nucleon-nucleus collisions are emitted in the direction of the incident nucleons, is often used in space vehicle shielding studies. The validity of this approximation has been tested by comparing calculations made with the angular distribution of secondary particles properly taken into account with calculations using the approximation. Comparisons between the calculations are given for both monoenergetic protons and a typical flare spectrum normally incident on slab shields followed by tissue. The results indicate that the approximation is sufficiently accurate to justify its use in obtaining estimates of the secondary particle contribution to the dose in many space shielding situations.

Reference

[1]Abstract of ORNL-TM-1848 (in preparation); work funded by National Aeronautics and Space Administration under NASA order R-104(1).

7.10 CALCULATIONS OF THE RADIATION HAZARD DUE TO EXPOSURE OF SUPERSONIC AIRCRAFT TO SOLAR-FLARE PROTONS[1]

M. Leimdorfer R. G. Alsmiller, Jr.
R. T. Boughner[2]

Monte Carlo transport calculations have been carried out to estimate the dose that travelers in supersonic aircraft will receive from a typical spectrum of solar-flare protons. The dose, from both primary protons and secondary particles, has been obtained as a function of depth in a tissue slab placed at various depths in the atmosphere. The incident spectrum is broken into eight energy regions, and the dose from the incident protons in each of these regions is presented.

References

[1]Abstract of *Nucl. Sci. Eng.* **27**, 151–157 (1967) and of ORNL-TM-1594 (Dec. 7, 1966); work funded by the National Aeronautics and Space Administration under NASA order R-104(1).
[2]Mathematics Division.

7.11 AN ESTIMATE OF THE PROMPT PHOTONS ARISING FROM COSMIC-RAY BOMBARDMENT OF THE MOON[1]

T. W. Armstrong R. G. Alsmiller, Jr.

Measurement of the photon spectrum from the moon using a lunar orbiting satellite is being planned. To investigate the spectrum that might be expected, an estimate has been made of the spectrum of photons leaking from the moon's surface due to (n,γ) and $(n,n'\gamma)$ reactions induced by neutrons produced from cosmic-ray bombardment. Photons arising from proton-nucleus interactions are not being considered at present.

The first step of the calculation consisted of estimating the neutron spectrum at several distances into the moon using the data of Lingenfelter *et al.*,[2] Arnold,[3] Newkirk,[4] and Hess *et al.*[5] (see Fig. 7.11.1). The spectrum at 0 g/cm^2 is the neutron leakage spectrum from the lunar surface calculated by Lingenfelter *et al.* At 30 and 100 g/cm^2 the spectra for $E > 2$ MeV are Arnold's estimates for a lunar composition, and the shape of the spectra for lower energies is based on Newkirk's calculations in the earth's atmosphere. The shape of the 200-g/cm^2 spectrum is based on measurements by Hess *et al.* in the earth's atmosphere and was normalized using Arnold's lunar spectrum. By interpolation the neutron spectra at other spatial points, $\phi(E,x)$, were obtained. The function $\phi(E,x)$ must, of course, be considered to be very approximate.

The energy and position of neutrons having (n,γ) or $(n,n'\gamma)$ reactions were sampled according to the joint probability density function

$$p(E,x) = \frac{\Sigma_\gamma(E)\,\phi(E,x)}{\int_0^\infty dx \int_{E_{min}}^{E_{max}} \Sigma_\gamma(E)\,\phi(E,x)},$$

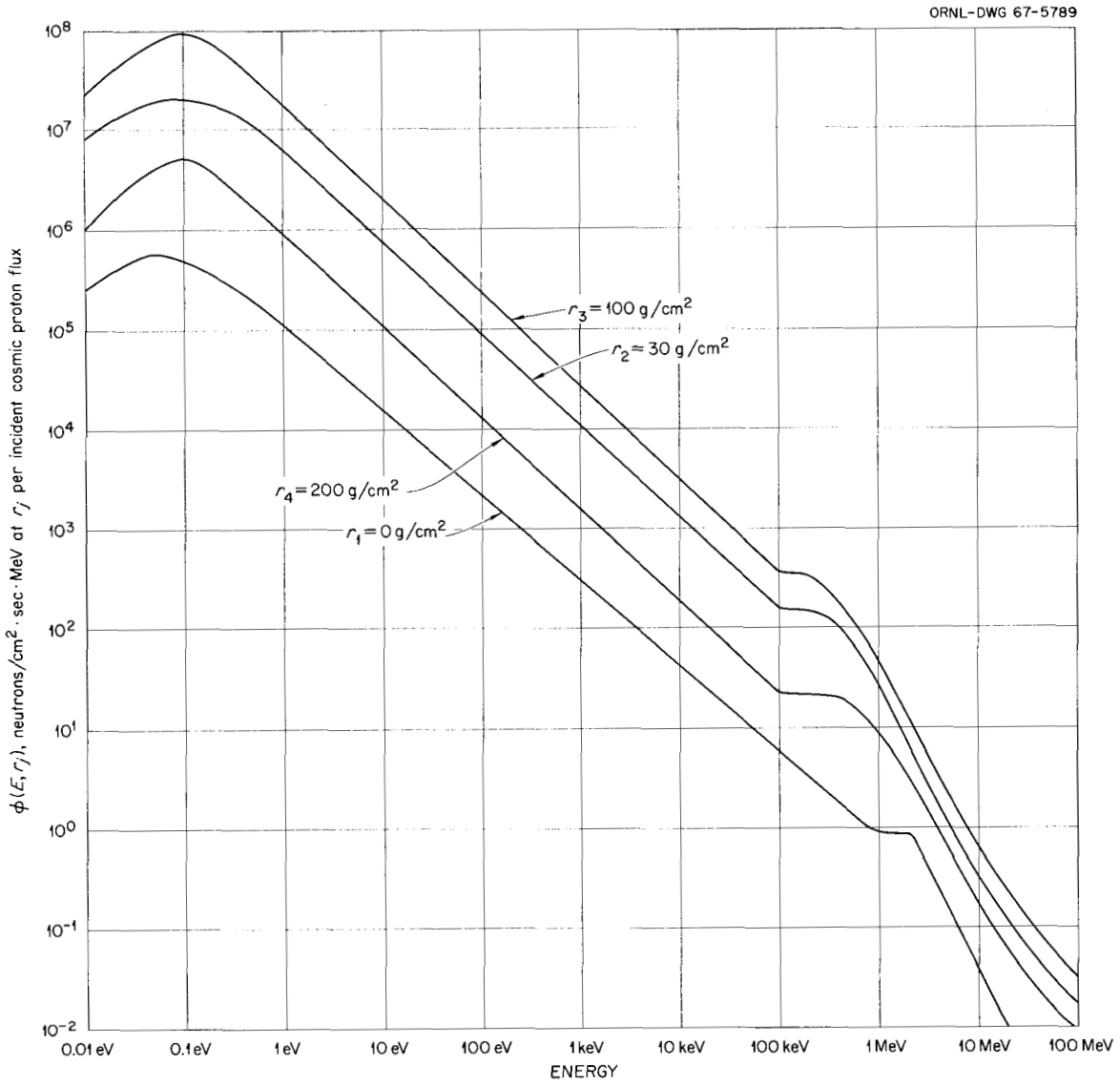

Fig. 7.11.1. Estimated Neutron Spectra in Moon Due to Cosmic-Ray Bombardment.

where $E_{min} = 10^{-8}$ MeV, E_{max} is the maximum neutron energy to be considered, and Σ_γ is the sum of the macroscopic capture and inelastic cross sections. Σ_γ was calculated using microscopic cross sections from the O5R cross-section library[6] and a lunar composition based on chrondritic meteorites. The composition assumed was (in at. %) O, 55.8; Si, 16.3; Mg, 15.2; Fe, 11.5; and Al, 1.2.

Selection of the photon energy, from both discrete and continuous distributions, was accomplished using the photon-production data (valid for neutron energies up to about 18 MeV) and the computer program developed in a related study by Leimdorfer and Boughner.[7] The photons were transported using the OGRE Monte Carlo program.[8]

At present, results have been obtained for neutron energies up to 18 MeV (Fig. 7.11.2). Similar calculations to include the higher energy neutrons (up to 100 MeV) using very approximate photon-production data are planned in order to obtain a rough estimate of the contribution of these high-energy neutrons to the photon leakage spectrum. If the high-energy neutrons prove to be important, then nuclear models for obtaining photon-production data of high-energy nucleons will be investigated.

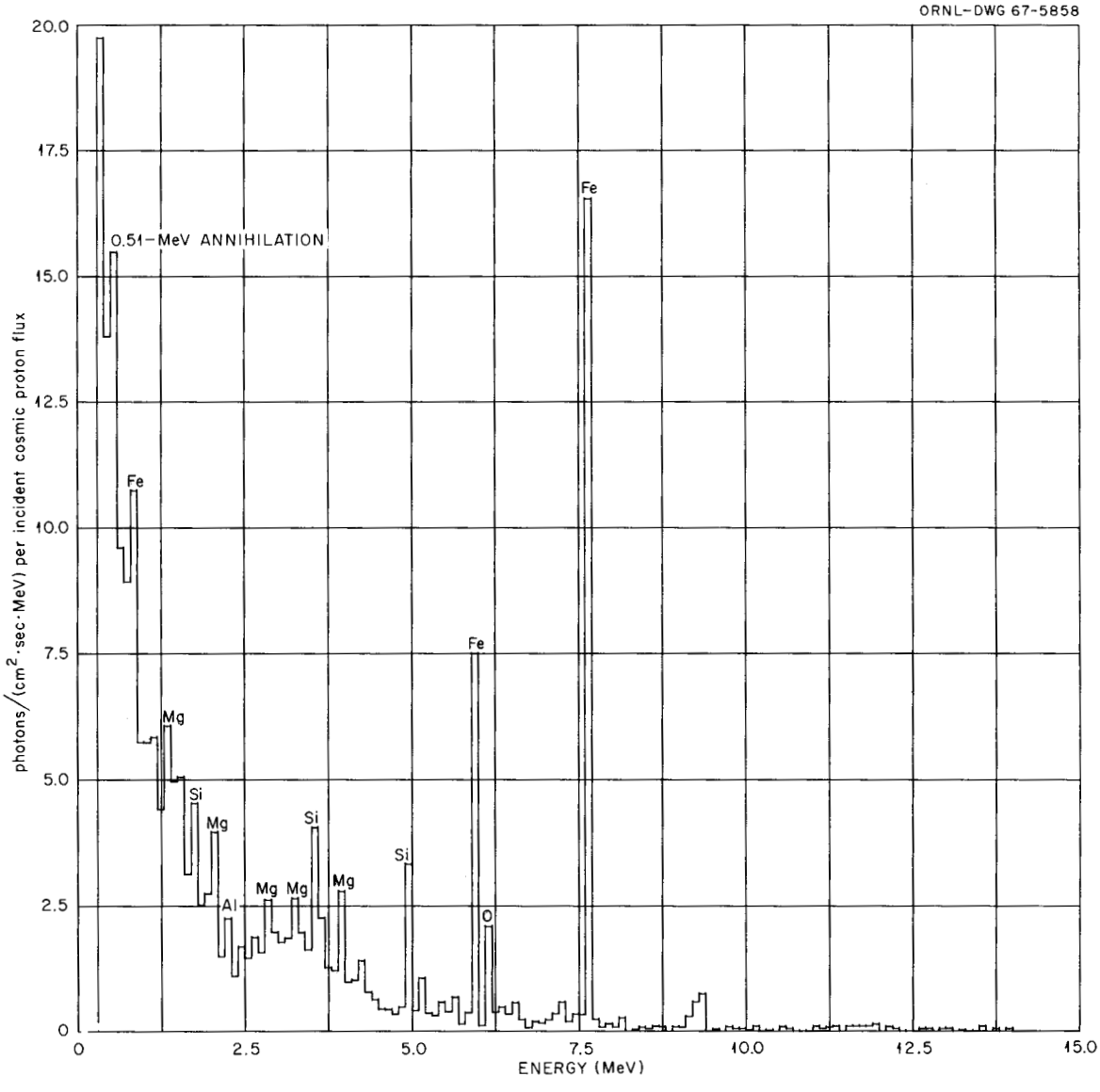

Fig. 7.11.2. Photon Leakage Spectrum from Lunar Surface.

References

[1]Work funded by National Aeronautics and Space Administration under NASA order R-104(1).

[2]R. E. Lingenfelter, E. H. Canfield, and W. N. Hess, *J. Geophys. Res.* **66**, 2665 (1961).

[3]J. R. Arnold, University of California – San Diego, private communication.

[4]L. L. Newkirk, *J. Geophys. Res.* **68**, 1825 (1963).

[5]W. N. Hess *et al.*, *Phys. Rev.* **116**, 445 (1959).

[6]D. C. Irving *et al.*, *O5R, A General-Purpose Monte Carlo Neutron Transport Code*, ORNL-3622 (1965).

[7]M. Leimdorfer and R. T. Boughner, "Monte Carlo Study of Method for Lunar (Surface) Analysis Based on Spectroscopy of Gamma Rays Following 14-MeV Pulsed-Neutron Bombardment," submitted to *Nuclear Instruments and Methods*.

[8]S. K. Penny, D. K. Trubey, and M. B. Emmett, *OGRE, A Monte Carlo System for Gamma-Ray Transport Studies, Including an Example (OGRE-P1) for Transmission Through Laminated Slabs*, ORNL-3805 (1966).

7.12 MODIFICATION AND FURTHER DEVELOPMENT OF THE NUCLEON TRANSPORT CODE, NTC[1]

D. C. Irving H. S. Moran W. E. Kinney

Several modifications to the Nucleon Transport Code NTC are described. Also, descriptions are provided for a few portions of the code which had previously been undocumented. Included in the report are the following:

1. description of PREP, a data preparation routine,
2. generalized framework for the High-Energy Analysis Program which handles the bookkeeping details and leaves the specialization to a particular problem to a few user-written routines,
3. listing of improvements made in the treatment of evaporation processes,
4. replacement of an older and incompletely documented version of O5R by the published version,
5. description of a general-purpose evaporation model program in O5R to treat inelastic scattering,
6. preparation of a special version of NTC to use a straightahead approximation.

Reference

[1]Abstract of ORNL-TM-1866 (in preparation).

7.13 PHOTONEUTRON PRODUCTION FROM 34- AND 100-MeV ELECTRONS IN THICK URANIUM TARGETS[1]

R. G. Alsmiller, Jr. H. S. Moran

The number of photoneutrons produced by 34- and 100-MeV electrons in targets of natural uranium and ^{235}U is calculated as a function of target thickness. For ^{235}U the number of neutrons produced by photofission is calculated separately. In the calculations only photoproduction is considered; that is, no attempt is made to correct or account for neutron-induced fission in the target.

Reference

[1]Abstract of ORNL-TM-1670 (Dec. 12, 1966); also submitted as a letter to *Nuclear Instruments and Methods*.

7.14 SHIELDING CALCULATIONS FOR A 400-MeV LINEAR ELECTRON ACCELERATOR

R. G. Alsmiller, Jr. J. Barish[1]
F. S. Alsmiller R. T. Boughner[2]
W. W. Engle, Jr.[1]

Calculations have been carried out to aid in the design of the shield for the 400-MeV linear electron accelerator which is to be built at the Massachusetts Institute of Technology.[3] Shielding calculations for an electron accelerator may conveniently be divided into four parts: (1) the electron-photon cascade which develops when a high-energy electron strikes the wall or target of the accelerator, (2) the photoneutrons which are produced by the cascade photons and which impinge on the inside of the shield, (3) the transport of the neutrons through the shield, and (4) the conversion of the neutron current that emerges from the shield to dose.

Electron-Photon Cascade

An IBM code for the study of the electron-photon cascade, which develops when a high-energy electron impinges on matter, has been written by Zerby and Moran.[4–6] Using this code, the photon track length from 400-MeV electrons in copper, which is needed to obtain the photoneutron yield, was calculated.

Photoneutron Production

The produced photoneutrons as a function of energy and angle have been calculated using the simplified models and parameters used by De Staebler.[7] Since the many assumptions involved in the calculation are discussed in detail by De Staebler, they will not be enumerated here, but it must be understood that the calculations are very approximate. At an electron energy of 400 MeV, double pion production is small and has been neglected. Single pion production, however, has been retained and, at least in the approximation used by De Staebler, contributes appreciably to photoneutron production.

Neutron Transport

Neutron transport through the shield has been carried out in three different approximations, each of which will be described separately.

Straightahead Approximation. – In this approximation it is assumed that when either an elastic or a nonelastic nuclear collision occurs all the collision products are emitted in the direction of the incident particle. The energy distribution of the reaction products is obtained by integrating the energy and angular distributions over all angles. The straightahead approximation is taken here to mean that all reaction products are emitted in the direction of the incident particle; i.e., no attempt is made to discriminate against particles emitted at large angles. Nonelastic nuclear collisions above 25 MeV are included in the calculations using data generated by Bertini,[8–10] and nonelastic collisions below 25 MeV are included by using a simplified version of standard evaporation theory. Elastic-scattering cross sections and angular distributions were taken from the compilation by Irving[11] for use in the O5R neutron transport code. Elastic scattering from heavy nuclei, silicon and oxygen, was included in the calculation in a continuous slowing-down approximation. Elastic scattering from hydrogen was included as a discrete process.

In the calculations this approximation was used to transport neutrons of all energies greater than 0.5 MeV, and neutrons below this energy were neglected. There is, of course, little justification for using the approximation to transport the lower energy neutrons, and it is to be expected that this calculation gives a considerable overestimate of the low-energy neutron flux emerging from the shield.

Straightahead Approximation Coupled to a Low-Energy Discrete Ordinates Calculation. – An estimate of the magnitude of the error in the straightahead calculations has been obtained by using an existing discrete ordinates code[12–14] to transport the low-energy (<14.9-MeV) neutrons. In this calculation the neutron flux per unit energy range calculated in the straightahead approximation was assumed to be correct at all energies up to a depth of 600 g/cm^2 and at all depths for energies greater than 14.9 MeV. Using the high-energy flux (at depths greater than 600 MeV) and the data on low-energy particle production from high-energy collisions, an energy- and angular- (assumed isotropic) dependent volume-distributed source term was calculated. This source term and the incident flux at 600 g/cm^2 were used in conjunction with the discrete ordinates code, and the low-energy (<14.9-MeV) neutron flux was calculated as a function of depth (>600 g/cm^2). The discrete ordinates code solves the complete angularly dependent transport equations, and thus the low-energy flux calculated in this way is much more reliable than that calculated in the straightahead approximation. It must be emphasized, however, that this flux is still quite approximate because it is based on the assumption that the straightahead approximation is valid at energies greater than 14.9 MeV.

Straightahead Approximation Coupled to a Monte Carlo Calculation. – There is available a code written by Kinney which will solve the transport equation for neutron energies of less than 400 MeV.[15] This code could in principle be used to obtain a solution to the neutron transport problem being considered. However, the code employs Monte Carlo methods and is not, at least in its present form, capable of yielding adequate statistical accuracy in the case of very thick shields. To estimate the error involved in the previously described transport methods, the Monte Carlo code has been used in conjunction with the straightahead approximation. In this calculation the flux calculated in the straightahead approximation at a depth of 750 g/cm^2 was used as a source in the Monte Carlo code, and the resulting neutron flux per unit energy range at all energies was calculated as a function of depth for a few collision mean free paths. The flux obtained in this manner is in principle more accurate than that obtained by either of the previous methods, but is, of course, still not definitive because it is dependent on the validity of the source used.

Dose

From the neutron current calculated in the various approximations, the dose as a function of depth in the shield was calculated using the current-to-dose conversion of Snyder and Neufeld (<0.5 MeV), Irving *et al.* (0.5 to 60 MeV), and Zerby and Kinney (>60 MeV). The conversion factors appropriate to normal incidence were used in all cases.

Calculations have been carried out using shields of silicon dioxide and silicon dioxide with 10%

water. The incident spectrum used was that calculated for emission at 90° from a 400-MeV electron in copper. This spectrum has a maximum neutron energy at 164 MeV. The geometry considered in the straightahead approximation and in the straightahead approximation coupled to the discrete ordinates code was a point source at the center of a spherical shield. In the Monte Carlo calculations the spherical shell was approximated by a semi-infinite slab. The dose as a function of depth in the silicon dioxide shield is shown in Fig. 7.14.1 and in the shield containing silicon dioxide with 10% water is shown in Fig. 7.14.2. In the case of the discrete ordinates calculation, two curves are shown, one in which the dose calculation includes only a contribution from neutrons with energy less than 14.9 MeV and one in which the dose calculation includes a contribution from neutrons of all energies. In this latter case, the neutrons with energy greater than 14.9 MeV are obtained from the straightahead calculation. The attenuation with distance (after approximate equilibrium is reached) of the curves obtained using the discrete ordinates code is approximately the same as that of the curve obtained using the straightahead approximation. Because of statistical uncertainties and because only relatively small distances are considered, it is difficult to determine an attenuation length from the Monte Carlo calculations, but it seems that this attenuation is different from that obtained in the other calculations.

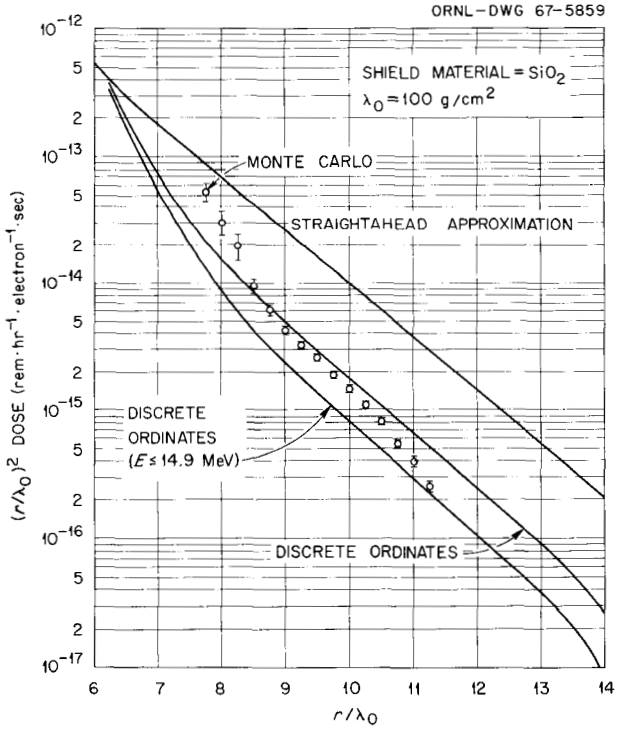

Fig. 7.14.1. $(r/\lambda_0)^2$ Dose vs Radius; Shield Material SiO_2.

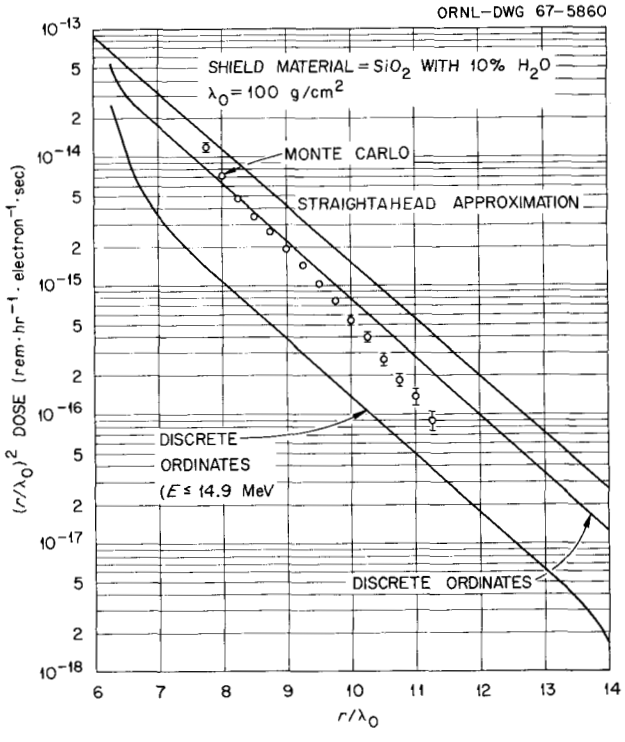

Fig. 7.14.2. $(r/\lambda_0)^2$ Dose vs Radius; Shielding Material SiO_2 with 10% H_2O.

References

[1]Computing Technology Center, Union Carbide Corporation, Oak Ridge.

[2]Mathematics Division.

[3]Calculations similar to those described here but varying somewhat in detail have also been carried out to aid in the shield design of the 150-MeV linear electron accelerator being built at the Oak Ridge National Laboratory.

[4]C. D. Zerby and H. S. Moran, *Studies of the Longitudinal Development of High-Energy Electron-Photon Cascade Showers in Copper*, ORNL-3329 (1962).

[5]C. D. Zerby and H. S. Moran, *A Monte Carlo Calculation of the Three-Dimensional Development*

of High-Energy Electron-Photon Cascade Showers, ORNL-TM-422 (1962).

[6]C. D. Zerby and H. S. Moran, *Neutron Phys. Div. Ann. Progr. Rept. Aug. 1, 1963*, ORNL-3499, Vol. II, p. 3.

[7]H. De Staebler, Jr., *Transverse Radiation Shielding for the Stanford Two-Mile Accelerator*, SLAC Report No. 9 (1962).

[8]H. W. Bertini, *Phys. Rev.* **131**, 1801 (1963), with erratum *Phys. Rev.* **138**, AB2 (1965).

[9]H. W. Bertini, *Nucl. Phys.* **87**, 138 (1966).

[10]R. G. Alsmiller, Jr., *et al.*, *Analytic Representation of Nonelastic Cross Sections and Particle-Emission Spectra from Nucleon-Nucleus Collisions in the Energy Range 25 to 400 MeV*, ORNL-4046 (1967).

[11]The master cross section tape for use in the O5R code, as well as references to all of the data used in making the compilation, is available on request from the Radiation Shielding Information Center of the Oak Ridge National Laboratory.

[12]W. W. Engle, Jr., and F. R. Mynatt, *ANISN, A One Dimensional Discrete Ordinates Transport Code with Anisotropic Scattering*, Computing Technology Center report (to be published).

[13]W. W. Engle, Jr., *A User's Manual for ANISN, A One Dimensional Discrete Ordinates Transport Code with Anisotropic Scattering*, K-1693 (1967).

[14]G. D. Joanou and J. S. Dudek, *GAM II, A B3 Code for the Calculation of Fast Neutron Spectra and Associated Multigroup Constants*, GA-4265 (1963).

[15]W. E. Kinney, *The Nucleon Transport Code, NTC*, ORNL-3610 (1964).

7.15 TRANSPORT CALCULATIONS FOR 500-MeV/c MUONS INCIDENT ON IRON ABSORBERS

M. Leimdorfer[1]

A computer program,[2,3] which solves the charged-particle transport equation using Monte Carlo techniques, has been applied previously to studies of the slowing down of muons of 100-BeV kinetic energy.[4] The same method of calculation has now been applied to a lower energy problem in which 500-MeV/c (404-MeV kinetic energy) muons are incident axially on circular iron cylinders of varying radii but infinite height. The main purpose of these calculations was to permit comparisons to be made with a recently published set of calculations[5] and experiments[6] pertaining to the same problem and also to further corroborate a simplified analytical method[7] which was used to calculate the lateral leakage, neglecting path-length straggling. An example of a comparison is shown in Fig. 7.15.1, which was taken from ref. 5 with our results added. The difference between the positions of the maxima of the two theoretical curves is due to the fact that different sets of stopping-power values[8,9] were used in the respective calculations. The difference in the total integrated ranges is equal to the observed difference between the maxima. The experimental curve indicates that the true range may lie somewhere between those of the calculations. The measured width of the distribution is larger than the corresponding theoretical value. This may be due to some background effect or other disturbance in the experiment.

A more detailed description of this work is being prepared.[10]

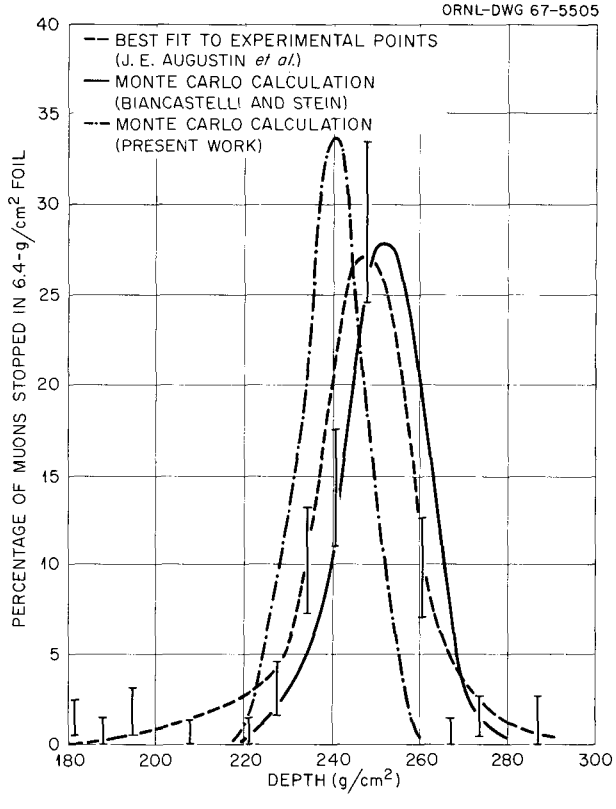

Fig. 7.15.1. Distribution of the Depth of Penetration of 500-MeV/c Muons in an Iron Absorber. The dashed line represents a best fit to the experimental points obtained in a spark chamber of 6.4-g/cm^2-thick foils.

References

[1]Consultant from Research Institute of National Defense, Stockholm, Sweden.

[2]C. Johansson and M. Leimdorfer, *A Monte Carlo Procedure for Calculating the Migration of Protons Taking Account Only of Electromagnetic Interactions*, FOA-4-A 4411-411 (January 1965).

[3]C. Johansson, *Program Description and User's Manual for PROTOS, a Computer Program for Treating Proton Slowing-Down Due to Atomic Collisions*, FOA-4-A 4436-411 (July 1965).

[4]R. G. Alsmiller, Jr., *et al., Neutron Phys. Div. Ann. Progr. Rept. May 31, 1966*, ORNL-3973, Vol. II, p. 74.

[5]R. Biancastelli and P. Stein, *A Montecarlo Computation of Multiple Scattering Effects*, ISS 66/26 (July 1966).

[6]J. E. Augustin *et al., Traces et Parcours d'Électrons, Muons et Pions dans une Chambre à Étincelles à Plaques Épaisses*, University of Paris Report LAL-1114 (September 1964).

[7]L. Eyges, *Phys. Rev.* **74**, 1534 (1948).

[8]W. H. Barkas and M. J. Berger, p. 103 in *Studies in Penetration of Charged Particles in Matter*, NAS-NRC Publication 1133 (1964).

[9]R. M. Sternheimer, *Phys. Rev.* **115**, 137 (1959).

[10]M. Leimdorfer, *The Transport of 500-MeV/c Muons in Iron*, ORNL-4132 (in preparation).

8. Experimental Studies for High-Energy Radiation Shielding

8.1 THE MASS AND ENERGY SPECTRA OF CHARGED REACTION PARTICLES FROM TARGETS BOMBARDED BY 60-MeV PROTONS[1]

F. E. Bertrand[2] R. W. Peelle
T. A. Love N. W. Hill[3]

An experiment to study the energy spectra of charged particles emitted from targets bombarded with 60-MeV protons has been discussed in previous annual reports.[4,5] The experiment was designed to detect and separate all types of charged reaction particles simultaneously, over the energy range from ~1 MeV to 60 MeV. The experimental system has been completed during the last year, and data have been obtained from several targets.

A schematic diagram of the detector array and electronics system is shown in Fig. 8.1.1. The detector system consists of a 100-μ and a 500-μ silicon surface-barrier detector followed by a lithium-drifted germanium total absorption detector.[6] The type of particle is determined by $\Delta E \times E$ methods when an event penetrates at least one detector and by time of flight when the event stops in the first detector. Total system energy resolution is ~180 keV (FWHM) for 60-MeV protons. A plastic scintillator with a rectangular slit cut in it is used as the detector system collimator for scattered particles. The scintillator produces a signal which is used as a veto pulse whenever a particle hits the scintillator instead of passing through the collimating slit. The use of this type of active collimator has resulted in a dramatic reduction of collimator slit edge scattering.

As is indicated in Fig. 8.1.1, every event detected in the counter telescope produces simultaneously a pulse in the fast logic system and in the slow system that is used for pulse-height analysis. The fast signals are used to set coincidence "flags," which indicate the counter in which the incident particle stopped, to provide time-of-flight data for the event, and to activate an anti-pile-up circuit.

The data from each event, which consist of pulse heights from four analog-to-digital converters and a series of flags which indicate coincidences and pile-up and pulser events, are read into an on-line PDP-8 computer which displays data in a variety of modes and writes events on IBM-compatible magnetic tape.

Figure 8.1.2 shows plots of energy loss (vertical axis) vs total energy for scattering from a CH target at 80°. The data shown in Fig. 8.1.2*a* are all events which penetrated the 100-μ (B) detector but stopped in the 500-μ (C) detector, while Fig. 8.1.2*b* displays all events which penetrated B and C and stopped in the total absorption detector. One observes complete separation between all particle types at all energies. The separation of particles in the time-of-flight identification system is equally as good down to approximately 1 MeV.

Data have been obtained for ^{54}Fe and ^{209}Bi at enough angles (~20) to provide good angular distributions for elastic and inelastic peaks. The angular range is from 15 to 160°. Data have been taken from CH and ^{56}Fe at fewer angles, but at a sufficient number to give a good integral of the cross sections over angle.

In addition to data obtained with 60-MeV protons as projectiles, a limited amount of data on CH, ^{16}O, ^{54}Fe, and ^{209}Bi have been obtained using incident protons of 40 MeV and incident alphas of 58 MeV.

Data reduction and interpretation are in early, preliminary states, but the general trend of the data can be determined from the spectra shown.

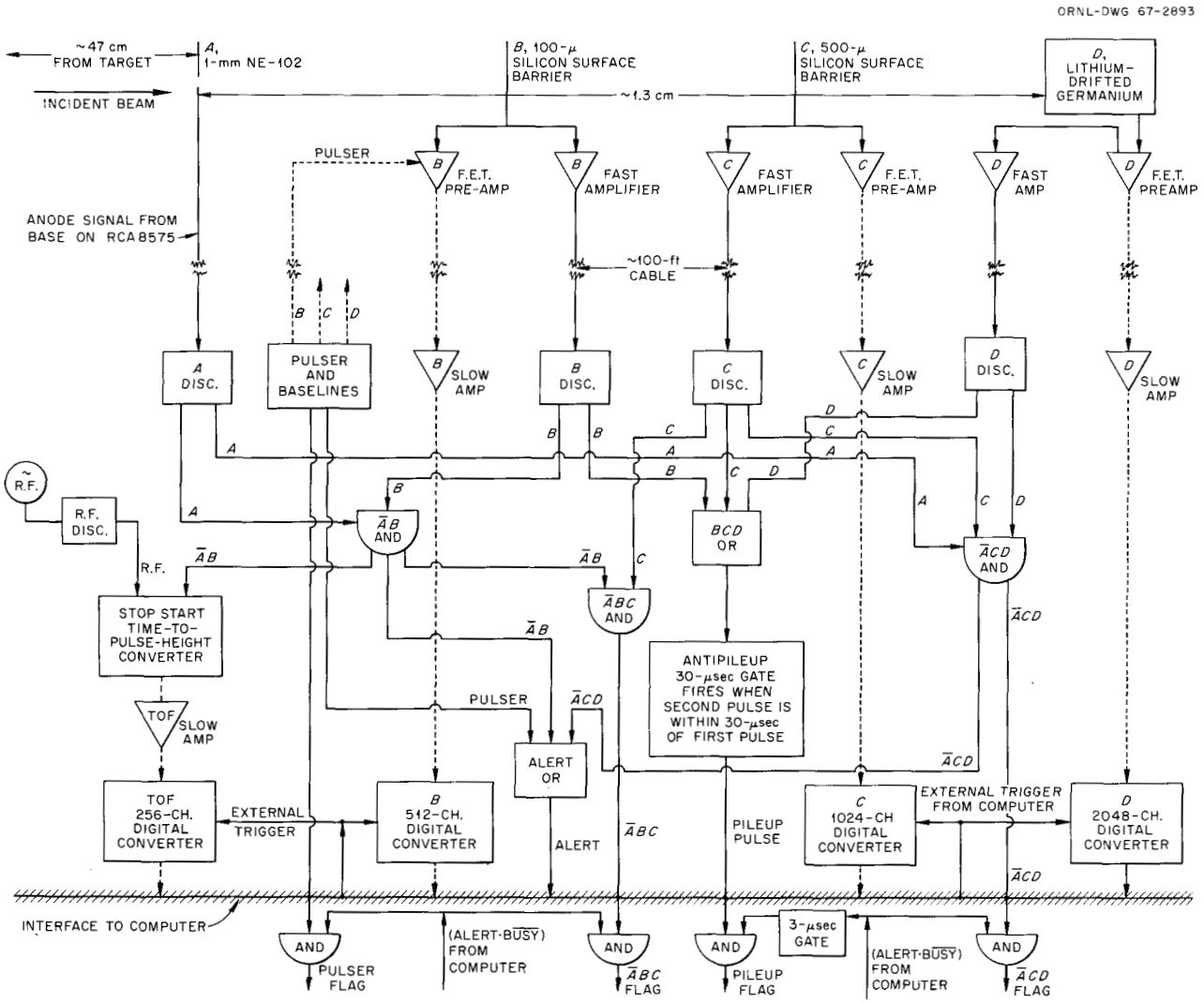

Fig. 8.1.1. Block Diagram of Electronics System. Slow signals are shown as dashed lines.

Figure 8.1.3 shows the spectra of protons, deuterons, tritons, helium-3, and alpha particles from ^{54}Fe at 60°. The data extend down to emission cutoff for all spectra except for the protons, where the lowest energy data is 1 MeV, a point at which identification in the time-of-flight system becomes ambiguous. It will be noticed that the shapes of all the spectra are quite similar, which is consistent in all the data analyzed thus far. In the case of ^{54}Fe, the spectrum of alpha particles exhibits an evaporation spectrum similar to that for the protons. No discrete peaks are shown in the triton, helium-3, or alpha-particle data because of poor statistics at this angle.

Shown plotted as a histogram on the proton data is a plot of the cascade-plus-evaporation spectrum obtained from the calculations of Bertini.[7] A plot of the predicted evaporation spectrum is shown for deuterons, tritons, helium-3 particles and alpha particles.

In Fig. 8.1.4 are shown the proton and deuteron spectra from ^{209}Bi at 30 and 60°. In these cases data are shown down to the lowest energy for particle emission. Predictions based on the Bertini code for the proton spectra are plotted in this figure also.

In the data analyzed thus far it is found that the cascade-plus-evaporation predictions fit the ex-

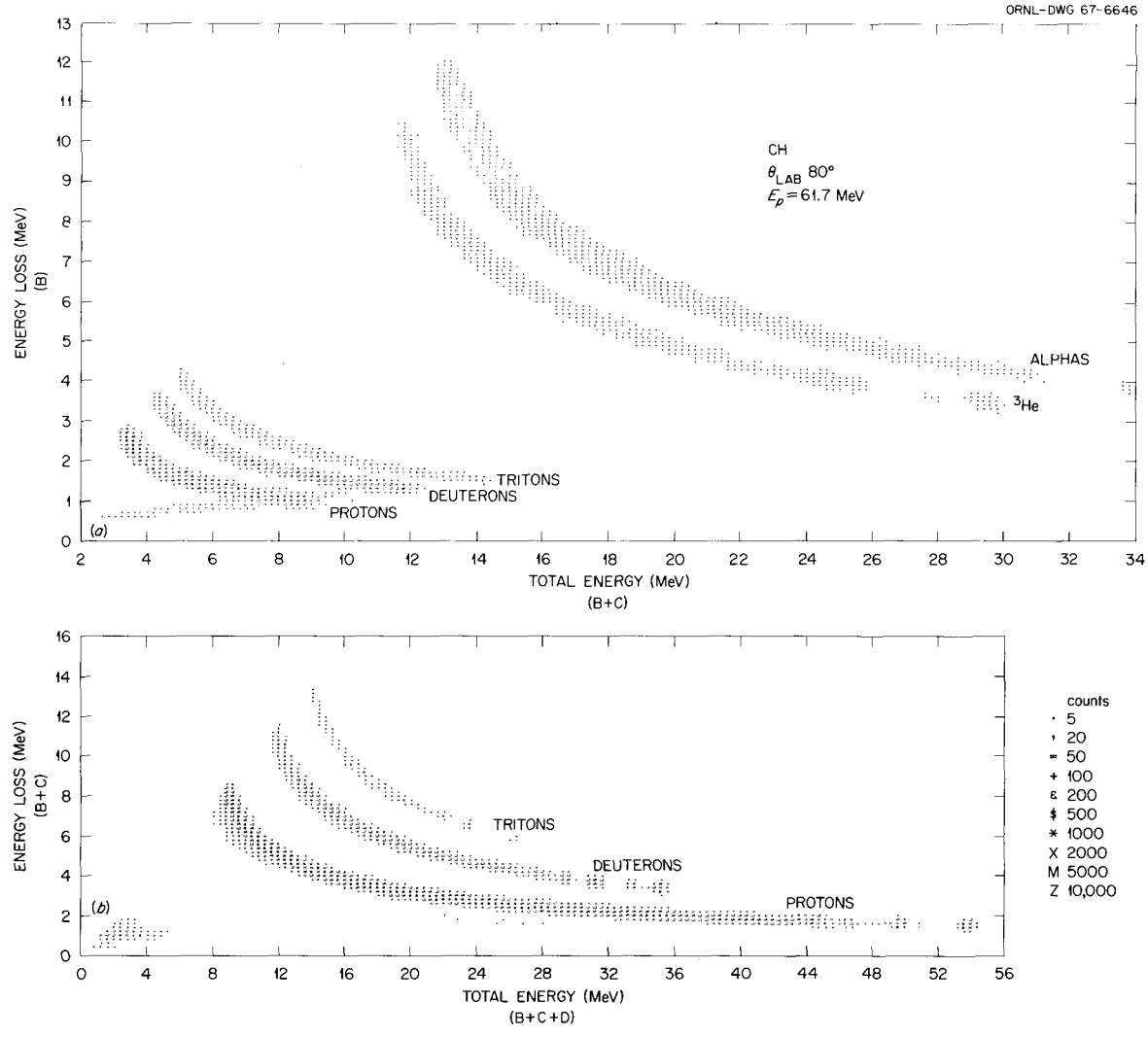

Fig. 8.1.2. Plot of Energy Loss vs Energy for Scattering from CH at 80°.

perimental data better at angles less than 45° than at larger angles. In the case of both ^{54}Fe and ^{209}Bi the prediction for the evaporation spectra is much above the experimental data. Even though the fits between the predictions and the experiment are imperfect, the fact that the agreement is as good as it is in the cascade regions is interesting when one considers the low (60-MeV) proton bombarding energy.

In addition to thorough analysis and interpretation of existing data it is planned in the near future to obtain data from targets of oxygen, aluminum, and tin using 60-MeV incident protons. An effort will also be made to extend the energy range of "unambiguous" detection below 1 MeV for all targets.

References

[1]Work funded by the National Aeronautics and Space Administration under NASA order R-104(1).

[2]Oak Ridge Associated Universities, Graduate Fellow.

[3]Instrumentation and Controls Division.

[4]F. E. Bertrand *et al.*, *Neutron Phys. Div. Ann. Progr. Rept. Aug. 1, 1965,* ORNL-3858, Vol. II, p. 85.

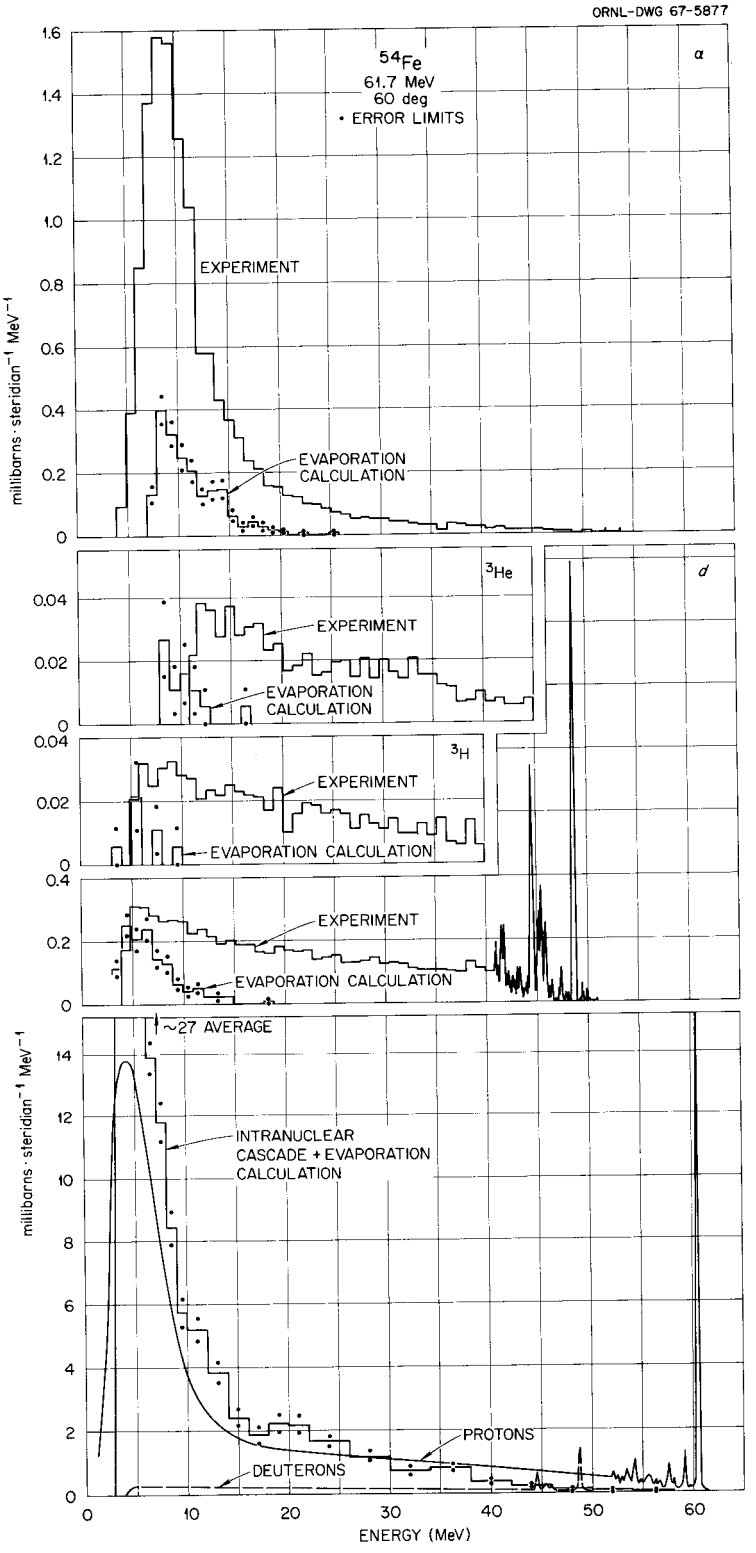

Fig. 8.1.3. Differential Cross Sections for Secondary p, d, t, ^{3}He, and ^{4}He Ions at 60° from 61-MeV Protons on ^{54}Fe.

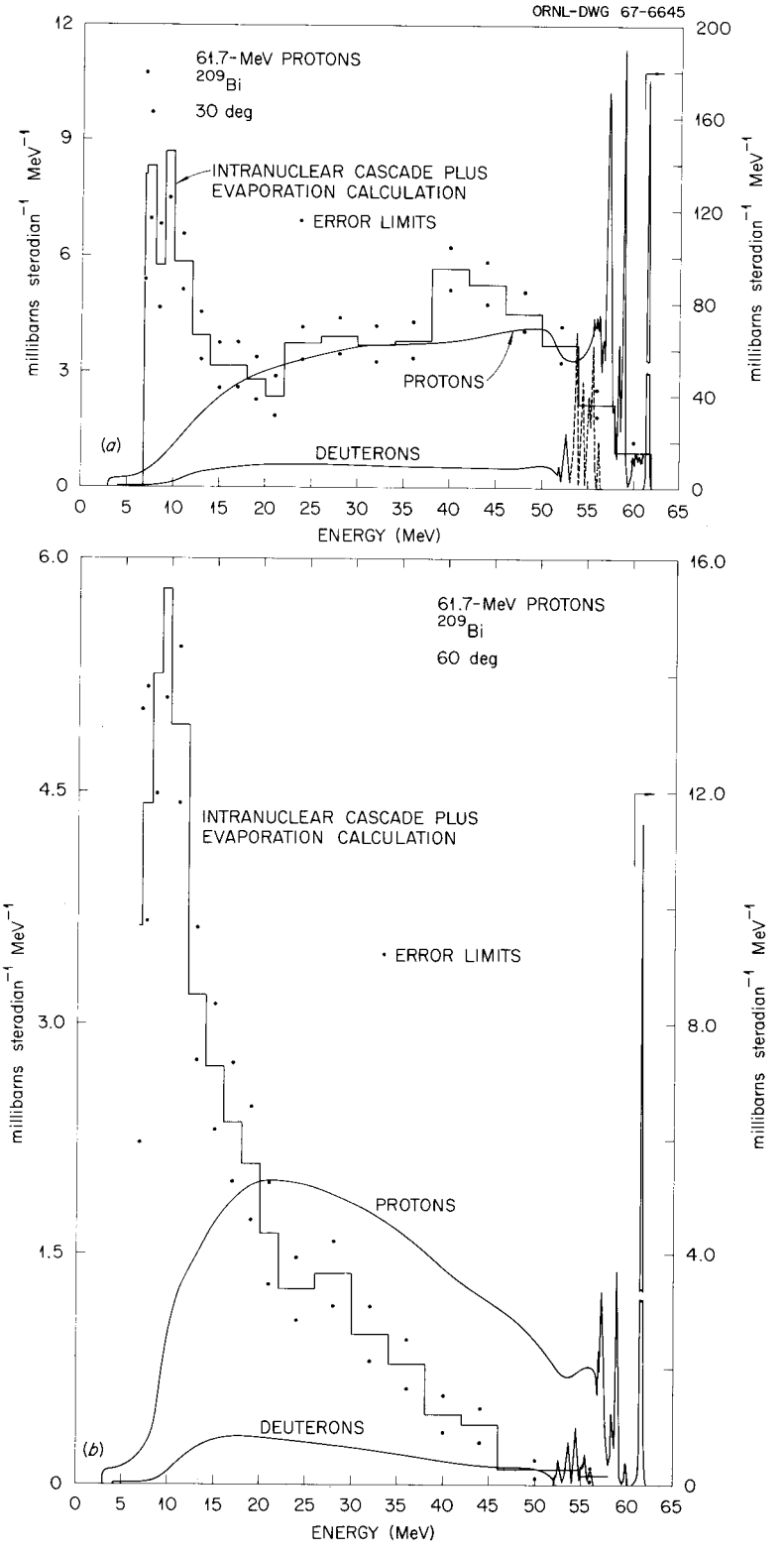

Fig. 8.1.4. Differential Cross Sections for Secondary Protons and Deuterons from 61-MeV Protons Incident on ^{209}Bi at 30° and 60°.

[5]F. E. Bertrand *et al., Neutron Phys. Div. Ann. Progr. Rept. May 31, 1966,* ORNL-3973, Vol. II, p. 96.

[6]F. E. Bertrand *et al., A Total-Absorption Detector for 60-MeV Protons Using Lithium-Drifted Germanium,* ORNL-TM-1462 (March 1966).

[7]H. W. Bertini, *Phys. Rev.* **131**, 1801 (1963); *Phys. Rev.* **138**, AB2 (1965).

8.2. NEUTRON AND PROTON SPECTRA FROM TARGETS BOMBARDED BY 160-MeV PROTONS[1]

J. W. Wachter W. R. Burrus
W. A. Gibson

Secondary neutron spectral data in the energy range between 50 and 160 MeV from targets bombarded by 160-MeV protons have been measured using a proton-recoil spectrometer. Secondary proton measurements were also made using this spectrometer. The target materials were H_2O, D, Be, C, Al, Cu, Co, and Bi, and measurements were made at 0, 10, 45, 60, and 135°. Target thicknesses ranged from thin targets in which the primary beam lost only a small amount of energy to thick targets in which the primary beam was completely stopped. The thin-target measurements are expressed as cross sections, and the remainder of the results are expressed as yields. Energy resolutions of 25 and 15% are associated with the neutron and proton spectra respectively. The results are compared with theoretical results obtained from Monte Carlo nuclear cascade codes.

Reference

[1]Abstract of paper submitted for journal publication; work funded by National Aeronautics and Space Administration under NASA order R-104(1).

8.3. SECONDARY PROTON AND NEUTRON SPECTRA FROM TARGETS BOMBARDED BY 450-MeV PROTONS[1]

W. A. Gibson J. W. Wachter
W. R. Burrus

Work continued on calculating the spectra of secondary neutrons and protons from data obtained by bombarding targets with 450-MeV protons at the University of Chicago cyclotron.[2-4] The elements studied were Be, C, Al, Cu, Co, Bi, and Pb, and the target thicknesses ranged from a few grams per square centimeter to 165 g/cm^2. The angles investigated were 0, 10, 20, 45, 60, 90, and 120°. The thin-target results are expressed as cross sections, and the thick-target results, because of the multiple nuclear interactions within the targets, are expressed as nucleon yield. A report on these measurements is being prepared for journal publication.

References

[1]Partially funded by the National Aeronautics and Space Administration under NASA order R-104(1).

[2]J. W. Wachter, W. R. Burrus, and W. A. Gibson, *Neutron Phys. Div. Ann. Progr. Rept. Aug. 1, 1965,* ORNL-3858, Vol. II, p. 88.

[3]J. W. Wachter, W. R. Burrus, and W. A. Gibson, *Neutron Phys. Div. Ann. Progr. Rept. May 31, 1966,* ORNL-3973, Vol. II, p. 88.

[4]W. A. Gibson, *Nucl. Instr. Methods* **46**, 29 (1967).

8.4. DIFFERENTIAL CROSS SECTIONS FOR THE PRODUCTION OF PROTONS IN THE REACTIONS OF ~160-MeV PROTONS ON NUCLEI[1]

R. W. Peelle T. A. Love
N. W. Hill[2] R. T. Santoro

Cross sections differential in both angle and energy were obtained by flight-time spectrometry for secondary protons above 20 MeV from 158-MeV protons on Be, C, H_2O, Al, Co, and Bi targets. Enough angles were studied to present rough angular distributions from aluminum and cobalt. All secondary charged particles were assumed to be protons, for which the energy resolution varied from 25 to 50%. The observed differential cross sections change smoothly with angle and target mass and show no peak corresponding to quasi-free scattering near the energy corresponding to free nucleon-nucleon scattering. The measurements are compared with others available at the same incident energy and with estimates based on intranuclear-cascade-plus-evaporation calculations. The observed cross sections are larger than the

estimated ones at angles of 90 and 120°, and at low energies for angles more forward than 45°. At 60° the observed cross sections are in accord with the Monte Carlo estimates.

References

[1]Abstract of ORNL-3887 (1966); work funded by the National Aeronautics and Space Administration under NASA order R-104(1).
[2]Instrumentation and Controls Division.

8.5. GAMMA RAYS FROM THE BOMBARDMENT OF ^{7}Li, Be, ^{11}B, C, O, Mg, Al, Co, Fe, AND Bi BY 16- TO 160-MeV PROTONS AND 59-MeV ALPHA PARTICLES[1]

W. Zobel F. C. Maienschein
J. H. Todd[2] G. T. Chapman

Determining the contribution of secondary gamma rays to the radiation dose produced by charged particles in space requires a knowledge of the cross sections for gamma-ray production by protons and alpha particles. The only previously available data of this type were for ~145-MeV protons. In the experiment reported here gamma-ray spectral measurements were made for protons of 16, 33, 56, and 160 MeV and for 59-MeV alpha particles incident on targets of low- and medium-Z materials. Absolute spectra were obtained, generally in the backward direction, with coincidence (pair) or anticoincidence (total absorption) scintillation spectrometers. The analysis method used to correct for the imperfect spectrometer response yielded quantitative error estimates for the spectra. A few measurements were made in the forward direction and at 90° to distinguish possible deviations from isotropy. From the spectra, cross sections were obtained for the production of specific gamma rays. Tables of these results include the probable nuclear reactions which produced the gamma rays. The production cross sections are plotted vs the average proton energy in the target for individual gamma rays for C, O, and Al, and the sums for all levels excited in these nuclei are compared with the total reaction cross sections and the total nonelastic cross sections predicted on the basis of intranuclear cascade calculations. The total cross sections for gamma-ray production are also plotted vs the atomic number A after division by A.

References

[1]Abstract of ORNL-4161 (in preparation); work funded by the National Aeronautics and Space Administration under NASA order R-104(1).
[2]Instrumentation and Controls Division.

8.6. NEUTRON YIELDS FROM (p,n) REACTIONS ON ^{9}Be, ^{14}N, ^{27}Al, ^{56}Fe, ^{115}In, ^{181}Ta, AND ^{208}Pb AT 15- AND 18-MeV BOMBARDING ENERGIES[1]

V. V. Verbinski M. Young[2]
W. R. Burrus J. D. Drischler

Neutron-production cross sections [i.e., (p,n) + (p,pn) + $2(p,2n)$] were measured as a function of neutron energy and angle for protons of 15- and 18-MeV bombarding energy. The neutron energy spectra showed appreciable structure for ^{9}Be and ^{14}N, as expected from level density considerations. In both cases the ground-state transition is quite strong. For ^{9}Be, at both 15- and 18-MeV proton bombarding energies, a persistent peak appears corresponding to roughly 2-MeV excitation energy of the ^{9}Be residual nucleus. In the case of ^{14}N an extremely strong neutron group appears at about 6 MeV below the ground-state group. For Al there is no appreciable structure except for a noticeable enhancement of ground-state transition. The high-Z nuclei showed no prominent levels, except ^{56}Fe. A prominent forward-directed peak appeared at 3 MeV below the ground-state-transition neutrons, a peak that corresponds to the isobaric analog level identified by Anderson *et al.*[3]

The neutron spectra were integrated over angle, $\sigma(E_i) = \Sigma_j \sigma(E_i,\theta_j)\,\Delta\Omega$, to produce poor-energy-resolution spectra. These spectra showed a low-energy evaporation component and a "precompound" component of higher energy for ^{115}In, ^{181}Ta, and ^{208}Pb. A fitting of these spectra, as well as those from ^{56}Fe and ^{27}Al, was made according to the statistical model of Griffin,[4] and the parameter g was obtained for each nucleus. The parameter g is equal to the density per MeV of single-particle states. This fitting also produces a ratio of evaporation to "precompound" neutrons for each isotope bombarded. The curves of angle-integrated cross sections vs neutron energy were also compared with the absolute cross sections vs energy predicted by the intranuclear cascade calculations

of Bertini,[5] and fair agreement was obtained for nearly all the isotopes.

References

[1]Work supported by National Aeronautics and Space Administration under NASA order R-104(1).

[2]Louisiana State University.

[3]J. D. Anderson, C. Wong, and J. W. McClure, *Phys. Rev.* **129**, 2718 (1963).

[4]J. J. Griffin, *Phys. Rev. Letters* **17**, 478 (1966).

[5]H. W. Bertini, *Monte Carlo Calculations on Intranuclear Cascades*, ORNL-3383 (1962).

8.7. A FORTRAN IV/63 PROGRAM PACKAGE FOR CALCULATING THE TIME CHANNEL RESPONSE FUNCTION IN NEUTRON TIME-OF-FLIGHT SPECTROSCOPY[1]

R. T. Santoro

Three computer programs – PTIME, TWALK, and CONVOL – for computing the time-channel response function for a neutron time-of-flight spectrometer are described. PTIME computes the time-jitter-smeared physical flight-time distribution for the target detector configuration where the incident beam and the detected neutrons are along the cylindrical axes of the target and detector respectively. The flight-time resolution and spectrometer efficiency are computed, and plotted results are provided. TWALK computes the neutron pulse-height spectrum and generates the time-slewing response function with the aid of the time-slewing curve. CONVOL performs the integral over the time-analyzer response function of the convolution of the physical flight-time distribution and the time-slewing response function. Instructions on the use of these codes with the CDC-1604 computer are given, along with input card formats required for execution. The methods of entabulation and interpolation of graphic data are included. Complete program listings are presented in appendices.

Reference

[1]Abstract of ORNL-TM-1836 (in preparation); work funded by the National Aeronautics and Space Administration under NASA order R-104(1).

8.8. "ELSA" – A COMPUTER PROGRAM TO CALCULATE THE ENERGY-LOSS STRAGGLING OF CHARGED PARTICLES IN ABSORBERS[1]

J. W. Wachter

The determination of the distribution in energy loss by charged particles traversing a given thickness of material is frequently important in designing experiments utilizing charged particle identification and/or energy determination using dE/dx counters[2,3] (see also Sect. 8.1).

As a charged particle passes through a medium it loses energy in discrete collisions with electrons. The amount of energy lost in each collision, as well as the distance between collisions, is statistical in nature, and in thin absorbers large fluctuations will occur in the total energy deposited in the absorber. For nonrelativistic protons the energy transfers are small and a near-Gaussian distribution of energy fluctuations results for absorbers in which the proton loses 10% or more of its energy. As the proton becomes relativistic, however, the maximum energy which can be transferred in each event increases, and the total energy loss results from a few collisions involving larger energy transfers. The fluctuations in the energy loss are no longer Gaussian but are described by skewed distribution functions. This effect has been examined in detail by Landau and by Symon[4–7] and more recent results have been summarized by Seltzer and Berger.[8]

A program has been written in FORTRAN II and IV for the IBM-7090 computer utilizing the Symon "thick absorber" solution to the problem.[5] Program options permit the energy loss constants to be changed either to those proposed by Peelle[9] or to constants computed on a density-averaged basis from elemental data. Output includes the weighted and unweighted parameters of the differential energy-loss distribution, as well as the mean, the probable energy loss, the FWHM, and the corresponding resolution. The differential and/or integral distributions (with specified normalization) may be plotted on-line as a print plot and by the Benson-Lehner plotter. Successive calculations may be combined in a single plot, allowing comparisons between different particles, different energies, or different absorbers (see Fig. 8.8.1).

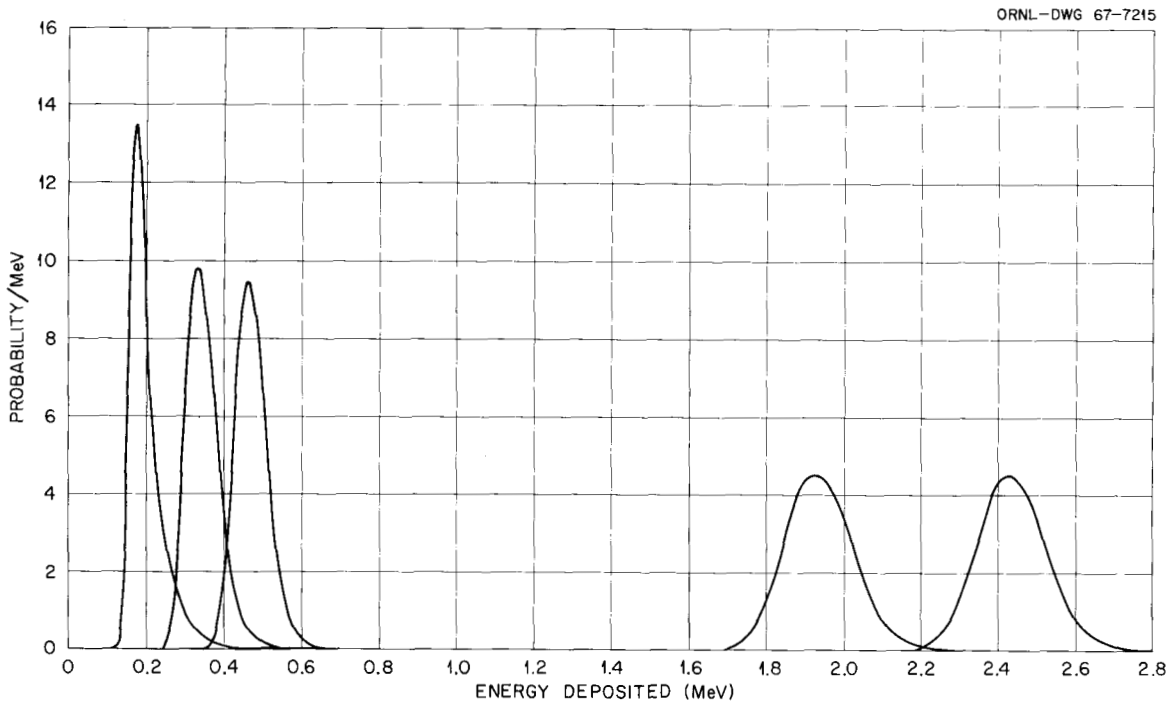

Fig. 8.8.1. Calculated Distributions in Energy Deposited in a 100-μ Silicon Detector (0.0233 g/cm^2) by 60-MeV Proton, Deuteron, Triton, ^{3}He, and Alpha Particles.

References

[1]Work partially funded by the National Aeronautics and Space Administration under NASA order R-104(1).

[2]W. A. Gibson *et al.*, *Nucl. Instr. Methods* **46**, 29 (1967).

[3]F. E. Bertrand *et al.*, *Neutron Phys. Div. Ann. Progr. Rept. May 31, 1966*, ORNL-3973, Vol. II, p. 85.

[4]L. Landau, *J. Phys. (USSR)* **4**, 201 (1944).

[5]K. R. Symon, Ph.D. Thesis (Harvard University, 1949).

[6]Cited by B. Rossi, *High Energy Particles*, Prentice Hall, New York, 1952, p. 22.

[7]Cited by D. M. Ritson, *Techniques of High Energy Physics*, Interscience, New York, 1961, p. 18.

[8]S. M. Seltzer and M. J. Berger, p. 187 in *Studies in Penetration of Charged Particles in Matter*, Nuclear Science Series No. 39, National Academy of Sciences, Washington, 1964.

[9]R. W. Peelle, *Rapid Computation of Specific Energy Losses for Energetic Charged Particles*, ORNL-TM-977 (1965).

Publications and Papers Presented at Scientific Meetings

PUBLICATIONS

ALSMILLER, R. G., Jr.

"High-Energy Nucleon Transport,'' ORNL-TM-1839 (June 6, 1967).

"High-Energy Nucleon Transport and Space Vehicle Shielding," *Nucl. Sci. Eng.* **27**, 158 (1967); ORNL-TM-1518 (July 1966).

ALSMILLER, R. G., Jr., F. S. ALSMILLER, and J. BARISH*

"The Effect of Charged-Particle Slowing Down on the Nuclear Cascade in Steel Initiated by 19.2-GeV/c Protons," ORNL-3854 (January 1967).

ALSMILLER, R. G., Jr., M. LEIMDORFER, and J. BARISH*

"Analytical Representation of Nonelastic Cross Sections and Particle-Emission Spectra from Nucleon-Nucleus Collisions in the Energy Range 25 to 400 MeV,'' *World-Wide News Compilations in Nuclear Physics, Nuclear Data* **2**(3), 333 (1966); ORNL-4046 (April 1967).

ALSMILLER, R. G., Jr., and H. S. MORAN

"Photoneutron Production from 34- and 100-MeV Electrons in Thick Uranium Targets," *Nucl. Instr. Methods* **51**, 339 (1967); ORNL-TM-1670 (Dec. 12, 1966).

"Electron-Photon Cascade Calculations and Neutron Yields from Electrons in Thick Targets,'' *Nucl. Instr. Methods* **48**, 109 (1967); ORNL-TM-1502 (June 17, 1966).

BERTINI, H. W.

"Effect of Error on Results of a Low-Energy Intranuclear Cascade Calculation," ORNL-3786 (1966).

"Secondary Particle Spectra from the Interaction of 30- to 340-MeV Protons on Complex Nuclei: Experimental Data and Comparison with Theory," ORNL-TM-1652 (Feb. 27, 1967).

"Results from Low-Energy Intranuclear-Cascade Calculation," *Nucl. Phys.* **87**, 138 (1966).

"Some Effects of Modified Evaporation Program on Calculations of Radiochemical Cross Sections and Particle Multiplicities for Protons on Carbon and Aluminum Targets,'' ORNL-TM-1549 (Nov. 14, 1966).

BERTINI, H. W., B. L. BISHOP, and M. P. GUTHRIE

"Representative Results in Graphical Form from Computer Production Runs of the Low-Energy Intranuclear-Cascade Calculation," ORNL-4128 (August 1967).

BERTINI, H. W., M. P. GUTHRIE, E. H. PICKELL, and B. L. BISHOP

"Literature Survey of Radiochemical Cross-Section Data Below 425 MeV," ORNL-3884 (October 1966).

BERTRAND, F. E., J. K. DICKENS, and T. A. LOVE

"Distorted-Wave Analysis of Inelastic Scattering of 61.7-MeV Protons from ^{60}Ni," ORNL-TM-1875 (June 9, 1967).

---

*Non-Division personnel.

BERTRAND, F. E., R. W. PEELLE, T. A. LOVE, R. J. FOX,* N. W. HILL,* and H. A. TODD*
"A Total-Absorption Detector for 60-MeV Protons Using Lithium-Drifted Germaninum,'' ORNL-TM-1462 (March 1966).

BURRUS, W. R., J. A. HARVEY,* F. C. MAIENSCHEIN, J. W. REYNOLDS,* and J. G. SULLIVAN*
"Proposal to Acquire a Data-Handling System for the Oak Ridge Electron Linear Accelerator,'' ORNL-TM-1746 (Jan. 17, 1967).

BURRUS, W. R., and B. W. RUST*
"Significance Arithmetic for FORTRAN," ORNL-TM-1249 (Nov. 4, 1966).

CALLIHAN, A. D.
"Standardization in Critical Experiments, Chemical Processes, Fissile-Material Transport, and Other Assorted Topics," *Nucl. News* **10**(2), 34 (1967).

CLARK, F. H. S.
"Variance of Certain Flux Estimators Used in Monte Carlo Calculations," *Nucl. Sci. Eng.* **27**, 235 (1967).

"Variance of the Surface-Crossing Flux Estimator Used in Monte Carlo Calculations," ORNL-TM-1548 (June 8, 1966).

"Importance of Epithermal Neutrons Relative to Thermal Neutrons in Absorbed Dose," *Health Phys.* **13**, 296 (1967).

"Determinations of Shield Requirements for Neutron Sources," ORNL-TM-1655 (Oct. 5, 1966).

"Report of a Meeting of a Working Committee on Shielding Conventions,'' ORNL-TM-1604 (Nov. 8, 1966).

CLARK, F. H. S., and N. A. BETZ*
"Results of the Analysis by Monte Carlo of Fast-Neutron Shielding Properties of Compound Cubical and Spherical Shields," ORNL-4009 (September 1966).

"Importance Sampling Devices for Selecting Track Lengths and Directions After Scatter in O5R," ORNL-TM-1484 (Aug. 5, 1966).

CLARK, F. H. S., N. A. BETZ,* and J. BROWN*
"Monte Carlo Calculations of the Penetration of Normally Incident Neutron Beams Through Concrete," ORNL-3926 (January 1967).

CLIFFORD, C. E., E. A. STRAKER, F. J. MUCKENTHALER, V. V. VERBINSKI, R. M. FREESTONE, Jr., K. M. HENRY, and W. R. BURRUS
"Measurements of the Spectra of Uncollided Fission Neutrons Transmitted Through Thick Samples of Nitrogen, Oxygen, Carbon, and Lead: Investigation of the Minima in Total Cross Sections," *Nucl. Sci. Eng.* **27**, 299 (1967); ORNL-TM-1656 (Rev.) (Mar. 3, 1967).

COLE, R. K.,* R. DITTMAN,* H. S. SANDHU,* C. N. WADDELL,* and J. K. DICKENS
"The $^{19}F(p,\alpha)^{16}O$ and $^{19}F(p,^{3}He)^{17}O$ Reactions at 30.5 MeV," *Nucl. Phys.* **A91**, 665 (1967); ORNL-TM-1585 (Aug. 23, 1966).

COLEMAN, W. A., and R. E. MAERKER
"Differential Neutron Current Albedos for Concrete in the Incident Energy Range 0.5 eV to 200 keV," ORNL-3967 (see below for Vol. I).

Vol. II. "Results of Monte Carlo Calculations for an Incident Angle of 0 deg" (November 1966).

Vol. III. "Results of Monte Carlo Calculations for an Incident Angle of 45 deg" (November 1966).

Vol. IV. "Results of Monte Carlo Calculations for an Incident Angle of 60 deg'' (November 1966).

Vol. V. "Results of Monte Carlo Calculations for an Incident Angle of 75 deg" (November 1966).

Vol. VI. "Results of Monte Carlo Calculations for an Incident Angle of 85 deg" (November 1966).

*Non-Division personnel.

COLEMAN, W. A., R. E. MAERKER, and F. J. MUCKENTHALER
"Differential Neutron Current Albedos for Concrete in the Incident Energy Range 0.5 eV to 200 keV. I. Description of Monte Carlo Calculation and TSF Experiment and Comparison of Calculated and Experimental Results," ORNL-3967 (March 1967).

COLEMAN, W. A., R. E. MAERKER, F. J. MUCKENTHALER, and P. N. STEVENS*
"Calculation of Doubly Differential Current Albedos for Monodirectional Beams of Epicadmium Neutrons Incident on Concrete and Comparison of the Reflected Subcadmium Component with Experimental Results," ORNL-TM-1554 (Sept. 27, 1966).

"Calculation of Doubly Differential Current Albedos for Epicadmium Neutrons Incident on Concrete and Comparison of the Reflected Subcadmium Component with Experiment," *Nucl. Sci. Eng.* **27**, 411 (1967).

COVEYOU, R. R., V. R. CAIN, and K. J. YOST
"Adjoint and Importance in Monte Carlo Application," *Nucl. Sci. Eng.* **27**, 219 (1967); ORNL-4093 (April 1967).

COVEYOU, R. R., and R. D. MacPHERSON
"Fourier Analysis of Uniform Random Number Generators," *J. Assoc. Computing Machinery* **14**(1), 100 (1967).

CRITICAL EXPERIMENTS FACILITY STAFF
"A Safety Analysis of the Oak Ridge Critical Experiments Facility," ORNL-TM-349, Rev. 1 (February 1967).

CRUME, E. C.,* and E. B. JOHNSON
"Criticality Safety Tests for Rover Reactor Fuel Elements," ORNL-TM-1704 (1967) (Confidential).

DICKENS, J. K., and E. EICHLER*
"The $^{91}Zr(d,p)^{92}Zr$ Reaction at $E_d = 6.25$ MeV," ORNL-TM-1868 (May 19, 1967).

DICKENS, J. K., E. EICHLER,* R. J. SILVA,* and I. R. WILLIAMS*
"Level Structure of ^{92}Mo," *Phys. Letters* **21**(6), 657 (1966).

El-SHISHINI, M. M.,* and W. ZOBEL
"Temperature Dependence of the Response of Lithium-Drifted Germanium Detectors to Gamma Rays," ORNL-TM-1295 (September 1966).

ENGLE, W. W., Jr.*
"A User's Manual for ANISN – A One-Dimensional Discrete Ordinates Code with Anisotropic Scattering," K-1693† (1967).

FELDMAN, H. A.
"Relations Between the Moments and Cumulants of a Probability Distribution," ORNL-TM-1624 (Nov. 4, 1966).

"Effects of Faulty Random Number Generators on Monte Carlo Calculations," ORNL-TM-1625 (July 12, 1967).

FREESTONE, R. M., Jr.
"Monte Carlo Calculations of the Neutron Flux Within a $^{10}B_4C$ Shell," ORNL-TM-1816 (June 9, 1967).

GIBSON, W. A.
"Design of Photomultiplier Socket Assembly with High Gain and Clean Output Signals for Tubes Viewing Organic Scintillator Light Pulses," *Rev. Sci. Instr.* **37**(5), 631 (1966).

GIBSON, W. A., W. R. BURRUS, J. W. WACHTER, and C. F. JOHNSON*
"Proton Recoil Spectrometer for Neutron Spectra Between 50 and 450 MeV," *Nucl. Instr. Methods* **46**, 29 (1967); ORNL-TM-1525 (June 2, 1966).

---

*Non-Division personnel.

†Work supported by Neutron Physics Division.

HOLLAND, L. B., L. W. GILLEY, J. W. POSTON,* and D. R. WARD
"Operational Problems with the Health Physics Research Reactor," *Nucl. Safety* **8**, 179 (1967).

IRVING, D. C., R. G. ALSMILLER, Jr., F. S. ALSMILLER, H. S. MORAN, and J. BARISH*
"The Secondary-Particle Contribution to the Dose from Solar-Flare Protons Incident Isotropically on Slab Shields," *Nucl. Sci. Eng.* **25**, 363 (1966).

IRVING, D. C., R. G. ALSMILLER, Jr., and H. S. MORAN
"Tissue Current-to-Dose Conversion Factors for Neutrons with Energies from 0.5 to 60 MeV," *Nucl. Instr. Methods* **51**, 129 (1967); ORNL-TM-1522 (Dec. 7, 1966); ORNL-4032 (1967).

JOHNSON, E. B.
"Critical Lattices of High Flux Isotope Reactor Fuel Elements," ORNL-TM-1808 (Mar. 20, 1967).

JOHNSON, E. B., and R. K. REEDY, Jr.
"Criticality of Lattices of Heat Transfer Reactor Experiment Fuel Elements," ORNL-TM-1566 (July 20, 1966).

JUNG, L.
"Experimental Verification of a Geometrical Shielding Transformation," ORNL-TM-1603 (September 1966).

KAM, F. B. K., and F. H. S. CLARK
"Fission Spectrum Neutron Dose Rate Attenuation and Gamma-Ray Exposure Dose Buildup Factors for Lithium Hydride," *Nucl. Applications* **3**(7), 433 (1967); ORNL-TM-1744 (Jan. 13, 1967).

KAM, F. B. K., and K. D. FRANZ*
"ACTIFK, A General Analysis Code for O5R," ORNL-3856 (September 1966).

LEIMDORFER, M., R. G. ALSMILLER, Jr., and R. T. BOUGHNER*
"Calculations of the Radiation Hazard Due to Exposure of Supersonic Aircraft to Solar Flare Protons," *Nucl. Sci. Eng.* **27**, 151 (1967); ORNL-TM-1594 (Dec. 7, 1966).

LEIMDORFER, M., and J. BARISH*
"A Method of Representing Two-Dimensional Distributions for Use in Monte Carlo Calculations," ORNL-4002 (January 1967).

LEIMDORFER, M., and R. T. BOUGHNER*
"Monte Carlo Study of Method for Lunar (Surface) Analysis Based on Spectroscopy of Gamma Rays Following 14-MeV Pulsed Neutron Bombardment," *Nucl. Instr. Methods* **50**, 302 (1967).

LEWIN, J.
"TSF-SNAP Reactor Safety Analysis Report," ORNL-4058 (Rev.) (June 21, 1967).

LOVE, T. A., R. T. SANTORO, R. W. PEELLE, and N. W. HILL*
"Absolute Efficiency Measurements of NE-213 Organic Phosphors for Detecting 14.4- and 2.6-MeV Neutrons," ORNL-3893 (September 1966).

MAERKER, R. E., and V. R. CAIN
"AMC: A Monte Carlo Code Utilizing the Albedo Approach for Calculating Neutron and Capture Gamma-Ray Distributions in Rectangular Concrete Ducts," ORNL-3964 (August 1967).

MAERKER, R. E., and F. J. MUCKENTHALER
"Monte Carlo Calculations, Using the Albedo Concept, of the Fast-Neutron Dose Rates Along the Center Lines of One- and Two-Legged Square Concrete Open Ducts and Comparison with Experiment," *Nucl. Sci. Eng.* **27**, 423 (1967); ORNL-TM-1557 (Sept. 21, 1966).

"Neutron Fluxes in Concrete Ducts Due to Incident Epicadmium Neutrons: Calculations and Experiments," ORNL-TM-1794 (May 17, 1967).

*Non-Division personnel.

"Measurements and Single-Velocity Calculations of Differential Angular Thermal-Neutron Albedos for Concrete," *Nucl. Sci. Eng.* **26**, 339 (1966); ORNL-4090 (August 1967).

"Calculations, Using the Albedo Concept, of Thermal-Neutron Fluxes Along the Center Lines of One-, Two-, and Three-Legged Square Concrete Open Ducts Arising from Thermal Neutrons Entering Duct Mouths: Comparison with Experiments," ORNL-TM-1758 (Feb. 13, 1967).

MARSHALL, J. D.,* and M. B. Wells*
"Simplified Method for Calculating Nitrogen-Capture and Fission-Product Gamma-Ray Doses Inside Underground Concrete Structures," RRA-71† (June 11, 1967).

"The Effect of Cutoff Energy on Monte Carlo Calculated Gamma-Ray Dose Rates in Air," RRA-M67† (Oct. 31, 1966).

MASKEWITZ, B. F., B. L. McGILL, and J. GURNEY
"Bibliography of the Computer Codes Literature Examined by the Radiation Shielding Information Center," ORNL-RSIC-15 (July 1966).

MIHALCZO, J. T.
"Uranium (93.2%) Metal Cylinders with Thin Stainless-Steel Reflectors," *Nucl. Sci. Eng.* **25**, 439 (1966).

"Multiplication Factor of Uranium Metal by One-Velocity Monte Carlo Calculations," *Nucl. Sci. Eng.* **27**, 557 (1967).

MOONEY, L. G.,* and M. B. WELLS*
"Effects of Neutron-Energy Spectrum in Air on the Neutron-Induced Dose in Concrete Undergound Structures," RRA-M65† (Oct. 31, 1966).

"The Shielding Effectiveness of Single Compartment Concrete Underground Structures Against Neutrons from Nuclear Weapons," RRA-T64† (Dec. 1, 1966). (Classified).

MORRISON, G. W.,* J. T. MIHALCZO, and D. C. IRVING
"ACTIVT – An O5R Monte Carlo Analysis Routine for Calculation of Activation," ORNL-TM-1674 (Oct. 3, 1966).

NESTOR, C. W.,* and H. C. CLAIBORNE
"Heating in Infinite Cylinders by Uniform Gamma-Ray Sources (Technical Note)," *Nucl. Sci. Eng.* **27**, 464 (1967).

PEELLE, R. W.
"Nuclear Reaction Cross Sections for Spacecraft Shield Design," ORNL-TM-1892 (June 16, 1967).

"Multiple Coulomb Scattering into a Detector in Charged Particle Coincidence Measurements Between Reaction Products," *Nucl. Instr. Methods* **51**, 315 (1967); ORNL-TM-1517 (June 16, 1966).

PEELLE, R. W., and P. M. AEBERSOLD
"Energy Parameters for Light Nuclides in Monte Carlo Nuclear Evaporation Programs Based on EVAP," ORNL-TM-1538 (Oct. 17, 1966).

PEELLE, R. W., T. A. LOVE, N. W. HILL,* and R. T. SANTORO
"Differential Cross Sections for the Production of Protons in the Reactions of 160-MeV Protons on Complex Nuclei," ORNL-3887 (September 1966).

PEREY, C. M., and F. G. PEREY
"Deuteron Optical-Model Analysis with Spin-Orbit Potential," *Phys. Rev.* **152**, 923 (1966); ORNL-TM-1529 (June 6, 1966).

PEREY, F. G.
"Filling in Gaps with Cross Sections Calculated from Theory," p. 235 in *Conference on Neutron Cross-Section Technology, March 22–24, 1966, Washington*, P. B. Hemmig, editor, TID-4500, Conf.-660303.

---

*Non-Division personnel.

†Work supported by Neutron Physics Division.

"Polarization from the Generalized Optical Potential," p. 191 in *Proceedings of the 2nd International Symposium on Polarization Phenomena of Nucleons, Karlsruhe, September 6–10, 1965*, P. Huber and H. Schopper, editors, Birkhauser-Verlag, Stuttgart, Germany, 1966.

PEREY, F. G., and G. R. SATCHLER*
"The Optical Model Potential for Deuterons," *Nucl. Phys.* **A97**, 515 (1967).

PEREY, F. G., and J. P. SCHIFFER*
"Anomalous Isotope Shift of the Nuclear Charge Radius," *Phys. Letters* **17**(6), 324 (1966).

PUTZULU, D. I., P. M. AEBERSOLD, and W. R. BURRUS
"Description of the TERP System, A FORTRAN II/63, IV/63, 360 System for Efficient Interpolation," ORNL-TM-1706 (Dec. 8, 1966).

RAFFETY, S. J., and J. T. THOMAS
"Experimental Determination of Safe Handling Procedures for High Flux Isotope Reactor Fuel Elements Outside the Reactor," ORNL-TM-1488 (July 1966).

RUST, B. W.,* and W. R. BURRUS
"'PUT-5' and 'TAKE-5' – Two Magnetic Tape Systems Routines for the PDP-8," ORNL-TM-1805 (Mar. 22, 1967).

"'Big Hoop' and 'Little Hoop' – Two 'Peter T. Hooper' Routines for Checking the Data Break on a PDP-8," ORNL-TM-1795 (Mar. 22, 1967).

"Super-Flickers – An On-Line Data Acquisition System for the PDP-8," ORNL-TM-1878 (June 1, 1967).

RUST, B. W.,* W. R. BURRUS, and C. SCHNEEBERGER
"A Simple Algorithm for Computing the Generalized Inverse of a Matrix," *Communications Assoc. Computing Mach.* **9**(5), 381 (1967).

SANTORO, R. T.
"System Response Functions for Flight-Time Spectrometry of Secondary Fast Neutrons," ORNL-4114 (August 1967).

SANTORO, R. T., F. E. GILLESPIE,* and P. M. AEBERSOLD
"Constant-Current Source for Instrument Calibration," *Rev. Sci. Instr.* **37**(7), 919 (1966).

SCHNEEBERGER, C., W. R. BURRUS, and B. RUST*
"A Fortran Subroutine Package for Linear Programming," ORNL-TM-1250 (July 18, 1967).

SCHUTTLER, R. J.*
"Efficiency of Organic Scintillators for Fast Neutrons," ORNL-3888 (July 1966).

SELPH, W. E.*
"Neutron and Gamma-Ray Albedos," Chapter 4 of *Weapons Radiation Shielding Handbook*, L. S. Abbott, H. C. Claiborne, and C. E. Clifford, editors, Defense Atomic Support Agency, Washington, DASA-1892-2 (June 1967).

SELPH, W. E.,* and H. C. CLAIBORNE
"Methods for Calculating Effects of Ducts, Access Ways, and Holes in Shields," Chapter 5 of *Weapons Radiation Shielding Handbook*, L. S. Abbott, H. C. Claiborne, and C. E. Clifford, editors, Defense Atomic Support Agency, Washington, DASA-1892-1 (December 1966).

SCOTT, W. W.
"Estimates of Primary and Secondary Particle Doses Behind Aluminum and Polyethylene Slabs Due to Incident Solar-Flare and Van Allen Belt Protons," ORNL-RSIC-18 (July 1967).

SCOTT, W. W., and R. G. ALSMILLER, Jr.
"Comparison of Results Obtained with Several Proton Penetration Codes," ORNL-RSIC-17 (July 1967).

STRAKER, E. A.
"Calculations of the Transport of Neutrons from Fission and 14-MeV Point Sources in an Infinite Medium of Air," ORNL-TM-1547 (Aug. 9, 1966).

*Non-Division personnel.

STRAKER, E. A., and V. R. CAIN
"A Note on Subroutine CEASE (O5R:EVAP), A Modification of EVAP in O5R," ORNL-TM-1552 (Aug. 31, 1966).

THOMAS, J. T.
"Criticality of Large Systems of Subcritical U(93) Components," ORNL-CDC-1 (1967).

TRUBEY, D. K.
"Radiation Shielding Information Center," p. 45 in *Panel Discussion Information for Nuclear Technology*, TID-22972 (June 20, 1966); *Nucl. News* **10**(1), 24 (1967).

TRUBEY, D. K., and F. H. S. CLARK
"Comment on Attix Article 'The Meanings of First Collision Dose'," *Health Phys.* **13**, 298 (March 1967).

TRUBEY, D. K., B. F. MASKEWITZ, and S. K. PENNY
"Computer Codes for Shielding Calculations," *Nucleonics* **24**(8), 112 (1966).

VERBINSKI, V. V.
"Slowing Down Spectra of Neutrons in Lithium Hydride," *Nucl. Sci. Eng.* **27**, 51 (1967).

"Angular Distributions of Low-Energy Neutrons Leaking from Various Scattering Materials," *Nucl. Sci. Eng.* **27**, 67 (1967).

VERBINSKI, V. V., and M. S. BOKHARI
"A Fast-Neutron Spectrometer for Reactor Environments," *Nucl. Instr. Methods* **46**, 309 (1967); ORNL-TM-1546 (June 7, 1966).

VERBINSKI, V. V., M. S. BOKHARI, J. C. COURTNEY,* and G. E. WHITESIDES*
"Measurements and Calculations of Spectral and Spatial Details of Fast-Neutron Flux in Water Shields," *Nucl. Sci. Eng.* **27**, 283 (1967).

VERBINSKI, V. V., J. C. COURTNEY,* and N. BETZ*
"A Method of Evaluating Fast-Neutron Differential Scattering Cross Sections with Short Experimental Runs," ORNL-TM-1769 (Feb. 28, 1967).

WACHTER, J. W., W. R. BURRUS, and W. A. GIBSON
"Neutron and Proton Spectra from Targets Bombarded by 160-MeV Protons," ORNL-TM-1781 (Mar. 3, 1967).

WEBSTER, J. W.
"Point-Set Representation of ^{238}U Cross Sections; Values and a Fortran Program for Computation," ORNL-TM-1448 (June 1966).

"Calculated Neutron Multiplication Factors of Uniform Aqueous Solutions of ^{233}U and ^{235}U," ORNL-CDC-2 (July 1967).

WESTON, L. W., R. GWIN, G. De SAUSSURE, R. W. INGLE,* R. R. FULLWOOD,* and R. W. HOCKENBURY*
"Measurement of the Neutron Fission and Capture Cross Sections for ^{233}U in the Energy Region 0.4 to 1000 eV," ORNL-TM-1751 (Apr. 26, 1967).

WILSON, J. H.,* and L. B. HOLLAND
"Calculations of the Power Distribution in the TSR-II," ORNL-TM-1821 (June 14, 1967).

YOST, K. J.
"A Formalism for the Calculation of Neutron-Capture Gamma-Ray Spectra," ORNL-TM-1867 (June 9, 1967).

*Non-Division personnel.

PAPERS

Topical Conference on Bases for Nuclear Spin-Parity Assignments, Gatlinburg, Tennessee, November 11, 12, and 13, 1965 – papers abstracted in *Bulletin of the American Physical Society*, Series II, Vol. 11, No. 4.

MIHALCZO, J. T., "Sensitivity of Neutron-Spectrum-Dependent Quantities in Uranium (93.2% ^{235}U) Metal Assemblies to Inelastic-Scattering Models of ^{235}U" (p. 651).

PEREY, F. G., "Spin Parities from DWBA Analysis of Inelastic Scattering'' (p. 598).

Topical Conference on Neutron Cross-Section Technology, Washington, D. C., March 22–24, 1966 – papers abstracted in *Bulletin of the American Physical Society*, Series II, Vol. 11, No. 4.

PEREY, F. G., "Filling in Gaps with Cross Sections Calculated from Theory'' (p. 647).

1966 Spring Meeting of the American Physical Society, Washington, D. C., April 25–28, 1966 – papers abstracted in *Bulletin of the American Physical Society*, Series II, Vol. 11, No. 3.

HARLOW, M. V., Jr., J. A. BIGGERSTAFF,* Y. CASSAGNOU,* W. E. KINNEY, J. W. McCONNELL,* F. G. PEREY, and P. H. STELSON,* "Fast-Neutron Scattering Using Time-of-Flight Techniques" (p. 351).

STELSON, P. H.,* Y. CASSAGNOU,* F. G. PEREY, J. W. McCONNELL,* and M. V. HARLOW, Jr., "Neutron Spectra from the ^{59}Co(p,n) ^{59}Ni and ^{65}Cu(p,n) ^{65}Zn Reactions'' (p. 365).

1966 Annual Meeting of the American Nuclear Society, Denver, Colorado, June 20–23, 1966 – papers summarized in *Transactions of the American Nuclear Society*, Vol. 9, No. 1.

COLEMAN, W. A., R. E. MAERKER, and F. J. MUCKENTHALER, "Calculation and Measurement of the Differential Angular Current Albedo for Subcadmium Neutrons Emergent from Concrete Due to Incident Monodirectional Beams of Epicadmium Neutrons" (p. 146).

HOLLAND, L. B., L. W. GILLEY, J. W. POSTON,* and D. R. WARD, "Operational Problems with the Health Physics Research Reactor" (p. 281).

JOHNSON, E. B., "Critical Parameters of Uranium (1.95) Metal Cylindrical Annuli" (p. 185).

KISTNER, G.,* and J. T. MIHALCZO, "The SORA Critical Experiments'' (p. 184).

MAERKER, R. E., and F. J. MUCKENTHALER, "Calculation of the Fast-Neutron Dose Rate Along the Center Line of Both a Straight and a Two-Legged Square Concrete Duct Using the Albedo Concept and Comparison with Experiment" (p. 147).

MIHALCZO, J. T., "Rossi-Alpha Measurements in Subcritical Uranium-Metal Cylinders'' (p. 175).

TRUBEY, D. K., "Radiation Shielding Information Center" (p. 212).

11th Annual Meeting of the Health Physics Society, Houston, Texas, June 27–30, 1966.

ALSMILLER, R. G., Jr., "High-Energy Nucleon Transport."

IRVING, D. C., R. G. ALSMILLER, Jr., and H. S. MORAN, "Tissue Current-to-Dose Conversion Factors for Neutrons with Energies from 0.5 to 60 MeV."

IAEA Symposium on Neutron Monitoring for Radiological Protection, Vienna, Austria, August 29–September 2, 1966.

VERBINSKI, V. V., W. R. BURRUS, R. M. FREESTONE, Jr., and R. E. TEXTOR,* "Proton-Recoil Neutron Spectrometry with Organic Scintillators.''

International Conference on Nuclear Physics, Gatlinburg, Tennessee, September 12–17, 1966.

DICKENS, J. K., F. G. PEREY, and R. J. SILVA,* "Nonlocal Effects in the Distorted Wave Theory of Stripping Reactions."

International Conference on Radiation Measurements in Nuclear Power, September 12–16, 1966, Berkeley, England – papers published in *Radiation Measurements in Nuclear Power*, Barthlomew Press, Dorkin, England.

---

*Non-Division personnel.

VERBINSKI, V. V., and M. S. BOKHARI, "Design and Operation of a Fast Neutron Spectrometer for Measuring Reactor Spectra" (paper 3.16, p. 246).

VERBINSKI, V. V., W. R. BURRUS, R. M. FREESTONE, Jr., and R. E. TEXTOR,* "Fast-Neutron Spectrometry with Thick Organic Scintillators in Reactor-Type Measurements" (paper 3.11, p. 220).

International Conference on Fast Critical Experiments and Their Analysis, October 10–13, 1966, Argonne, Illinois – proceedings published in ANL-7320.

KISTNER, G.,* and J. T. MIHALCZO, "Critical Experiments with a Mockup of the Repetitively Pulsed Reactor, SORA" (p. 586).

LOTTIN, A.,* L. W. WESTON, G. De SAUSSURE, and J. H. TODD,* "Ratio of Capture to Fission in ^{239}Pu at keV Neutron Energies" (p. 22).

MIHALCZO, J. T., "Prompt-Neutron Time Behavior in Delayed-Critical Coupled Uranium-Metal Cylinders" (p. 237).

THOMAS, J. T., "Monte Carlo Calculations of Fast Multicomponent Critical Systems" (p. 299).

Conference on Nuclear Data – Microscopic Cross Sections and Other Basic Data for Reactors, International Atomic Energy Agency, October 17–21, 1966, Paris, France – proceedings published in *Nuclear Data for Reactors*, IAEA, Vienna, 1967.

De SAUSSURE, G., L. W. WESTON, R. GWIN, R. W. INGLE,* J. H. TODD,* R. W. HOCKENBURY,* R. R. FULLWOOD,* and A. LOTTIN,* "Measurement of the Neutron Capture and Fission Cross Sections and of Their Ratio Alpha for ^{233}U, ^{235}U, and ^{239}Pu" (Vol. II).

1966 Winter Meeting of the American Nuclear Society, Pittsburgh, Pennsylvania, October 30–November 3, 1966 – papers summarized in *Transactions of the American Nuclear Society*, Vol. 9, No. 2.

IRVING, D. C., R. G. ALSMILLER, Jr., and H. S. MORAN, "Tissue Current-to-Dose Conversion Factors for Neutrons with Energies from 0.5 to 60 MeV" (p. 359).

LEIMDORFER, M., R. G. ALSMILLER, Jr., and R. T. BOUGHNER,* "Calculations of the Radiation Hazard Due to Exposure of Supersonic Aircraft to Solar Flare Protons" (p. 335).

MAERKER, R. E., and F. J. MUCKENTHALER, "Calculations Using the Albedo Concept of the Subcadmium Flux Along the Center Lines of One-, Two-, and Three-Legged Square Concrete Ducts Arising from Incident Subcadmium Neutrons: Comparison with Experiment" (p. 368).

MARSHALL, J. D.,* and M. B. WELLS,* "The Effect of Cutoff Energy on Monte Carlo Gamma-Ray Dose Rates in Air"† (p. 343).

MIHALCZO, J. T., "Sensitivity of Neutron-Spectrum-Dependent Quantities in Uranium (93.2% ^{235}U) Metal Assemblies to Inelastic-Scattering Models of ^{235}U" (p. 489).

MOONEY, L. G.,* and M. B. WELLS,* "Effects of Neutron-Energy Spectrum in Air on the Neutron-Induced Dose in Concrete Underground Structures"‡ (p. 344).

MORRISON, G. W.,* G. W. WHITESIDES,* and D. C. IRVING, "Adjoint Monte Carlo Calculations for Enriched-Uranium-Metal Assemblies" (p. 440).

MYNATT, F. R.,* N. M. GREENE,* and W. W. ENGLE, Jr.,* "On the Application of Discrete-Ordinates Transport Theory to Deep-Penetration Fast-Neutron-Dose Calculations in Water"† (p. 366).

STRAKER, E. A., "Measurements of the Spectra of Uncollided Fission Neutrons Transmitted Through Thick Samples of Nitrogen, Oxygen, Carbon, and Lead" (paper presented at informal session of the Shielding Division, but not published).

STRAKER, E. A., and M. B. EMMETT,* "Fast-Neutron Collimator Studies" (p. 355).

---

*Non-Division personnel.

†Work supported by Neutron Physics Division.

WEBSTER, J. W., and E. B. JOHNSON, "Criticality of Aqueous Solutions of 5%-Enriched Uranium" (p. 514).

WESTON, L. W., R. GWIN, G. De SAUSSURE, R. W. INGLE,* R. R. FULLWOOD,* and R. W. HOCKENBURY,* "Simultaneous Measurements of the ^{233}U Fission and Capture Cross Sections" (p. 220).

WESTON, L. W., R. GWIN, G. De SAUSSURE, R. W. INGLE,* R. R. FULLWOOD,* and R. W. HOCKENBURY,* "Measurements of the Neutron Capture and Fission Cross Sections of ^{233}U from 0.5 to 100 eV" (paper presented at special session, but not published).

National Topical Meeting of the American Nuclear Society, Las Vegas, Nevada, December 13–15, 1966 – papers published in *Proceedings, Nuclear Criticality Safety,* SC-DC-67-1305.

CALLIHAN, A. D., "Standardization for Nuclear Criticality Control" (p. 105).

JOHNSON, E. B., "The National Criticality Data Center" (p. 79).

THOMAS, J. T., "A Method for Estimating Critical Conditions of Large Arrays of Uranium" (p. 189).

Topical Meeting of the American Nuclear Society, Texas A and M University, College Station, Texas, January 22–24, 1967.

MIHALCZO, J. T., "Rossi-Alpha and Pulsed Neutron Measurements in Subcritical Coupled Uranium-Metal Cylinders."

5th Annual Student Conference of the American Nuclear Society, Gatlinburg, Tennessee, April 6–8, 1967.

COLEMAN, W. A., "A Study to Determine Some of the System Characteristics of an Intense Neutron Generator Based on a Proton Accelerator Using Monte Carlo Methods."

SOLOMITO, M., "Neutron Flux-to-Dose Conversion Factors for Tissue."

1967 Spring Meeting of the American Physical Society, Washington, D. C., April 24–27, 1967 – papers abstracted in *Bulletin of the American Physical Society,* Series II, Vol. 12, No. 4.

BERTINI, H. W., "Intermediate-Energy Intranuclear-Cascade Calculation" (p. 380).

KINNEY, W. E., J. A. BIGGERSTAFF,* J. K. DICKENS, M. V. HARLOW, Jr., J. W. McCONNELL,* F. G. PEREY, and P. H. STELSON,* "Neutron Cross Sections for ^{56}Fe from 4.5 to 7.6 MeV" (p. 475).

PEREY, F. G., J. A. BIGGERSTAFF,* J. K. DICKENS, W. E. KINNEY, J. W. McCONNELL,* and P. H. STELSON,* "Inelastic Scattering of 7.6-MeV Neutrons" (p. 512).

1967 Annual Meeting of the American Nuclear Society, San Diego, California, June 11–15, 1967 – papers summarized in *Transactions of the American Nuclear Society,* Vol. 10, No. 1.

ALSMILLER, R. G., Jr., "High-Energy Nucleon Transport" (p. 384).

ALSMILLER, R. G., Jr., M. LEIMDORFER, and J. BARISH,* "Analytical Representation of Nonelastic Cross Sections and Particle-Emission Spectra from Nucleon-Nucleus Collisions in the Energy Range 25 to 400 MeV" (p. 386).

CAIN, V. R., "Application of S_n Adjoint Flux Calculations to Monte Carlo Biasing" (p. 399).

JOHNSON, E. B., "Critical Lattices of U(4.89) Metal Rods in Water" (p. 190).

MAERKER, R. E., and F. J. MUCKENTHALER, "Calculations Using the Albedo Concept of the Subcadmium Flux Along the Center Lines of One-, Two-, and Three-Legged Square Concrete Ducts Arising from Incident Epicadmium Neutrons: Comparison with Experiment" (p. 396).

MARSHALL, J. D.,* and M. B. WELLS,* "Simplified Method for Calculating Nitrogen-Capture and Fission-Product Gamma-Ray Doses Inside Underground Concrete Structures"† (p. 406).

---

*Non-Division personnel.

†Work supported by Neutron Physics Division.

MIHALCZO, J. T., "Prompt-Neutron Decay in Delayed-Critical Assemblies of Three Interacting Cores" (p. 242).

MORRISON, G. W.,* J. R. KNIGHT,* and D. C. IRVING, "Prompt-Neutron Decay Constants Calculated in Highly Enriched Uranium Metal Assemblies" (p. 223).

PEELLE, R. W., "Nuclear Reaction Cross Sections for Spacecraft Shield Design" (p. 385).

STRAKER, E. A., and M. B. EMMETT,* "Sensitivity of Calculations of Neutron Transport in Oxygen to Various Cross-Section Sets" (p. 392).

TRUBEY, D. K., "A Calculation of the Components of the Exposure in a Basement Due to Fallout" (p. 404).

WESTON, L. W., R. GWIN, G. De SAUSSURE, R. W. INGLE,* R. R. FULLWOOD,* and R. W. HOCKENBURY,* "Simultaneous Measurements of the ^{233}U Fission and Capture Cross Sections" (p. 220).

Annual Meeting of the Society for Industrial and Applied Mathematics, Washington, D. C., June 12–15, 1967.

COVEYOU, R. R., "Mathematics of Random Number Generation."

Conference on Reactor Operating Experience, American Nuclear Society, Atlantic City, New Jersey, July 24–25, 1967.

HOLLAND, L. B., and D. R. WARD, "TSR-II Control Mechanism Development and Operational Experience."

---

*Non-Division personnel.

ORNL-4134
UC-34 – Physics

INTERNAL DISTRIBUTION

1. L. S. Abbott
2. F. S. Alsmiller
3. R. G. Alsmiller, Jr.
4. T. W. Armstrong
5. J. Barish (K-25)
6. H. W. Bertini
7. F. E. Bertrand
8. N. A. Betz
9. J. A. Biggerstaff
10. R. T. Boughner
11. T. V. Blosser
12. J. Brown
13. W. R. Burrus
14. V. R. Cain
15. A. D. Callihan
16. G. T. Chapman
17. H. C. Claiborne
18. F. H. S. Clark
19. C. E. Clifford
20. W. A. Coleman
21. R. R. Coveyou
22. S. N. Cramer
23. G. deSaussure
24. H. Derrien
25. J. K. Dickens
26. L. Dresner
27. J. D. Drischler
28. E. Eichler
29. J. F. Ellis
30. M. B. Emmett
31. W. W. Engle, Jr. (K-25)
32. W. E. Ford, III (K-25)
33. Hemma Francis
34. J. L. Fowler
35. K. D. Franz (K-25)
36. R. M. Freestone, Jr.
37. C. Y. Fu
38. T. Gabriel
39. W. A. Gibson
40. L. W. Gilley
41. J. H. Gillette
42. N. M. Greene (K-25)
43. Jane Gurney
44. M. P. Guthrie
45. R. Gwin
46. V. M. Hamrick
47. J. A. Harvey
48. Henrietta Hendrickson
49. K. M. Henry, Jr.
50. B. D. Holcomb (K-25)
51. L. B. Holland
52. J. L. Hull
53. R. W. Ingle
54. D. C. Irving
55. E. B. Johnson
56. W. H. Jordan
57. F. B. K. Kam
58. M. A. Kastenbaum
59. D. T. King
60. W. E. Kinney
61. J. R. Knight (K-25)
62. R. Kuebbing
63. C. E. Larson
64. J. Lewin
65. E. C. Long (K-25)
66. A. Lottin
67. T. A. Love
68. J. J. Lynn
69. H. G. MacPherson
70. R. E. Maerker
71. D. W. Magnuson
72–122. F. C. Maienschein
123. J. J. Manning
124. A. L. Marusak
125. B. F. Maskewitz
126. J. W. McConnell
127. J. T. Mihalczo
128. H. S. Moran
129. G. W. Morrison (K-25)
130. F. J. Muckenthaler
131. F. R. Mynatt (K-25)
132–133. R. B. Parker
134. R. W. Peelle
135. C. M. Perey
136. F. G. Perey
137. R. Perez
138. J. W. Poston
139. D. I. Putzulu

140. T. R. Puryear
141. S. J. Raffety
142. J. J. Ritts
143. R. J. Rodgers (K-25)
144. E. R. Rohrer
145. R. Roussin
146. B. W. Rust (K-25)
147. R. T. Santoro
148. G. R. Satchler
149. E. G. Silver
150. M. J. Skinner
151. E. Solomito
152. P. H. Stelson
153. P. N. Stevens
154. P. Stewart (K-25)
155. J. R. Stockton
156. E. A. Straker
157. R. Textor (K-25)
158. J. T. Thomas
159. J. H. Todd
160. D. K. Trubey
161. W. C. Tunnell
162. J. W. Wachter
163. D. R. Ward
164. J. W. Webster
165. A. M. Weinberg
166. G. Westley (K-25)
167. L. W. Weston
168. C. Whitehead (K-25)
169. G. W. Whitesides (K-25)
170. G. C. Williams
171. L. R. Williams (K-25)
172. H. Yamakoshi
173. G. Young
174. K. J. Yost
175. W. Zobel
176. G. Dessauer (consultant)
177. B. C. Diven (consultant)
178. W. N. Hess (consultant)
179. M. H. Kalos (consultant)
180. L. V. Spencer (consultant)
181. Radiation Shielding Information Center
182. Biology Library
183–185. Central Research Library
186. Reactor Division Library
187–188. ORNL Y-12 Technical Library, Document Reference Section
189–238. Laboratory Records Department
239. Laboratory Records ORNL R.C.

EXTERNAL DISTRIBUTION

240–539. Given external distribution
540. P. B. Hemmig, Division of Reactor Development, U.S. Atomic Energy Commission, Washington, D.C.
541. I. F. Zartman, Division of Reactor Development, U.S. Atomic Energy Commission, Washington, D.C.
542. J. A. Swartout, Union Carbide Corporation, New York, New York
543. W. W. Grigorieff, Assistant to the Executive Director, Oak Ridge Associated Universities, Oak Ridge, Tennessee
544. Research and Development Division, AEC, ORO
545–858. Given distribution as shown in TID-4500 under Physics category (25 copies – CFSTI)